OptiPerformer

Examples from Govind P. Agrawal's Book Fiber-Optic Communication Systems

OptiSystem Project Simulator

Version 8.0



OptiPerformer

Examples from Govind P. Agrawal' Book
Fiber-Optic Communication Systems

OptiSystem Project Simulator

Copyright © 2010 Optiwave
All rights reserved.

All OptiPerformer documents, including this one, and the information contained therein, is copyright material.

No part of this document may be reproduced, stored in a retrieval system or transmitted in any form or by any means whatsoever, including recording, photocopying, faxing, etc., without prior written approval of Optiwave.

Disclaimer
Optiwave makes no representation or warranty with respect to the adequacy of this documentation or the programs which it describes for any particular purpose or with respect to its adequacy to produce any particular result. In no event shall Optiwave, its employees, its contractors, or the authors of this documentation be liable for special, direct, indirect, or consequential damages, losses, costs, charges, claims, demands, or claim for lost profits, fees, or expenses of any nature or kind.

Technical support

If you purchased Optiwave software from a distributor that is not listed here, please send technical questions to your distributor.

Optiwave — Canada/US

Tel (613) 224-4700
Fax (613) 224-4706
E-mail support@optiwave.com
URL www.optiwave.com

Cybernet Systems Co., Ltd. — Japan

Tel +81 (03) 5297-3342
Fax +81 (03) 5297-3646
E-mail owtech@cybernet.co.jp
URL www.cybernet.co.jp

Optiwave Europe — Europe

Tel +33 (0) 494 08 27 97
Fax +33 (0) 494 33 65 76
E-mail support@optiwave.com
URL www.optiwave.eu

Table of contents

Introduction 1

Basic Concepts of Optical Communication Systems 5

Optical NRZ and RZ Modulation Formats 7
Lightwave System Components 11

Optical Fibers 15

Fiber Dispersion 17
Chirped Gaussian Pulses 21
Attenuation Coefficient 29
Stimulated Light Scattering - Raman 31
SPM and XPM 33
Four-Wave Mixing 35

Optical Transmitters 37

LED Spectral Distribution 39
LED Modulation Response 41
Light-Current Characteristics 45
Direct Modulation and External Modulation 47
Laser Intensity Noise 49

Optical Receivers 51

Receiver Design 53
Receiver Shot and Thermal Noise 57
Receiver PIN x APD 59
Receiver BER and Q Factor 61
Minimum Received Power 63
ER Induced Sensitivity Degradation 65

Lightwave Systems 67

Power Budget 69
Power Management for Ring Networks 71
Dispersion Induced Degradation 85

Multichannel Systems 87

Fabry-Perot Filter 89
Uniform FBG Filter 91
AWG Demultiplexer 93
Star Coupler 95
Optical Cross-Connects 97
Channel Multiplexing 99
Channel Demultiplexing by FWM 101
Interchannel Crosstalk at ADM in A Ring Network 103
Subcarrier Multiplexing 107

Optical Amplifiers 109

EDFA Basic Concepts 111
Booster Amplifier 117
In-Line Amplifier 119
Preamplifier 121
SLA Cascaded in-line Amplifiers: Soliton Pattern Effect at 10 Gb/s in SMF 123
SLA Gain Recovery 127
SLA Gain Saturation of Chirped and Super Gaussian Pulses 141
SLA Gain Saturation of Gaussian Pulses 149
Raman Gain and Bandwidth 159
Raman Gain Saturation 161
Broadband Flat Gain Raman Amplifier 163
Pumping Requirements 165
Multichannel Amplification 169
Optical Preamplifiers 171
Power Boosters 173
Metro EDFA 175
Cascaded In-Line Amplifiers 177
EDFA Dynamic 179

Dispersion Management 181

Dispersion Compensation Techniques 183
Precompensation Technique using SOA 189
40 Gbps Transmission System 195
Dispersion Compensation with FBG 203
Fiber Nonlinearities and Dispersion 205
Negative Dispersion Fiber and Applications for Metro Networks 211
Migrating to 10 Gbps Metro System and Dispersion Limited Transmission 215

Soliton Systems 221

Fundamental and Higher-Order Solitons 223
Interaction of A Pair of Fundamental Solitons 227
Average Soliton Regime 229
Interaction of Multicolor Solitons 231

Advanced Lightwave Systems 233

Intensity Modulation Formats (NRZ, RZ, AMI, DB) 235
DPSK Modulation and Demodulation 251
QPSK Modulation and Demodulation 257
100 Gbps PM-QPSK 263
OD8PSK Modulation and Demodulation 265
4-QAM OFDM Modulation and Demodulation 269

Optical Signal Processing 273

Nonlinear Optical Loop Mirror 275
Parametric Amplifiers 277
Wavelength Conversion Based on FWM in SOA 279
Wavelength Conversion Based on XGM in SOA 283
Wavelength Conversion Based on XPM in HNLF 287
Data-Format Conversion Based on XPM in HNLF 291
SPM Based 2R Regenerator for RZ Signal 293
XPM Based 3R Regenerator for RZ Signal 295

Introduction

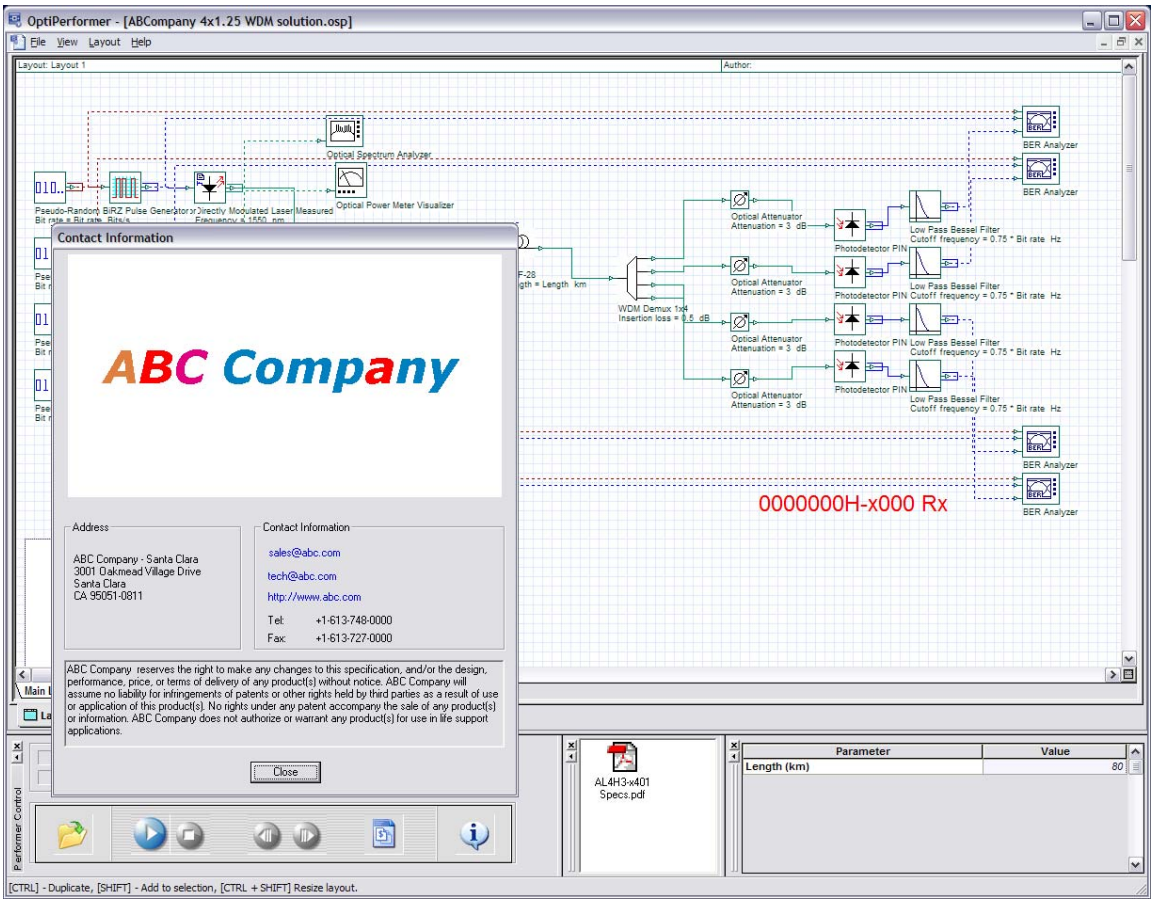
OptiPerformer is a software tool that enables technical sales and marketing teams of component and system vendors to powerfully and cost-effectively demonstrate their products. The demonstration is carried out using design scenarios that accurately project performance characteristics of real systems built using vendor components or subsystems. By using OptiPerformer, an application engineer can easily demonstrate the benefits of a product, or propose different scenarios for the product, without having to develop the full depth of R&D-level technical knowledge typical of proficient OptiSystem users.

OptiPerformer's capabilities are derived from Optiwave's award-winning OptiSystem product, an optical system design tool that enables users to plan, test, and simulate almost every type of optical link in the physical layer of a broad spectrum of optical networks. OptiSystem addresses the needs of research scientists and optical telecom engineers, and offers the benefits of dramatic reductions of investment risk and time-to-market, rapid, low-cost prototyping, and global insight into system performance.

OptiPerformer extends OptiSystem's simulation power beyond an organization's R&D department, addressing the needs of the 'customer-facing' team. OptiPerformer features key streamlined functionality and enhanced ease-of-use, enabling technical-sales and marketing oriented users to convincingly demonstrate to their potential customers the value of their specific component solution. Further to this, potential customers can simulate and validate component and system vendors proposed component and sub-system performance versus competing offers within the virtual environment of OptiPerformer.



Figure 0-1: OptiPerformer GUI



OptiPerformer can be distributed and used by both system and component vendors, as well as their customers and prospects.

Main features

The main features of the OptiPerformer interface include:

Feature	Description
Graphical user interface	A comprehensive Graphical User Interface (GUI) controls the optical component layout, component models, and presentation graphics. The Performer Control window provides simple, easy-to-use button controls for simulation control.
Mixed signal representation	OptiSystem handles mixed signal formats for optical and electrical signals in the Component Library. OptiSystem calculates the signals using the appropriate algorithms related to the required simulation accuracy and efficiency.
Quality and performance algorithms	In order to predict the system performance, OptiSystem calculates parameters such as BER and Q-Factor using numerical analysis or semi-analytical techniques for systems limited by inter symbol interference and noise.
Advanced visualization tools	Advanced visualization tools produce OSA Spectra, Oscilloscope, and Eye diagrams. Also included are WDM analysis tools listing signal power, gain, noise figure, and OSNR.
State-of-the-art calculation data-flow	The Calculation Scheduler controls the simulation by determining the order of execution of component modules according to the selected data flow model. The main data flow model that addresses the simulation of the transmission layer is the Component Iteration Data Flow (CIDF). The CIDF domain uses run-time scheduling, supporting conditions, data-dependent iteration, and true recursion.

Notes:

Chapter 1 - Basic Concepts of Optical Communication Systems

This chapter contains the following examples.

- Optical NRZ and RZ Modulation Formats
- Lightwave System Components

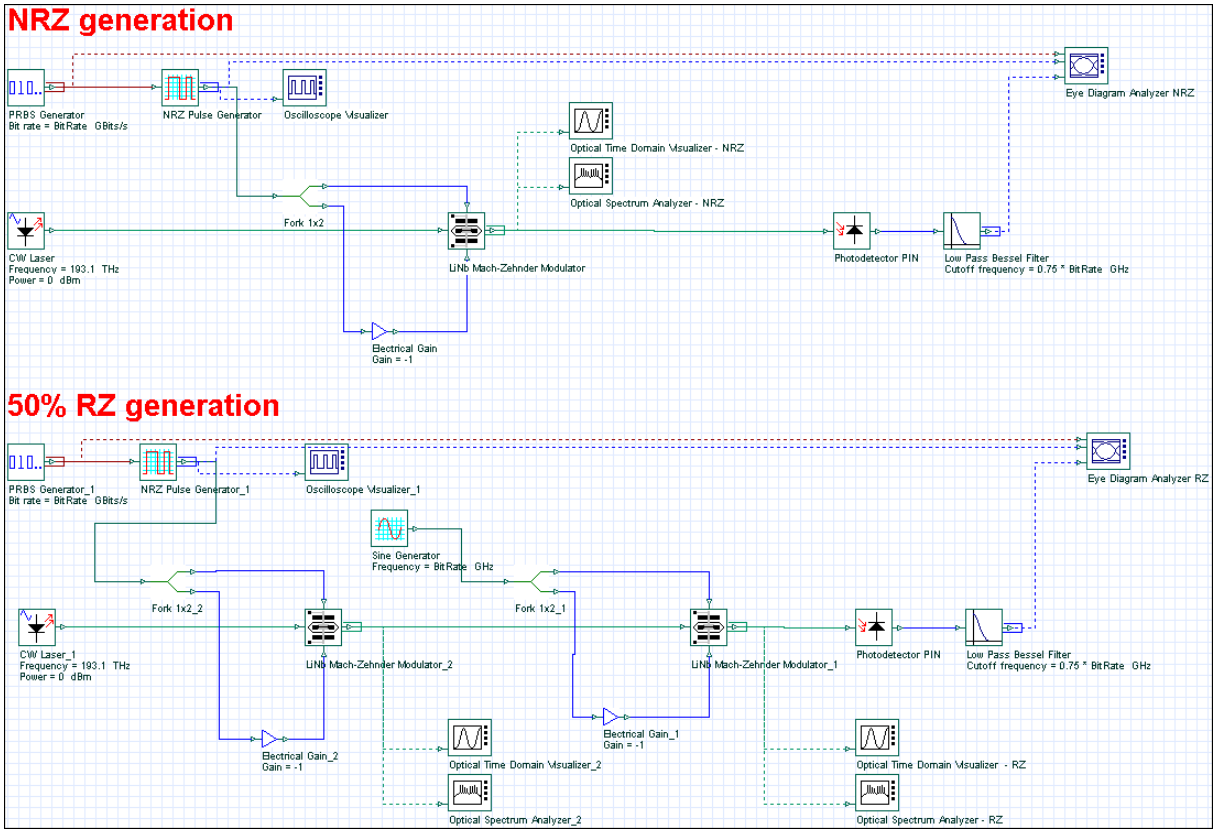
Notes:

Optical NRZ and RZ Modulation Formats

Optical NRZ RZ formats.osp

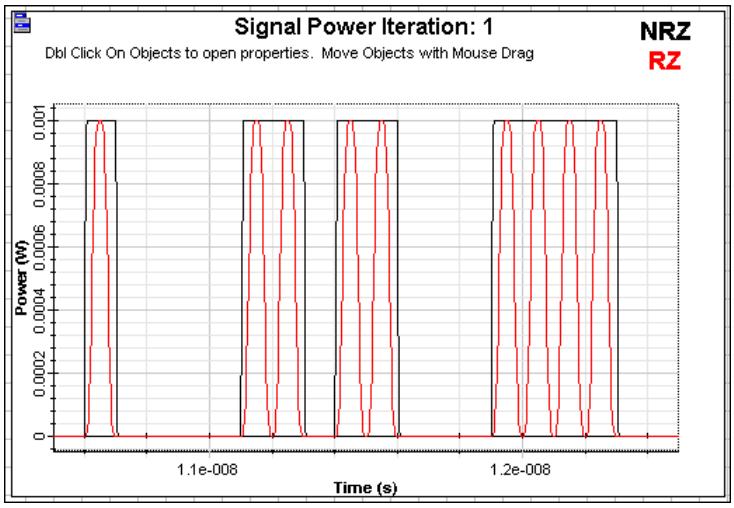
There are two typical choices for the modulation format of an optical signal. These are shown in the project file "*Optical NRZ RZ formats.osp*" and are known as the return-to-zero (RZ) and nonreturn-to-zero (NRZ).

Figure 1-1: Layout - NRZ and RZ modulation formats



In the RZ format, each pulse that represents bit 1 is shorter than the bit slot, and its amplitude returns to zero before the bit duration is over. In the NRZ format, the pulse remains on throughout the bit slot and its amplitude does not drop to zero between two or more successive bits. As a result, pulse width varies depending on the bit pattern, whereas it remains the same in the case of RZ format.

Figure 1-2: NRZ and RZ (Amplitude vs. Time)



An advantage of the NRZ format is that the bandwidth associated with the bit stream is smaller than that of the RZ format by about a factor of 2 simply because on-off transitions occur fewer times.

Figure 1-3: Spectrum of NRZ and RZ signals

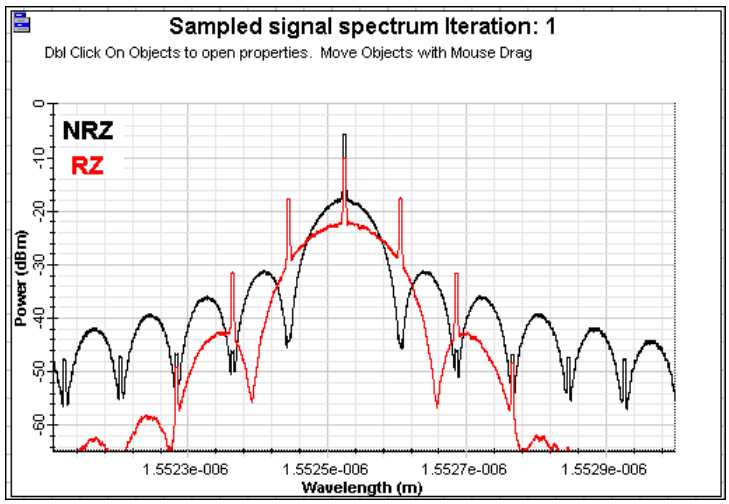
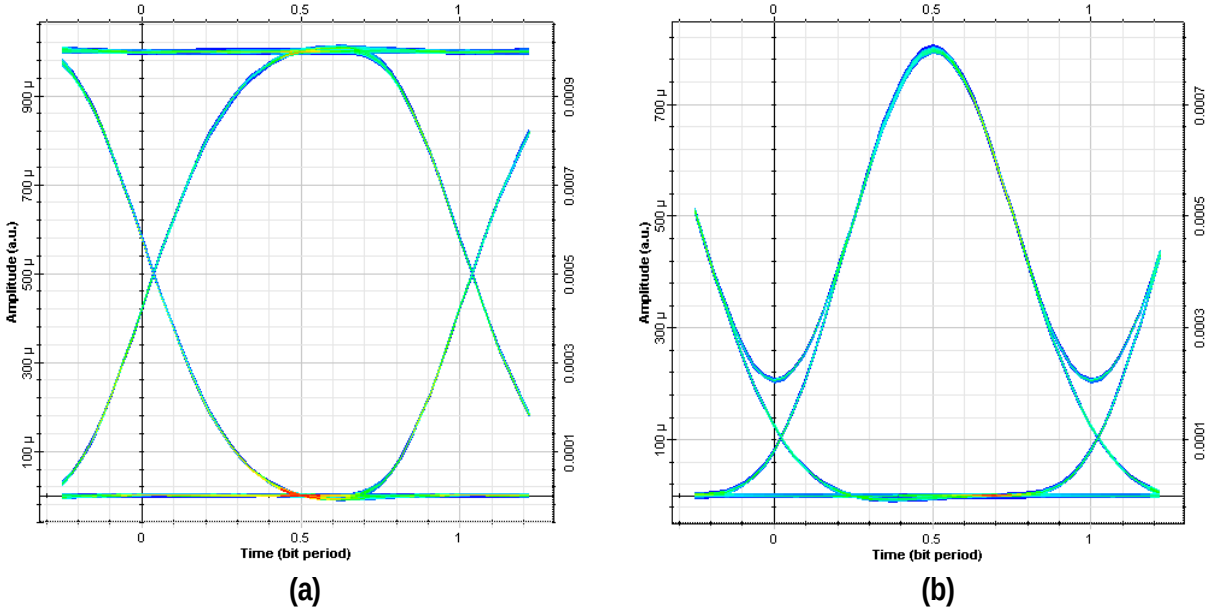


Figure 1-4: Eye diagrams of (a) NRZ and (b) RZ signals



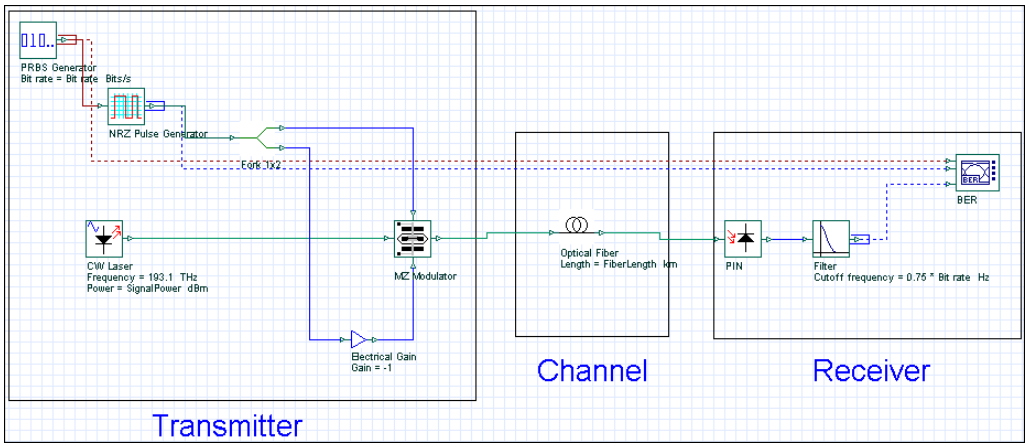
Notes:

Lightwave System Components

Lightwave system components.osp

Project "*Lightwave system components.osp*" shows a generic block diagram of an optical communication system. It consists of a communication channel with a transmitter in the front and a receiver at the back.

Figure 1-5: Layout - Lightwave system components



(a) Communication Channel

The role of the communication channel is to transport the optical signal from transmitter to receiver without distorting it. Most lightwave communication systems use optical fibers as the communication channel because fibers can transmit light with a relatively small amount of power loss.

Fiber loss is, of course, an important design issue, as it determines directly the repeater spacing of a long-haul lightwave system. Another important design issue is fiber dispersion, which leads to broadening of individual pulses inside the fiber.

In order to observe the effects of loss and dispersion in the optical signal the user can change the values of fiber length and visualize the degradation of the signal at the receiver stage.

Figure 1-6: Received eye diagram after 50 km of fibe

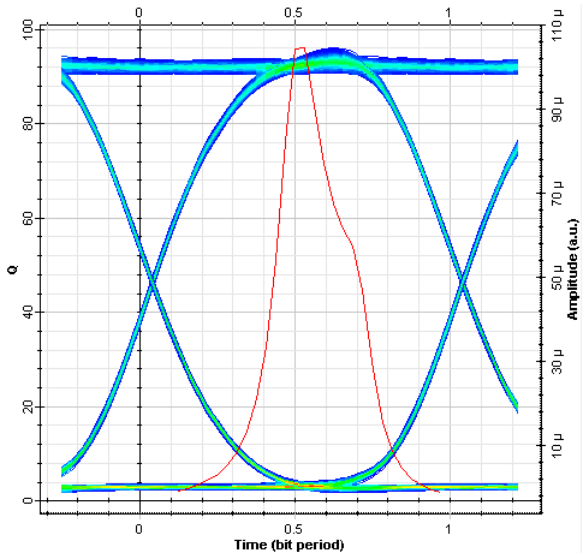


Figure 1-7: Received eye diagram after 100 km of fiber

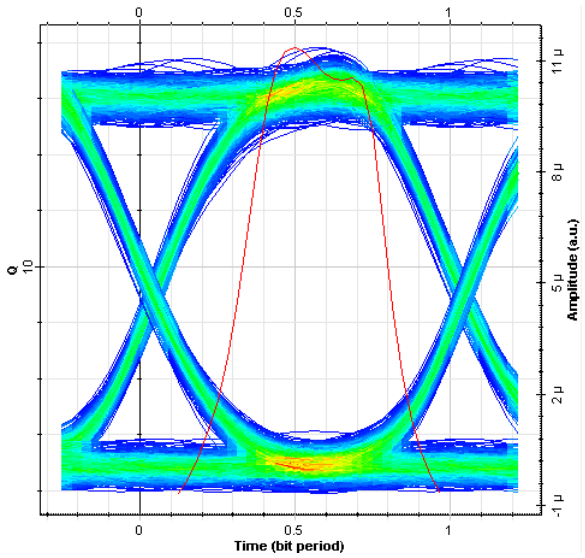
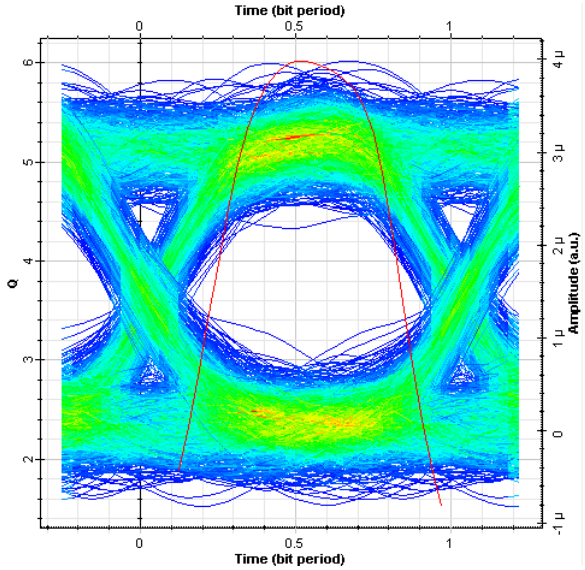


Figure 1-8: Received eye diagram after 126 km of fiber



(b) Optical Transmitters

The role of the optical transmitter is to convert the electrical signal into optical form and to launch the resulting optical signal into the optical fiber. It consists of an optical source, an electrical pulse generator and an optical modulator.

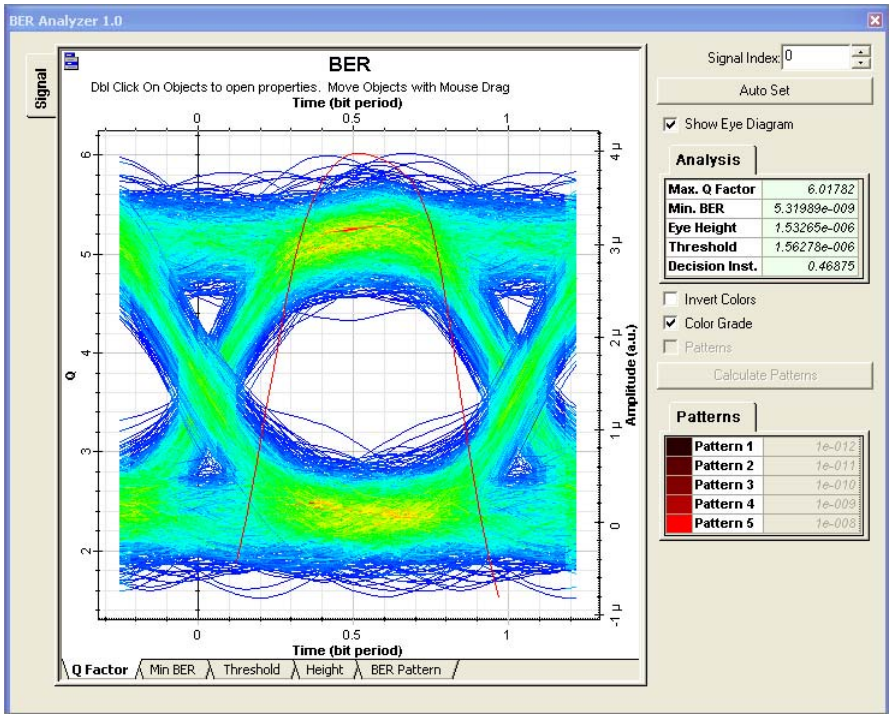
The launched power is an important design parameter, as it indicates how much fiber loss can be tolerated. It is often expressed in units of dBm with 1 mW as the reference level.

(c) Optical Receivers

An optical receiver converts the optical signal received at the output end of the optical fiber back into the original electrical signal. It consists of a photodetector, a filter and a demodulator. Usually the received signal is in the form of optical pulses representing 1 and 0 bits and it is converted directly into an electrical current. Such a scheme is referred to as intensity modulation with direct detection (IM/DD). Demodulation is done by a decision circuit that identifies bits as 1 or 0, depending on the amplitude of the electrical current.

The performance of a digital lightwave system is characterized through the bit- error rate (BER). It is customary to define the BER as the average probability with incorrect bit identification. Most lightwave systems specify a BER of 10^{-9} as the operating requirement. For this project, a laser output power of 0 dBm with 126 km of fiber length will lead to an output signal with BER of 10^{-9}.

Figure 1-9: Received eye diagram and BER after 126 km of fiber



Chapter 2 - Optical Fibers

This chapter contains the following examples.

- Fiber Dispersion
- Chirped Gaussian Pulses
- Attenuation Coefficient
- Stimulated Light Scattering - Raman
- SPM and XPM
- Four-Wave Mixing

Notes:

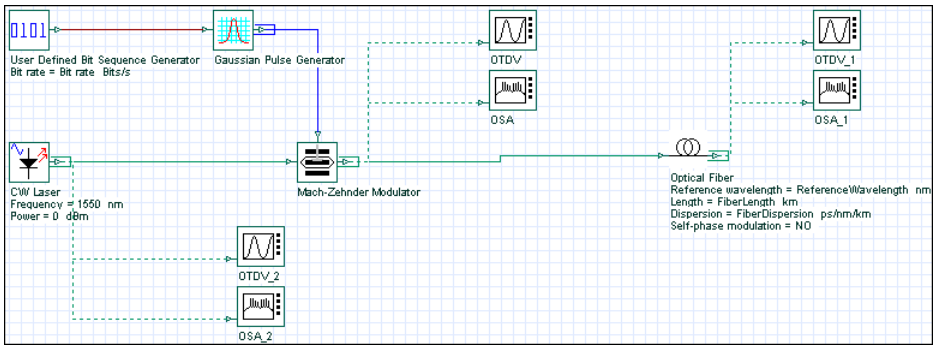
Fiber Dispersion

Fiber dispersion.osp

In this example we demonstrate the influence of the group velocity dispersion in SMF at 1.55 μm using externally modulated optical sources. The fiber dispersion is set to D = 16.75 ps/nm-km @ 1550 nm, attenuation and fiber nonlinearity are not considered in this example. We consider the unchirped pulse and neglect the influence of the initial pulse shape.

Externally modulated laser with a small spectral width is used as an optical source. A transmission bit rate of 10 Gb/s is considered in the layout which is shown in Figure 2-1:

Figure 2-1: Layout - Externally modulated laser

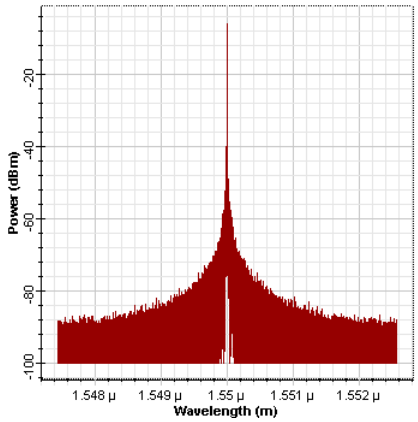


For simulation, we consider duty cycle = 0.5, T_{FWHM} = 50 ps, T_0 = 30.03 ps, $L_D = T_0^2/|\beta_2|$ = 42.24 km, $\Delta\omega = 1/T_0$= 33.3 GHz, and $\sigma_\omega \sim 2\pi \times 10$ MHz. Figure 2-2 shows the generated spectrum of the CW laser. Since $\sigma_\omega/\Delta_\omega$ << 1, for the spread of the pulse width, we can expect the validity of the following formula :

$$\frac{\sigma^2}{\sigma_0^2} = 1 + \left(\frac{\beta_2 z}{2\sigma_0^2}\right)^2 = 1 + \left(\frac{z}{L_D}\right)^2 \qquad \textbf{(2-1)}$$

where σ_0 is the RMS width of the input Gaussian pulse $\sigma_0 = T_0/(\sqrt{2})$. Eq. 2-1 shows that to get 4 times increase of the pulse width a distance of approximately $4L_D$ (~ 169 km) is needed.

Figure 2-2: Spectrum of the CW laser



(Note that to get enough spectral resolution a very large time window was used with a sequence length of 2048 bits and 64 samples per bit).

Obtained results after the simulation are presented in Figure 2-3, Figure 2-4, and Figure 2-5.

Figure 2-3: Pulse profile after the modulator (T_{FWHM} = 50 ps)

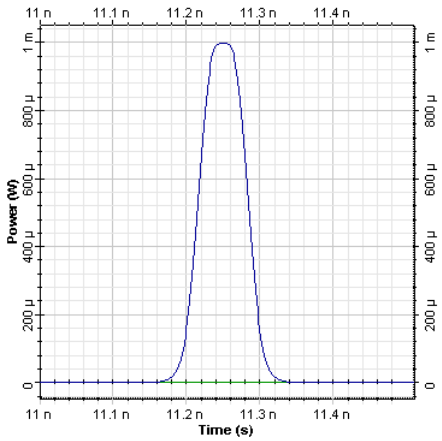


Figure 2-4: Spectrum after the modulator

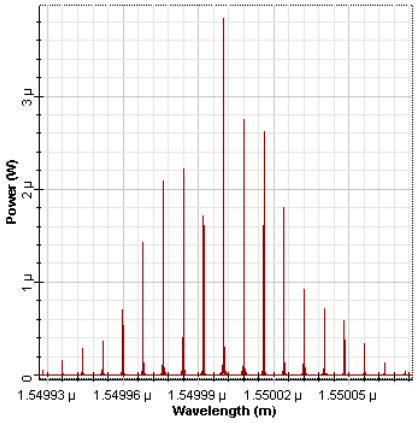
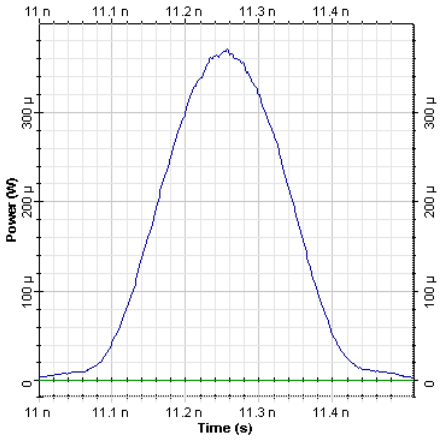


Figure 2-5: Pulse profile after propagation in 169 km of SMF (T_{FWHM} = 197.7 ps)



As can be seen that the pulse width increases approximately 3.95 times (cf. Eq. 2-1).

Reference:

[1] G.P. Agrawal, *Nonlinear Fiber optics*, third edition, Academic Press, 2001.

Notes:

Chirped Gaussian Pulses

Chirped Gaussian pulses.osp

Chirped Gaussian pulses - Dispersion compensation.osp

(a) Chirped Gaussian pulses

In this example we show the influence of the GVD on the spatial evolution of the pulse width of initially chirped Gaussian pulses. Again, attenuation and fiber nonlinearity are not considered. The general expression for the spatial evolution of pulse width in dispersive media is given by Eq. 2-2:

$$\frac{\sigma^2}{\sigma_0^2} = \left(1 + \frac{C\beta_2 z}{2\sigma_0^2}\right)^2 + (1 + V_\omega^2) \times \left(\frac{\beta_2 z}{2\sigma_0^2}\right)^2 \qquad \textbf{(2-2)}$$

Where: C is the initial chirp of the pulse

σ is the root-mean-square (RMS) width of the pulse

$V_\omega = 2\sigma_\omega\sigma_0 = (\sqrt{2}\sigma_\omega)/(\Delta\omega)$ is the parameter describing the relative contribution of spectral width of the source and of the pulse

$\sigma_0 = T_0/(\sqrt{2})$, where T_0 is the initial pulse width

$D = -\frac{2\pi c}{\lambda^2}\beta_2$

$\Delta\omega = 1/T_0$ is the spectral width of the unchirped Gaussian pulse

The typical value of D = 16.75 ps/nm-km at 1.55 μm for SMF leads to β_2 = -21.35 ps^2/km. For the considered optical source (source with small spectral width) the limiting transmission distances are determined by the pulse width and the GVD. For such source, the dispersive action of the medium is described by the dispersion length $L_D = T_0^2/|\beta_2|$, which characterizes the pulse spreading in dispersive medium. In this case, for the initially unchirped pulse, if $V_\omega \ll 1$, Eq. 2-2 can be simplified into Eq. 2-3:

$$\frac{\sigma^2}{\sigma_0^2} = 1 + \left(\frac{\beta_2 z}{2\sigma_0^2}\right)^2 = 1 + \left(\frac{z}{L_D}\right)^2 \qquad \textbf{(2-3)}$$

If for a Gaussian pulse we assume duty cycle = 0.5, then

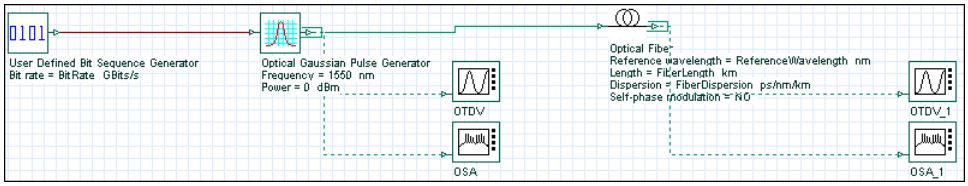
B = 2.5 Gb/s -> T_B = 400 ps -> T_{FWHM} = 200 ps -> T_0 = 120.12 ps -> L_D = 675.86 km -> $\Delta\omega$ = 8.3250 GHz -> $\sigma_\omega/(\Delta\omega) \ll 1$

B = 10 Gb/s -> T_B = 100 ps -> T_{FWHM} = 50 ps -> T_0 = 30.03 ps -> L_D = 42.24 km -> $\Delta\omega$ = 33.3 GHz -> $\sigma_\omega/(\Delta\omega) \ll 1$

B = 40 Gb/s -> T_B = 25 ps -> T_{FWHM} = 12.5 ps -> T_0 = 7.51 ps -> L_D = 2.64 km -> $\Delta\omega$ = 133.16 GHz -> $\sigma_\omega/(\Delta\omega) \ll 1$

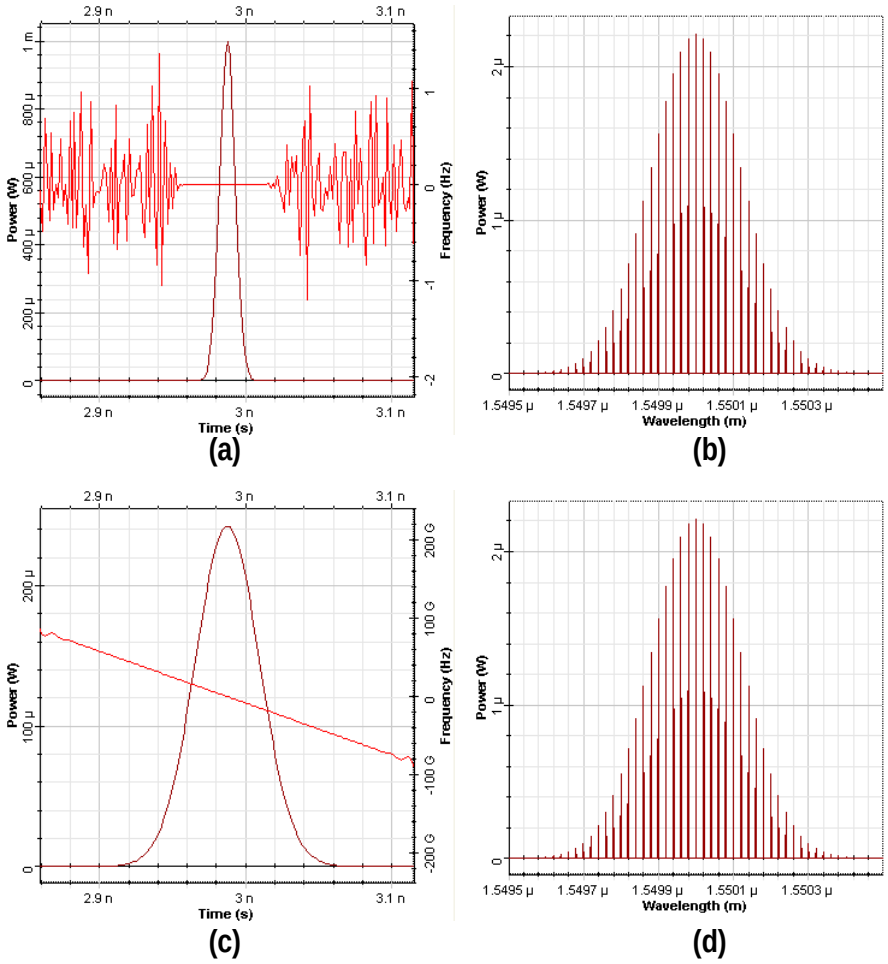
Let us consider B= 40 Gb/s. In accordance with Eq. 2-3, at 4 x L_D = 10.56 km the width of the initially unchirped pulse will increase approximately 4 times. This can be demonstrated with the project *Chirped Gaussian pulses.osp* which has the following layout:

Figure 2-6: Layout - Chirped Gaussian pulses



The obtained results for 40 Gb/s transmission, duty cycle = 0.5 and D = 16.75 ps/nm-km at 1.55 μm are shown in Figure 2-7.

Figure 2-7: (a) Initial pulse shape (intensity and chirp) (b) Initial pulse spectrum (c) Pulse shape after propagation in 10.56 km of SMF (intensity and chirp) (d) Pulse spectrum after propagation in 10.56 km of SMF.



As expected (cf. Eq. 2-3), an increase of the initially unchirped pulse width by approximately 4 times can be clearly seen. Note the appearance of the negative chirp of the pulse after transmission in 10.56 km of fiber in anomalous group velocity dispersion region (Figure 2-7(c)). Because the GVD is the only included effect in the calculation, no changes in the spectrum can be observed after the transmission.

Now, we consider the pulse evolution of the initially chirped pulse (chirp parameter C = -2) for a transmission distance of 10.56 km. From Eq. 2-2 we see that when $C\beta_2 > 0$ the broadening of the pulse is increased with comparison to unchirped initial pulse. Results are shown in Figure 2-8 and Figure 2-9.

Figure 2-8: Initial chirped pulse shape (C = -2). Note the negative initial chirp shown in the figure.

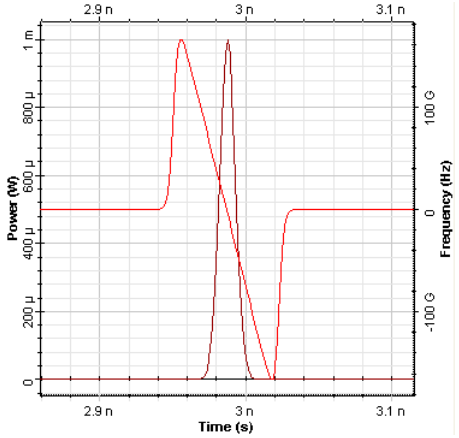
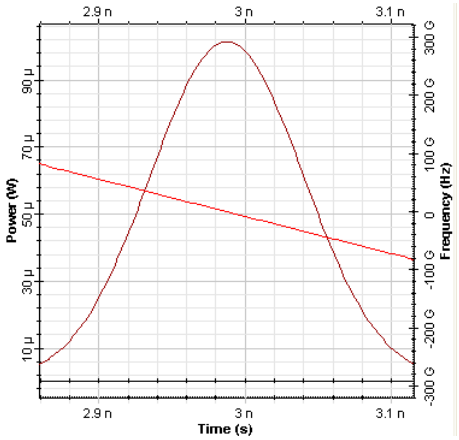


Figure 2-9: Increase of pulse width after propagation in 10.56 km of SMF.



As we can see from Figure 2-9, after only 10.56 km of SMF, the pulse width increases approximately 11.52 times or much more as compared to the case of initially unchirped pulse.

However, if we substitute $C\beta_2 < 0$ in Eq. 2-2, the pulse compression could be expected. To demonstrate this type of behavior, we consider an initial chirped pulse with C = 2 and a transmission distance of 1.056 km.

Results are shown in Figure 2-10 and Figure 2-11.

Figure 2-10: Initial chirped pulse shape (C = 2, T_{FWHM} = 12.5 ps). Note the positive initial chirp shown in the figure.

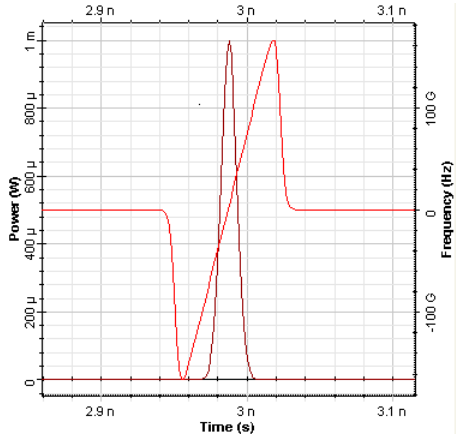
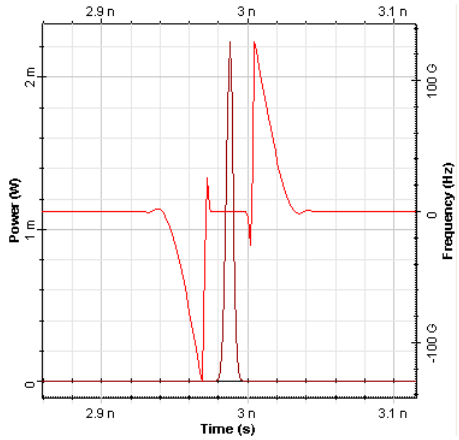


Figure 2-11: Decrease of pulse width (TFWHM = 5.6 ps) after propagation in 1.056 km of SMF.

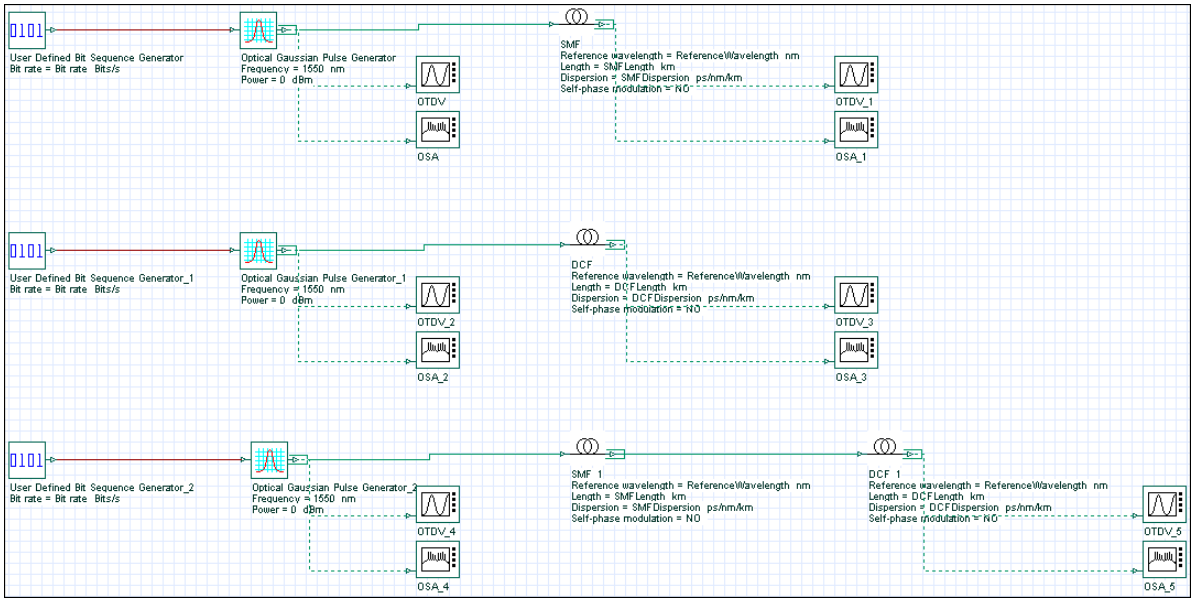


As we can see, pulse width gets reduced approximately two times as compared to its initial value after propagation in 1.056 km of SMF.

(b) Chirped Gaussian pulses - Dispersion compensation

Now, we will pay attention to the cancellation of chirp in single mode fiber (SMF) and dispersion compensation fiber (DCF). The project has the following layout (Figure 2-12):

Figure 2-12: Layout - Chirped Gaussian pulses - Dispersion compensation



We choose the following parameters for SMF and DCF:

D_{SMF} = 16 ps/nm-km, $DispersionSlope_{SMF}$ = 0.08 ps/nm^2-km, α = 0.2 dB/km and L_{SMF} = 10 km.

D_{DCF} = -80 ps/nm-km, $DispersionSlope_{DCF}$ = 0.08 ps/nm^2-km, α = 0.5 dB/km and L_{DCF} = 2 km.

The initial Gaussian pulse profile can be seen in Figure 2-13.

Figure 2-13: Initial Gaussian pulse profile

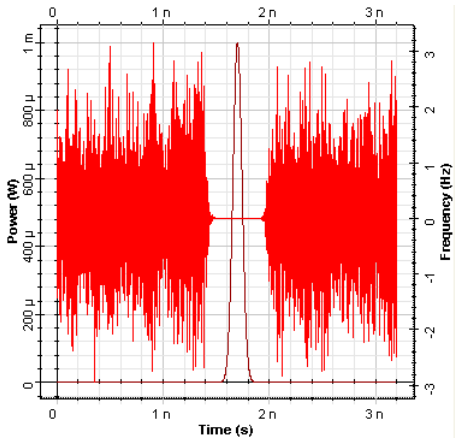
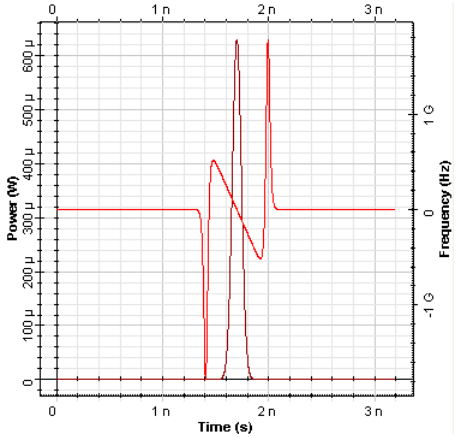


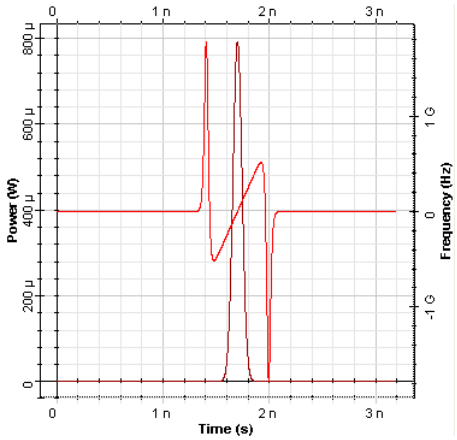
Figure 2-14: Pulse profile after propagation in 10 km of SMF



If the pulse is sent to 10 km of SMF, the pulse profile after propagation is given in Figure 2-14.Note the negative chirp appeared after the propagation.

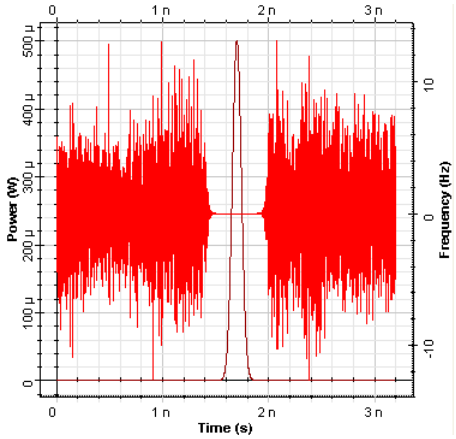
If the pulse is sent to 2 km of DCF, the pulse profile after the propagation is given in Figure 2-15, and there is a positive chirp being developed.

Figure 2-15: Pulse profile after propagation in 2 km of DCF



Note that the obtained chirp after 2 km of DCF is with opposite sign as compared to after 10 km of SMF, which would lead to complete compensation of dispersion if we put the DCF after the SMF. Simulation result for this case is given in Figure 2-16. As can be seen, after dispersion compensation, no chirp is observed and hence the complete recovery of the pulse is achieved.

Figure 2-16: Pulse profile after propagation in 10 km of SMF and 2 km of DCF



References:

[1] G.P. Agrawal, *Nonlinear Fiber optics*, third edition, Academic Press, 2001.

[2] G.P. Agrawal, *Fiber-Optic Communication Systems*, 4th ed., John Wiley & Sons, INC, 2010.

Attenuation Coefficient

Attenuation coefficient.osp

Project file "*Attenuation coefficient.osp*" shows power loss in the fiber. In this example a basic 50 km fiber link is designed. The system works in 1.3 μm window and the loss of fiber at this wavelength is 0.5 dB/km. Fiber is spliced after every 5 km and has two connectors of 1 dB loss at both ends. Splice loss is 0.2 dB. The channel loss in total is 50 x 0.5 dB + 2 x 1 dB + 9 x 0.2 dB = 28.8 dB. You can see the received signal power by double clicking on power meter after you run the simulation with 24 dBm launched power, the received power is -4.8 dBm.

The received power changes when the connector attenuation is changed. As an additional work, change the attenuation constant of the fibers and repeat your calculation with this new parameter. Check the validity of your calculation by running a new simulation with this new attenuation constant.

Notes:

Stimulated Light Scattering - Raman

Raman spectrum - With broad band source signal.osp

Raman spectrum - With two pump signals.osp

Project file "*Raman spectrum - With broad band source signal.osp*" and "*Raman spectrum - With two pump signals.osp*" shows SRS in spectral domain for two different cases. In the first case, a signal at 1450 nm (pump) is multiplexed with the broad band source signal. You can see how the spectrum of the signal from broadband source is affected. Fiber acts as a Raman amplifier such that longer wavelengths are amplified by the shorter ones. In this example, some power is transferred from the pump to other broad band spectrum components. As can be seen from the spectrum, the gain is a function of wavelength. In the second case, we have used two pump signals and swept the separation between them. You can see how the gain spectrum is changed depending on the separation of the pumps. Note also that the power of the second pump increases as its wavelength increases, because it sees more and more gain according to the gain spectrum.

Notes:

SPM and XPM

SPM.osp

XPM and GV mismatch.osp

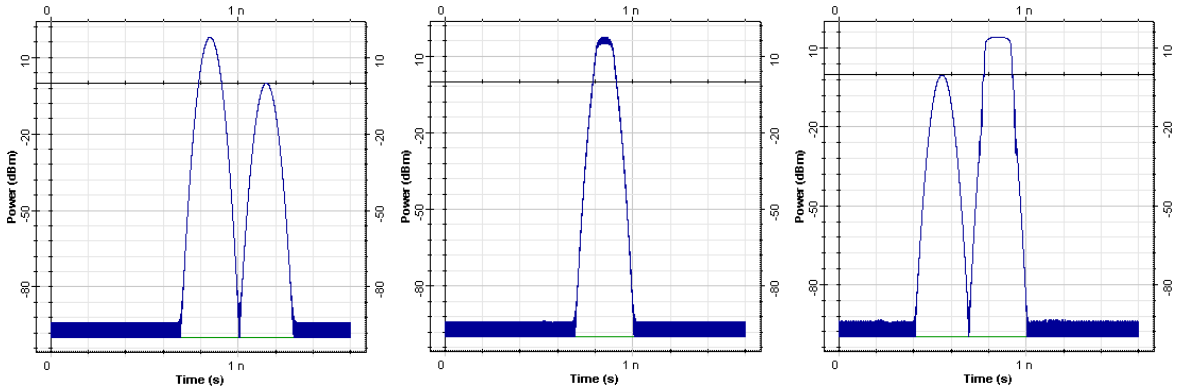
(a) Self Phase Modulation (SPM)

Project file "*SPM.osp*" shows how SPM affects the spectral shape of a Gaussian pulse. In this example, we enable only the SPM effect for our fiber model; all other effects are set to off. You can see the spectral shape of the pulse depending on its power using the OSA at the fiber end. The nonlinear phase shift depends on input pulse power and nonlinear parameter. Changing the effective area of the fiber changes the nonlinear parameter. You can re-run the simulation with different effective areas and see how the results are changed. Since dispersion effect is set to off, you will not see any change on the pulse intensity profile. In fact, nonlinear phase shifts with time, resulting in frequency chirp, which in turn affects the pulse shape through group velocity dispersion (GVD). You can see this by setting the GVD effect on and re-run the simulation. In that case, you will see that pulse goes through a contraction phase when the dispersion parameter D is positive ($\beta_2 < 0$, anomalous-GVD). With correct parameters you can even get a "soliton". As an extra work, try to see what happens when the dispersion is negative ($D < 0$, $\beta_2 > 0$).

(b) Cross Phase Modulation (XPM) and GV mismatch

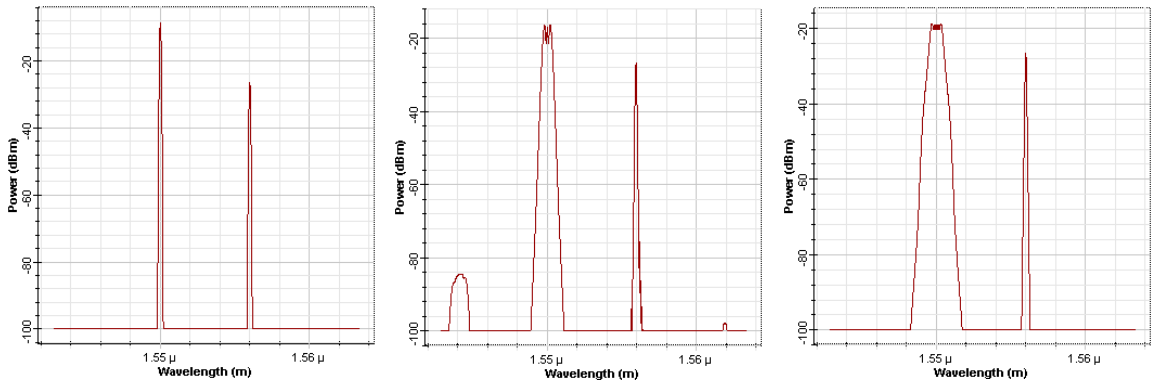
Project file "*XPM and GV mismatch.osp*" demonstrates that XPM induced distortions can be canceled out, if the dispersion is sufficiently high. As in the case of SPM, there is no pulse broadening introduced by XPM if there is no GVD to transform the spectral broadening to pulse broadening. On the other hand, walk off between the channels because of GVD also tends to lessen the impact of XPM. In this example, we consider two isolated pulses in different channels propagating in a lossless fiber, and the signal pulse will sweep across the pump pulse when propagating in the fiber. When the signal pulse is overlapped with the leading edge of the pump pulse, the signal pulse will receive a red shift due to rising intensity of the interfering pulse. As the pulses walk through each other, and trailing edge of the pump pulse is superimposed with the signal pulse, the signal pulse receives a blue shift. In fact, the net frequency shift experienced by a particular part of the signal pulse is proportional to the integral of the derivative of the intensity of the pump pulse. Therefore, when the pulses have completely walked through each other, there is no residual effect.

Figure 2-17: Pulse relative positions (a) input (b) after 12.5 km of fiber(c) after 25 km of fiber



Here we have considered two 50 ps pulses with an initial 300 ps center-to-center separation. The channels are separated by 6 nm. Dispersion of the fiber is set to -4 ps/nm-km. The signal pulse has a lower power than the pump pulse. As shown in Figure 2-17, the pulses are perfectly superimposed after 12.5 km of fiber, and are separated again after 25 km of fiber. Since power of the signal pulse is low, SPM is negligible. However, XPM should be large because the power of pump pulse is high. The spectrum of signal and pump at the input, after 12.5 km of fiber, and after 25 km of fiber are shown in Figure 2-18. You can see that the spectrum broadening of the signal due to XPM is smaller than the spectrum broadening of the pump pulse arising from SPM by looking at the spectrum at 12.5 km. Note that, pulses are completely overlapped at this distance. You can also see the new spectrum components generated by FWM. At 25 km, the pulses are separated and effects of XPM have completely vanished, while the effect of SPM on the pump pulse remains. So, this example has demonstrated that dispersion can reduce the effects of XPM.

Figure 2-18: Power spectrum (a) input (b) after 12.5 km of fiber and (c) after 25 km of fiber



Reference:

[1] *Optical Fiber Telecommunications IIIa*, ed. by I. Kaminov and T. Koch, chapter "*Fiber Nonlinearities and their Impact on Transmission Systems*" by F. Forghieri, R. Tkach and A. Chraplyvy

Four-Wave Mixing

FWM.osp

Project file "*FWM.osp*" demonstrates the FWM effect. When three optical fields with carrier frequencies f_1, f_2, and f_3 co-propagate inside the optical fiber simultaneously, nonlinear effect generate a fourth field whose frequency f_4 is related to other frequencies by a relation $f_4 = f_1 \pm f_2 \pm f_3$. In principle, several frequencies corresponding to different plus and minus signs combinations are possible. In practice, the frequency combinations of the form $f_4 = f_1 + f_2 - f_3$ are most troublesome. For an N channel system, $M = \frac{1}{2}(N^3 - N^2)$ mixing products are generated. In this example, when the 3 channels are equidistant, some of the generated fields by FWM overlap with existing channels. Therefore, you will not be able to see all the mixing products in the spectrum for this case. When the 3 channels are not equidistant, you can see all the mixing products in the spectrum. You can also see that the above given formula is satisfied and the number of generated mixing product is 9. You can change the separation between channels to see how the spectrum is affected.

Notes:

Chapter 3 - Optical Transmitters

This section contains the following examples.

- LED Spectral Distribution
- LED Modulation Response
- Light-Current Characteristics
- Direct Modulation and External Modulation
- Laser Intensity Noise

Notes:

LED Spectral Distribution

LED spectral distribution.osp

The spectral distribution of light sources affects the performance of optical communication systems through fiber dispersion. The spectral distribution is governed by the spectrum of spontaneous emission and typically follows a Gaussian shape. Figure 3-1 shows the layout for "*LED spectral distribution.osp*". It generates the output spectrum of a typical 1300 nm LED with 50 nm of spectral width (Figure 3-2 and Figure 3-3).

Figure 3-1: Layout - LED spectral distribution

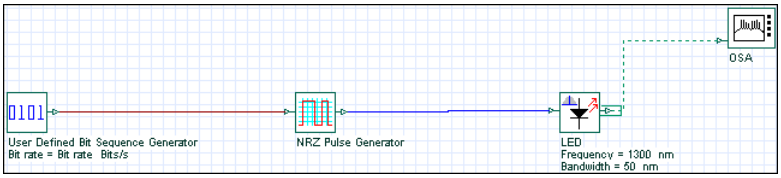


Figure 3-2: Output spectrum of LED

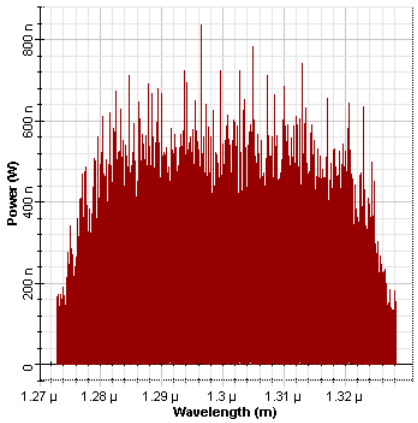
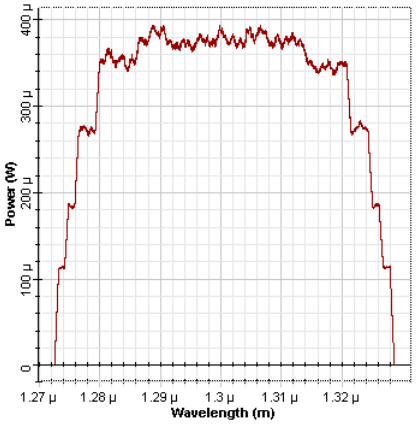


Figure 3-3: Output spectrum of LED with 1 nm resolution bandwidth

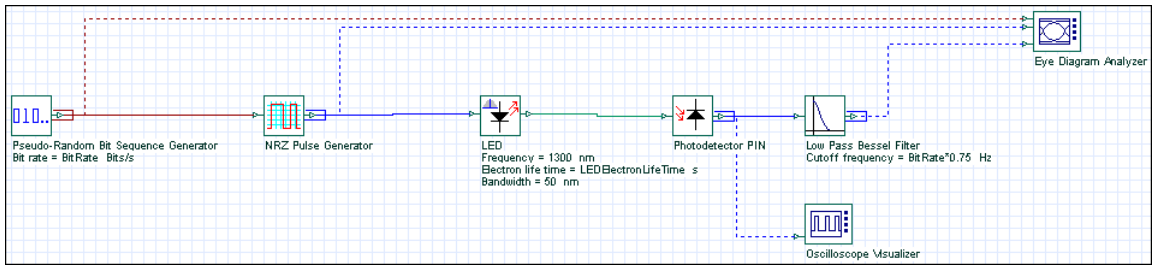


LED Modulation Response

LED modulation response.osp

The modulation response of LEDs depends on carrier dynamics and is limited by the carrier lifetime. The LED 3-dB modulation bandwidth is defined as the modulation frequency at which the LED transfer function is reduced by 3 dB or by a factor of 2. Figure 3-4 shows the layout for "*LED modulation response.osp*".

Figure 3-4: Layout - LED modulation response



The project "*LED modulation response.osp*" shows the closure of the eye diagram when the modulation bit rate increases from 100 MB/s to 400 MB/s (Figure 3-5, Figure 3-6, Figure 3-7, and Figure 3-8). This phenomenon occurs because of the LED modulation response. Reducing the carrier lifetime value will increase the LED modulation response.

Figure 3-5: LED modulation at 100 MB/s

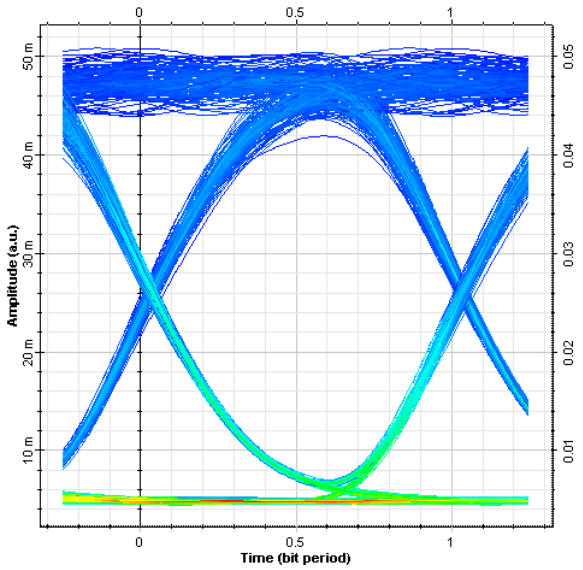


Figure 3-6: LED modulation at 200 MB/s

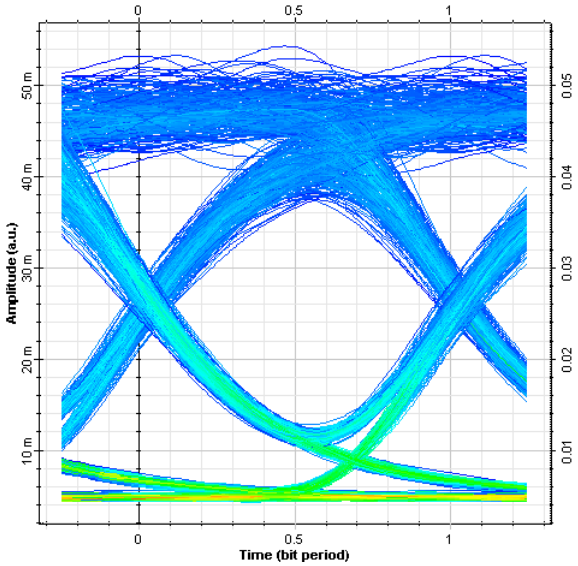


Figure 3-7: LED mdulation at 300 MB/s

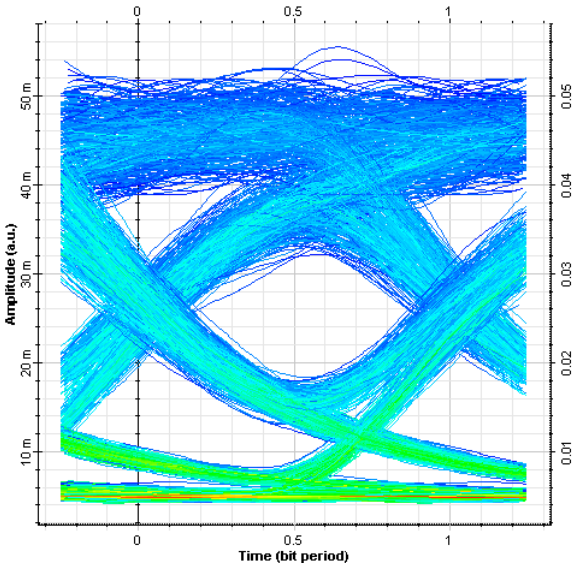


Figure 3-8: LED modulation 400 MB/s

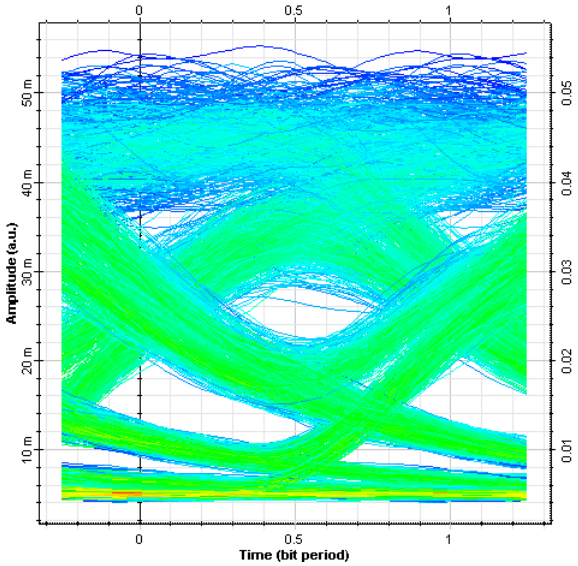
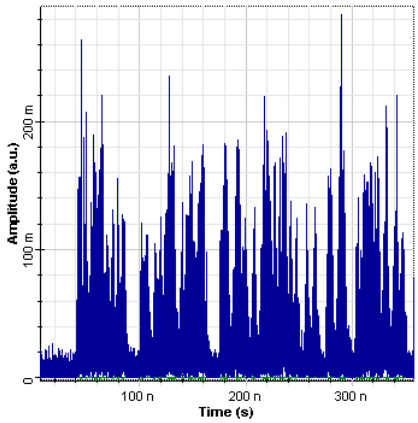


Figure 3-9 shows the electrical signal after the photodetector and before the electrical filter.

Figure 3-9: Electrical signal - LED modulation at 400 MB/s



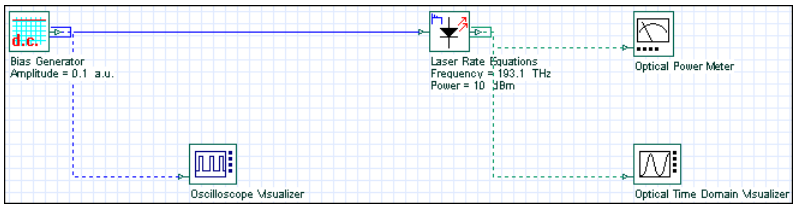
Notes:

Light-Current Characteristics

Semiconductor laser L-I curve.osp

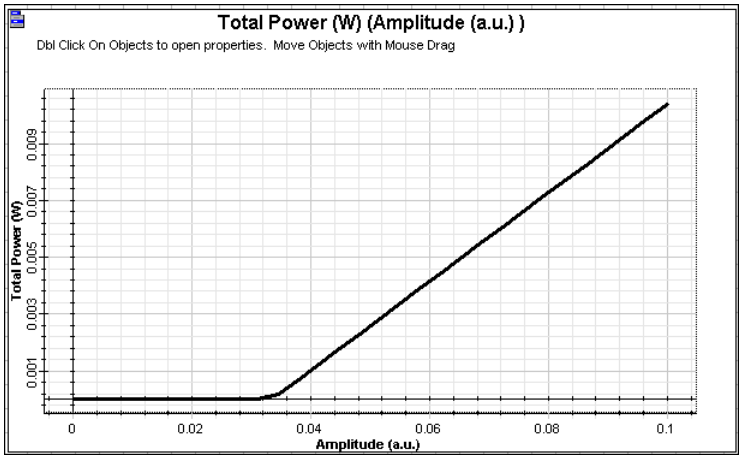
The Light-Current (L-I) curve characterizes the emission properties of a semiconductor laser, as it indicates not only the threshold level but also the current that needs to be applied to obtain a certain amount of power. Project "*Semiconductor laser L-I curve.osp*" (Figure 3-10) generates the L-I curve of a laser.

Figure 3-10: Layout - Semiconductor laser L-I curve



The L-I curve is generated after sweeping the parameter "Amplitude" of the Bias Generator component from 0.01 to 100 mA. After running the simulation, results are given in Figure 3-11 (it can also be accessed from the report page).

Figure 3-11: Laser L-I curve



Notes:

Direct Modulation and External Modulation

Semiconductor laser large signal modulation.osp

Direct modulation vs External modulation.osp

Amplitude modulation in semiconductor lasers is accompanied by phase modulation. A time-varying phase is equivalent to transient changes in the mode frequency from its steady-state value. Such a pulse is called chirped. The project "*Semiconductor laser large signal modulation.osp*" (Figure 3-12) generates the amplitude and signal chirp for a directly modulated semiconductor laser. Figure 3-13 shows the amplitude and signal chirp for the directly modulated semiconductor laser

Figure 3-12: Layout - Semiconductor laser large signal modulation

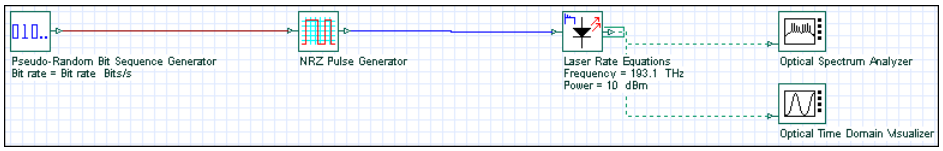


Figure 3-13: Amplitude and signal chirp for directly modulated semiconductor laser

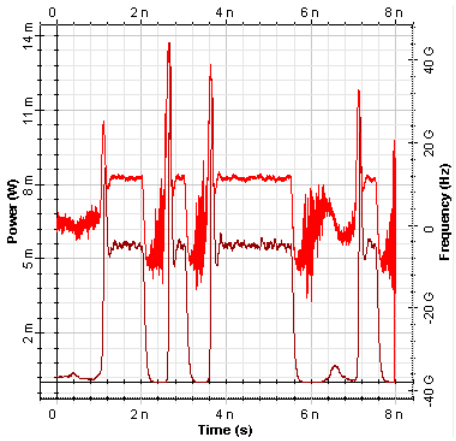
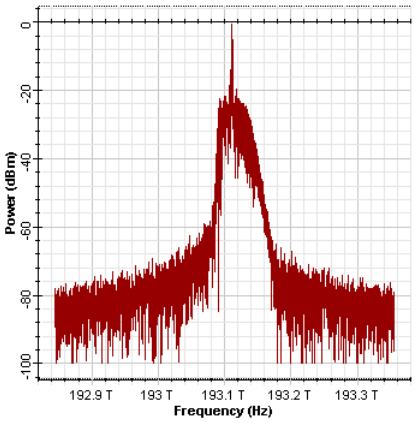


Figure 3-14: Output spectrum

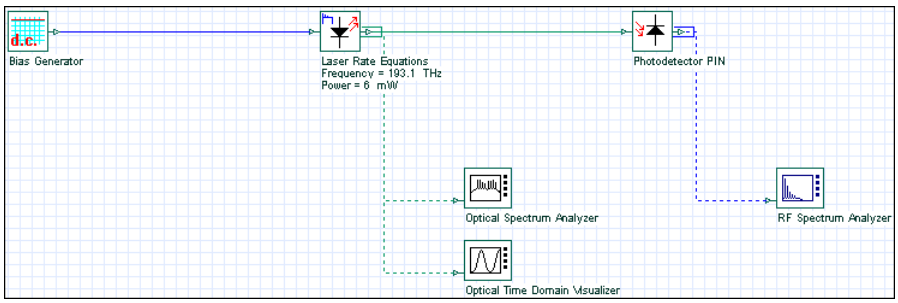


Laser Intensity Noise

Laser intensity noise.osp

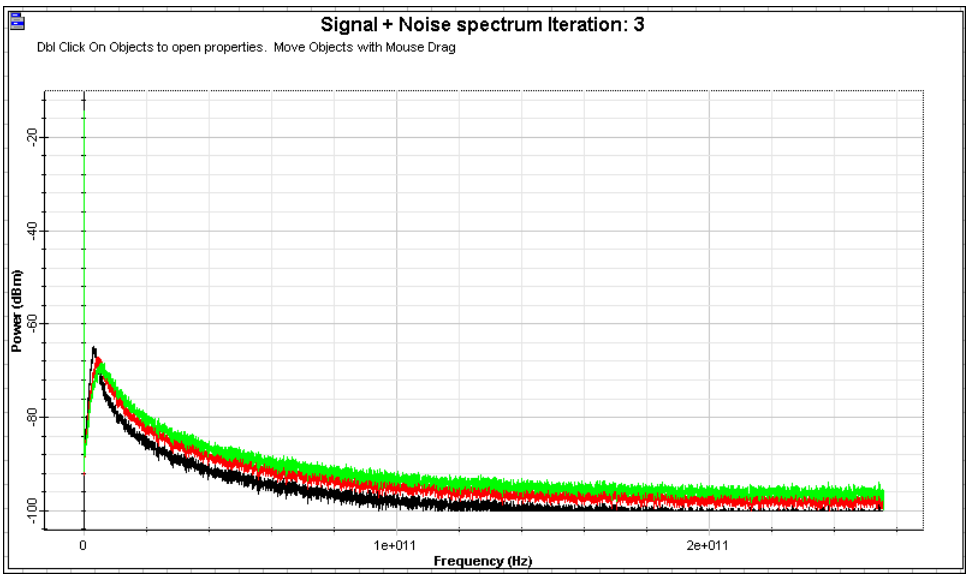
Project "*Laser intensity noise.osp*" (Figure 3-15) shows the laser spectral under CW operation at several power levels.

Figure 3-15: Layout - Laser intensity noise



The laser exhibits fluctuations in its intensity, phase and frequency even when the laser is biased at a constant current with negligible current fluctuations (Figure 3-16).

Figure 3-16: Laser intensity noise (from report page)



Notes:

Chapter 4 - Optical Receivers

This section contains the following examples.

- Receiver Design
- Receiver Shot and Thermal Noise
- Receiver PIN x APD
- Receiver BER and Q Factor
- Minimum Received Power
- ER Induced Sensitivity Degradation

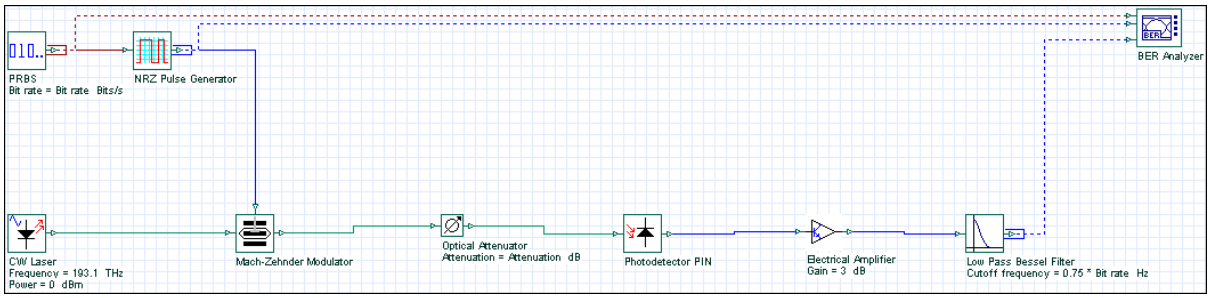
Notes:

Receiver Design

Receiver design.osp

The design of an optical receiver depends largely on the modulation format used by the transmitter. Project "*Receiver design.osp*" (Figure 4-1) shows a digital receiver design. Its components can be arranged into three groups, the front end, the linear channel and the data-recovery section.

Figure 4-1: Layout - Receiver design

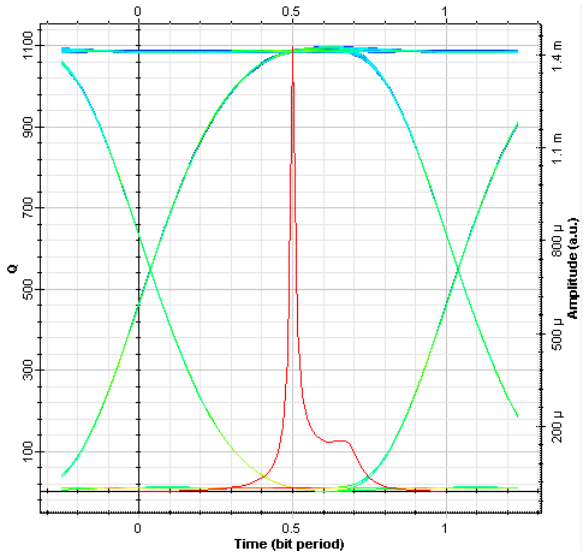


The front-end of a receiver consists of a photodiode with a built in preamplifier, the linear channel consists of a high-gain amplifier and an low-pass filter and the data recovery is done by the BER Analyzer with a built in clock recovery and decision circuit.

The linear channel has a low pass filter that shapes the pulse. The receiver noise is proportional to the receiver bandwidth and can be reduced by using a low-pass filter whose bandwidth is smaller than the bit rate. The pulse spreads beyond the time slot. Such spreading can interfere with the detection of neighboring bits, the phenomenon referred to as intersymbol interference (ISI).

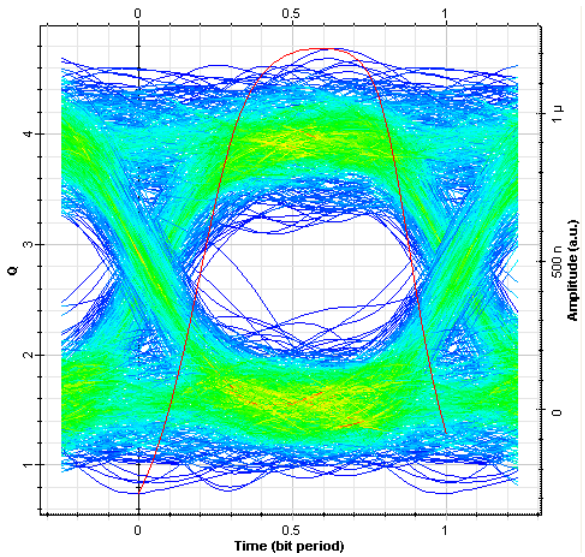
When the attenuation is 0 dB, the ideal eye diagram is shown as below: (Figure 4-2)

Figure 4-2: Received eye diagram (ideal)



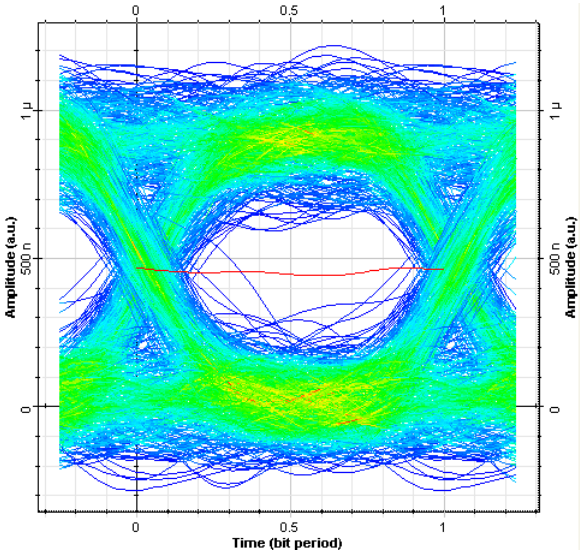
By setting the attenuation to 32 dB, you can observe the degraded eye diagram (Figure 4-3).

Figure 4-3: Received eye diagram (degraded)



The decision circuit compares the output from the linear channel to a threshold, at a decision instant determined by the clock recovery circuit, and decides whether the signal corresponds to bit 1 or bit 0. The optimum threshold level is calculated for each decision instant in order to minimize the BER (Figure 4-4).

Figure 4-4: Received eye diagram and threshold vs. decision time instant



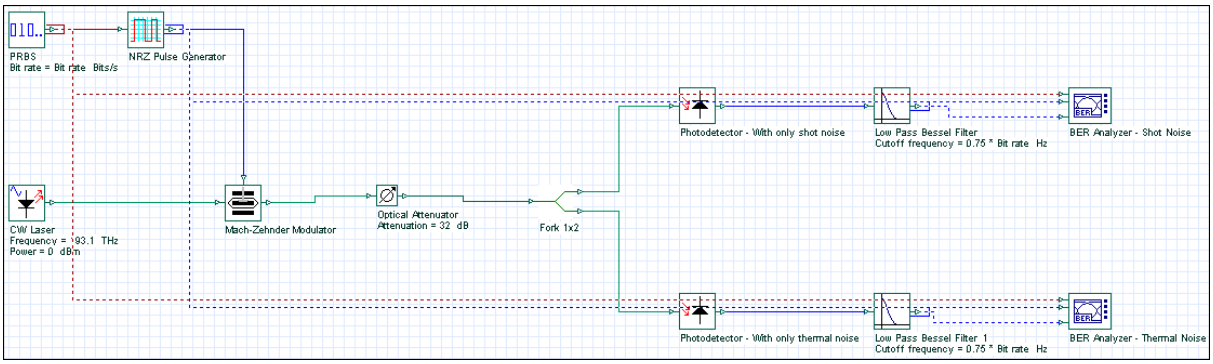
Notes:

Receiver Shot and Thermal Noise

Receiver shot and thermal noise.osp

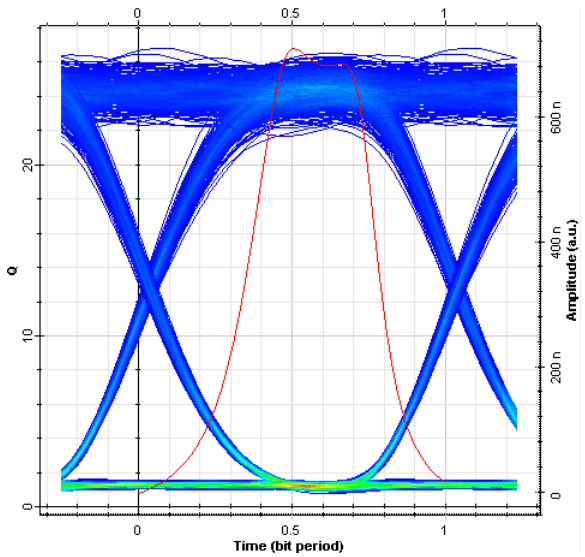
There are two fundamental noise mechanisms in a photodetector: shot noise and thermal noise. The project "*Receiver shot and thermal noise.osp*" (Figure 4-5) shows the signal degraded by thermal and shot noise in the PIN photodetector. The low-pass filter has cutoff frequency of the same value as the bit rate.

Figure 4-5: Layout - Receiver shot and thermal noise



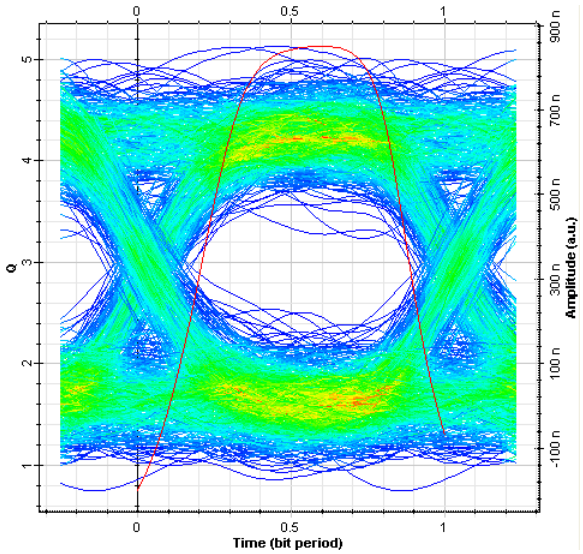
The upper system has the photodetector without thermal noise; the only noise generated at the output is the shot noise. You can observe that the shot noise is signal amplitude dependent (Figure 4-6).

Figure 4-6: Receiver shot noise



The lower system has the photodetector without shot noise; the only noise generated at the output is the thermal noise. You can observe the thermal noise is signal amplitude independent (Figure 4-7).

Figure 4-7: Receiver thermal noise

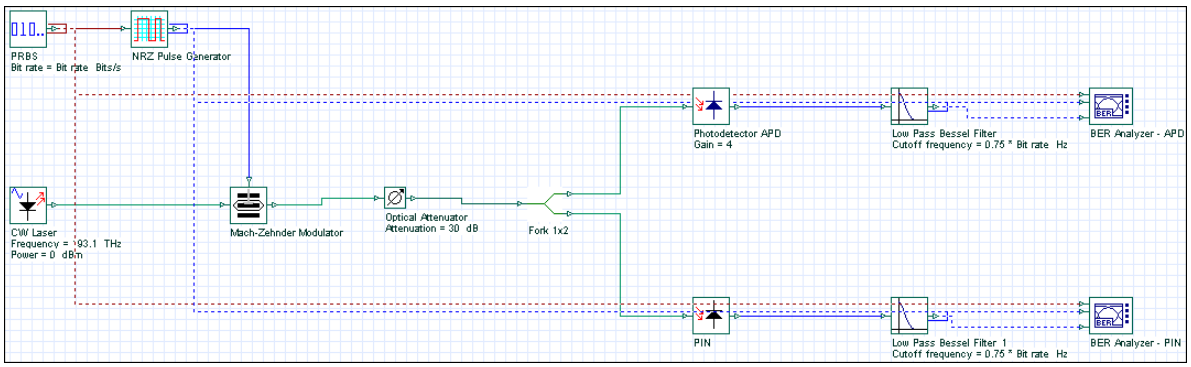


Receiver PIN x APD

Receiver PIN x APD.osp

Optical receivers with APD generally provide a higher SNR for the same incident optical power. The improvement is due to the internal gain that increases the photocurrent by the multiplication factor M. The project "*Receiver PIN x APD.osp*" (Figure 4-8) shows a comparison with two systems using PIN and APD, respectively.

Figure 4-8: Layout - Receiver PIN x APD



When the gain factor of the APD photodetector is set to 3.5, the eye diagram has a Q factor higher (Figure 4-9) than the eye diagram generated using the PIN photodetector (Figure 4-10).

Figure 4-9: Q factor - APD

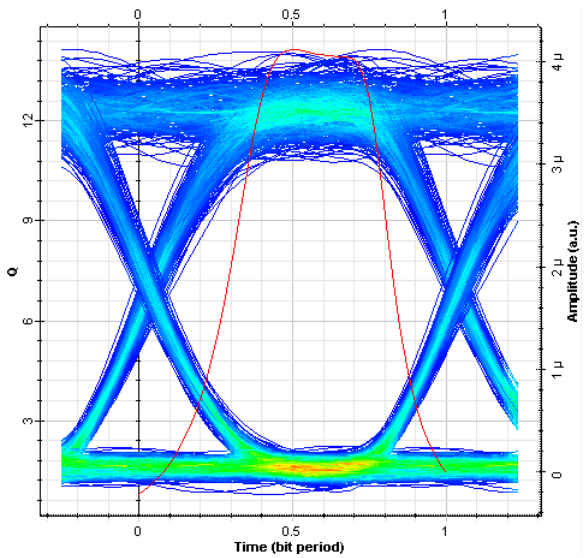
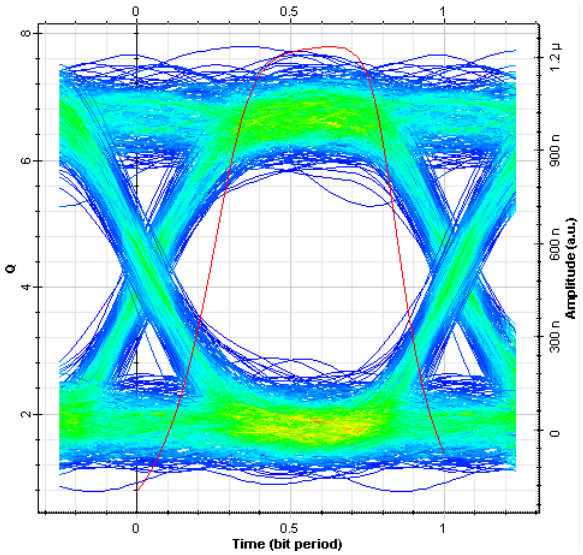
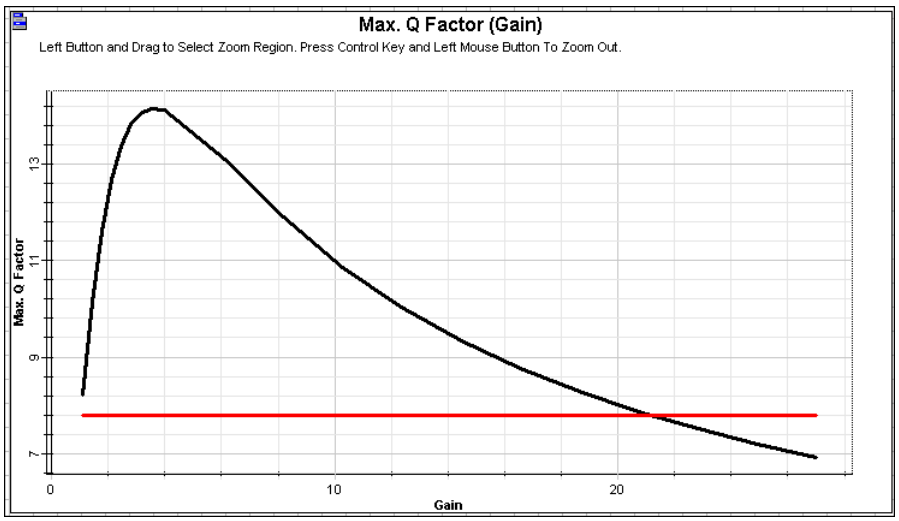


Figure 4-10: Q factor - PIN



If we increase the gain factor then there is a limit where the shot noise will degrade the system performance, therefore it's important to find the optimum APD gain. If we run the same simulation varying the value of the gain factor we can observe the evolution of the Q factor (Figure 4-11).

Figure 4-11: Q factor vs. APD gain



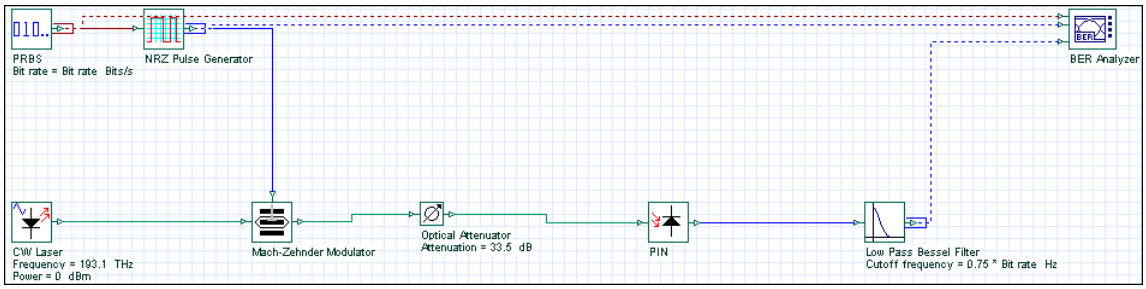
In this case, for a gain higher than 21.2, there is no advantage of using the APD (which is represented by the black line), compared to using PIN (which is represented by the red line), since it will not improve the receiver sensitivity.

Receiver BER and Q Factor

Receiver BER - Q factor.osp

The performance criteria for digital receivers, is governed by the bit-error-rate (BER), defined as the probability of incorrect identification of a bit by the decision circuit of the receiver.

Figure 4-12: Layout - Receiver BER - Q factor



The project "*Receiver BER - Q factor.osp*" generates the BER and Q factor at the data recovery stage for different values of input power. In the project, by changing the attenuator attenuation, we can calculate not only Q- Factor versus attenuation (Figure 4-13) and BER versus attenuation (Figure 4-14), but also the BER versus Q factor (Figure 4-15).

Figure 4-13: Q factor vs. attenuation

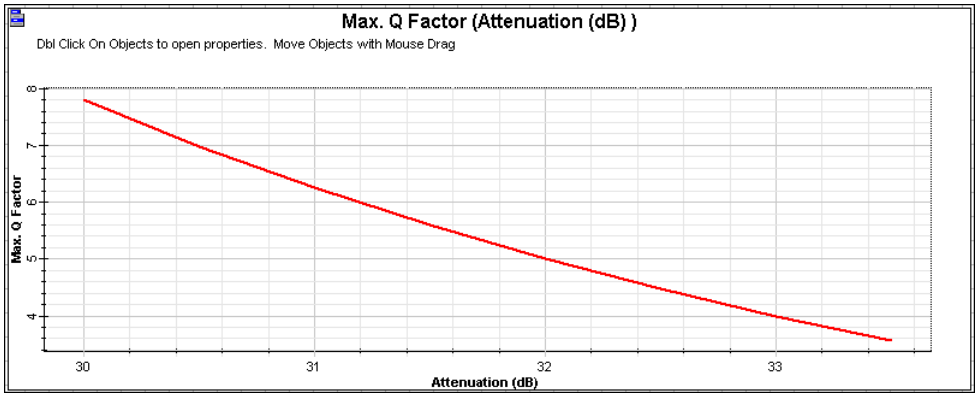


Figure 4-14: BER vs. attenuation

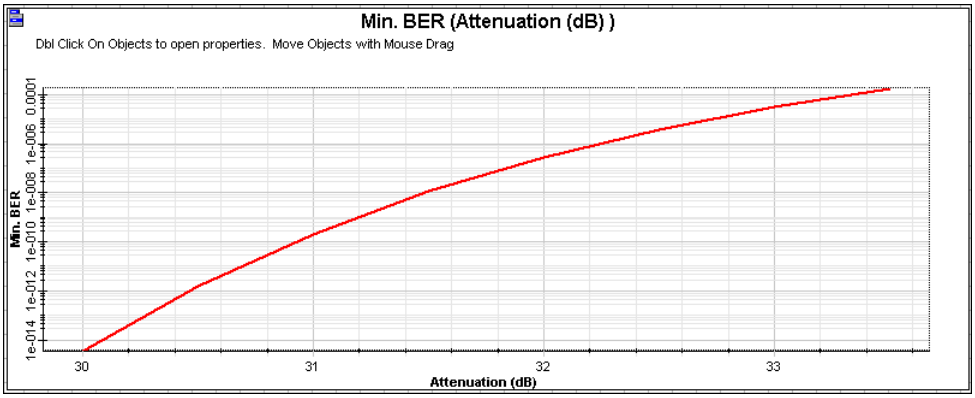
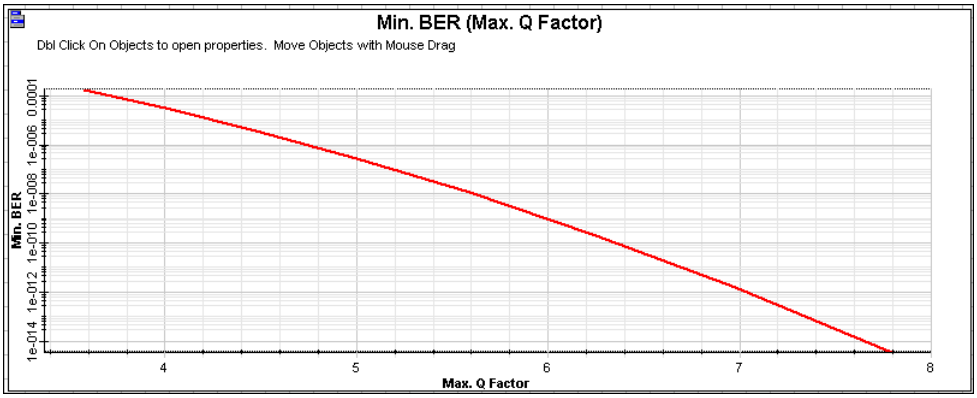


Figure 4-15: BER vs. Q factor

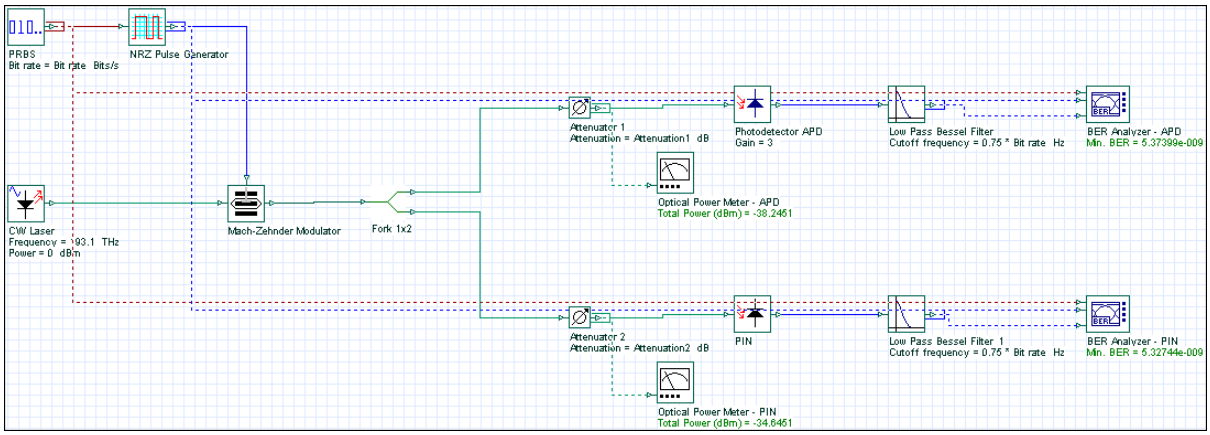


Minimum Received Power

Receiver – Minimum received power.osp

The project "*Receiver – Minimum received power.osp*" (Figure 4-16) shows the minimum optical power that a receiver needs to operate reliably with a BER below a specific value. In this example we calculate this input power by targeting a BER of 10^{-9} (which means a Q factor equals to 6) for a PIN photodetector and an APD.

Figure 4-16: Layout - Receiver - Min. received power



This example shows that the receiver sensitivity by using the PIN is -34.65 dBm (Figure 4-17). When using the APD with a gain equals to 3 the sensitivity increases to -38.25 dBm (Figure 4-18). Figure 4-19 and Figure 4-20, show the corresponding eye diagrams for the case when using PIN and APD receivers, respectively.

Figure 4-17: Optical power when using PIN

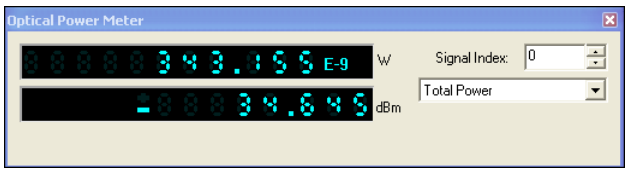


Figure 4-18: Optical power when using APD

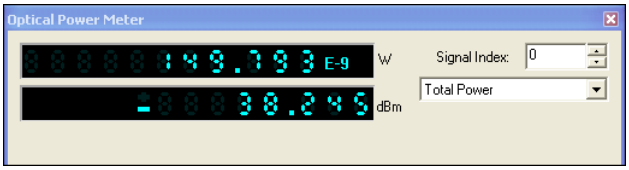


Figure 4-19: Eye diagram when using PIN

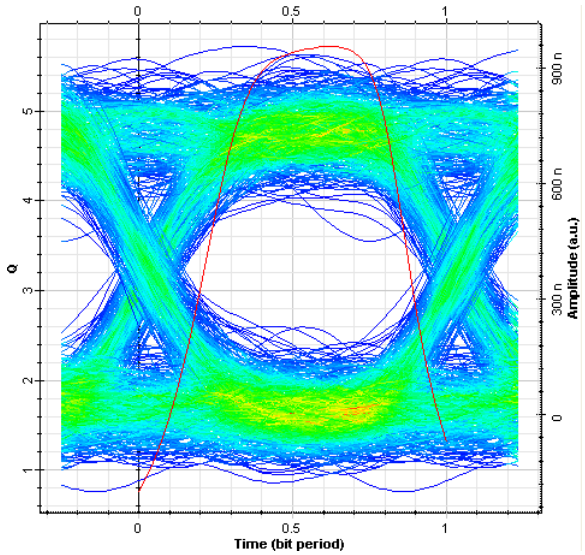
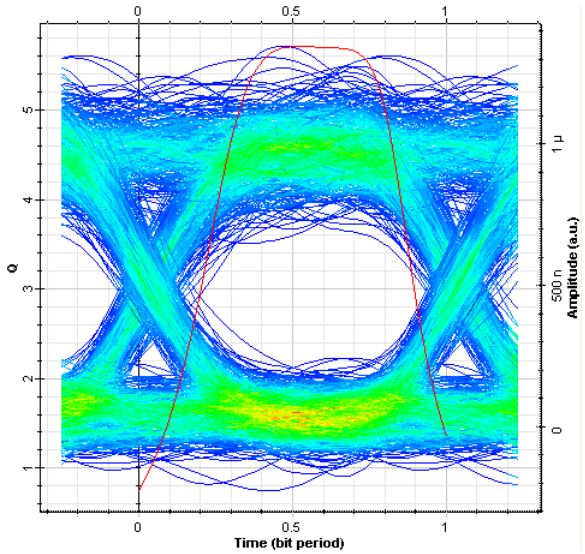


Figure 4-20: Eye diagram when using APD

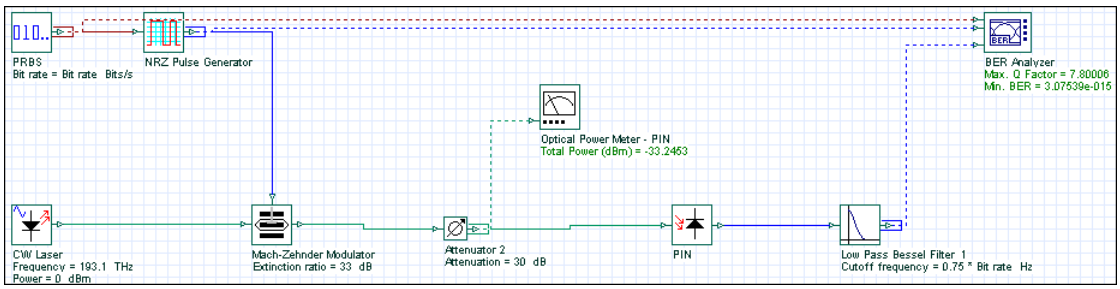


ER Induced Sensitivity Degradation

Sensitivity degradation - ER.osp

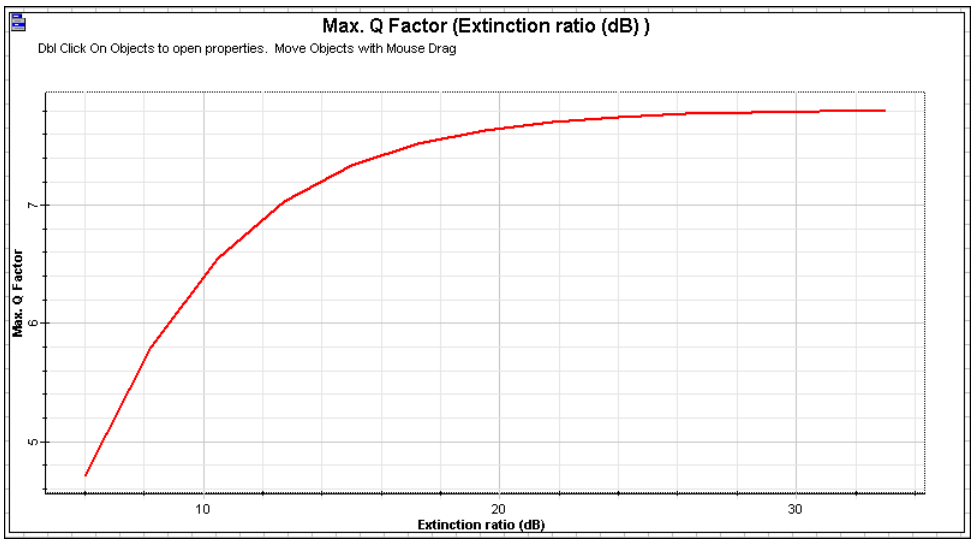
A simple source of power penalty is related to the energy carried by 0 bits. Some power is emitted by transmitters even in the off-state. In the project "*Sensitivity degradation - ER.osp*" (Figure 4-21), we have an externally modulated laser where you can specify the extinction ratio (ER) at the modulator.

Figure 4-21: Layout - Sensitivity degradation - ER



In this project we vary the value of the ER and we calculate the Q factor at the receiver. The variation of Q factor versus extinction ratio has been shown in Figure 4-22.

Figure 4-22: Q factor vs. extinctino ratio



Notes:

Chapter 5 - Lightwave Systems

This section contains the following examples.

- Power Budget
- Power Management for Ring Networks
- Dispersion Induced Degradation

Notes:

Power Budget

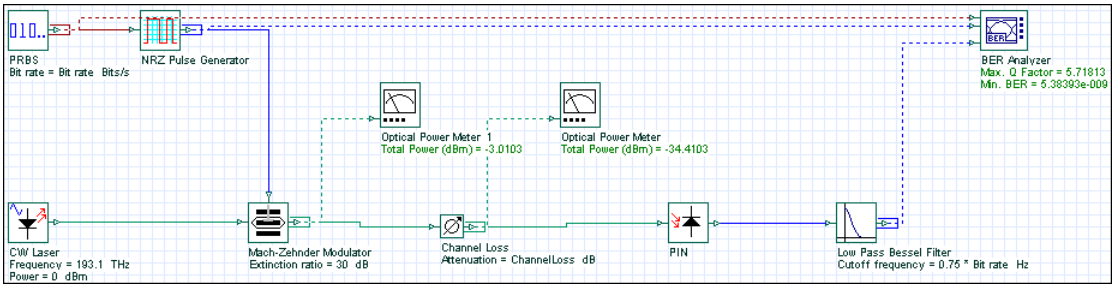
System design - Power budget.osp

The purpose of power budget is to ensure that enough power will reach the receiver to maintain a reliable performance during the entire system lifetime. The minimum average power required by the receiver is the receiver sensitivity. The average launch power is generally specified for each transmitter with optical powers expressed in dBm.

In order to estimate the maximum fiber length we should specify the output power of the transmitter and the receiver sensitivity. We can also specify a system margin. The purpose of the system margin is to allocate a certain amount of power to additional sources of power penalty that may develop during the system lifetime.

The project "*System design - Power budget.osp*" shows (Figure 5-1) a system designed using a receiver with -34.4 dBm sensitivity and an externally modulated transmitter with output power of -3.0 dBm.

Figure 5-1: Layout - System design - Power budget



Using a system margin of 0 dB the total loss allocated for the channel will be:

Channel Loss = Transmitter power - System Margin - Receiver Sensitivity

Therefore, Channel Loss = -3 + 34.4 = 31.4 dB

For a typical fiber with attenuation of 0.25 dB/km, the maximum distance the light can propagate in this system would be 125.6 km. In this case, we are not including the dispersion effect which will limit the system performance.

Notes:

Power Management for Ring Networks

Optical power level management in metro networks - No amplifier.osp

Gain variation of EDFA depending on input power.osp

Optical power level management in metro networks - Lumped amplification.osp

Optical power level management in metro networks - Unity gain.osp

Project files "*Optical power level management in metro networks - No amplifier.osp*", "*Gain variation of EDFA depending on input power.osp*", "*Optical power level management in metro networks - Lumped amplification.osp*", and "*Optical power level management in metro networks - Unity gain.osp*" consider the power budgeting for metro networks. They show alternative amplifier implementations in the network and their effect to system performance. Details of calculations are also included in this example.

Case I: No amplifier option

Optical power level management in metro networks - No amplifier.osp

In this example, our goal is to design a basic ring network without amplification and discover the power related issues.

Metro networks using ring topology are expected to have more dynamic traffic pattern compared to most long-haul networks. In addition to this, they are expected to have optically transparent nodes with minimum number of regenerators being used. Therefore, we need to consider all the optical power variations. These variations may result from the wavelength dependent loss in fibers, wavelength dependent gain in amplifiers, and channel to channel insertion loss variation in the multiplexers/demultiplexers etc. These optical degradations accumulate along the links until the optical termination. Due to dynamic nature of the network, only proper dynamic power level management can reduce them. Let us consider first the loss elements.

Optical Add/Drop Multiplexers (OADMs) introduce insertion loss. It contains two parts: deterministic and random. In fact, loss varies with the wavelength. The loss of fiber depends on fiber type and wavelength. Variation of optical switch types and different path lengths in the network will result in a random loss, which is difficult to predict.

There are several limiting factors in terms of power in the network. These are nonlinear effects, receiver sensitivity, and losses in the fiber, OADMs, OXCs etc.

Typical loss values are given in Table 5-1.

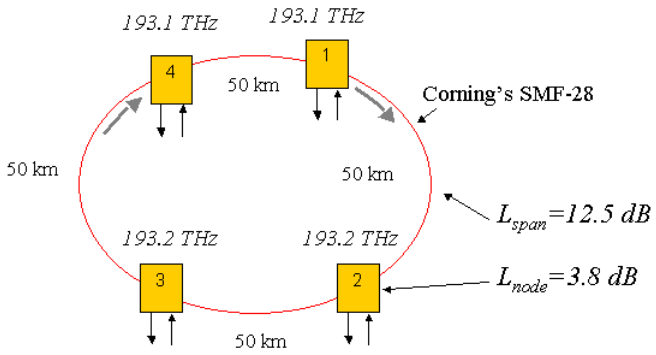
Table 5-1: Typical losses for components used in metro links

Symbol	Description	Loss value
L_{mon}	Tap loss for monitoring	0.2 dB
L_{conn}	Loss of a connector	0.25 dB
L_{splice}	Loss of a splice	0.15 dB
L_{span}	Loss of a fiber span	0.25 dB/km
L_{mux}	Loss of a multiplexer	4 dB
L_{demux}	Loss of a demultiplexer	4 dB
L_{foadm}	Loss of a fixed OADM	2 dB
L_{roadm}	Loss of a re-configurable OADM	10 dB

Total allowable loss depends on the transmitted power and receiver sensitivity. Receiver sensitivity is also a function of bit rate, and in this example, the receiver has a sensitivity of -34.4 dBm. The allowable loss is given by $L_{allowable} = P_{transmitted} - P_{sensitivity}$. Assuming two splices and six connectors total loss at each node is given by $L_{node} = 2 \times L_{splice} + 6 \times L_{conn} + L_{foadm}$.

Let us consider a typical WDM metro ring at 2.5 Gbps with 200 km in circumference with four intermediate fixed OADMs as shown in Figure 5-2. In this network, node 1 and 4 communicate on channel 1 whereas node 2 and 3 communicate on channel 2. Design project is given in "*Optical power level management in metro networks - No amplifier.osp*" file.

Figure 5-2: A basic optical ring network with four nodes and two channels



Without any inline amplification, the allowable loss by using externally modulated source is $L_{allowable} = 0 - (-34.4) = 34.4$ dB (if we assume the transmitter output power to be 0 dBm). Node (including two splices and six connectors) and span loss are $L_{node} = 2 \times 0.15 + 6 \times 0.25 + 2 = 3.8$ dB and $L_{span50km} = 50 \times 0.25 = 12.5$ dB, respectively. Therefore, the total loss will be $12.5 \times 4 + 3.8 \times 4 = 65.2$ dB.

Comparing the allowable loss and total loss in the network shows that it is not a good idea to make a design without amplification. Of course, increasing power is another option, but nonlinear effects may

become important impairments at high powers. In this case, the required transmitter output power will be 65.2 – 34.4 = 30.8 dBm/channel. Note transmitter output power means the power after the modulator; while CW laser power mentioned later on means the output power of the CW laser. Let us now discuss these nonlinear effects [1,2].

Self-Phase Modulation

The effect of SPM is to chirp the pulse and broaden its spectrum. As a rough design guideline SPM effects are negligible when $P_0 < \alpha/\gamma$ where $\gamma = (n_2\omega_0)/(cA_{eff})$ [$W^{-1}km^{-1}$] is the non-linearity coefficient, P_0 is the peak power and α is the loss parameter. For the fiber we used γ = 1.3 $W^{-1}km^{-1}$. Therefore, SPM effects can be negligible when the peak power is below 192.3 mW or 22.8 dBm.

Cross-Phase Modulation

When two or more pulses of different wavelengths propagate simultaneously inside fibers, their optical phases are affected not only by SPM but also by XPM. Fiber dispersion converts phase variations into amplitude fluctuations. XPM induced phase shift should not affect the system performance if the GVD effects are negligible. As a rough estimate, the channel power is restricted with $P_{th} < \alpha/(\gamma(2N_{ch}-1))$ where N_{ch} is the number of channels.

For a two channel system, limiting power is around 64.1 mW (18.1 dBm). Separation between channels also affects the XPM. Increase in the separation will decrease the penalty which originates from XPM.

Four-Wave Mixing

FWM is the major source of nonlinear cross-talk for WDM communication systems. It can be understood from the fact that beating between two signals generates harmonics at difference frequencies. If the channels are equally spaced new frequencies coincide with the existing channel frequencies. This may lead to nonlinear cross-talk between channels. When the channels are not equally spaced, most FWM components fall in between the channels and add to overall noise. FWM efficiency depends on signal power, channel spacing, and dispersion. If the GVD of the fiber is relatively high $|\beta_2|$ > 5 ps^2/km, FWM efficiency factor almost vanishes for a typical channel spacing of 50 GHz or more. If the channel is close to zero dispersion wavelength of the fiber, considerably high power can be transferred to FWM components. To reduce the effect of FWM to the system performance, one can use either uneven channel spacing or use dispersion-management technique.

Stimulated Raman Scattering

Because of SRS, short wavelength channels act as pump for longer wavelength channels. In a WDM system, the SRS will impair the system performance such that energy is transferred from the short-wavelength to the long-wavelength channels. The Raman threshold for a single channel system is given by Eq. 5-4:

$$P_{th} \approx \frac{16A_{eff}}{g_R L_{eff}} \qquad \textbf{(5-4)}$$

where

$$L_{eff} = \frac{1 - e^{-\alpha L}}{\alpha} \quad \textbf{(5-5)}$$

and it is approximately equal to $1/\alpha$ for long fibers. In fact, the Raman threshold is a function of the number of the channels and channel power. For a single channel system it is around 500 mW near 1.55 μm if g_R = 1 x 10^{-13} m/W. For a 20 channel system P_{th} exceeds 10 mW whereas it is around 1 mW for a 70 channel system. For a single channel system, the SRS has little impact on system performance.

Stimulated Brillouin Scattering

It results from the interaction of light with acoustic wave in fiber and scatters power backward. Back scattered light is downshifted in frequency from the original signal frequency. Threshold level depends on effective core area and effective fiber length and is given below:

$$P_{th} \approx \frac{21 A_{eff}}{g_B L_{eff}} \quad \textbf{(5-6)}$$

Typical value for g_B is around 5 x 10^{-11} m/W.The threshold value also depends on modulation format, source linewidth and duration of pulse. Some values for threshold power are given as below:

(1) 9 dBm for CW light

(2) 12 dBm for externally modulated transmitter

(3) >18 dBm for externally modulated transmitter with source wavelength dither.

Generally speaking, SBS has little effect on system performance.

Figure 5-3 shows the Q factor for channel 1 at the receiver end versus the launched CW laser power, when no amplifier is used. This figure shows that after about 20 dBm of launched CW laser power (as predicted) nonlinearity becomes an issue and Q factor starts to decay.

Figure 5-3: Q factor versus launched CW laser power at node 4 when no amplifier is used

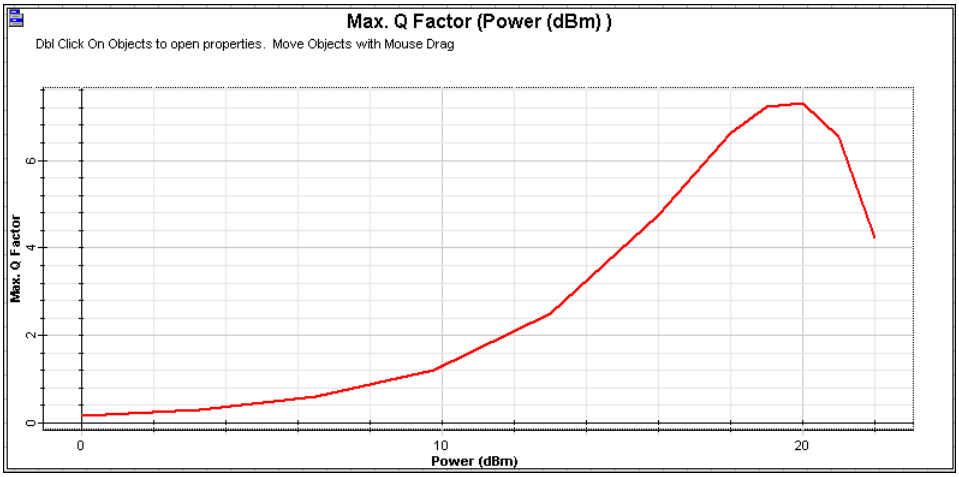


Figure 5-4 shows OSNR at the receiver with respect to launched CW laser power. Figure 5-5, Figure 5-6, and Figure 5-7 show the eye diagram for the launched CW laser power of 13 dBm/channel, 20 dBm/channel, and 22 dBm/channel; respectively. From these figures we can conclude that, limiting factor below 20 dBm region is mainly OSNR whereas above this value, it is nonlinearity. This example shows that non-linearity may become an issue in no- amplifier ring networks.

Figure 5-4: OSNR versus launched CW laser power at node 4 when no amplifier is used

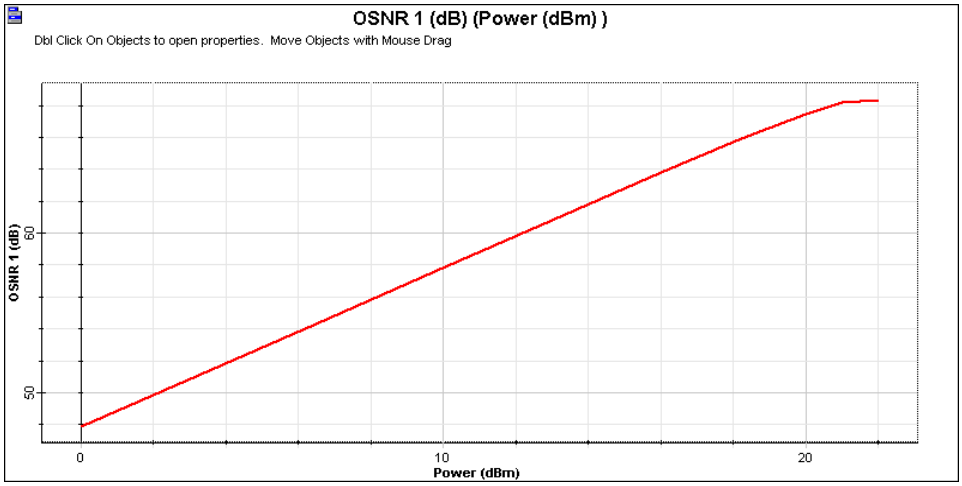


Figure 5-5: Eye diagram at the receiver when the launched CW laser power is 13 dBm

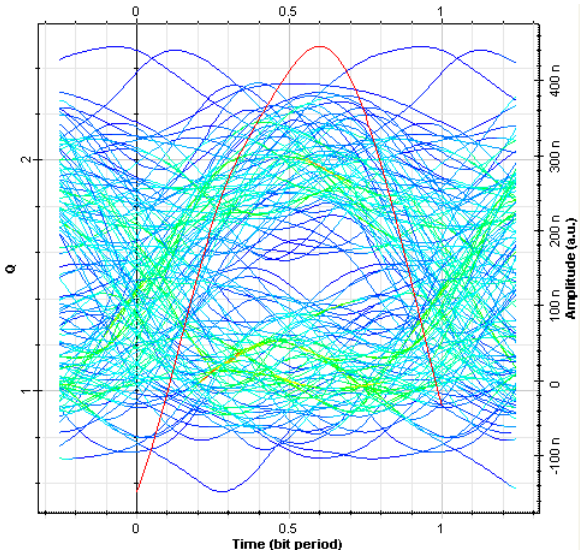


Figure 5-6: Eye diagram at the receiver when the launched CW laser power is 20 dBm

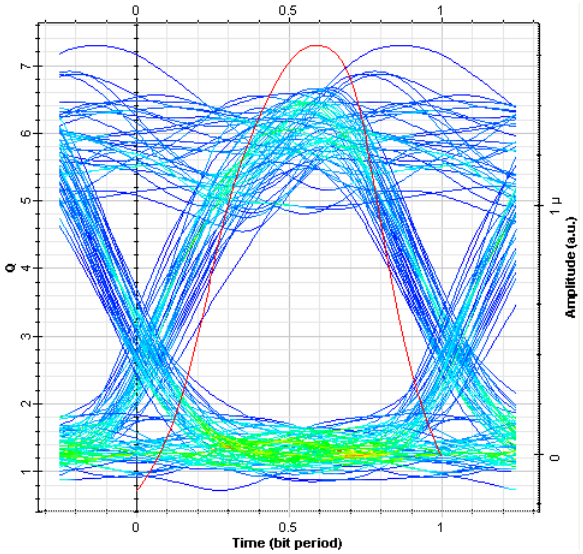
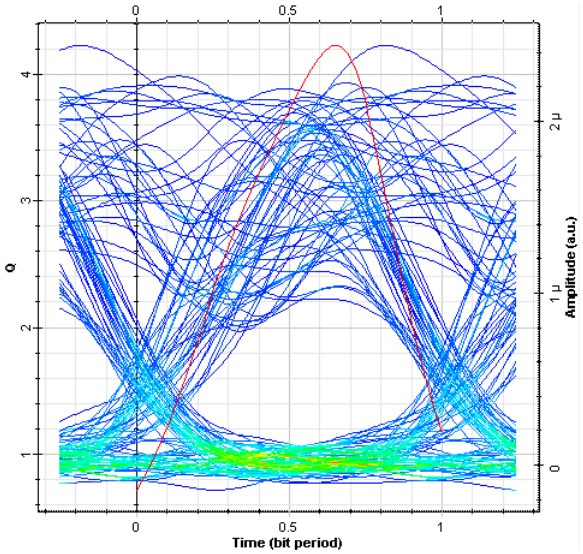


Figure 5-7: Eye diagram at the receiver when the launched CW laser power is 22 dBm



Case II: Lumped amplification

Gain variation of EDFA depending on input power.osp

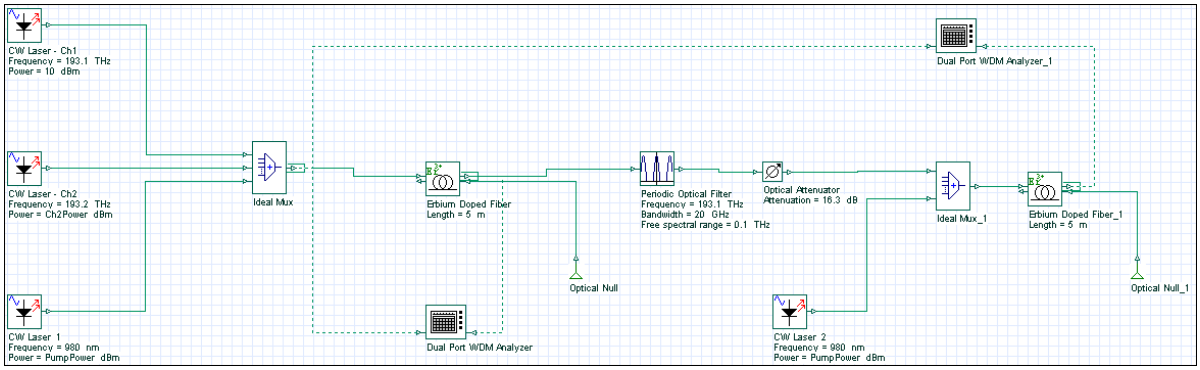
Optical power level management in metro networks - Lumped amplification.osp

Metro ring networks have more dynamic traffic pattern compared to most long-haul networks. In this configuration we need to consider all the optical power variations resulting from the wavelength dependent loss in the fiber, wavelength dependent gain in the amplifiers, channel to channel insertion loss variation in the multiplexers/demultiplexers, etc. These optical degradations accumulate along the links and may grow very fast depending on the path followed by the wavelength. Due to dynamic nature of the network, only proper dynamic power level management can reduce them. Typical values for the loss elements are given in the Table 5-1.

In this example we consider compensation of the loss in fibers and ADMs using amplifiers. To do so, let's first investigate the amplifier gain characteristics.

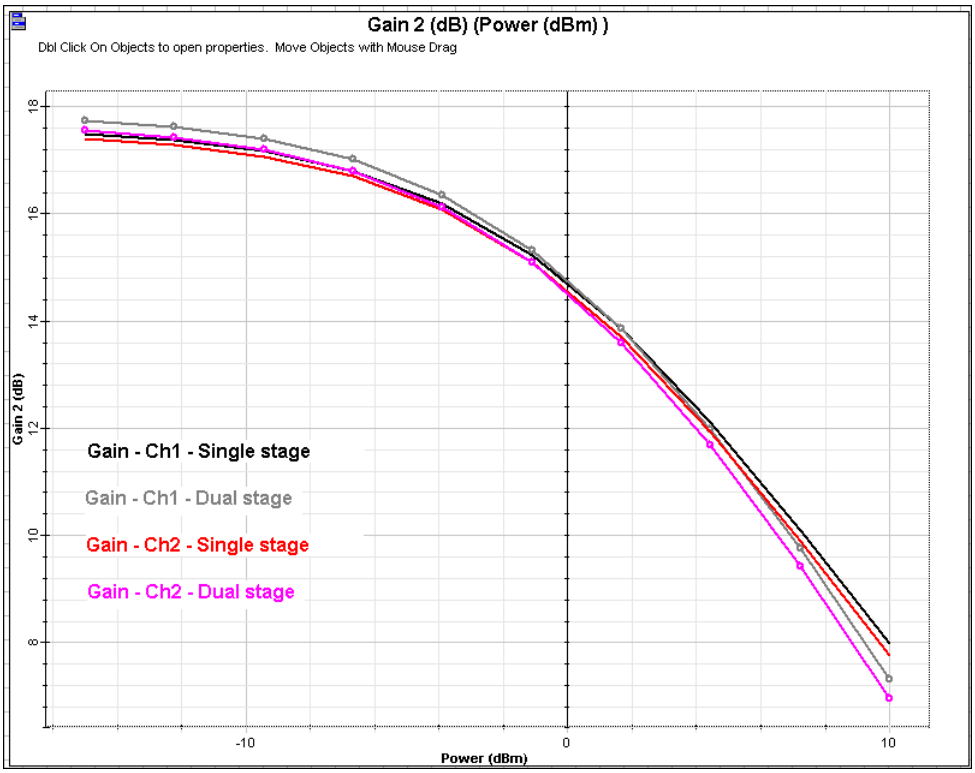
The gain of the optical amplifier changes with the input power. This is shown below (Figure 5-8) for two cascaded EDFA amplifiers (each with a fiber length of 5 m, and pump power at 980 nm is 15 dBm), we consider a 16.3 dB loss between the amplifiers to model the total span and node loss. Two channels (one @ 193.1 THz of which the power is swept from -15 dBm to 10 dBm, another one @ 193.2 THz with a constant power of 0 dBm) are used as the input signals. The gain of each channel versus the power of channel 1 signal is shown in Figure 5-9.

Figure 5-8: Layout - Gain variation of EDFA depending on input power



The project file is "*Gain variation of EDFA depending on input power.osp*". When the span losses of different spans in the ring are different, the input power of different amplifier will be different. Therefore, depending on the path of the signal, each communication link between two nodes will experience different amplification. Besides, the optical gain of an amplifier is also wavelength dependent. To eliminate these effects, pump control, variable attenuator at the input or gain tilt compensating amplifier/filter can be used.

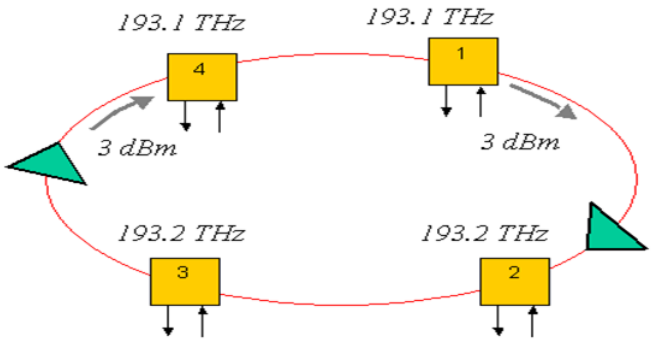
Figure 5-9: Value and shape of optical gain depending on input power



Let us now consider a typical WDM metro ring at 2.5 Gbps with 200 km in circumference with four intermediate fixed OADMs as shown in Figure 5-10. In this network, node 1 and 4 communicate on

channel 1 whereas node 2 and 3 communicate on channel 2. Design project is given in "*Optical power level management in metro networks - Lumped amplification.osp"* file.

Figure 5-10: Ring network layout with two amplifiers



Assuming a transmitter output power of -3 dBm (approximately a launched CW laser power of 0 dBm) and receiver sensitivity of -34.4 dBm, the amount of amplification needed in the ring is:

$G_{required}$ = -34.4 + 3 x 0.25 x 50 + 3 x 3.8 – (-3) = 17.5 dB

This gain can be obtained by using two EDFAs each with a gain of 9 dB as shown in Figure 5-10. In this configuration, two amplifiers are placed just before node 2 and node 4. However, this implementation of lumped amplification prevents the flexibility of adding new nodes into the ring [2,3].

Measured signal power and OSNR at the receiver is given below (Figure 5-11) when two 9 dB amplifiers are used. Figure 5-12 shows the eye diagram for this case, and the Q factor is 5.7.

Figure 5-11: Measured signal power and OSNR at the receiver

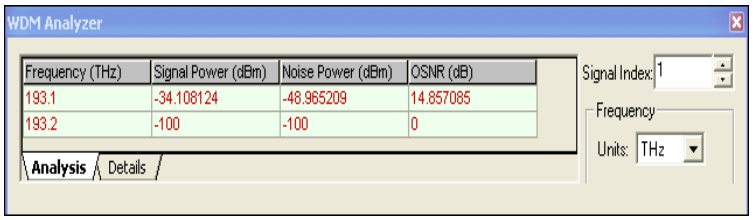
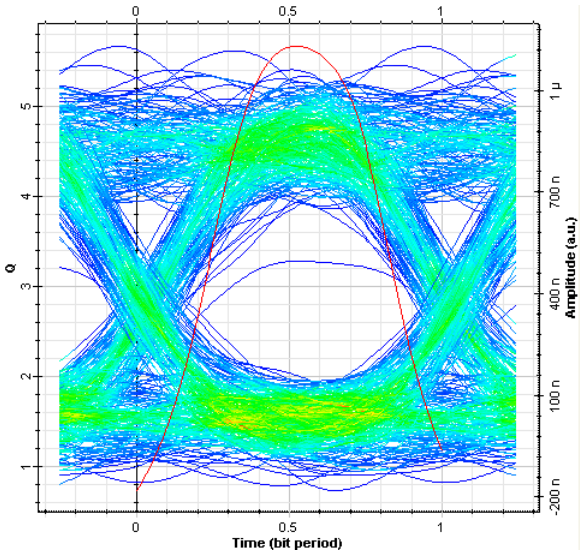


Figure 5-12: Eye diagram at node 4 when two amplifiers with 9 dB gain each are inserted before node 4 and node 2



Even though this configuration will do the job for a static configuration, it will not allow the addition of new node or complex wavelength routing schemes where one signal may follow different paths depending on the routing.

Case III: Unity gain approach

Optical power level management in metro networks_Unity gain.osp

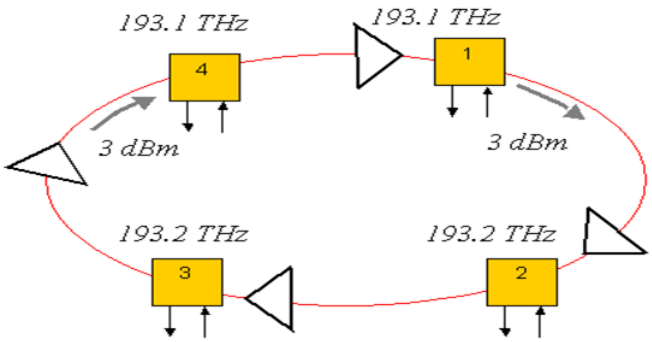
In optical ring topology, we need to consider all the optical power variations resulting from the wavelength dependent loss in fiber, wavelength dependent gain in amplifiers, and channel to channel insertion loss variation in multiplexers/demultiplexers etc. These optical degradations accumulate along the links and may grow very fast depending on the path followed by the wavelength. Due to dynamic nature of the network, only proper dynamic power level management can reduce them. Typical values for the loss elements are given in Table 5-1. We have also discussed the characteristics of optical amplifiers and placement of amplifiers at certain points in network in Case II. In the two cases discussed above we have seen that no amplifier is not a good choice for loss compensation since required high power may trigger fiber nonlinearity. Even though lumped loss compensation seems to do the job in terms of good eye diagram, it is not the best considering the dynamic nature of metropolitan networks.

In this example we will show an alternative approach, so called unity gain approach. In this approach, each amplifier matches the loss of one node and span. The loss that need to be compensated will be the node (L_{node} = 2 x 0.15 + 6 x 0.25 + 2 = 3.8 dB) and span ($L_{sapn50km}$ = 50 x 0.25 = 12.5 dB) loss preceding it. For this approach, an amplifier with modest gain of 16.3 dB at each node can be used. This approach is only economically feasible with a low cost-compact optical amplifier yet the best one considering dynamic routing in the network.

Let us now consider a typical WDM metro ring at 2.5 Gbps with 200 km in circumference with four intermediate fixed OADMs as shown in Figure 5-13. In this network node 1 and 4 communicate on channel 1 whereas node 2 and 3 communicate on channel 2. Loss of each span and node is compensated at the node following the span. Gain of each amplifier is 16.3 dB. Design project is given

in "*Optical power level management in metro networks - Unity gain.osp"* file. This configuration is scalable. Moreover, regardless of path followed by a certain wavelength, the power is always balanced [1-4].

Figure 5-13: Ring network layout with amplifier at each node



Eye diagrams of channel 1 at node 4 are shown in Figure 5-14, when CW laser power is 0.6 dBm. Figure 5-15, on the other hand, shows the eye diagram at node 4 when the CW laser power is -26 dBm. Figure 5-16 shows the Q factor versus the power of the CW laser.

Figure 5-14: Eye diagram of channel 1 at node 4 when CW laser power is 0.6 dBm and bit rate is 2.5 Gbps

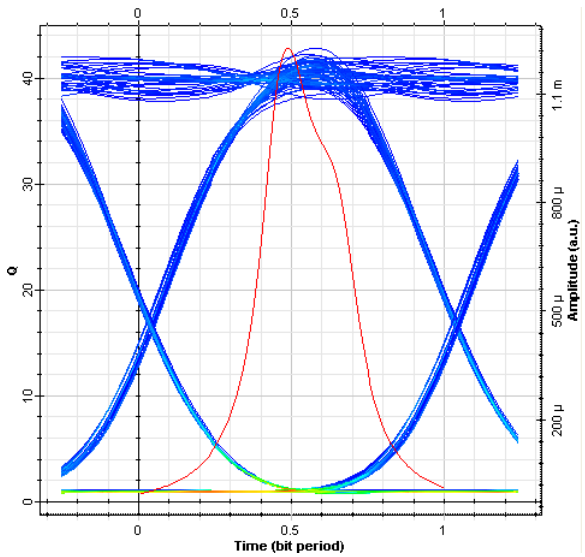


Figure 5-15: Eye diagram of channel 1 at node 4 when CW laser power is -26 dBm and bit rate is 2.5 Gbps

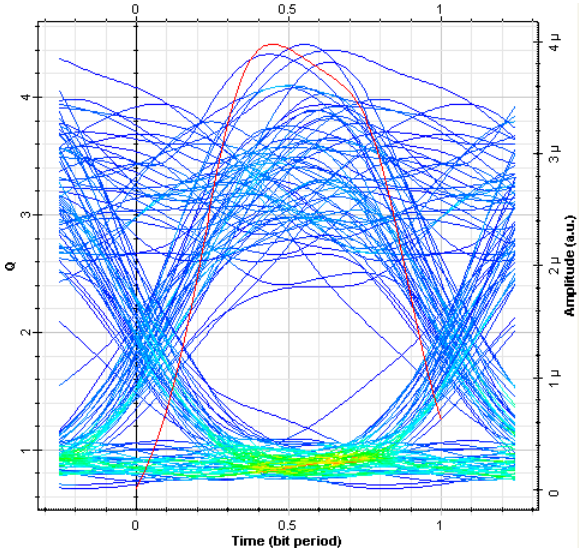
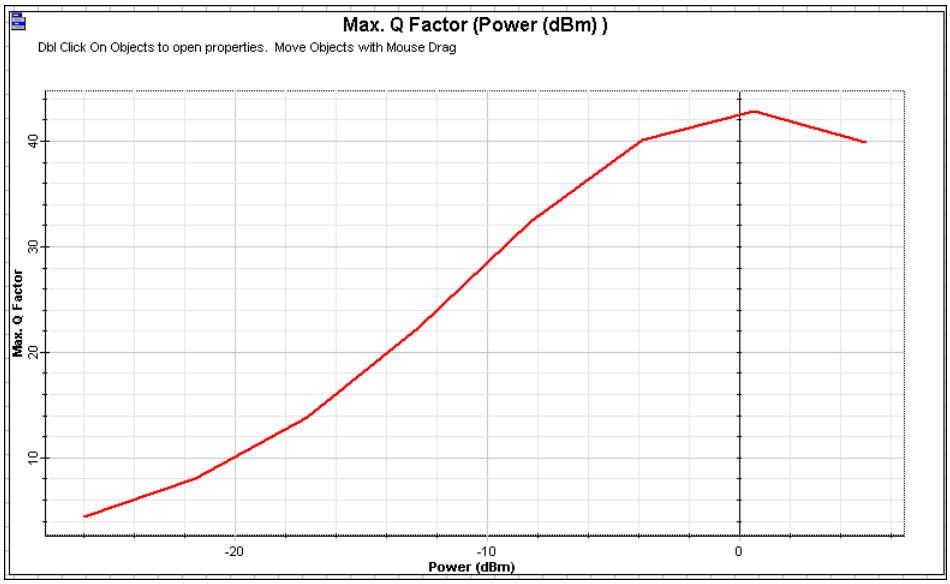


Figure 5-16: Q factor versus CW laser power at node 4 when bit rate is 2.5 Gbps



References:

[1] S. Bigo et. al., “Investigation of cross-phase modulation limitation over various types of fiber infrastructures”, IEEE Photon. Tech. Lett. 11, pp. 605, 1999.

[2] T.S. El-Bawab et. al., “Design considerations for transmission systems in optical metropolitan networks”, Opt. Fib. Tech. 63, pp. 213, 2000

[3] R. Ramaswami and K.N. Sivarajan, *Optical Networks: A Pactical Perspective*, Morgan Kaufmann, 1998.

[4] S. Shiba et. al., “Optical power level management in metro networks”, NFOEC’01, 2001.



Notes:

Dispersion Induced Degradation

Dispersion vs power.osp

Project file "*Dispersion vs power.osp*" shows that the dispersion broadening penalty of the system using un-chirped NRZ input pulses is lower when the dispersion is positive. In this example, a 10 Gb/s NRZ signal is transmitted through two nominally identical 150 km of fibers with opposite signs of dispersion. For the first case, fiber has –2.27 ps/nm-km dispersion and for the second case it is +2.27 ps/nm-km. Power of the CW laser is swept from 2 dBm to 20 dBm for these two cases. This simulation shows that system penalty when a negative dispersion fiber is used is larger than when a positive dispersion fiber is used. The penalty in the negative dispersion fiber arises from the pulse broadening due to SPM. However, in the case of positive dispersion, nonlinear pulse compression interacts with dispersion, resulting in negative power penalties. Up to about 18.3 dBm of input power, the Q factor increases with the input power when the dispersion is positive (Figure 5-17).

Figure 5-17: Q factor versus input power for negative and positive dispersion fibers

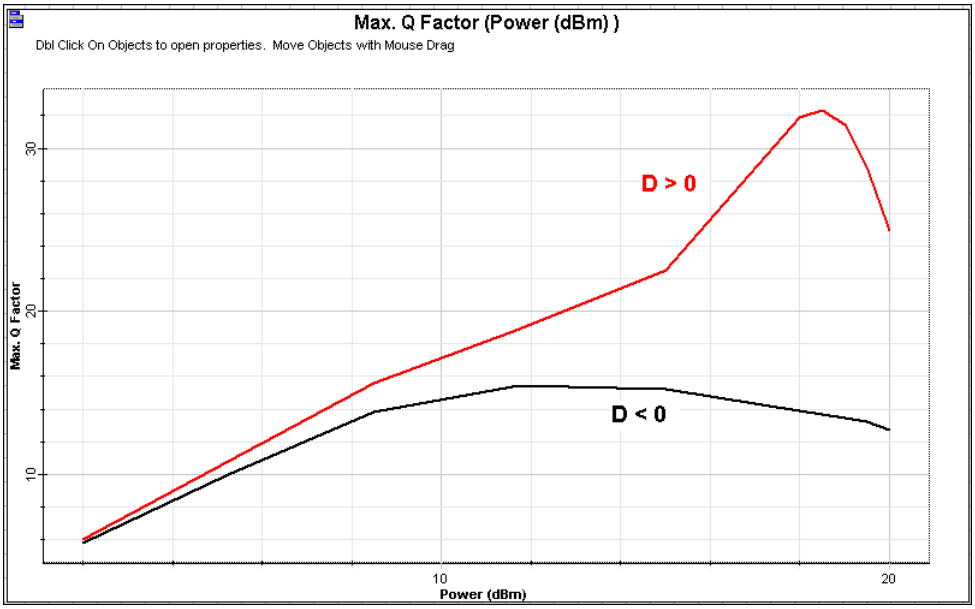
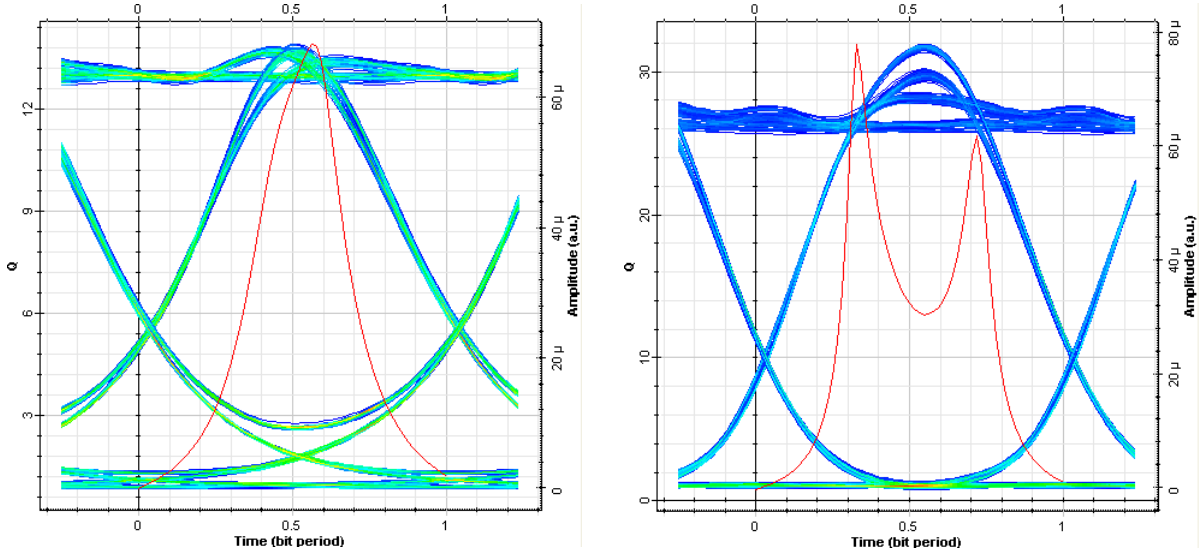


Figure 5-18 compares negative and positive dispersion cases when the input power is 18 dBm.

Figure 5-18: Eye diagrams (a)after 150 km of negative dispersion fiber (b) after 150 km of positive dispersion fiber



Reference:

[1] *Optical Fiber Telecommunications IIIa*, Eds: I. Kaminov and T. Koch, chapter “Fiber Nonlinearities and their Impact on Transmission Systems” by F. Forghieri, R. Tkach and A. Chraplyvy.

Chapter 6 - Multichannel Systems

This section contains the following examples.

- Fabry-Perot Filter
- Uniform FBG Filter
- AWG Demultiplexer
- Star Coupler
- Optical Cross-Connects
- Channel Multiplexing
- Channel Demultiplexing by FWM
- Interchannel Crosstalk at ADM in A Ring Network
- Subcarrier Multiplexing

Notes:

Fabry-Perot Filter

Fabry-Perot filter.osp

The project "*Fabry-Perot filter.osp*" (Figure 6-1) shows the transmission response of a Fabry- Perot filter used as a tunable optical filter. The frequency spacing between two successive transmission peaks is known as free spectral range (Figure 6-2).

Figure 6-1: Layout - Fabry-Perot filter

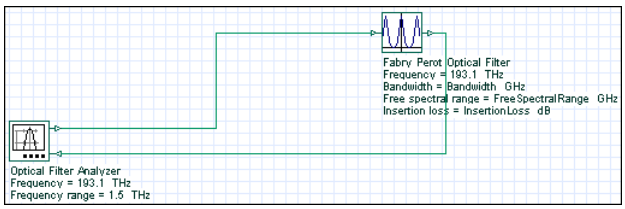
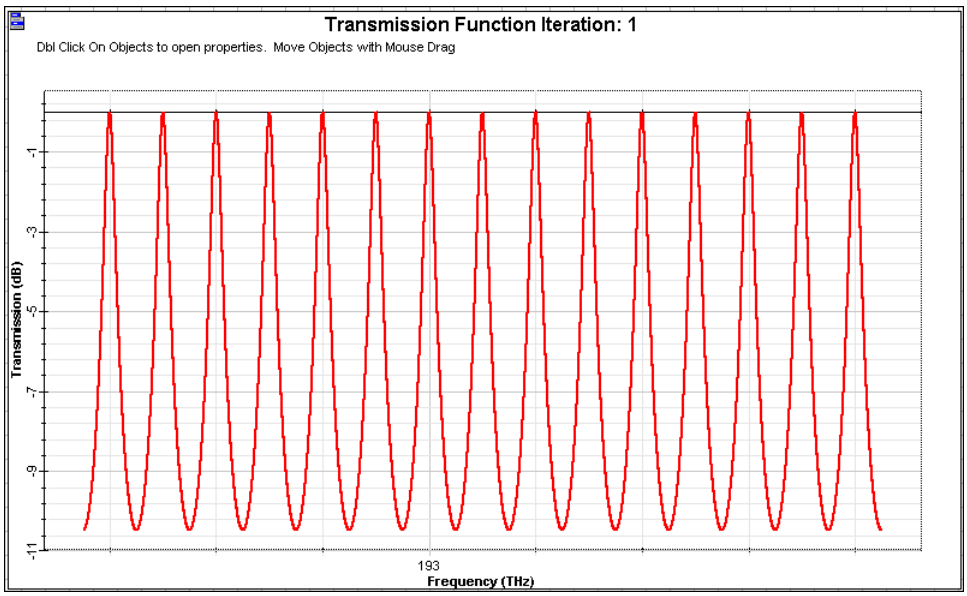


Figure 6-2: Fabry-Perot filter transmission response



Notes:

Uniform FBG Filter

FBG filter transmission.osp

A separate class of optical filters makes use of the wavelength selectivity provided by a Bragg grating. The project "*FBG filter transmission.osp*" (Figure 6-3) shows the transmission response of a uniform FBG filter (Figure 6-4).

Figure 6-3: Layout - FGB filter transmission

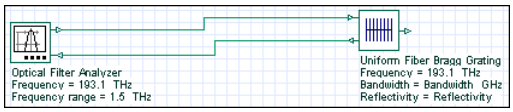
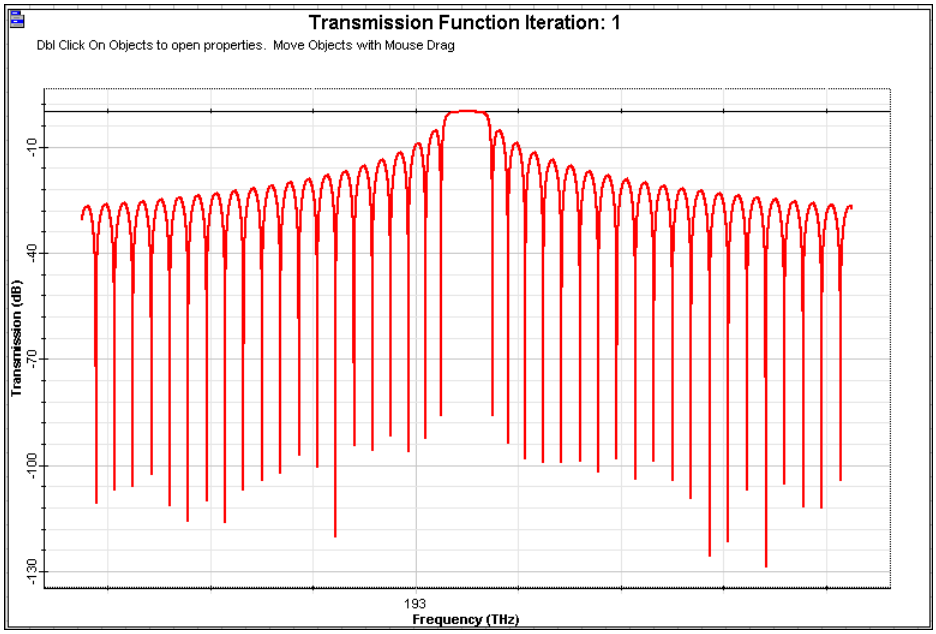


Figure 6-4: FBG filter transmission response



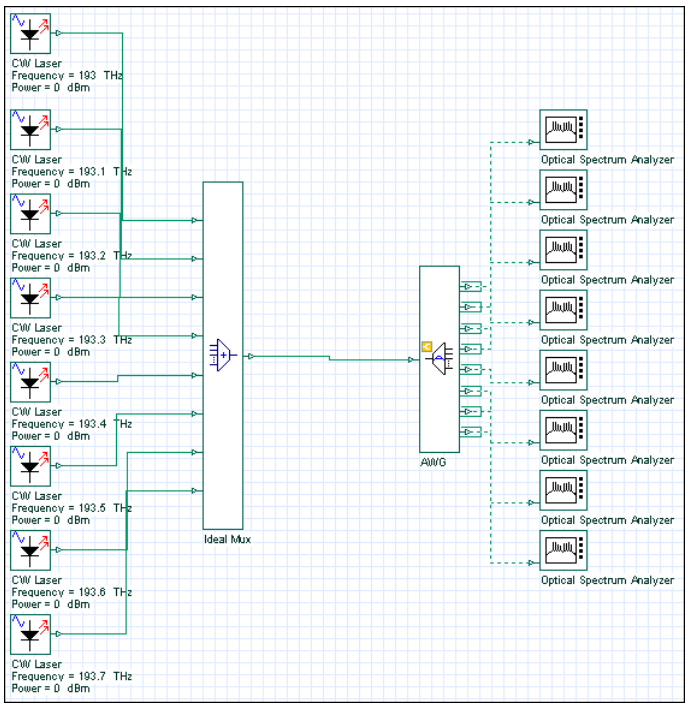
Notes:

AWG Demultiplexer

AWG demultiplexer.osp

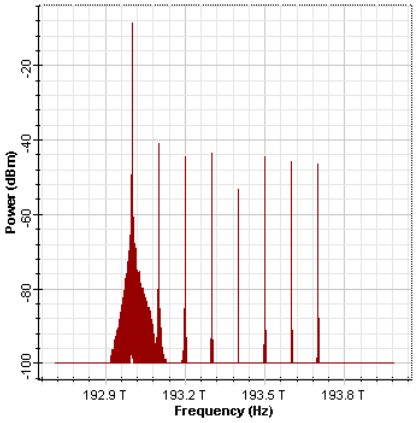
Fiber Bragg gratings can be used for making all fiber demultiplexers. The project "*AWG demultiplexer.osp*" (Figure 6-5) shows an Array waveguide grating (AWG) demultiplexer.

Figure 6-5: Layout - AWG demultiplexer



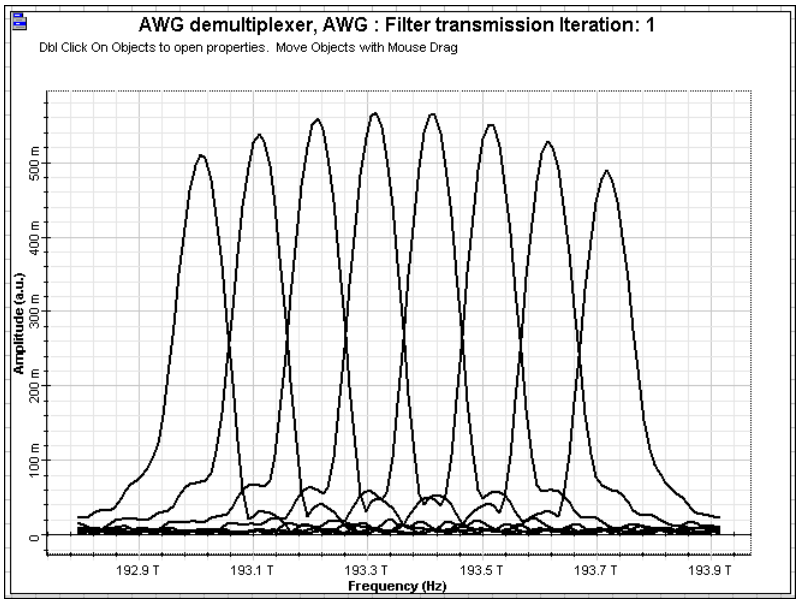
The OSA at the AWG output shows the selected WDM channel. For the first channel, the AWG output has been shown in Figure 6-6.

Figure 6-6: AWG output



The AWG transmission response is shown in Figure 6-7.

Figure 6-7: AWG transmission response

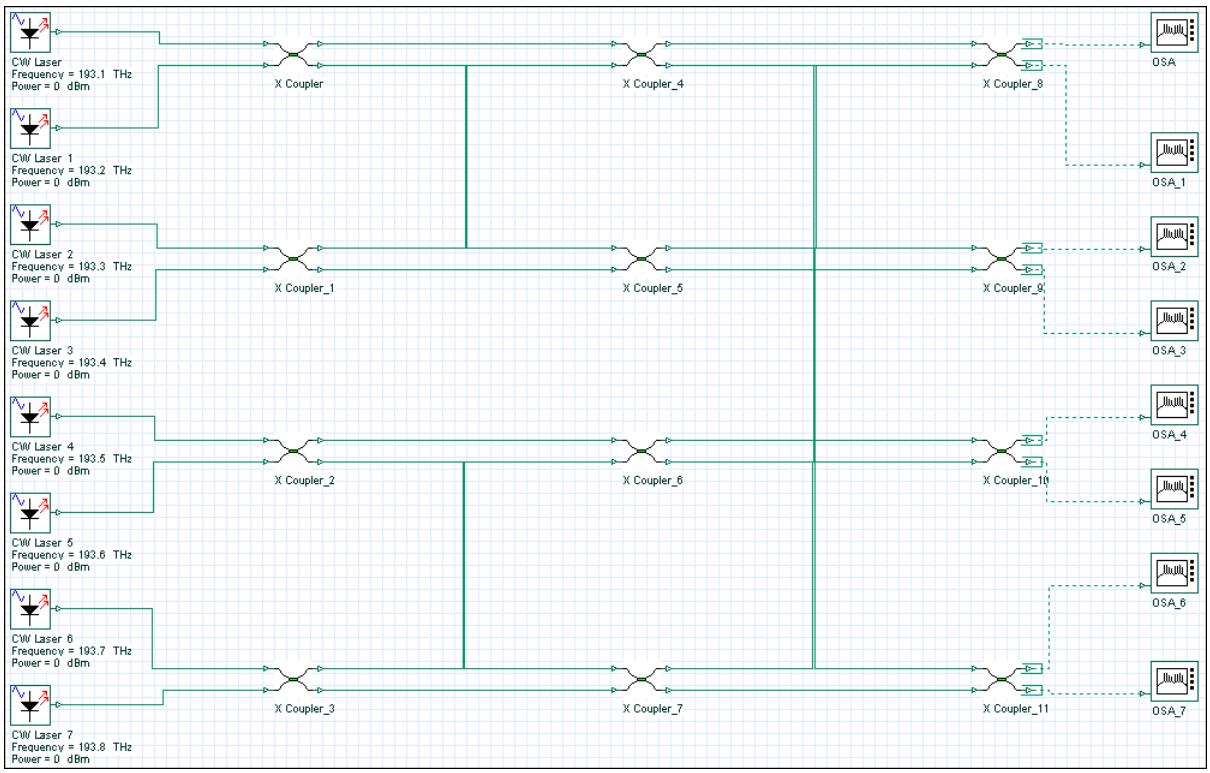


Star Coupler

Star couplers.osp

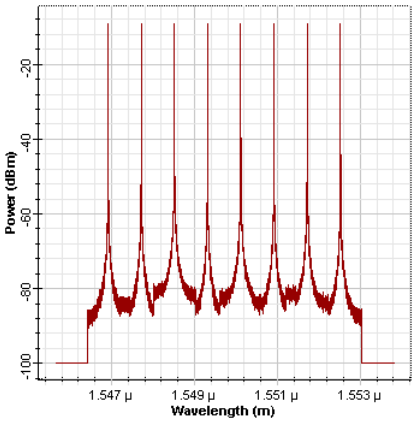
The role of a star coupler is to combine the optical signals entering its multiple input ports and divide them equally amongst its output ports. The project "*Star couplers.osp*" (Figure 6-8) shows a star coupler with 8 input ports, each port has a transmitter working at different wavelengths.

Figure 6-8: Layout - Star coupler



The output of the star coupler can be visualized by attaching an OSA at any of the output ports (Figure 6-9).

Figure 6-9: Output spectrum

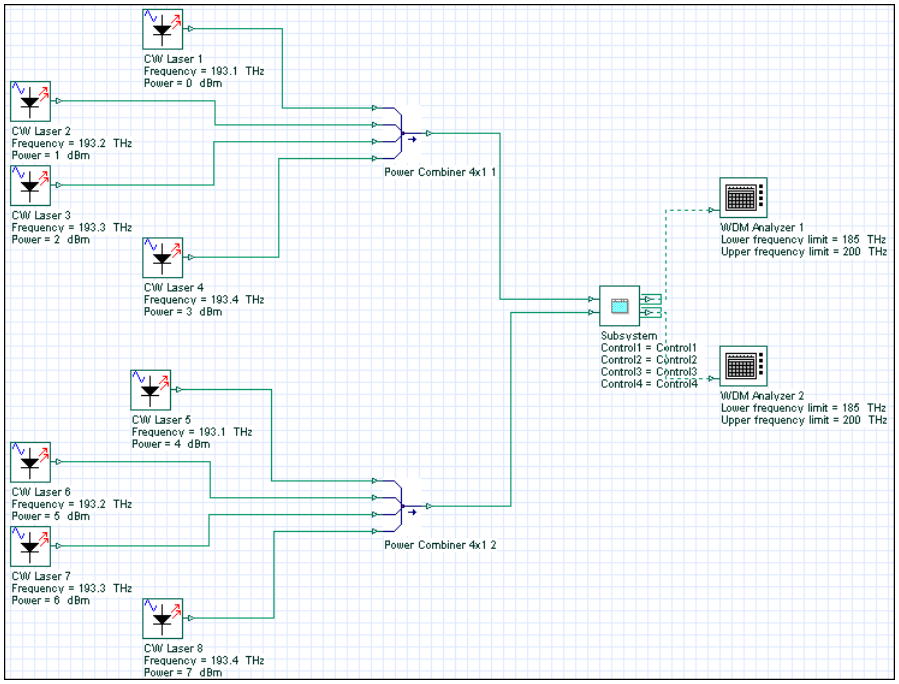


Optical Cross-Connects

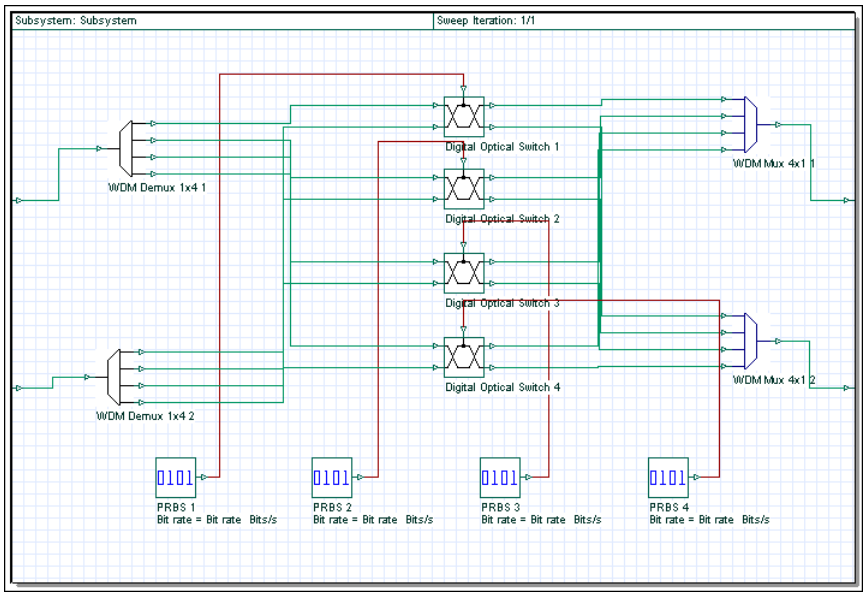
OXC project.osp

The development of wide-area WDM networks requires wavelength routing that can reconfigure the network while maintaining its transparent nature. Project "*OXC project.osp*" (Figure 6-10) shows an optical cross connects with 2 input ports and 2 output ports, each port accommodates 4 wavelengths:

Figure 6-10: (a) Layout - OXC project (b) subsystem structure



(a)



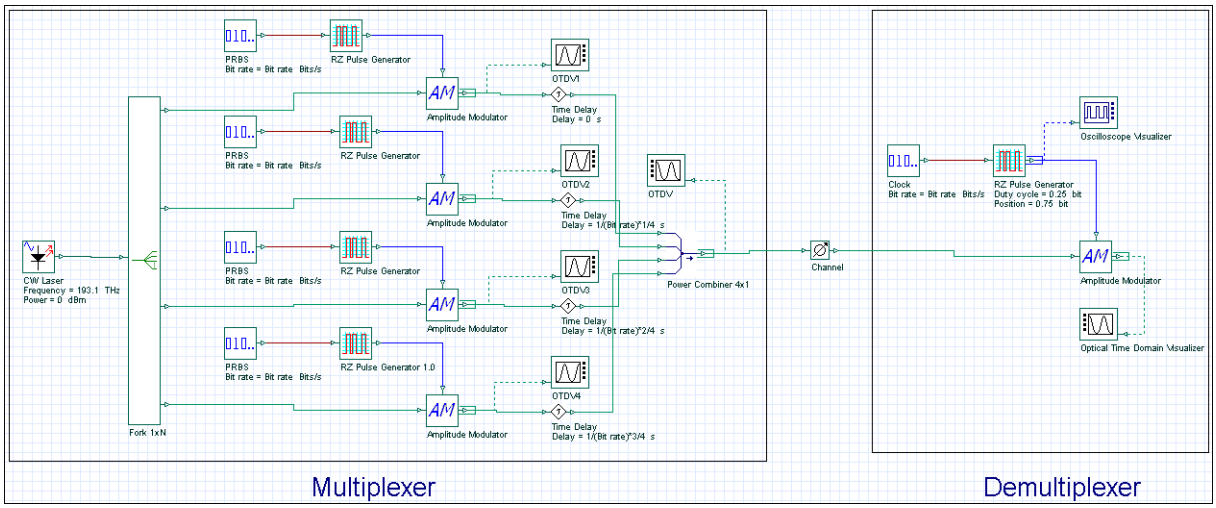
(b)

Channel Multiplexing

OTDM multiplexer.osp

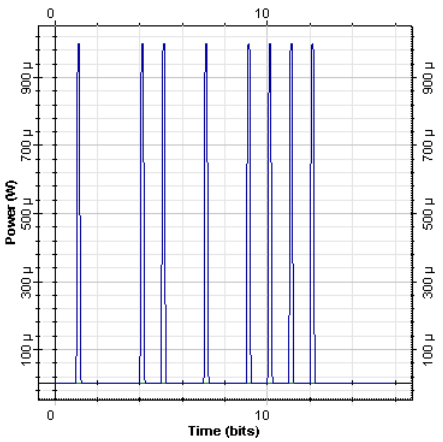
In optical time-division multiplexing (OTDM) systems, several optical signals modulated at the bit rate B using the same carrier frequency, are multiplexed optically to form a composite optical signal at a bit rate N x B, where N is the number of multiplexed optical channels. This has been shown in the project "*OTDM multiplexer.osp*" (Figure 6-11).

Figure 6-11: Layout - OTDM multiplexer



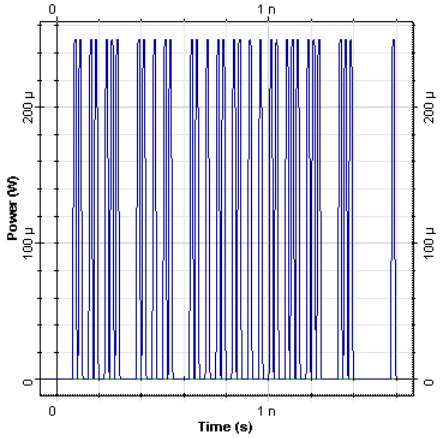
Each modulator generates short pulses with 10 Gb/s bit rate.

Figure 6-12: Pulses after modulator



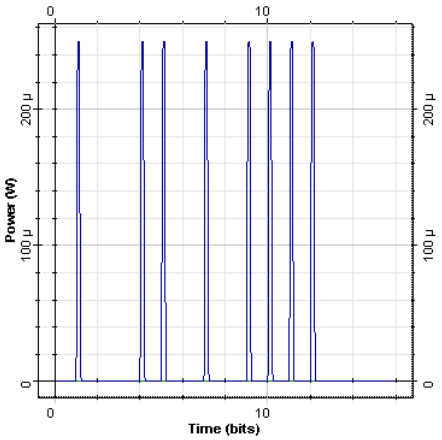
The signals are combined in order to generate a 40 Gb/s signal at the multiplexer output (Figure 6-13).

Figure 6-13: Pulses after multiplexer



The demultiplexer stage uses a modulator working with a 10 Gb/s clock. In this example the output signal for the first channel is shown in Figure 6-14.

Figure 6-14: Pulses after the demultiplexer for the first channel

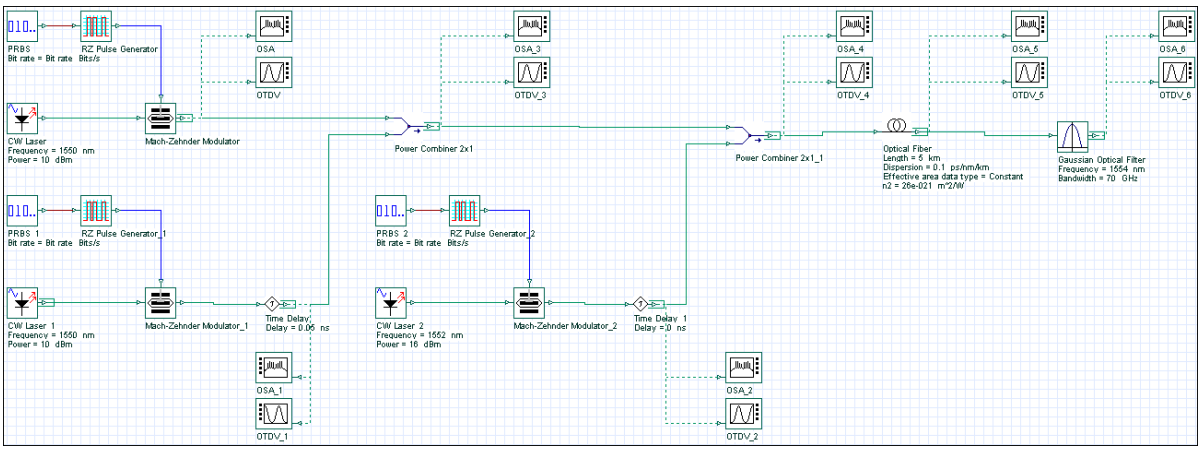


Channel Demultiplexing by FWM

DeMUX by FWM.osp

Project file "*DeMUX by FWM.osp*" generates a demultiplexing scheme that makes use of FWM in nonlinear fiber. In this configuration, the optical TDM signal at 1550 nm is launched together with the clock signal at a different frequency of 1552 nm into fiber. The clock signal acts as a pump for the FWM process. A new pulse train is generated at a third frequency (1554 nm), which is an exact replica of the channel that needs to be demultiplexed. An optical band-pass filter centered at 1554 nm is then used to separate the demultiplexed channel from the optical TDM signal and clock signal.

Figure 6-15: Layout - DeMUX by FWM



Notes:

Interchannel Crosstalk at ADM in A Ring Network

Interchannel crosstalk at ADM in a ring network.osp

Project file "*Interchannel crosstalk at ADM in a ring network.osp*" analyzes the effect of linear interchannel crosstalk in a ring network. The ring network in this example contains four nodes. One can see the crosstalk effect by looking at the eye diagram as well as the optical spectrum. Crosstalk is originated from the filters in ADMs.

Inter-channel cross-talk can arise from a variety of sources. One example of this is an optical filter or ADM that selects one channel (drop) and passes others over the network. Another example is an optical switch (switching different wavelengths) where cross-talk arises owing to imperfect isolation between the switch ports. Other cross-talk types are amplifier induced, router induced, XPM induced, etc. [1]. A particular signal can accumulate cross-talk from different elements and channels over the network. Cross-talk can be reduced by using several techniques such as wavelength dilation and filter cascading. In this example, we will investigate the effect of inter-channel cross-talk at ADM in a ring network. The project is given in "*Interchannel crosstalk at ADM in a ring network.osp*". This network contains 4 nodes and these nodes communicate over two channels at 193 THz and 193.1 THz as shown in Figure 6-16. We have considered a bit rate of 10 Gb/s. ADMs at each node is modeled by using WDM add and drop components. WDM add and drop components are created by using 4th order Bessel filters. The ring is ended with a ring control component that can circulate the signals in the ring for a given number of times. The distance between the nodes is 12.5 km and we inserted an ideal amplifier just before node 2 to compensate for the fiber loss.

Figure 6-16: A basic ring network with 4 nodes

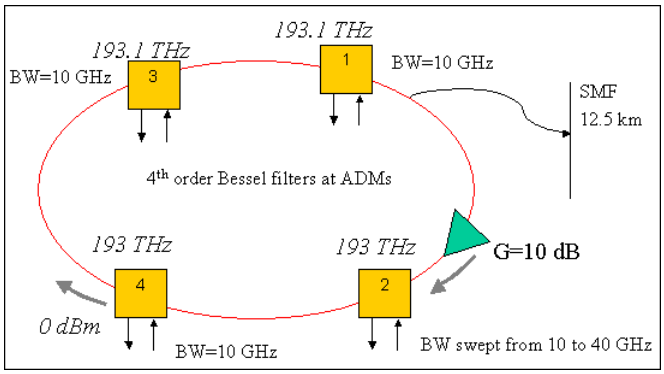
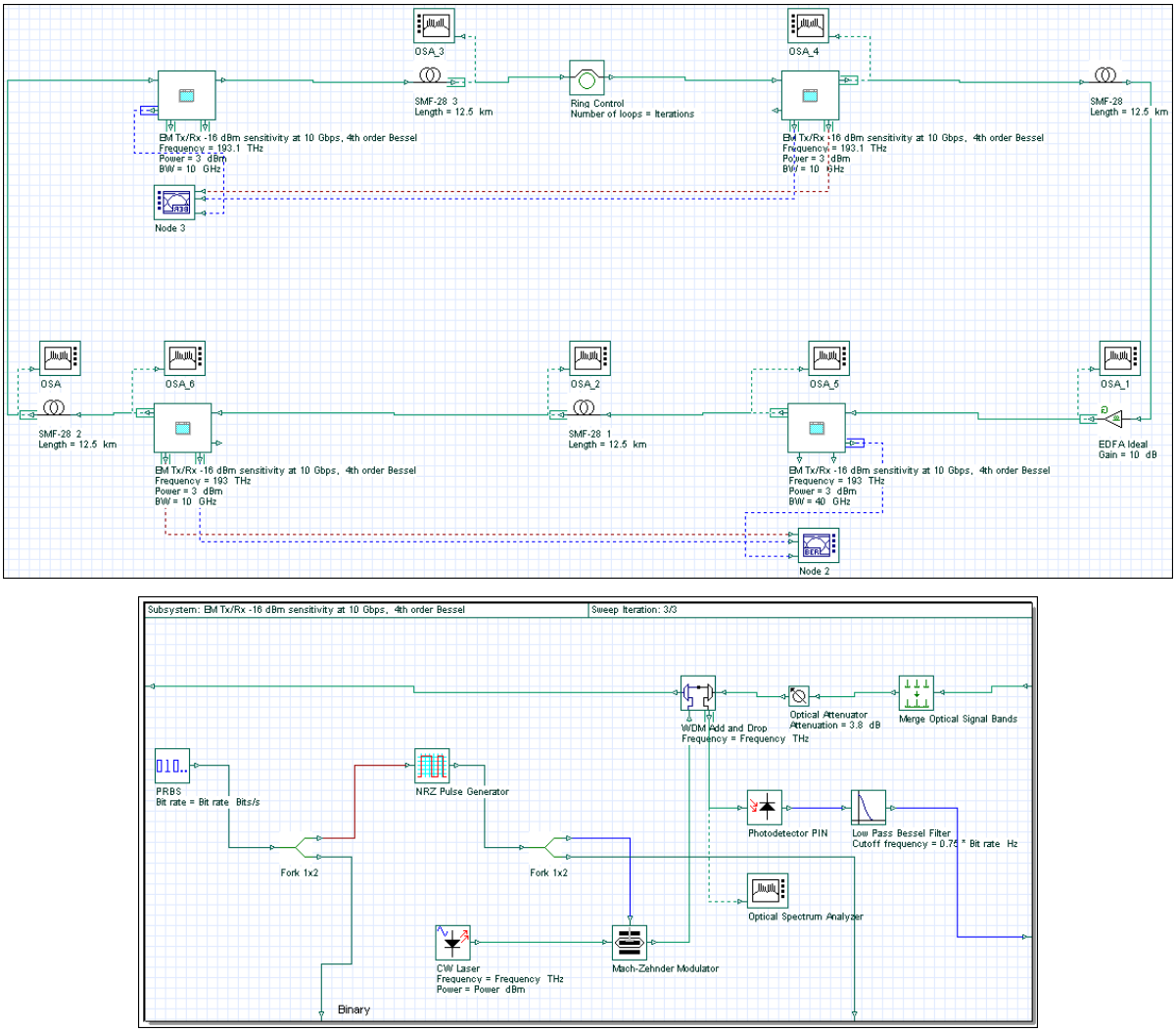


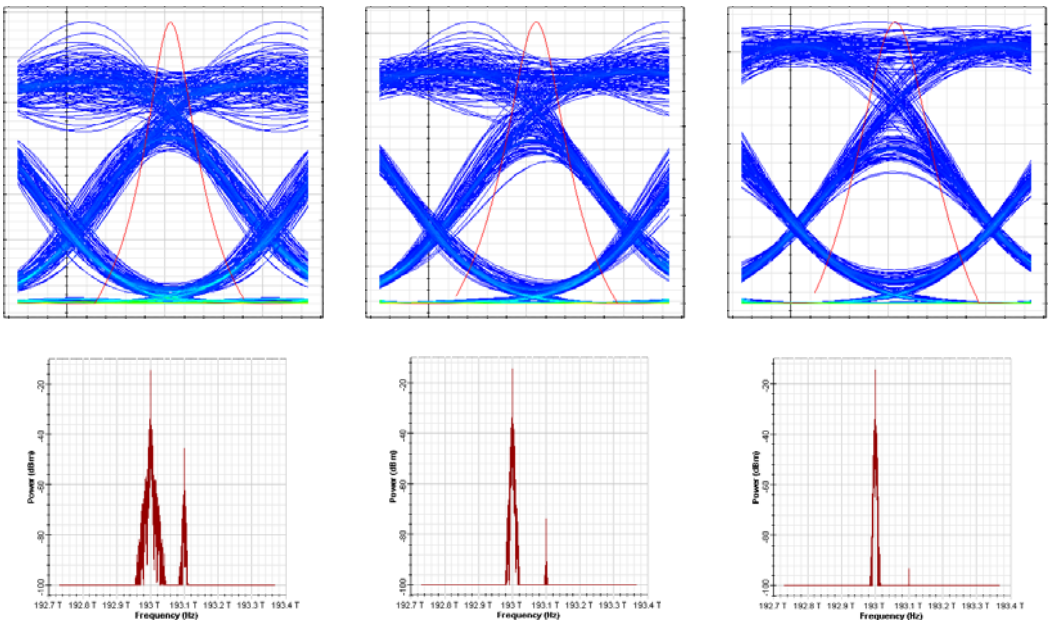
Figure 6-17: (a) Layout of a ring network (b) structure of the subsystem "EM Tx/Rx - 16 dBm sensitivity at 10 Gbps, 4th order Bessel"



To show the effect of inter-channel cross-talk, we have swept the bandwidth of the filters in ADM of node 2 from 10 to 40 GHz. The eye diagrams and power spectra at node 2 for several bandwidths are given in Figure 6-18. Of course this type of characteristic of the ADM at node 2 will also affect the received signals at other nodes and other channel performances.

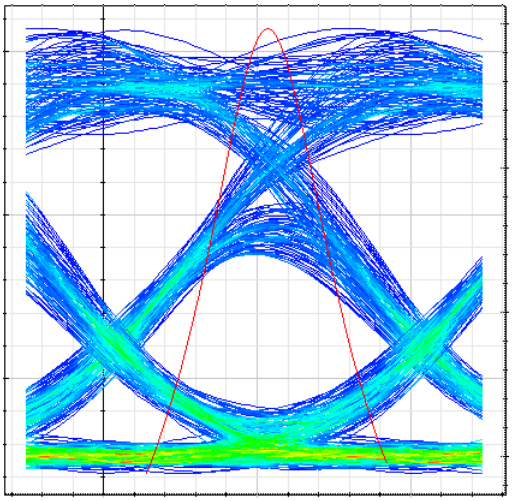
Figure 6-19 shows the eye diagram at node 3 which communicates on channel 1 at 193.1 THz.

Figure 6-18: Eye diagrams and corresponding power spectra at node 2 when bandwidth of the filters in node 2 is (a) 40 GHz (b) 17.5 GHz and (c) 10 GHz



(a) **(b)** **(c)**

Figure 6-19: Eye diagram of the signal dropped at node 3 that communicates on channel 1 at 193.1 THz



References:

[1] G.P. Agrawal, *Fiber-Optic Communication Systems*, 4th ed., John Wiley & Sons, INC., 2010.

[2] T. Gyselings et. al, “Crosstalk analysis of multi-wavelength optical cross connects”, J. Light. Tech. 17, pp. 1273, 1999.

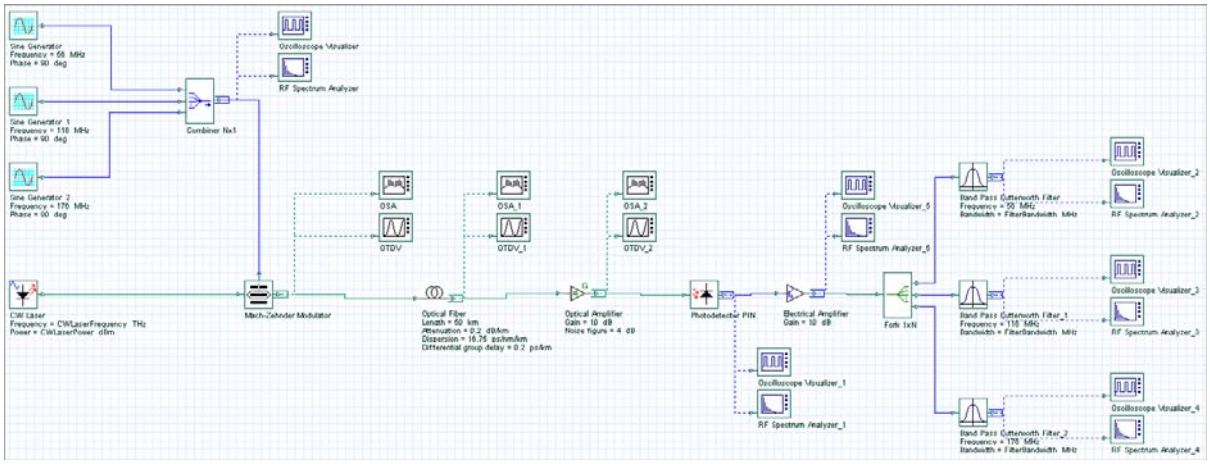
[3] R. Ramaswami and K.N. Sivarajan, Optical Networks: A practical Perspective, Morgan Kaufmann, 1998.

Subcarrier Multiplexing

Subcarrier multiplexing.osp

Project file "*Subcarrier multiplexing.osp*" generates an analog SCM lightwave system designed with a single optical carrier at 193.1 THz. Three sinusoidal signals (0.5+0.5*sin(ω_0*t)) with frequencies of 56 MHz, 116 MHz, and 176 MHz are first combined in electronic domain and then used to modulate the amplitude of an optical carrier. Light is sent to fiber and at the receiver end, subcarriers are separated by filters.

Figure 6-20: Layout - Subcarrier multiplexing



Notes:

Chapter 7 - Optical Amplifiers

This section contains the following examples.

- EDFA Basic Concepts
- Booster Amplifier
- In-Line Amplifier
- Preamplifier
- SLA Cascaded in-line Amplifiers: Soliton Pattern Effect at 10 Gb/s in SMF
- SLA Gain Recovery
- SLA Gain Saturation of Chirped and Super Gaussian Pulses
- SLA Gain Saturation of Gaussian Pulses
- Raman Gain and Bandwidth
- Raman Gain Saturation
- Broadband Flat Gain Raman Amplifier
- Pumping Requirements
- Multichannel Amplification
- Optical Preamplifiers
- Power Boosters
- Metro EDFA
- Cascaded In-Line Amplifiers
- EDFA Dynamic

Notes:

EDFA Basic Concepts

EDFA Basic Concepts - Gain Spectrum.osp

EDFA Basic Concepts - Gain Saturation.osp

EDFA Basic Concepts - Amplifier Noise.osp

The sample files in this example show the basic characterization of the Erbium doped fiber amplifier. We have considered the three design versions namely, (a) Gain Spectrum (b) Gain Saturation and (c) Amplifier noise. These enable the characterization of the gain, noise figure and output power under unsaturated and saturated conditions. These examples refer to the topics: Gain Spectrum and Bandwidth, Gain Saturation, and Amplifier Noise, respectively.

In these examples the amplifier performance is characterized by using sweeps for the input parameters of the amplifier. In examples *Gain Spectrum* and *Amplifier Noise*, the signal wavelength is swept; while in example *Gain Saturation*, we sweep the input power for the cases: small signal input power (-30 dBm) and saturated input signal power (0 dBm).

For each design version we have plotted three graphs showing the Output Signal Power, Gain, and Noise Figure as a function of the sweep parameter. In the project, some components settings can be modified and the simulations can be repeated in order to analyze the amplifier performance.

The input parameters which are critical in the numerical solution of coupled rate and propagating equations are displayed in Erbium doped fiber component. The gain and noise figure are calculated using the power results. Figure 7-1 shows the cross-section file used in the projects.

Figure 7-1: Cross-section (absorption curve in black and emission curve in red) file used in the Erbium doped fiber component

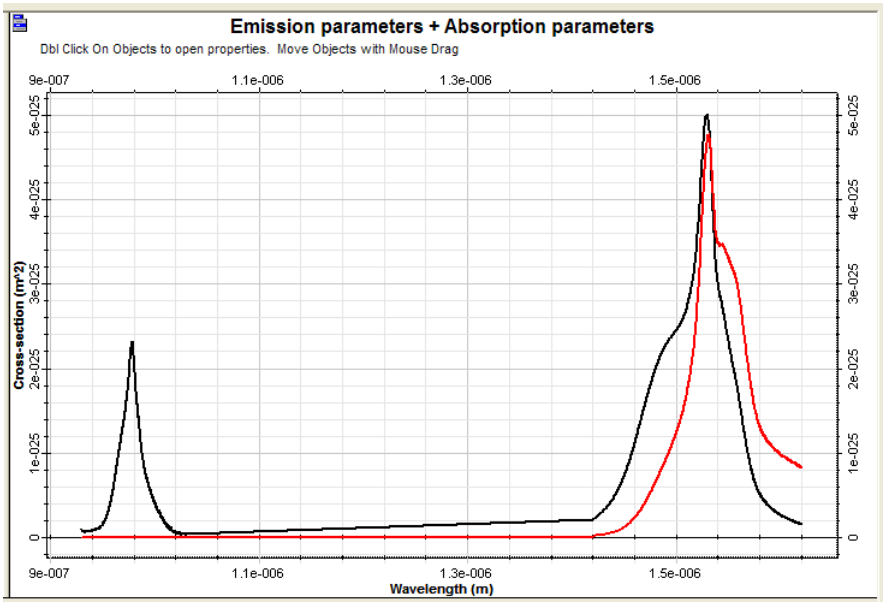
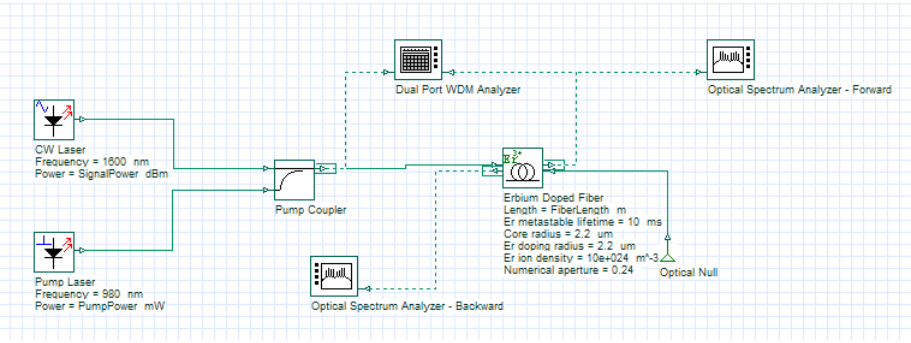


Figure 7-2: Layout - EDFA basic concepts



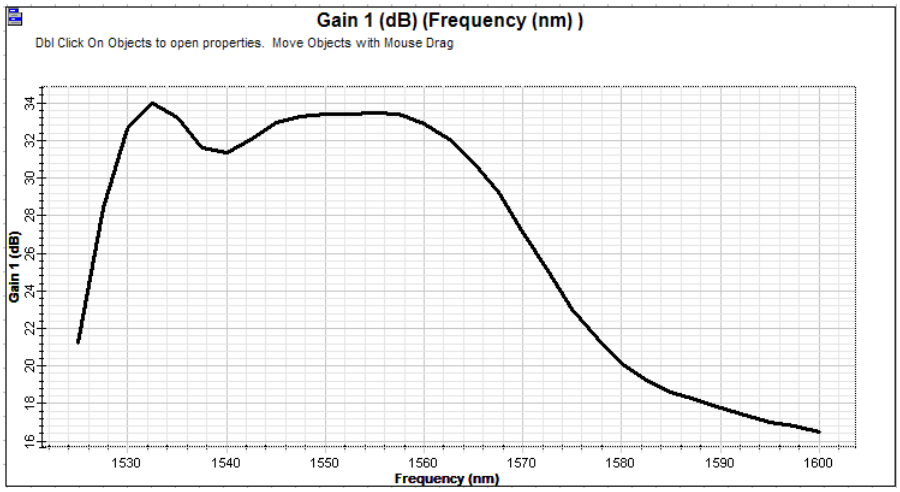
The basic layout used in the calculations for each version is shown in Figure 7-2.

Version - Gain Spectrum

In this first version named *Gain Spectrum* the signal wavelength of the CW laser signal is swept from 1525 nm to 1600 nm which enables evaluating the spectral gain and the bandwidth of the amplifier.

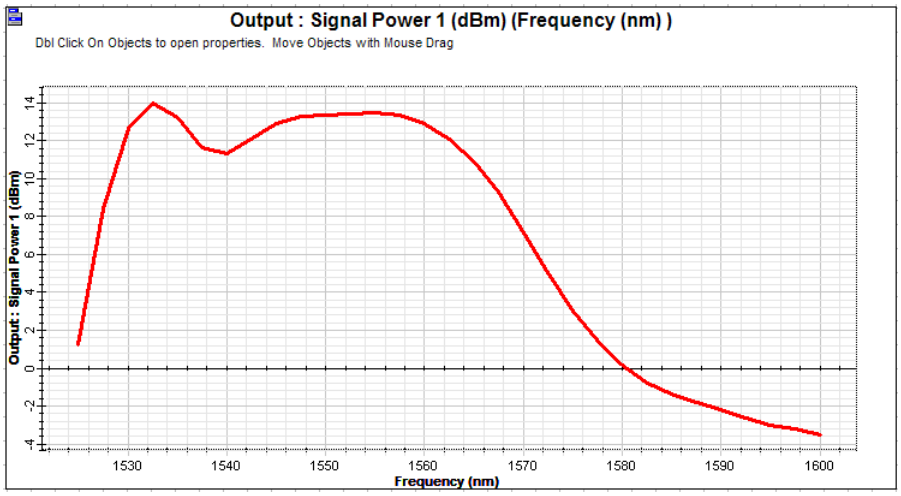
The spectral gain calculated for -20 dBm of input signal power is shown in Figure 7-3.

Figure 7-3: Gain versus signal wavelength (given in [nm] unit) with signal input power equals to -20 dBm



An additional graph that can be checked in the Gain Spectrum version is the output power versus signal wavelength as shown in Figure 7-4.

Figure 7-4: Signal output power versus signal wavelength (given in [nm] unit) calculated with a signal input power equals to -20 dBm



Version - Gain Saturation

The version Gain Saturation enables evaluating the amplifier performance as a function of the signal input power. The signal input power is swept from small signal to large signal regime, i.e. - 40 dBm to 0 dBm. The amplifier performance in terms of gain, output power and noise figure are shown in Figure 7-5, Figure 7-6 and Figure 7-7, respectively.

Figure 7-5: Gain vs. signal input power

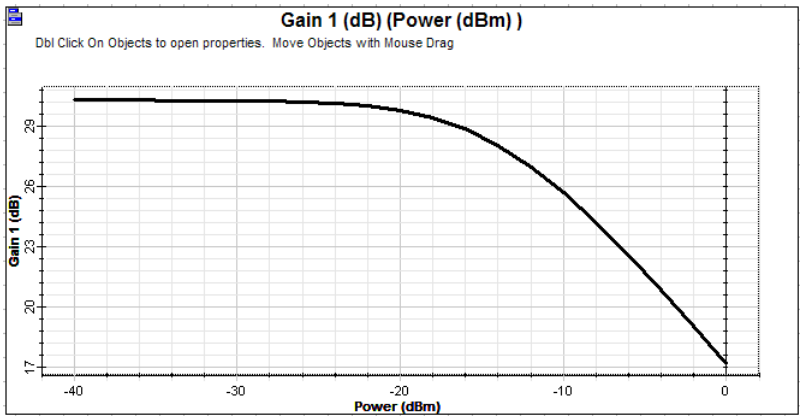


Figure 7-6: Amplified signal power vs. input signal power

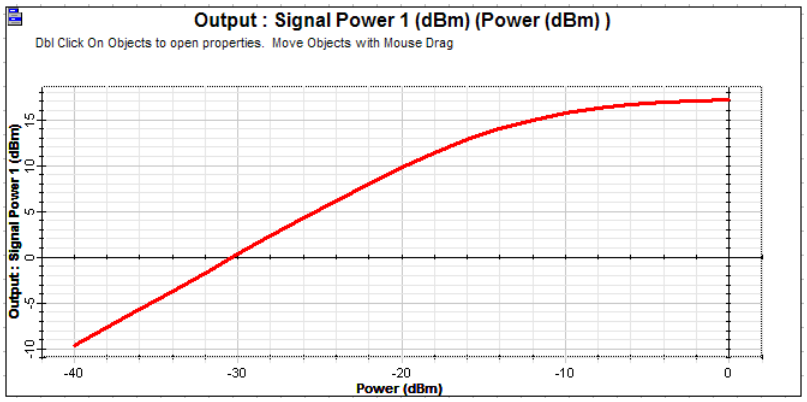
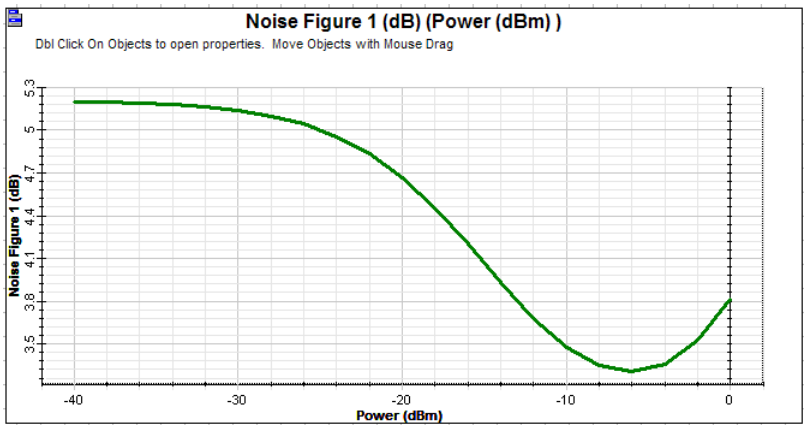


Figure 7-7: Noise figure vs. input signal power



Version - Amplifier Noise

The signal wavelength is the parameter swept in this version, which enables calculating the spectral noise of the amplifier. The total noise power versus signal wavelength is shown in Figure 7-8. Signal and pump power can be changed for further evaluation of the amplifier performance.

Figure 7-8: Amplifier noise characterization

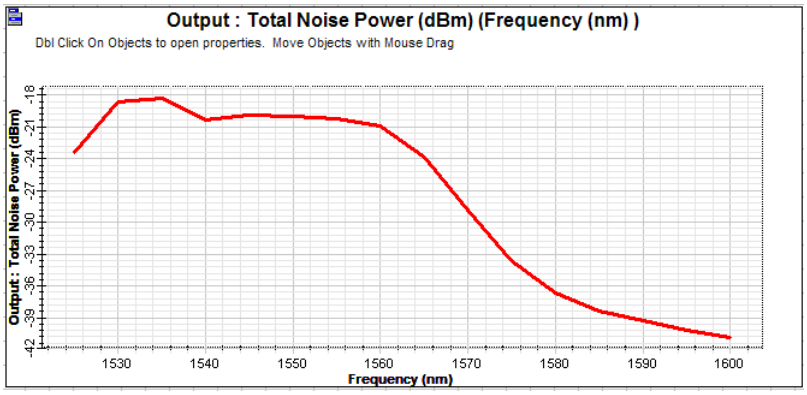
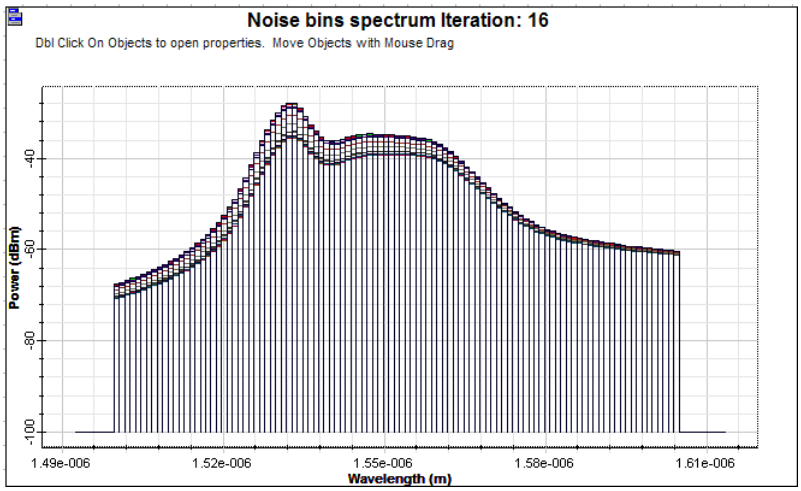


Figure 7-9 shows the ASE spectrum stored after calculating each iteration of the signal wavelength.

Figure 7-9: Noise bins as a function of wavelengths used in the calculations. Each curve in this graph is resulted from different iterations.



Notes:

Booster Amplifier

Booster Amplifier.osp

The project file "*Booster amplifier.osp*" shows the characterization of a booster/power amplifier setup in a single heavily doped erbium-doped fiber, bidirectionally pumped by two 980 nm-pump lasers. In this case, large signal input power is considered because large signal input power contributes to obtain high output power, which is a requirement to booster/power amplifiers. As a consequence, moderate gain will be observed in this case. The low noise figure requirement for EDFAs is not so tight here, where an increase in NF can be tolerated. It is important to mention that typical configurations of booster amplifiers include multiple Er-doped fiber stages.

Figure 7-10 shows the layout of the booster amplifier. Bidirectional pump was used to produce the typical pump scheme observed in booster amplifiers. The optical spectrum analyzer connected at the output port 1 shows the amplified signal obtained after running this project file. The component dual port WDM analyzer gives the calculated results performed to all the propagating signals and pump.

The output power, gain and noise figures calculated as a function of signal input power are shown in Figure 7-11, Figure 7-12, and Figure 7-13**,** respectively. It is possible to observe the gain being compressed as a function of the increasing signal input power as shown in Figure 7-12.

The noise figure curve is calculated by sweeping the signal input power to the booster amplifier assuming identical input parameters. There is a region in the curve where NF is minimized as a function of the signal input power.

Figure 7-10: Layout - Booster amplifier

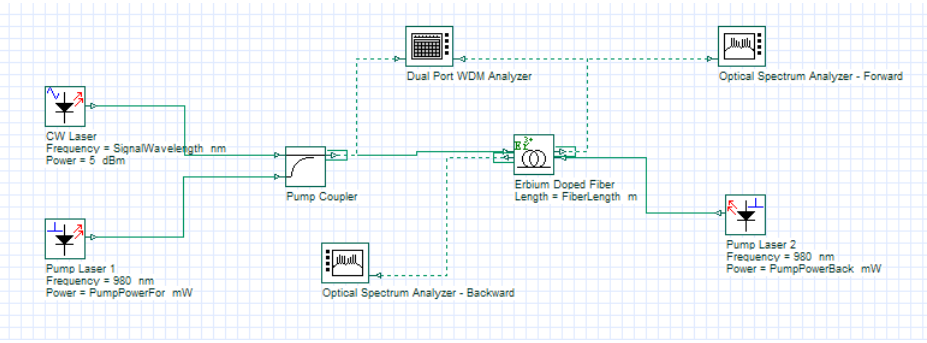


Figure 7-11: Signal output power vs. signal input power calculated for the booster amplifier

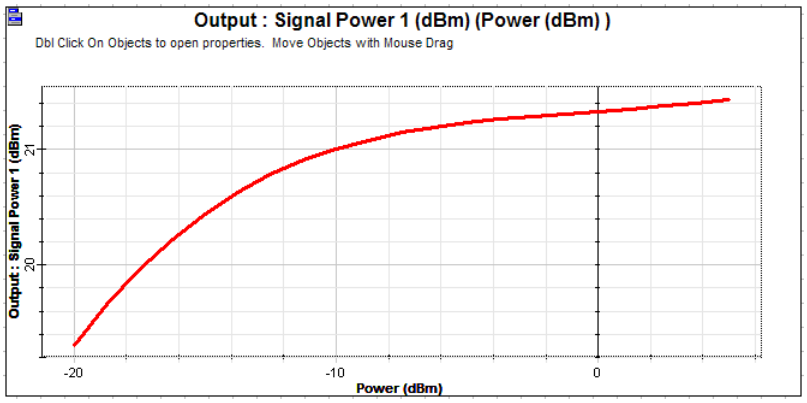


Figure 7-12: Gain vs. signal input power calculated for the booster amplifier

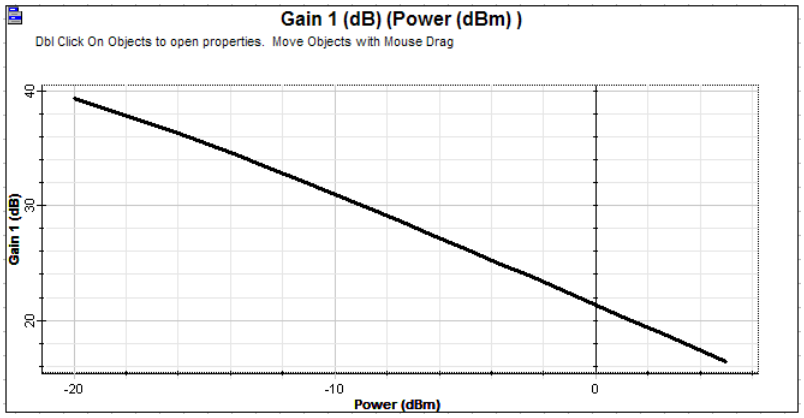
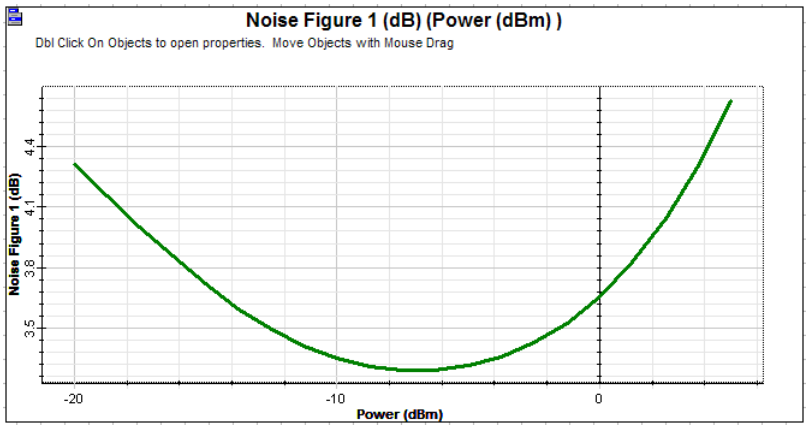


Figure 7-13: Noise figure vs. signal input power calculated for the booster amplifier



The power of both pump lasers (co- and counter-propagating) as well as the Er-doped fiber length can be modified.

In-Line Amplifier

In-line Amplifier.osp

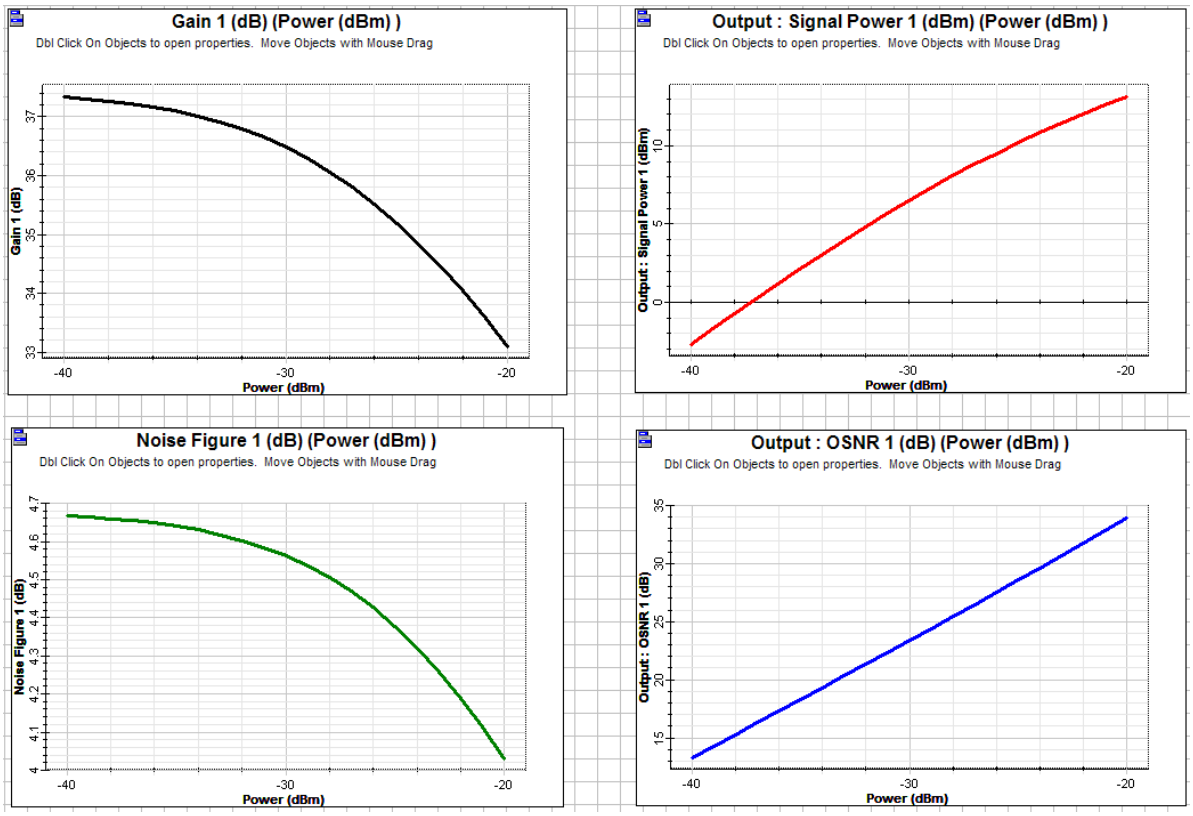
In-line Amplifier - Co & Counter-propagating Pump.osp

The project file "*In-line amplifier.osp*" shows the characterization of an in-line amplifier setup in a single erbium-doped fiber stage, pumped by one 980 nm- pump laser.

In this case, small signal input power is considered to obtain high gain and small noise figure values. The signal input power is swept from -40 dBm to -20 dBm that enables checking the gain, noise figure, output power and OSNR as a function of signal input power.

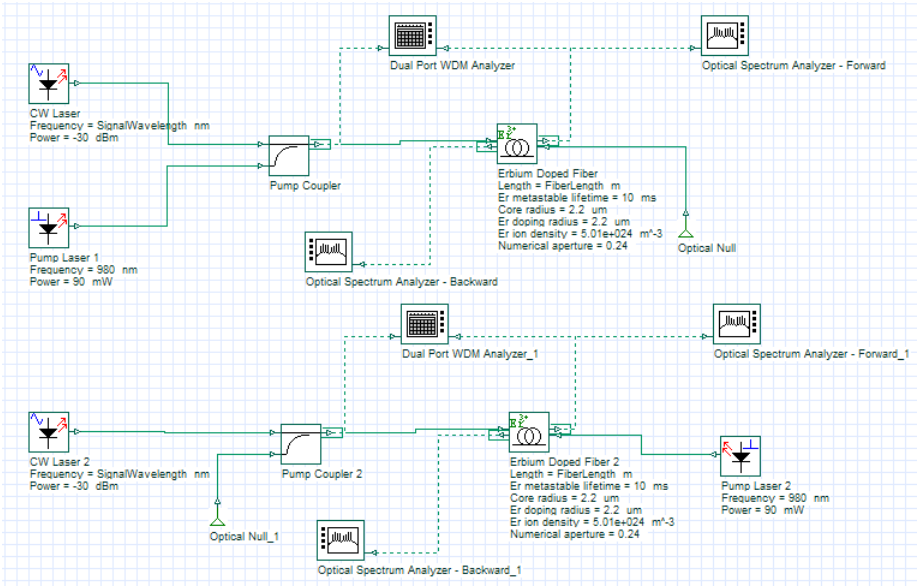
After sweeping iterations over the signal input power, the amplifier performance can be checked in the graphs displayed on the report page, as shown in Figure 7-14.

Figure 7-14: Graphs presenting the inline amplifier performance setup in a co-propagating pump scheme



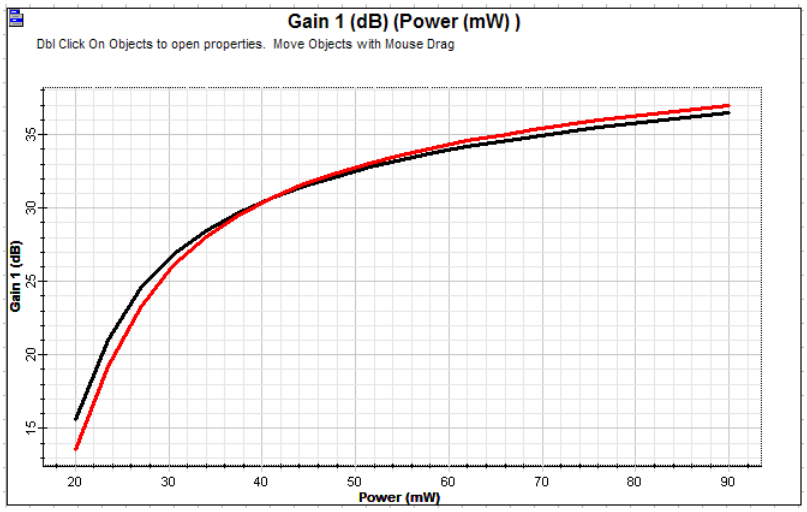
Comparison of two different pump schemes that consider co- and counter-propagating pump are available in "*In-line Amplifier - Co & Counter-propagating Pump.osp*" file, of which the layout is shown in Figure 7-15. The performance of the inline amplifier with co- and counter-propagating pump schemes can be seen in the graphs of gain, noise figure and output power displayed in the report page.

Figure 7-15: Layout - In-line amplifier with co- & counter-propagating pump schemes



The amplifier performance in case of co- and counter-propagating pump schemes can be compared through graphs available. Pump wavelength equal to 980 nm was considered in both cases. The gain versus pump power is shown in Figure 7-16 considering the co- and counter-pump schemes that enable evaluating the most efficient pump scheme for the EDFAs.

Figure 7-16: Comparing gain performance of an EDFA setup in co- and counter-propagating pump schemes



Preamplifier

Preamplifier.osp

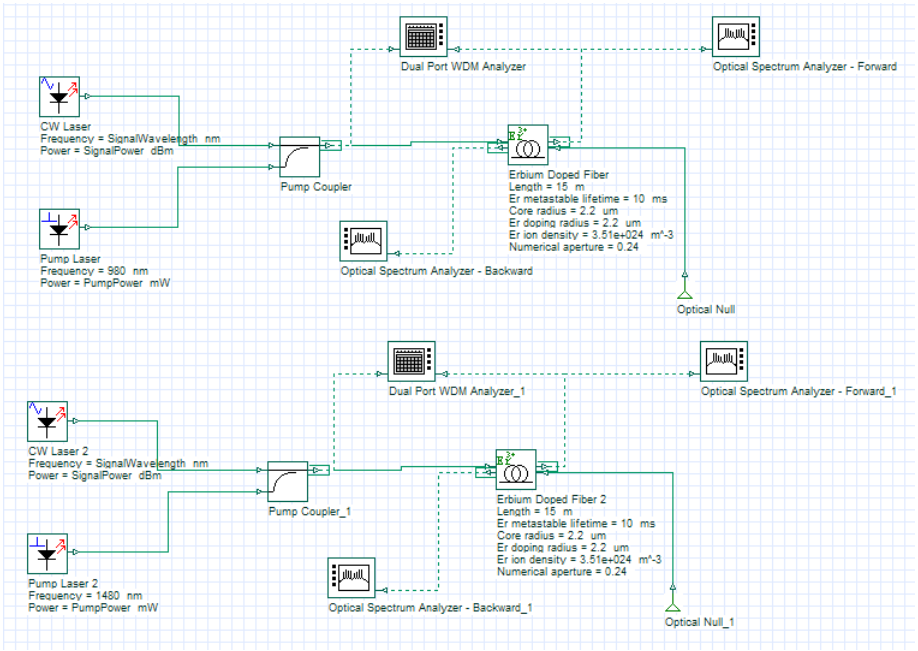
The project file "*Preamplifier.osp*" shows the characterization of an in-line amplifier setup in a single erbium-doped fiber stage, pumped by one pump laser in a co-pump scheme.

In this case, small signal input power is considered to obtain high gain and small noise figure values. The erbium doped fiber length is swept from 6 m to 15 m that enables checking the gain, noise figure, output power and OSNR as a function of fiber length. The pump wavelengths considered in the layout are 980 nm and 1480 nm.

In the two different versions, signal input power is -35 dBm at 1550 nm, respectively. The performance of the preamplifier for the pump wavelength can be seen in the graphs of gain, noise figure and output power displayed in the report page.

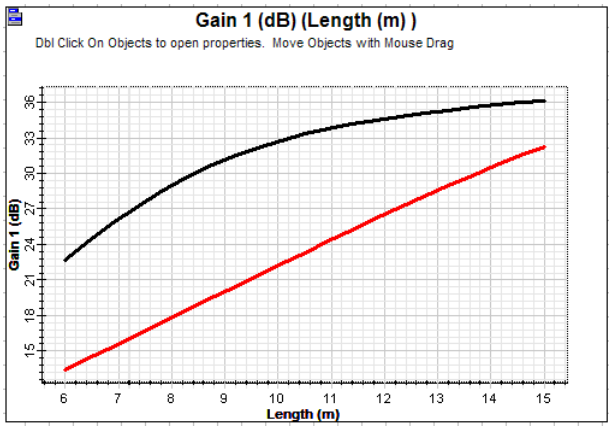
The basic layout used in this preamplifier example is shown in Figure 7-17.

Figure 7-17: Layout - Preamplifier



The gain for the preamplifier is shown in Figure 7-18. Different pump power, signal wavelength, and fiber parameters can be considered to perform additional simulations.

Figure 7-18: Gain vs. erbium doped fiber length considering 980 nm (black curve) and 1480 nm (red curve) as pump wavelength



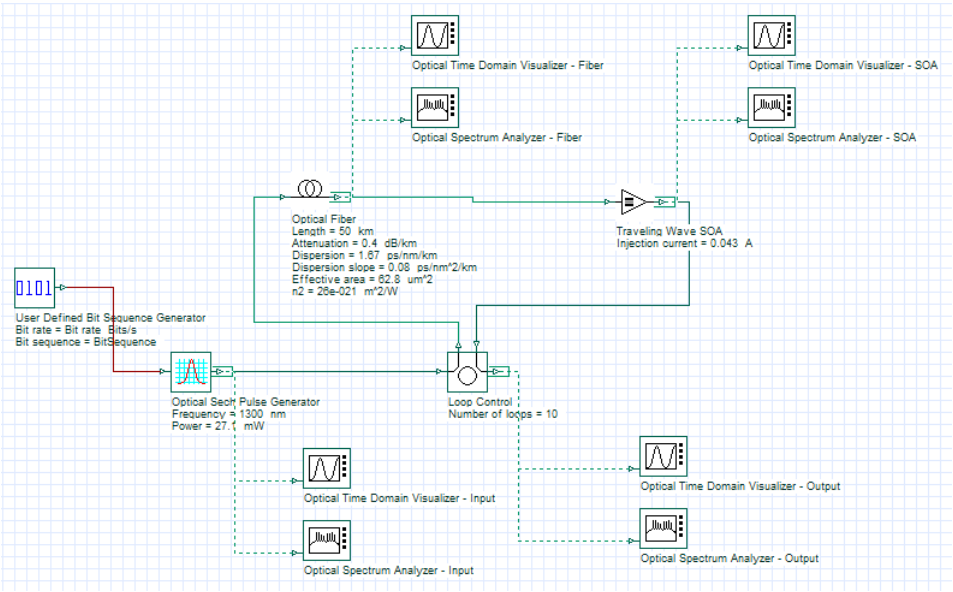
SLA Cascaded in-line Amplifiers: Soliton Pattern Effect at 10 Gb/s in SMF

SLA cascaded in-line amplifiers soliton pattern effect 10 Gb/s in SMF.osp

One of the possibilities to upgrade existing network of already installed standard single mode optical fibers operating at 1.3 μm is the use of SOA. The advantages of using SOA are the low dispersion of the SMF at this carrier wavelength and attractive features of semiconductor optical amplifiers. However, there are two major negative factors in the utilization of SOA as in-line optical amplifiers: (a) gain-saturation effects, which lead to non-equal amplification of pulses in the pattern (so called pattern effect) and (b) the chirp that pulse acquires after amplification.

The aim of this project is to demonstrate the pattern effect at 10 Gb/s transmission over a 500 km optical link consisting of SMF and in-line SOAs [1]. We consider the parameters similar to those in [1].

Figure 7-19: Layout - SLA cascaded in-line amplifiers - soliton pattern effect at 10 Gb/s in SMF



We fix B= 10 Gb/s -> T_B = 100 ps. The sequence length is 16 bit. The carrier wavelength of the pulse is λ ~ 1300 nm. The T_{FWHM} = 20 ps -> T_0 = 0.567 x T_{FWHM} = 11.34 ps. The input peak power is 21.7 mW.

We will consider SMF with a length of 50 km and loss of 0.4 dB/km. The parameter k_2 (= - $\lambda^2 D/(2\pi c)$) ~ -1.5 (ps^2/km) -> D ~ 1.67 (ps/nm.km) -> L_D (= $T_0^2/|k_2|$) ~ 85 km. After each fiber the signal will be amplified with SOA, therefore L_A ~ 50 km. Note that the condition $L_A < L_D$ is satisfied.

The Kerr nonlinearity coefficient γ equals to $n_2\omega_0/cA_{eff}$. For the fixed values of nonlinear refractive index $n_2 = 2.6 \times 10^{-20}$ m^2/W, $\omega_0/c = 2\pi/\lambda = 2\pi/1.3 \times 10^{-6}$ m^{-1}, and $A_{eff} = 62.8$ μm^2, γ will be 2 $W^{-1}km^{-1}$.

Figure 7-20, Figure 7-21, Figure 7-22, and Figure 7-23 show the initial pattern of pulses, and the same pattern of pulses after 200, 350 and 500 km of SMF with periodic amplification at every 50 km using SOA.

Figure 7-20: Initial pattern of pulses

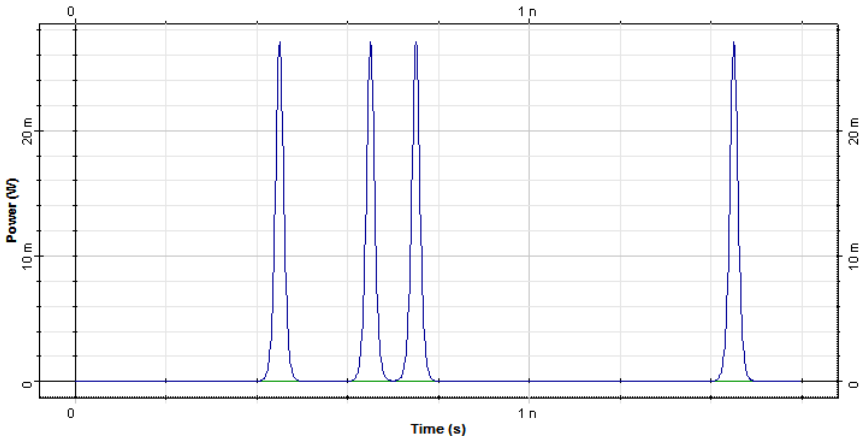


Figure 7-21: Pulses after 200 km of SMF with periodic amplification using SOA at every 50 km

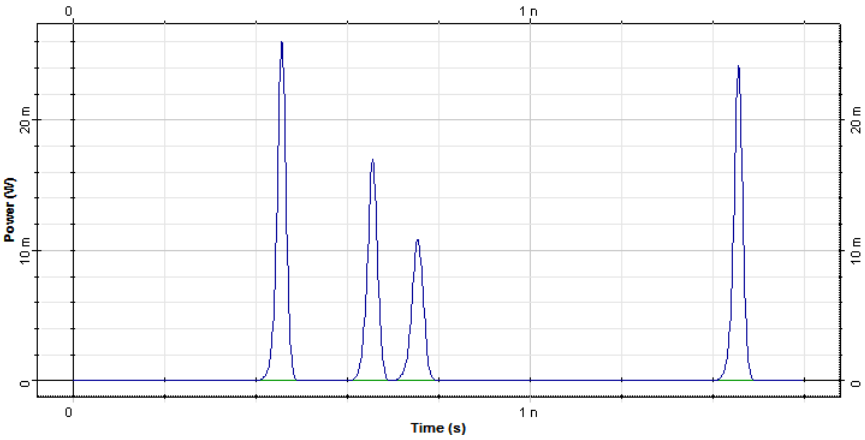


Figure 7-22: Pulses after 350 km of SMF with periodic amplification using SOA at every 50 km

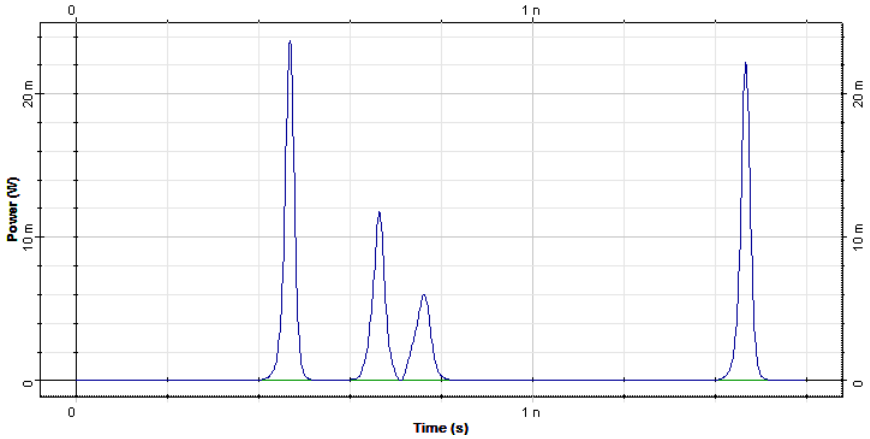
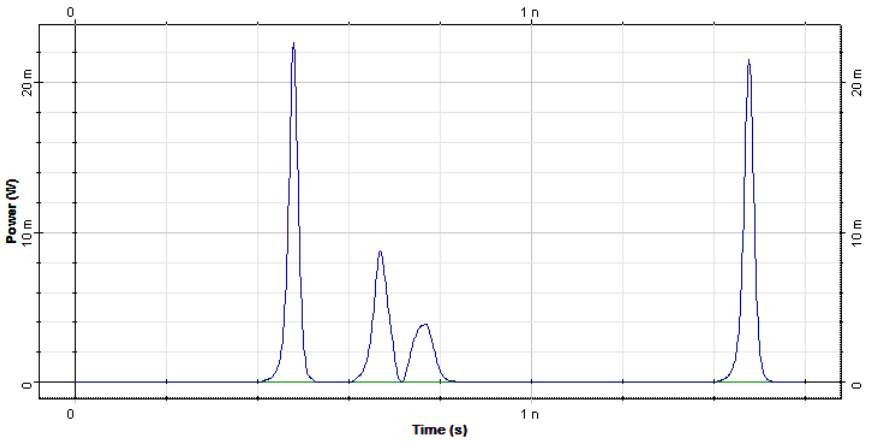


Figure 7-23: Pulses after 500 km of SMF with periodic amplification using SOA at every 50 km



Wha we can see form these figures is the pattern effect, which leads to reduction in the gain of the pulses after previous pulses.

References:

[1] M. Settembre, F. Matera, V. Hagele, I. Gabitov, A. W. Mattheus, and S. Turitsyn, “Cascaded optical communication systems with in-line semiconductor optical amplifiers”, Journal of Lightwave Technology, vol.15, pp. 962-967, 1997.

[2] F. Matera and M. Settembre, “Study of 1.3 μm transmission systems on standard step-index fibers with semiconductor optical amplifiers”, Optics communications, vol. 133, pp.463-470, 1997.

[3] G.P. Agrawal, *Fiber-Optic Communication Systems*, 4th ed., John Wiley & Sons, Inc., 2010.

Notes:

SLA Gain Recovery

SLA gain recovery.osp

When the pulse width becomes comparable to the carrier lifetime, the saturated gain has time to recover during the pulse. The recovery effect influences the shape and spectrum of the amplified pulse.

The aim of this project is to study this influence. Three subtopics will be considered:

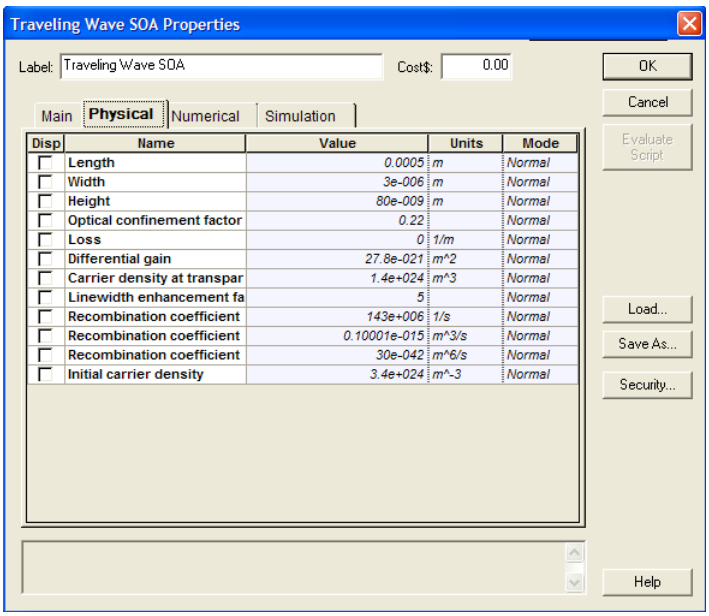
a) Partial gain recovery;

b) Complete gain recovery

c) Appearance of gain-saturation induced self-phase modulation.

SOA parameters considered are : carrier lifetime τ_C ~ 1.4 ns, G = 0.22 and E_{sat} = 5 pJ. Table 7-1 shows the physical parameters of SOA. The unsaturated single pass amplifier gain ~ 30 dB and Inner loss = 0 are used to make the comparison with [1].

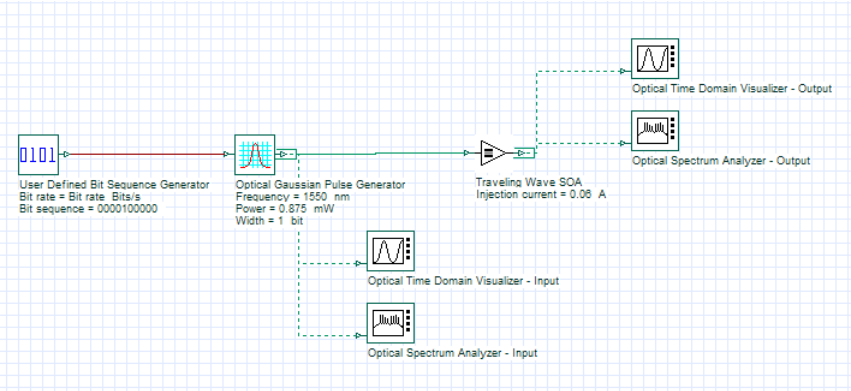
Table 7-1: Semiconductor optical amplifier parameters (physical)



Disp	Name	Value	Units	Mode
☐	Length	0.0005	m	Normal
☐	Width	3e-006	m	Normal
☐	Height	80e-009	m	Normal
☐	Optical confinement factor	0.22		Normal
☐	Loss	0	1/m	Normal
☐	Differential gain	27.8e-021	m^2	Normal
☐	Carrier density at transpar	1.4e+024	m^3	Normal
☐	Linewidth enhancement fa	5		Normal
☐	Recombination coefficient	143e+006	1/s	Normal
☐	Recombination coefficient	0.10001e-015	m^3/s	Normal
☐	Recombination coefficient	30e-042	m^6/s	Normal
☐	Initial carrier density	3.4e+024	m^-3	Normal

Figure 7-24 shows the layout of the project.

Figure 7-24: Layout - SLA gain recovery



(a) Partial gain recovery

As the carrier lifetime of SOA is: τ_C ~ 1.4 ns, we will consider here pulses with widths smaller than 1.4 ns. Keeping the ratio E_{in} / E_{sat} = 0.1, we will investigate the influence of the increase of the pulse duration which will approach the carrier lifetime but will remain smaller than it.

The bit rate B = 1 Gbps implies T_B = 1ns.

We will consider three pulses (pulse 1,2 and 3) with widths of 0.25 ns, 0.5 ns and 1 ns, respectively. In all the three cases, the ratio E_{in} / E_{sat} = 0.1 will be kept constant.

The parameters for pulse 1 are: duty cycle = 0.25, T_{FWHM} ~ 0.25 ns -> T_0 ~ 0.14 ns, and P_{in} = 3.5 mW. Therefore, T_0 /τ_C ~ 0.1.

Figure 7-25, Figure 7-26, Figure 7-27, and Figure 7-28 show the shape and spectrum of the initial and amplified pulse 1.

Figure 7-25: Shape of initial pulse 1

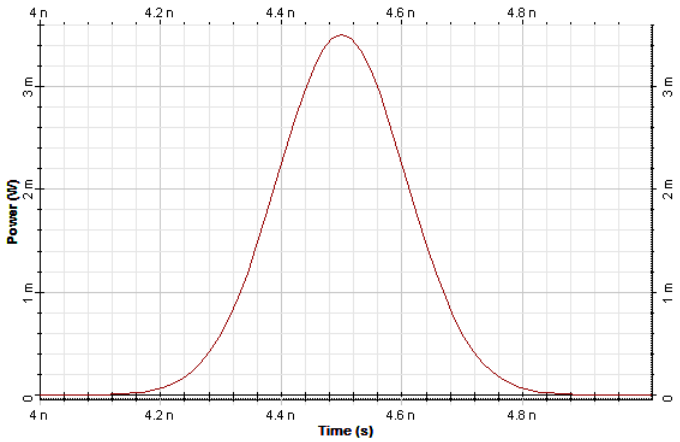


Figure 7-26: Spectrum of initial pulse 1

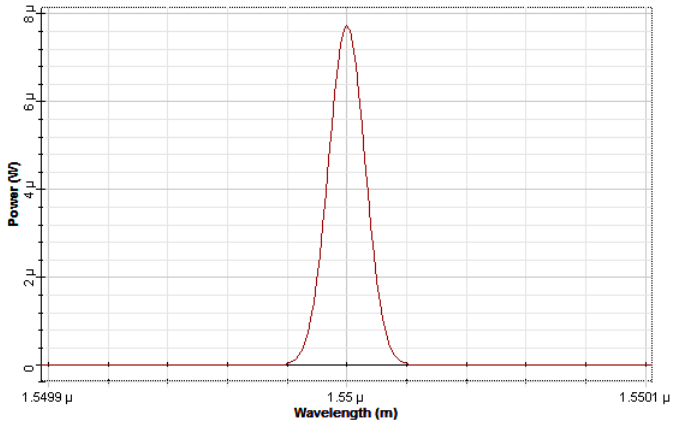


Figure 7-27: Shape of amplified pulse 1

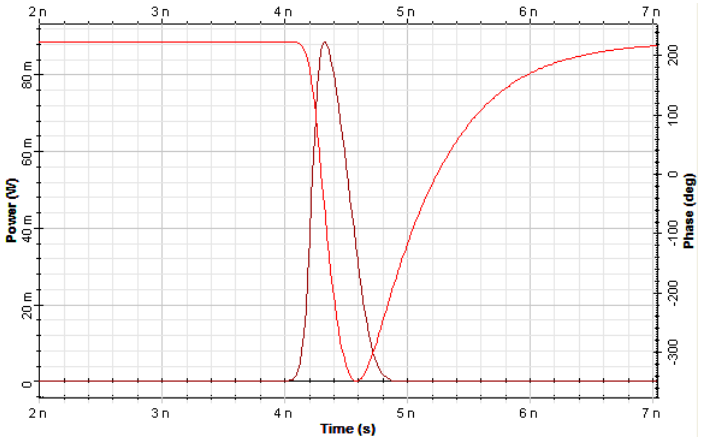
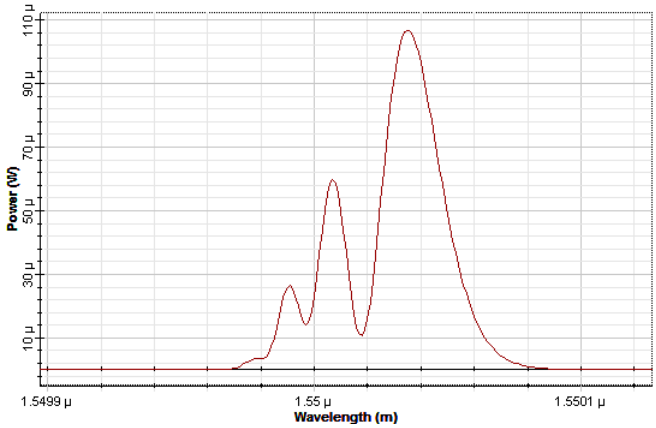


Figure 7-28: Spectrum of amplified pulse 1



The parameters for pulse 2 are: duty cycle = 0.5, T_{FWHM} ~ 0.5 ns -> T_0 ~ 0.28 ns, and P_{in} = 1.75 mW. Therefore, T_0 / τ_C ~ 0.2.

Figure 7-29, Figure 7-30, Figure 7-31, and Figure 7-32 show the shape and spectrum of the initial and amplified pulse 2.

Figure 7-29: Shape of initial pulse 2

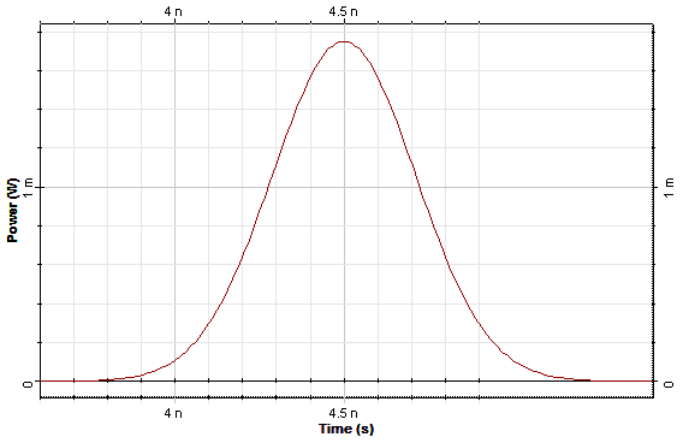


Figure 7-30: Spectrum of initial pulse 2

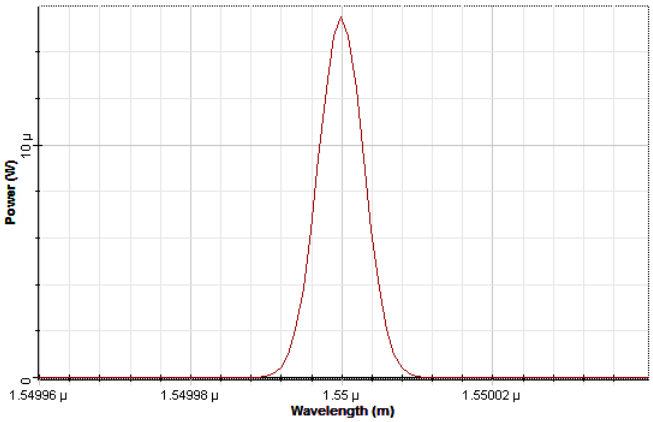


Figure 7-31: Shape of amplified pulse 2

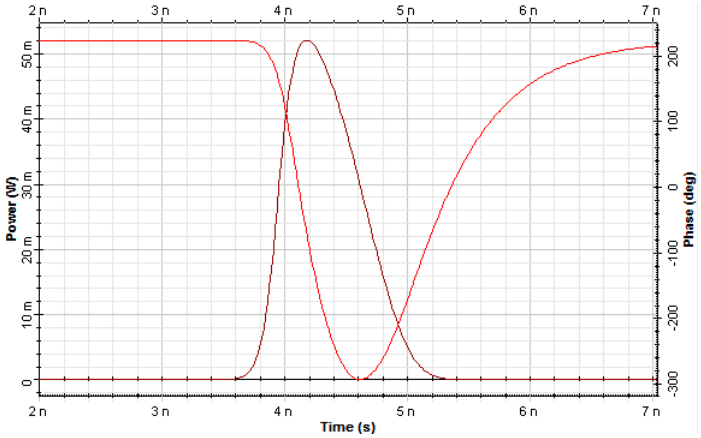
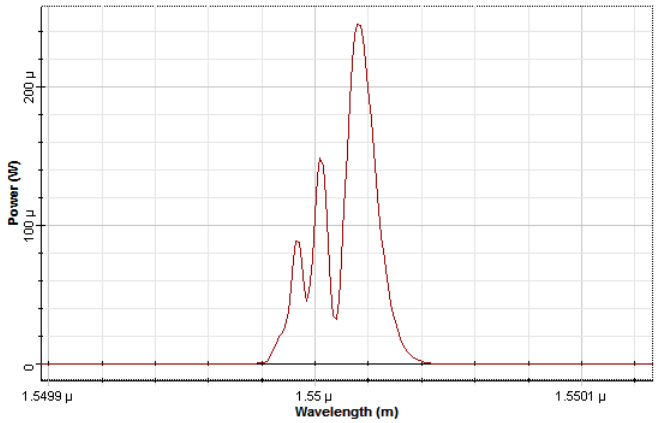


Figure 7-32: Spectrum of amplified pulse 2



The parameters for pulse 3 are: duty cycle = 1, T_{FWHM} ~ 1 ns -> T_0 ~ 0.567 ns, and P_{in} = 0.875 mW. Therefore, T_0 / τ_C ~ 0.4.

Figure 7-33, Figure 7-34, Figure 7-35, and Figure 7-36 show the shape and spectrum of the initial and amplified pulse 3.

Figure 7-33: Shape of initial pulse 3

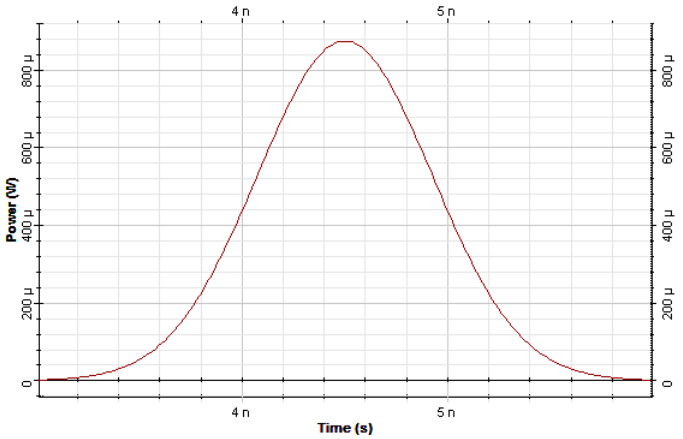


Figure 7-34: Spectrum of initial pulse 3

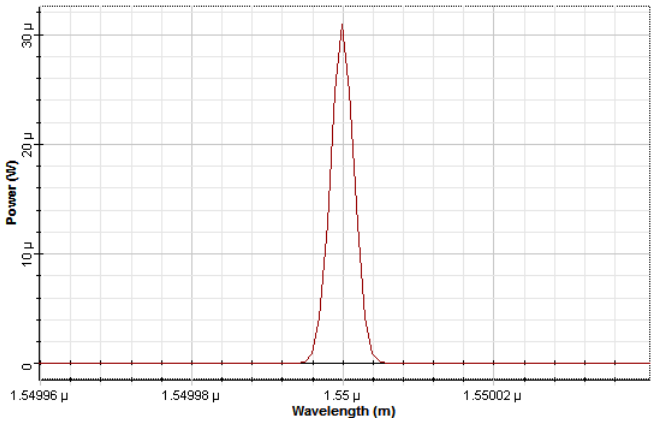


Figure 7-35: Shape of amplified pulse 3

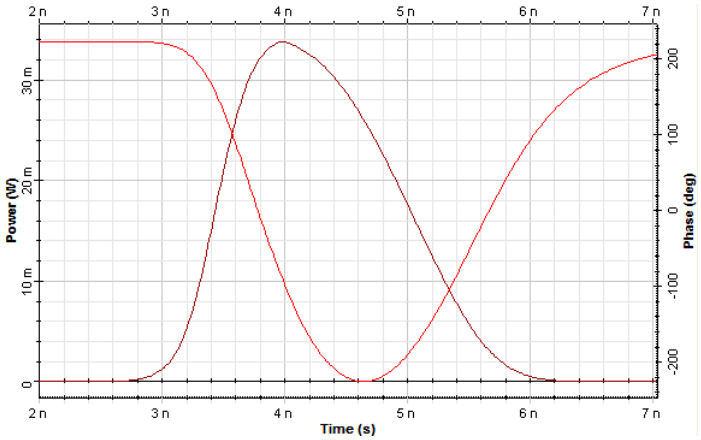
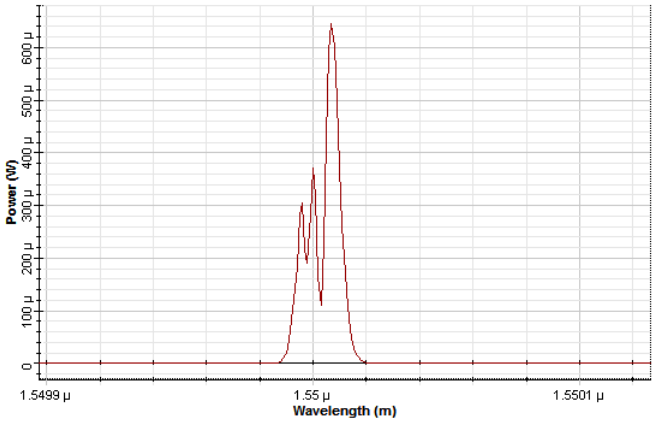


Figure 7-36: Spectrum of amplified pulse 3



Following properties of the three amplified pulses considered above can be observed. First, we see that by increasing the pulse width and keeping the ratio E_{in} / E_{sat} = 0.1, the pulse shape becomes broader and less asymmetrical than the input pulse. At the same time increasing the pulse width, the spectrum becomes less asymmetrical and the spectral shift reduces. Note the behavior of the phase that is shown in the figures of the shapes of amplified pulses. As the phase of amplified pulse gives the information for the gain we can see that for such pulses the gain doesn't have enough time to recover completely.

(b) Complete gain recovery (the quasi CW operation)

As the carrier lifetime of SOA is: τ_C ~ 1.4 ns, we will consider pulses with widths larger than 1.4 ns. The bit rate B = 100 Mbps implies T_B = 10 ns.

We will consider three pulses (pulse 4, 5 and 6) with widths of 2.5 ns, 5 ns and 10 ns, respectively. In all the three cases the ratio E_{in} / E_{sat} = 0.1 will be kept constant.

The parameters for pulse 4 are: duty cycle = 0.25, T_{FWHM} ~ 2.5 ns, T_0 ~ 1.42 ns, and P_{in} = 0.15 mW. Therefore, T_0 /τ_C ~ 1.8 and P_{in} / P_{sat} = 0.04. Figure 7-37, Figure 7-38, Figure 7-39, and Figure 7-40 show the shape and spectrum of the initial and amplified pulse 4.

Figure 7-37: Shape of initial pulse 4

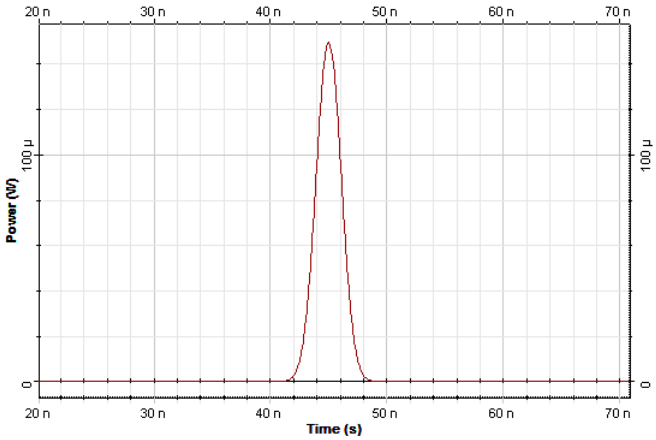


Figure 7-38: Spectrum of initial pulse 4

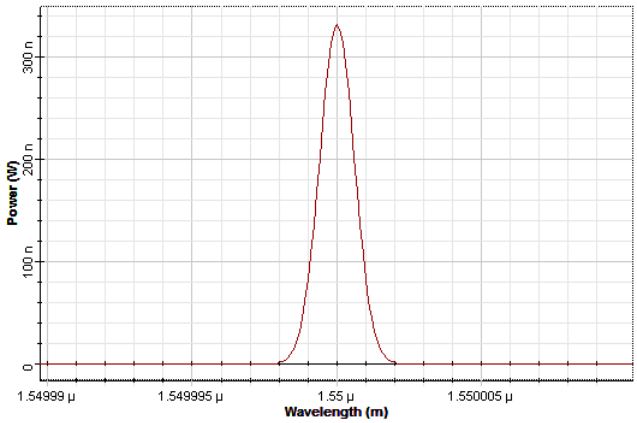


Figure 7-39: Shape of amplified pulse 4

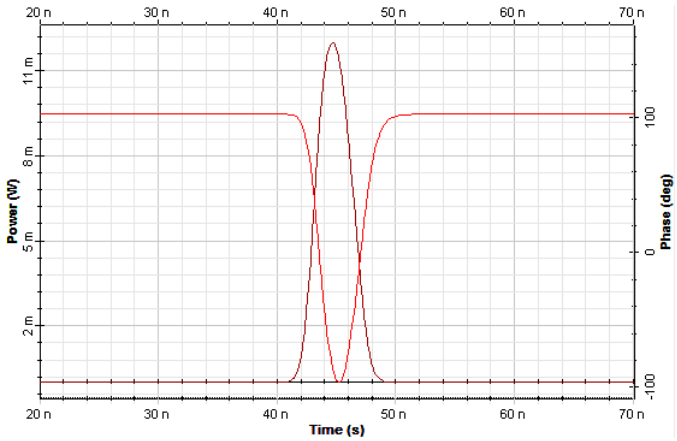
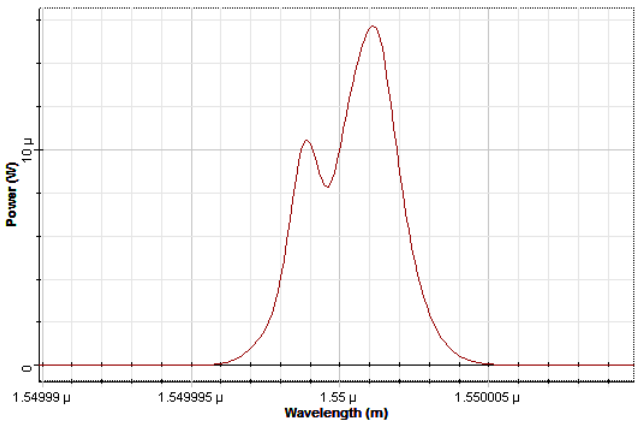


Figure 7-40: Spectrum of amplified pulse 4



The parameters for pulse 5 are: duty cycle = 0.5, T_{FWHM} ~ 5 ns -> T_0 ~ 2.83 ns, and P_{in} = 0.28 mW. Therefore, T_0 / τ_C ~ 3.6 and P_{in} / P_{sat} = 0.08.

Figure 7-41, Figure 7-42, Figure 7-43, and Figure 7-44 show the shape and spectrum of the initial and amplified pulse 5.

Figure 7-41: Shape of initial pulse 5

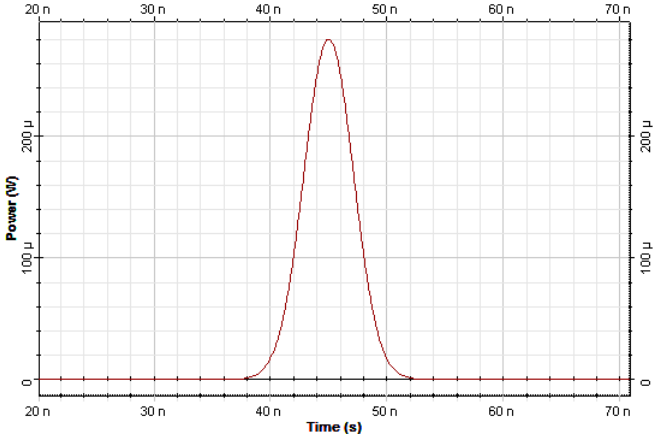


Figure 7-42: Spectrum of initial pulse 5

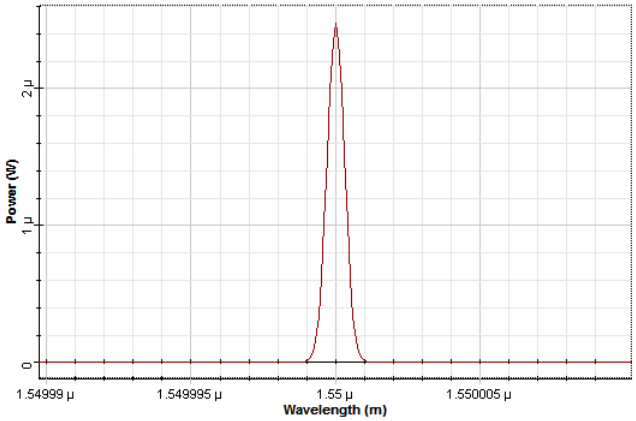


Figure 7-43: Shape of amplified pulse 5

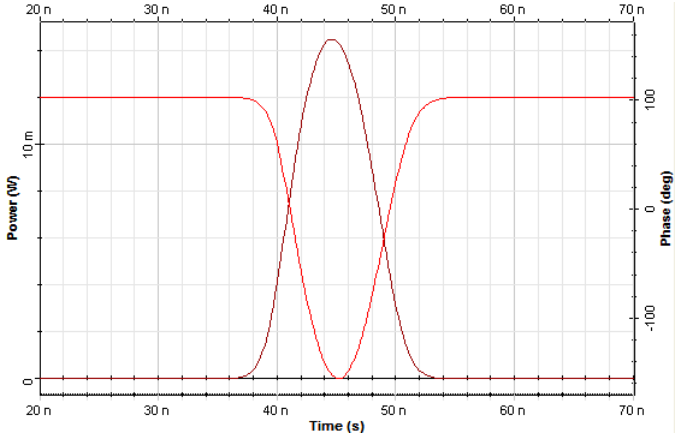
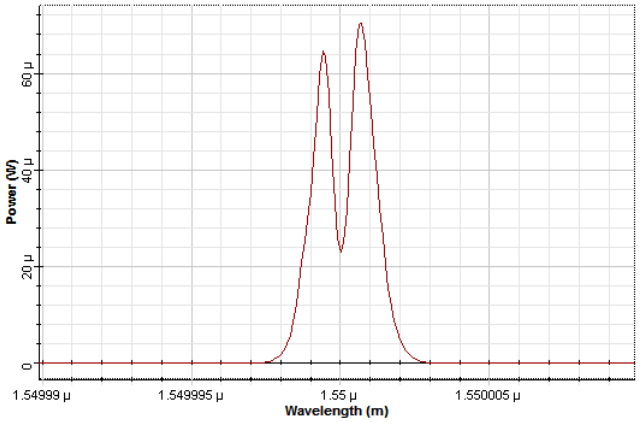


Figure 7-44: Spectrum of amplified pulse 5



The parameters for pulse 6 are: duty cycle = 1, T_{FWHM} ~ 10 ns -> T_0 ~ 5.67 ns, and P_{in} = 0.736 mW. Therefore, T_0 / τ_C ~ 7.1 and P_{in} / P_{sat} = 0.2.

Figure 7-45, Figure 7-46, Figure 7-47, and Figure 7-48 show the shape and spectrum of the initial and amplified pulse 6.

Figure 7-45: Shape of initial pulse 6

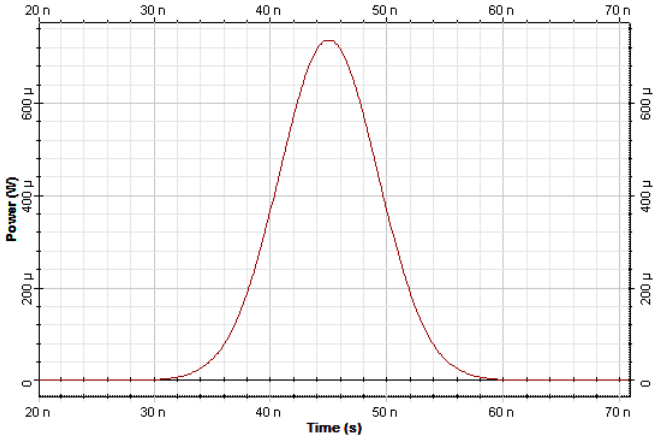


Figure 7-46: Spectrum of initial pulse 6

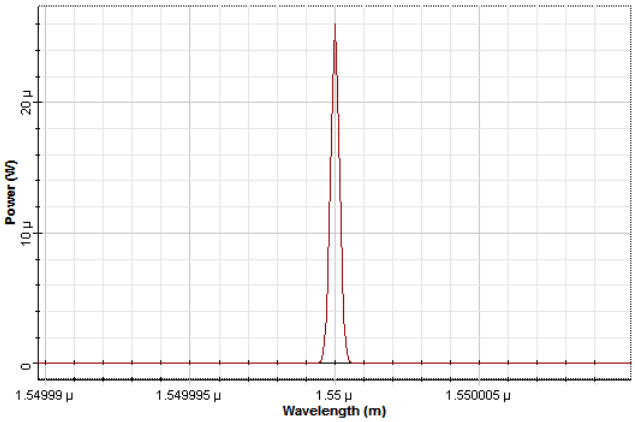


Figure 7-47: Shape of amplified pulse 6

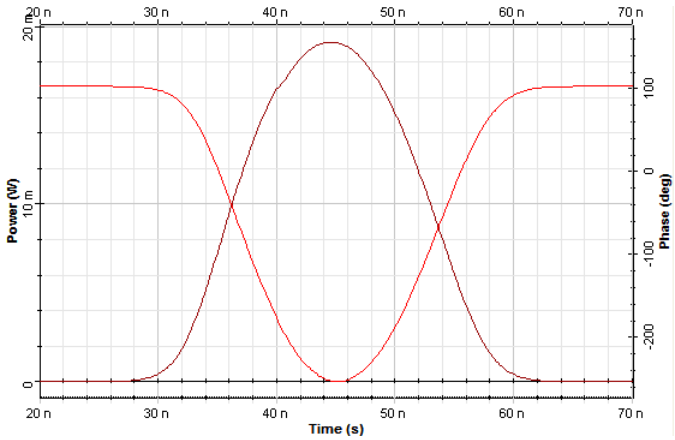
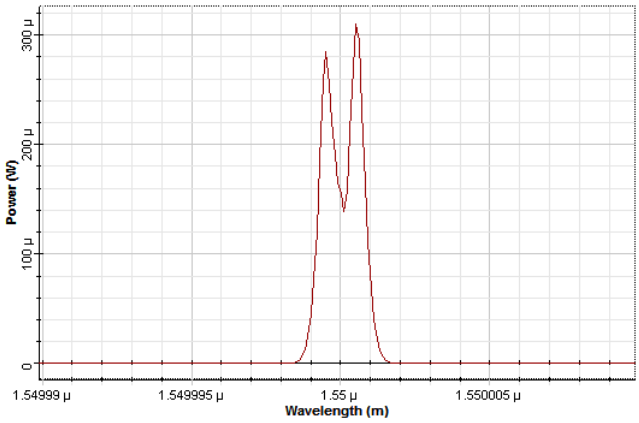


Figure 7-48: Spectrum of amplified pulse 6



We see from the properties of the last three amplified pulses that increasing the pulse width well above the carrier lifetime leads to much more symmetrical shapes of the amplified pulses. They become also much broader than the shapes of the corresponding initial pulses. At the same time increasing the pulse width the spectrum of the amplified pulses become less asymmetrical and the red shift continuously reduce. The phase is shown in the figures of the shapes of amplified pulses. We see now that for such pulses the gain has enough time to recover completely.

(c) Appearance of gain-saturation induced self- phase modulation

Now we will compare the obtained results for the pulse 6 (for which P_{in} / P_{sat} = 0.2) with that of P_{in} / P_{sat} = 0.4. To make this we will increase the initial power 10 times. The compared Results for the shapes and spectrum of the amplified pulses are shown in Figure 7-49 and Figure 7-50, respectively.

Figure 7-49: Comparision of results for the shapes of amplified pulses

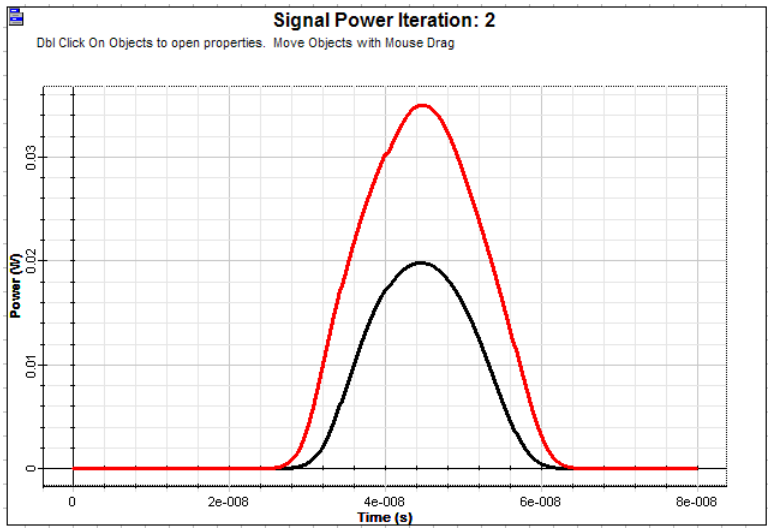
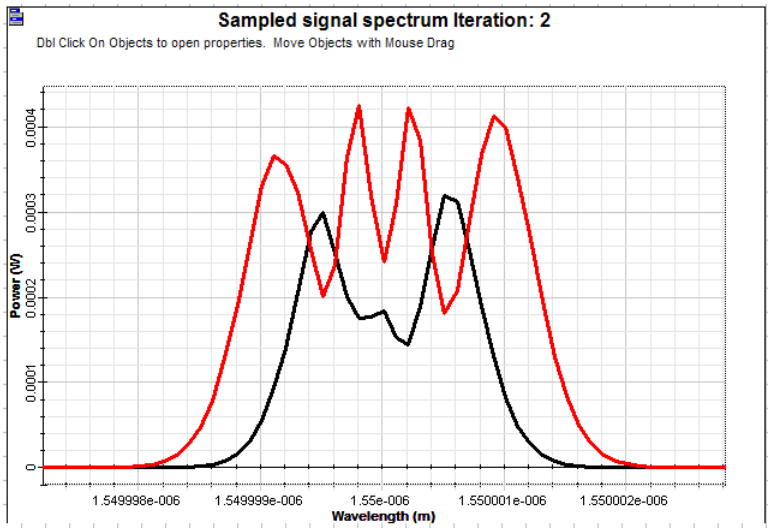


Figure 7-50: Comparision of results for the spectrum of the amplified pulses



Obtained spectrum for the complete gain recovery example exhibits the shape that is very similar to the case of pulse propagation in a medium with Kerr nonlinearity [2]. These spectrum show the concept of gain saturation induced self-phase modulation [1]. Note that such kinds of spectrum are possible only in the case of pulses longer than the carrier lifetime.

References:

[1] G.P. Agrawal and N.A. Olsson, “Self-phase modulation and spectral broadening of optical pulses in semiconductor laser amplifiers”, IEEE Journal of Quantum electronics, vol. 25, pp.2297-2306, 1989.

[2] G.P. Agrawal, *Nonlinear Fiber optics*, third edition, Academic Press, 2001.

Notes:

SLA Gain Saturation of Chirped and Super Gaussian Pulses

SLA gain saturation of chirped and super-gaussian pulses.osp

In this project we will study the effect of gain saturation induced self-phase modulation for the amplification of optical pulses. However, we will concentrate on the pulses with different shape and initial frequency shift. The chirped Gaussian input pulses are the pulses that are usually produced from directly modulated semiconductor laser.

We will consider the pulses with pulse width much shorter than the carrier lifetime. The carrier wavelength of the Gaussian pulse is 1.55 μm.

In the first part of this project we will consider chirped Gaussian pulses, and in the second part, the super Gaussian pulses.

Saturation of amplification of chirped Gaussian pulse

For the default values of physical parameters of SOA, we obtain the following values of the parameters:

Carrier lifetime τ_C ~ 1.4 ns

Saturation energy E_{sat} ~ 3.7 pJ

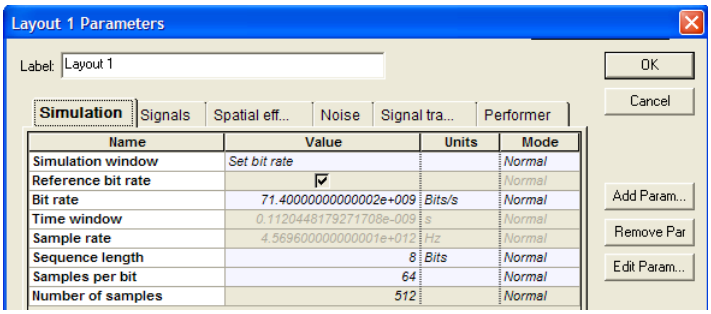
Amplification factor G_0 = 29 dB.

Note that as a typical value of the linewidth enhancement factor, α = 5 is chosen.

Gaussian pulse with the parameters: Energy E_0 ~ 0.73 pJ, T_{FWHM} = 14 ps -> P ~ 50 mW and the Chirp linewidth enhancement factor of 5 is considered.

To get the required carrier wavelength and power the parameters of the chirped and super optical Gaussian pulse generators have been fixed. To get chirped and super Gaussian pulse with desired T_{FWHM} = 14 ps, the global parameters have been chosen as shown in Table 7-2.

Table 7-2: Global parameters

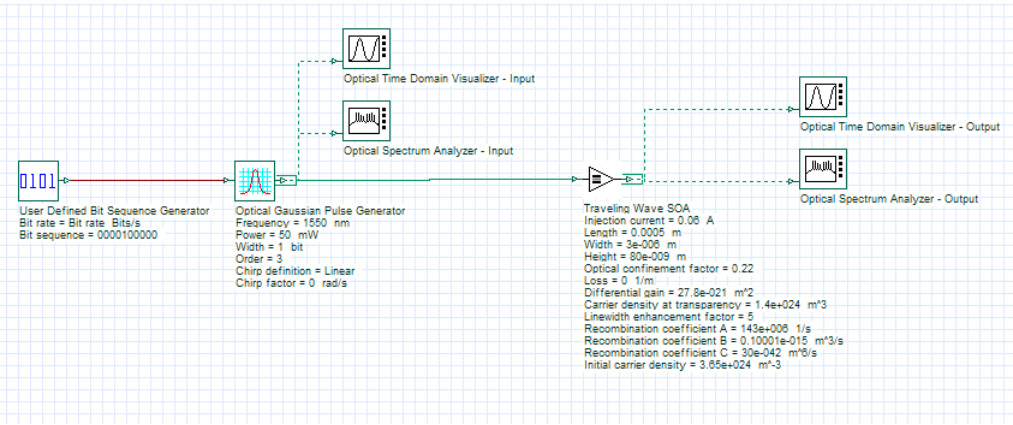


Name	Value	Units	Mode
Simulation window	Set bit rate		Normal
Reference bit rate	☑		Normal
Bit rate	71.40000000000002e+009	Bits/s	Normal
Time window	0.1120448179271708e-009	s	Normal
Sample rate	4.569600000000001e+012	Hz	Normal
Sequence length	8	Bits	Normal
Samples per bit	64		Normal
Number of samples	512		Normal

As a result, we get, $T_0 / \tau_C \sim 0.006$ and $E_0 / E_{sat} \sim 0.2$. According to the first ratio the input pulse width is much smaller than the carrier lifetime. The meaning of the second one is that pulse energy is comparable with the SOA saturation energy.

The project in which the amplification of the Gaussian pulse with SOA will be analyzed is shown in Figure 7-51.

Figure 7-51: Layout - SLA gain saturation of chirped and super Gaussian pulses



The shape and spectrum of the initial chirped Gaussian pulse are shown in Figure 7-52 and Figure 7-53. Note that the initial negative chirp is also shown in Figure 7-52.

Figure 7-52: Shape of the initial chirped Gaussian pulse

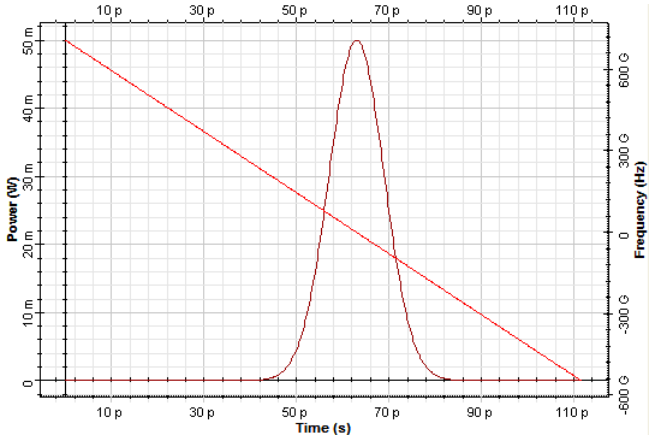
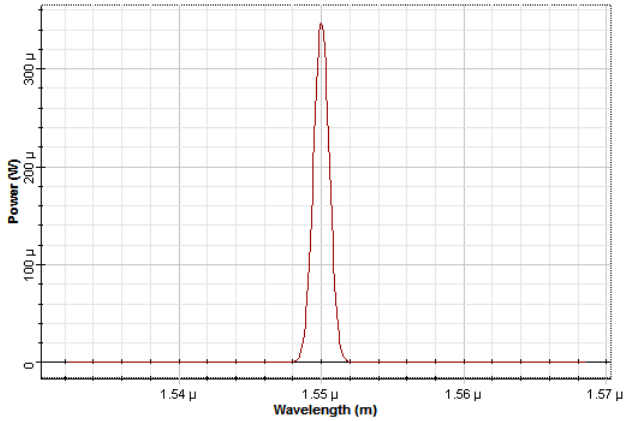


Figure 7-53: Spectrum of the initial chirped Gaussian pulse



Note that the frequency in Figure 7-52 decreases with time across the pulse, and this is usually referred to as negative chirp.

Figure 7-54 and Figure 7-55 show the shape and spectrum of the amplified chirped pulse.

Figure 7-54: Shape of the amplified chirped pulse

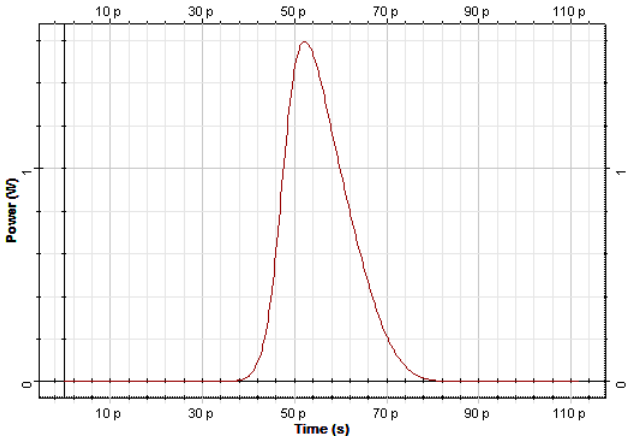


Figure 7-55: Spectrum of the amplified chirped pulse

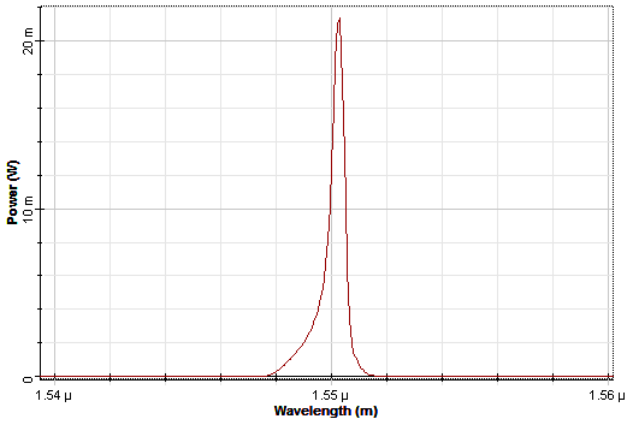


Figure 7-54 reveals already expected sharpening of the leading edge. Note the different form of the output pulse spectrum and the reduced red shift in comparison with the amplified Gaussian pulse.

In Figure 7-56, phase of the pulse after amplification is shown together with its shape. In Figure 7-57, the deformation of the initial negative chirp after amplification can be easily seen.

Figure 7-56: Shape and phase of the pulse after amplification

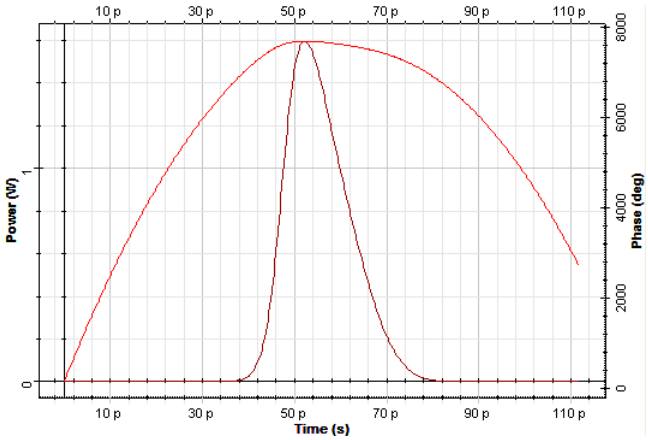
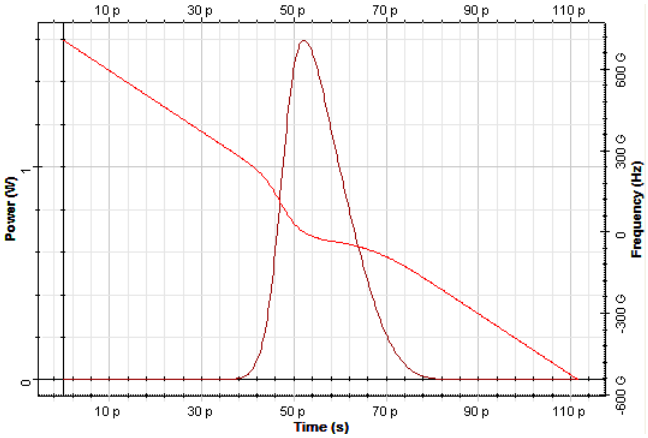


Figure 7-57: Deformation of the initial negative chirp after amplification



For negative initial chirp, the gain saturation induced red shift reduces. For the opposite sign of initial chirp the spectrum shifts even more to the red side than for the case of zero initial chirp.

Saturation of amplification of super-Gaussian pulse

The additional pulse parameter which is considered for the super Gaussian pulse is m = 3 (Note that the pulse now will be without initial chirp).

The shape and spectrum of the initial super Gaussian pulse are shown in Figure 7-58 and Figure 7-59.

Figure 7-58: Shape of the initial super Gaussian pulse

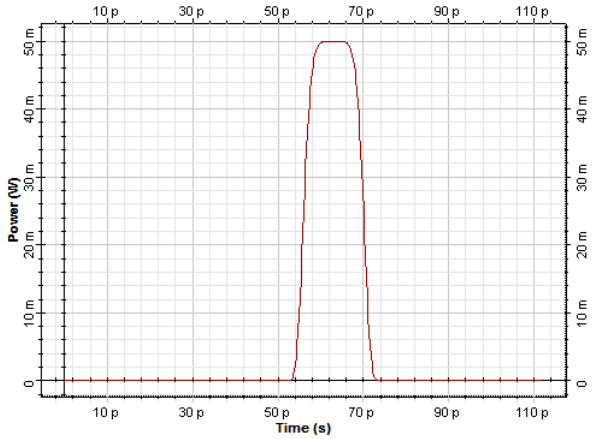


Figure 7-59: Spectrum of the initial super Gaussian pulse

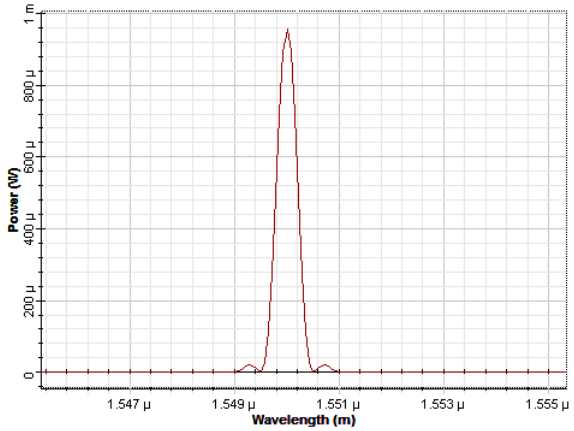


Figure 7-60 and Figure 7-61 show the shape and spectrum of the amplified super Gaussian pulse.

Figure 7-60: Shape of the amplified super Gaussian pulse

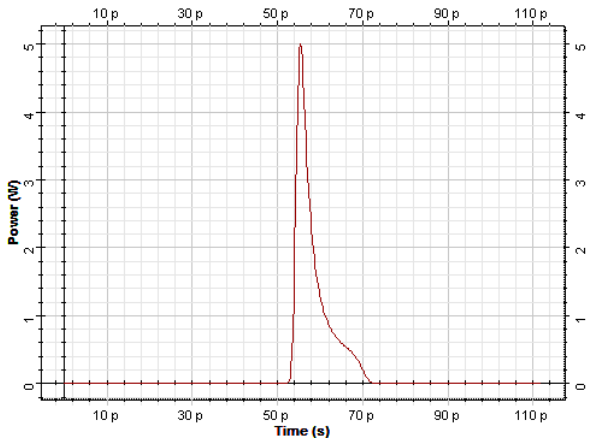
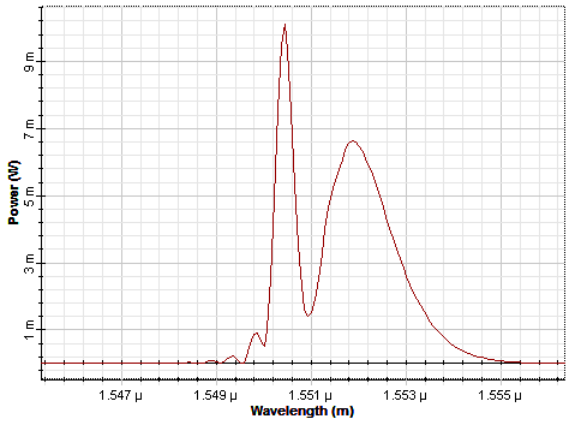


Figure 7-61: Spectrum of the amplified super Gaussian pulse



The output pulse has a long tail on the trailing edge and appears to be narrower than the input pulse. The situation is very different from the case of amplification of Gaussian pulse where the T_{FWHM} of the output pulse was larger than the input one.

The spectrum of the output spectrum has a multi-peak structure and very well expressed red shift. Comparison of this spectrum with the one of the amplified Gaussian pulse shows a clear difference. Therefore the form of the spectrum and amount of the red shift strongly depends on the initial pulse shape.

In Figure 7-62, phase of the pulse after amplification is shown together with its shape. In Figure 7-63, the formation of the chirp after amplification can be easily seen.

Figure 7-62: Shape and phase of the pulse after amplification

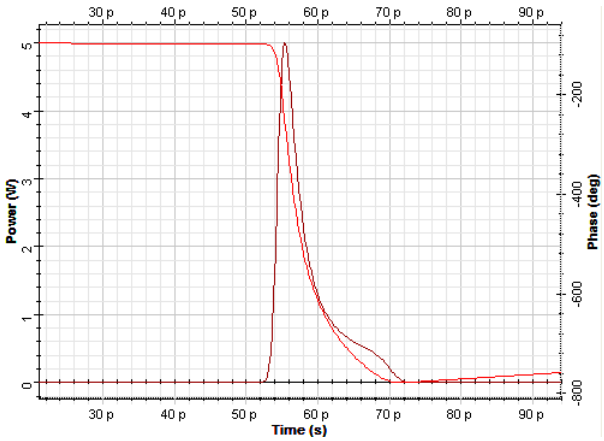
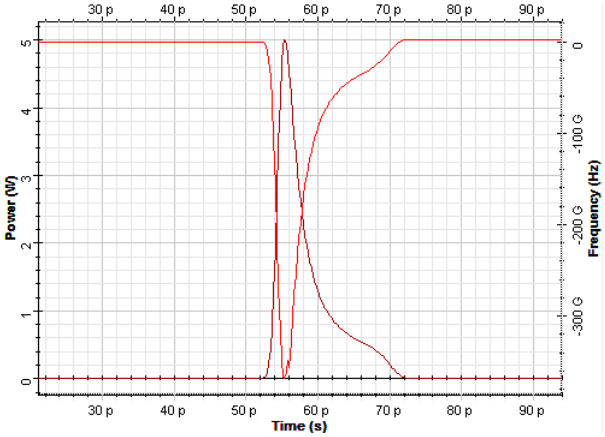


Figure 7-63: Formation of the chirp after amplification



In this project we described the basic properties of the chirped and super Gaussian pulse amplification with SOA component in OptiSystem software. We have shown that the shape and spectrum distortions with the amplification of SOA strongly depends on the shape and initial frequency modulation of the pulse. These properties can be very important in the case when pulses produced by directly modulated semiconductor lasers are amplified.

The obtained results are in complete agreement with results published in [1] and [2]:

References:

[1] G.P. Agrawal and N.A. Olsson, “Self-phase modulation and spectral broadening of optical pulses in semiconductor laser amplifiers”, IEEE Journal of Quantum electronics, vol. 25, pp.2297-2306, 1989.

[2] G.P. Agrawal, *Fiber-Optic Communication Systems*, 4th ed., John Wiley & Sons, INC., 2010.

SLA Gain Saturation of Gaussian Pulses

SLA gain saturation of Gaussian pulses.osp

SLA gain saturation of Gaussian pulses - Power.osp

SLA gain saturation of Gaussian pulses - Conf.osp

SLA gain saturation of Gaussian pulses - Loss.osp

Amplification of ultra-short optical pulses in SOA produces considerable spectral broadening and distortion due to the non-linear phenomenon of self-phase modulation. The physical mechanism behind SPM is gain saturation, which leads to intensity dependent changes of refractive index in response to variations in carrier density. Signal-gain saturation in SOA is caused by a reduction of the population inversion in the active layer due to an increase in stimulated emission. Gain saturation characteristics are especially important in optical repeaters and multi-channel amplifiers which require high-power operation.

In this project the effect of gain saturation induced self-phase modulation on the amplification of Gaussian pulse will be considered. We will consider the pulses with pulse width much shorter than the carrier lifetime. The carrier wavelength of the Gaussian pulse is 1.55 μm.

For these default values of physical parameters of SOA we obtain the following values of parameters:

The carrier lifetime τ_C ~ 1.4 ns

The saturation energy E_{sat} ~ 3.7 pJ

The amplification factor G_0 = 29 dB.

As a typical value of the linewidth enhancement factor, α = 5 is chosen. Note that we have chosen the internal losses to be zero. Such choice allows a comparison to be done with existing analytical solution (see the referred paper at the end of this section). We will also analyze the influence of the internal losses.

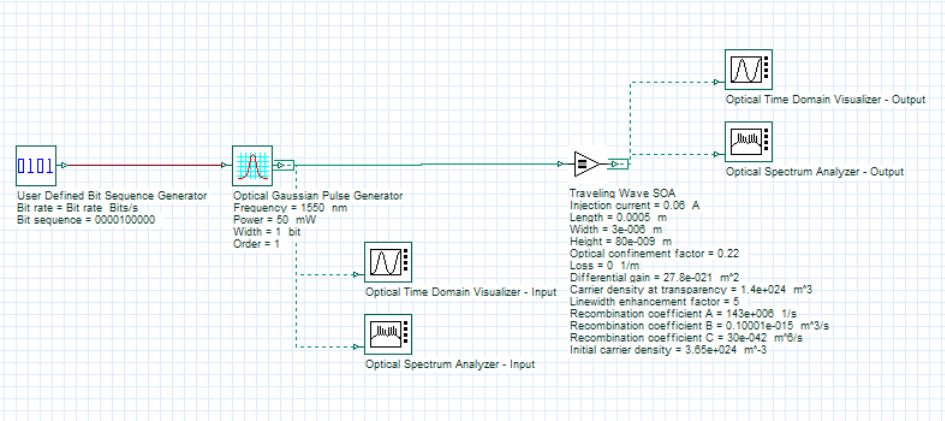
Gaussian pulse with following parameters is considered: Energy E_0 ~ 0.73 pJ, T_{FWHM} = 14 ps, and P ~ 50 mW. Note the large value of the pulse initial power. It allows in a best way to demonstrate the basic qualitative features of gain saturation induced properties of the pulse amplification. The influence of the value of the pulse initial power will be considered later in this section.

The global parameters have been chosen to get a Gaussian pulse with desired T_{FWHM} = 14 ps. As a result we get T_0 / τ_C ~ 0.006 and E_0 / E_{sat} ~ 0.2.

According to the first ratio the input pulse width is much smaller than the carrier lifetime. The meaning of the second one is that pulse energy is comparable with the SOA saturation energy.

The project layout for amplification of the Gaussian pulse with SOA is shown in Figure 7-64.

Figure 7-64: Layout - SLA gain saturation of Gaussian pulses



To illustrate the appearance of the gain saturation induced effects first we will show the amplification of very weak pulse. The shape and spectrum of the weak Gaussian pulse are shown in Figure 7-65 and Figure 7-66.

Figure 7-65: Shape of the weak Gaussian pulse

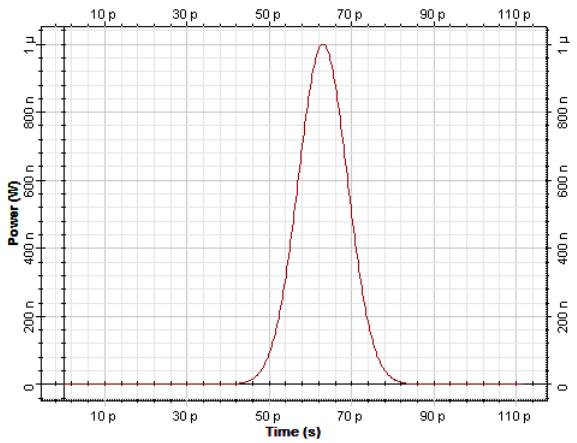


Figure 7-66: Spectrum of the weak Gaussian pulse

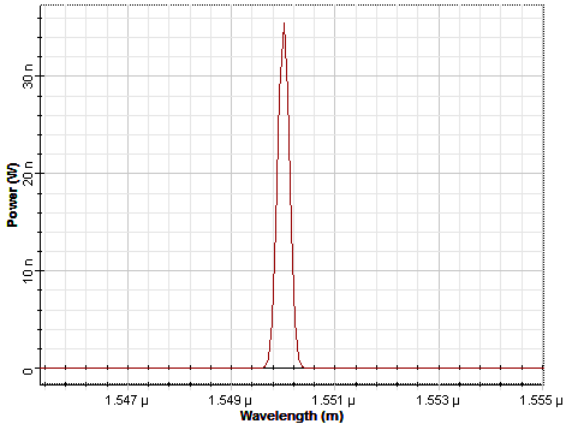


Figure 7-67 and Figure 7-68 show the shape and spectrum of the amplified weak pulse.

Figure 7-67: Shape of the amplified weak pulse

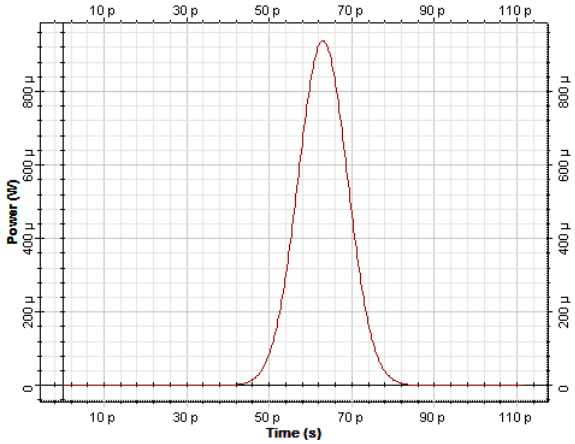
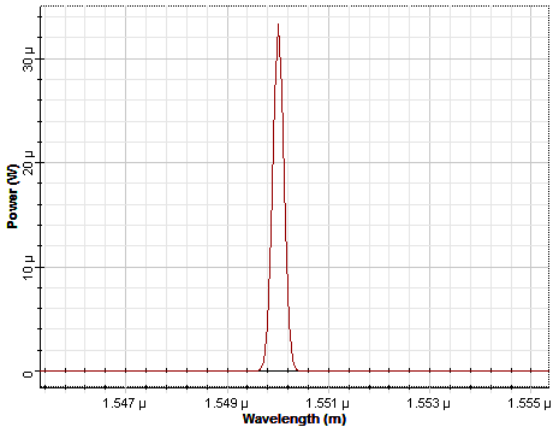


Figure 7-68: Spectrum of the amplified weak pulse



Comparison of the above figures shows that the pulse is amplified in unsaturated region. No qualitative changes in the spectrum of the amplified pulse could be observed.

Figure 7-69 and Figure 7-70 show the shape and spectrum of the initial Gaussian pulse, which will be amplified in saturation region.

Figure 7-69: Shape of the initial Gaussian pulse

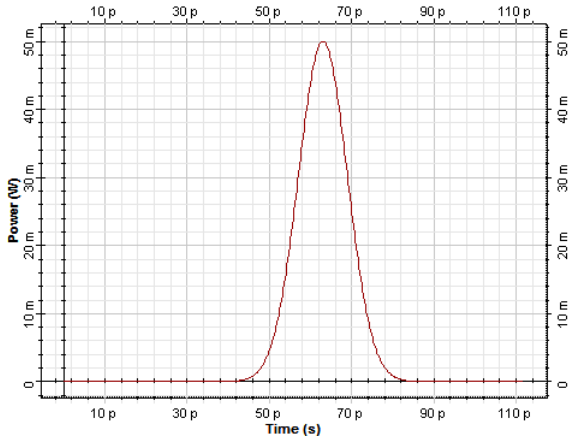


Figure 7-70: Spectrum of the initial Gaussian pulse

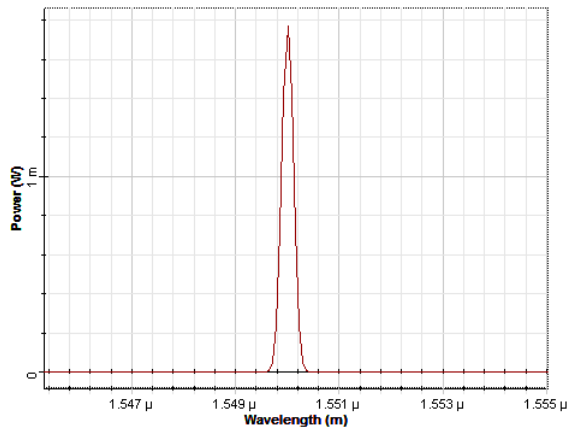


Figure 7-71 and Figure 7-72 show the shape and spectrum of the amplified pulse.

Figure 7-71: Shape of the amplified pulse

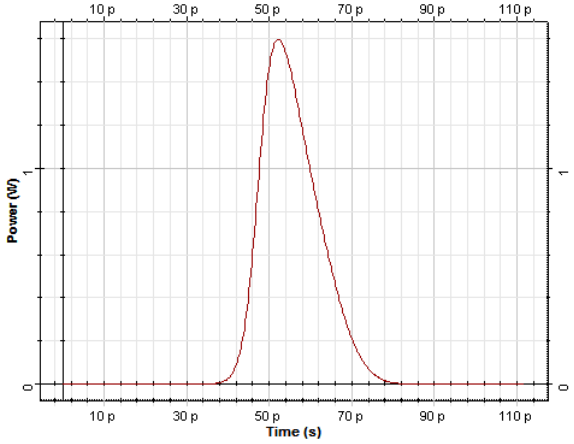


Figure 7-72: Spectrum of the amplified pulse

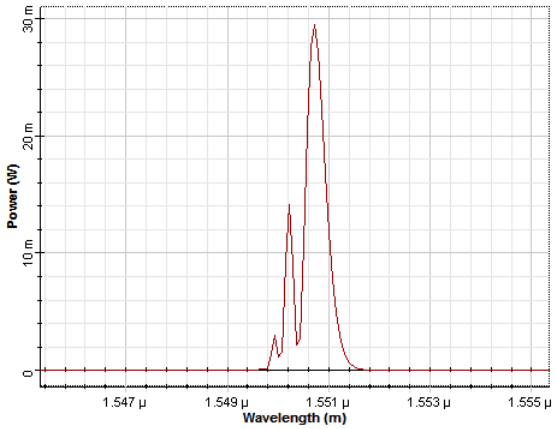


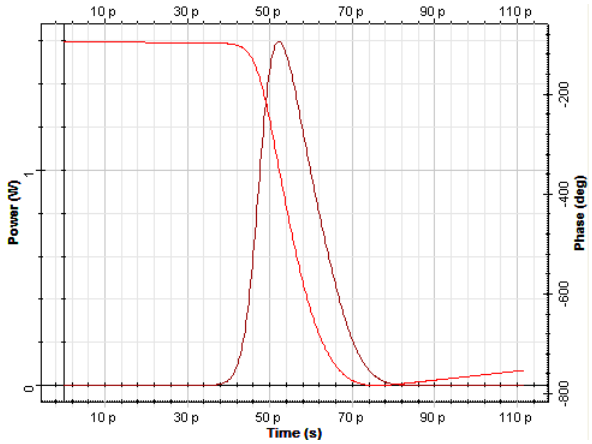
Figure 7-71 reveals that the amplified pulse becomes asymmetric so that its leading part is sharper compared with the trailing edge. Note that sharpening of the leading edge is a common feature of all amplifiers.

The pulse spectrum of the amplified pulse, however, reveals features that are particular for the SOA.

The spectrum develops a multi-peak structure and the dominant peaks shift toward longer (red) wavelengths. This red shift increases with the increase of the amplification factor. The red shift observed from this figure is ~ 0.001 μm (~ 120 GHz).

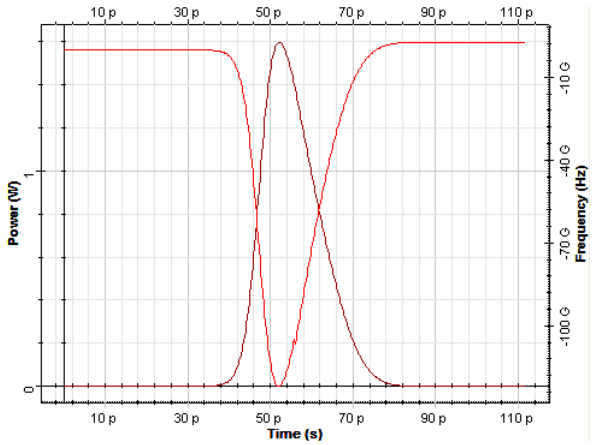
In Figure 7-73, the phase of the pulse after amplification is shown together with its shape. The important characteristic that has to be mentioned is that the phase follows the time evolution of the gain. We see that for such short pulse, gain has no time to recover (remember $T_0 / \tau_C \sim 0.006$).

Figure 7-73: Phase and shape of the pulse after amplification



In Figure 7-74, the gain saturation induced chirp across the pulse is shown together with its shape. Note that the initial Gaussian pulse was unchirped.

Figure 7-74: Gain saturation induced chirp across the pulse



The gain saturation induced chirp is negative across the entire pulse, therefore the instantaneous frequency is down shifted (the red shift) from the incident frequency. Nevertheless because of the fact that induced chirp increases towards the trailing part of the pulse, such chirp is known as positive one. From the theory of propagation of phase modulated pulses in the medium with group velocity dispersion [3], it follows that appearance of positive chirp can be used for pulse compression in the medium with anomalous group velocity dispersion. Let us now consistently analyze the influence of the initial power, optical confinement factor and inner losses on the observed properties. Note that in model used in [1,2], the inner losses have been neglected.

First we will see how the shape and spectrum of the amplified Gaussian pulse (for the same pulse and SOA parameters as above) change as a function of the initial pulse power. The values of the initial power considered are P = 5, 10, 20, 30, and 50 mW. In the first case we consider $E_0 / E_{sat} \sim 0.02$.

To get these results, mode sweep can be used.

In Figure 7-75 and Figure 7-76**,** the shape and spectrum of the amplified Gaussian pulse are shown for different initial powers.

Figure 7-75: Shape of the amplified Gaussian pulse for different initial powers

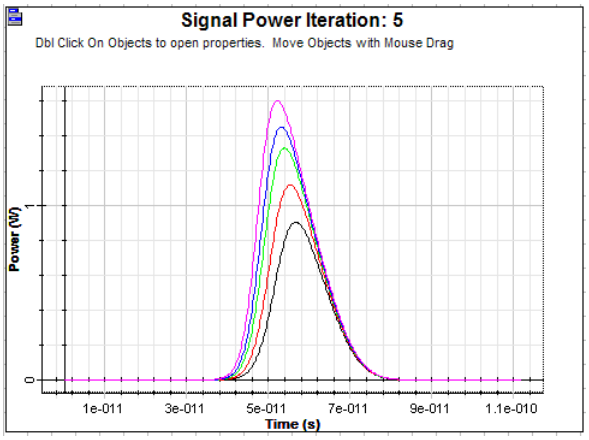
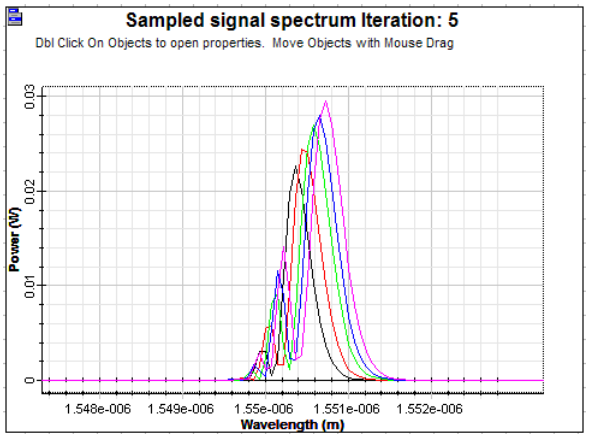


Figure 7-76: Spectrum of the amplified Gaussian pulse for different initial powers



As we could expect increasing the ratio E_0 / E_{sat} (for fixed pulse width) leads to increase in the number of the peaks in the spectrum along with the increase of the red shift.

In Figure 7-77 and Figure 7-78**,** the shape and spectrum of the amplified Gaussian pulse (for the same pulse and SOA parameters as above) are shown as a function of the optical confinement factor. The values of optical confinement factor considered are Γ = 0.1, 0.2, 0.3, 0.4 and 0.5.

Figure 7-77: Shape of the amplified Gaussian pulse (for the same pulse and SOA parameters as above) as a function of the optical confinement factor

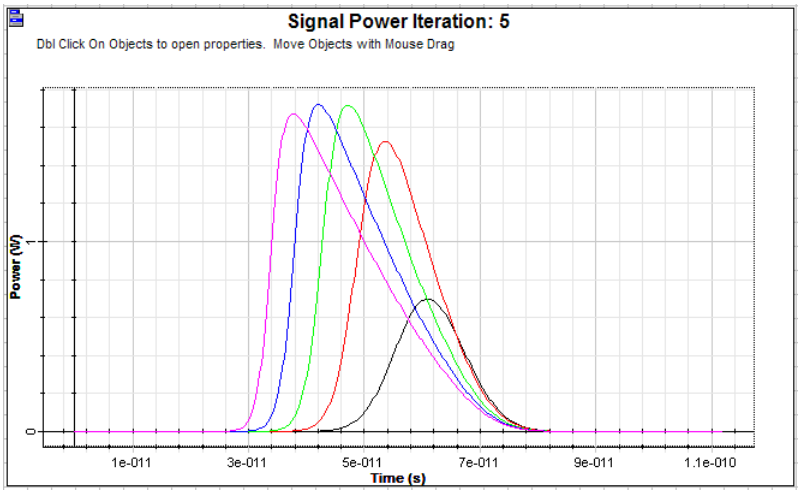
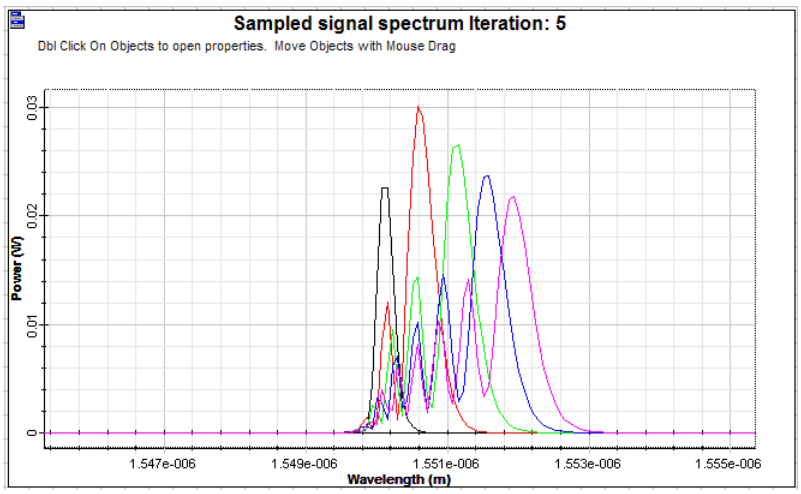


Figure 7-78: Spectrum of the amplified Gaussian pulse (for the same pulse and SOA parameters as above) as a function of the optical confinement factor



As we see the optical confinement factor influences the pulse spectrum and shape.

Figure 7-79 and Figure 7-80 show the shape and spectrum of the amplified Gaussian pulse (for the same pulse and SOA parameters as above) as a function of the internal losses. The values of internal losses considered are α_{int} = 0, 1000, 2000, 3000 and 4000 (1/m).

Figure 7-79: Shape of the amplified Gaussian pulse (for the same pulse and SOA parameters as above) as a function of the internal losses

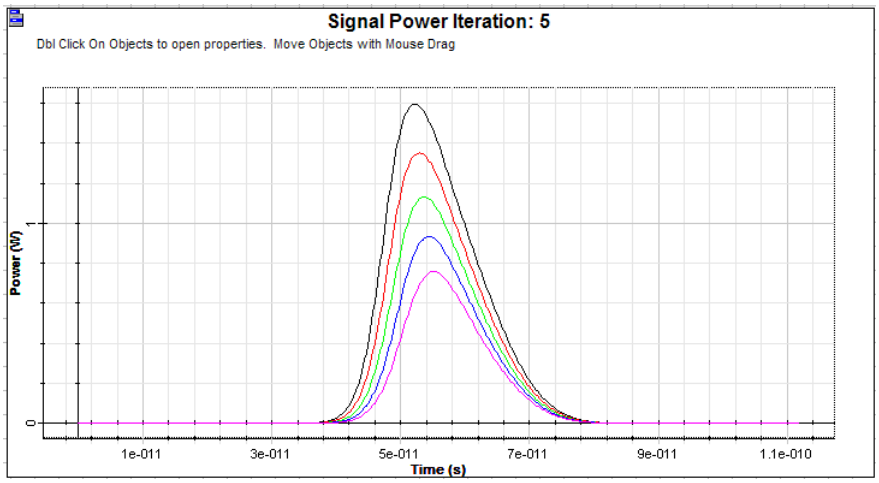
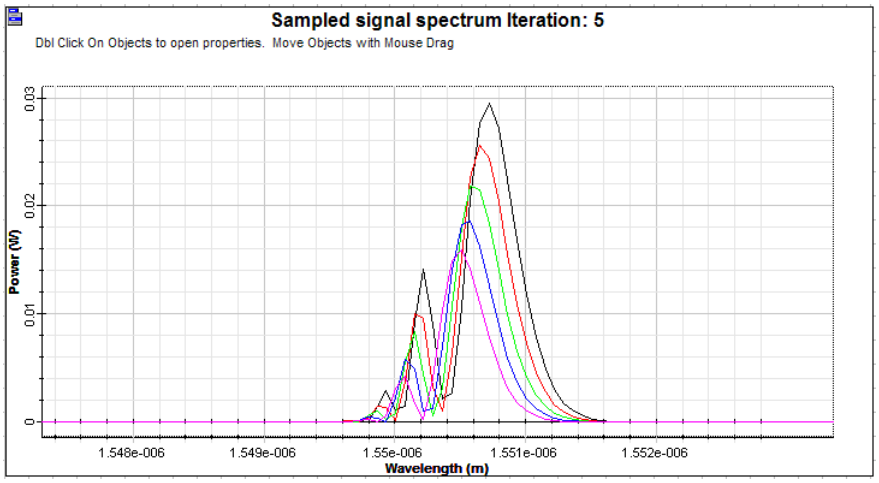


Figure 7-80: Spectrum of the amplified Gaussian pulse (for the same pulse and SOA parameters as above) as a function of the internal losses



As we can see, in contrast to the optical confinement factor, the internal losses do not influence the pulse spectrum and shape.

References:

[1] G.P. Agrawal and N.A. Olsson, “Self_phase modulation and spectral broadening of optical pulses in semiconductor laser amplifiers”, IEEE Journal of Quantum electronics, vol. 25, pp.2297-2306, 1989.

[2] G.P. Agrawal, *Fiber-Optic Communication Systems*, 4th ed., John Wiley & Sons, INC., 2010.

[3] G.P. Agrawal, *Nonlinear Fiber Optics*, third edition, Academic Press, 2001.

Notes:

Raman Gain and Bandwidth

Forward-Backward Raman amplification.osp

Project file "*Forward-Backward Raman amplification.osp*" demonstrates forward and backward Raman amplification in a 16-channel WDM system. This project file includes two configurations in the same project: one with forward pump and one with backward pump. 16 channels in 191 ~ 195.5 THz band, separated with 3 GHz are multiplexed and sent to Raman amplifier. The frequency difference between stokes and pump beam (Stokes shift) is important in SRS process. The Raman gain coefficient scales linearly with pump frequency. Maximum gain is obtained when the Stokes shift is about 13.2 THz. This example shows that, a relatively flat and high gain can be obtained when the frequency of the pump signal is about 206.75 THz, in which case the Stokes shift is about 13.3 THz for the center channel. In fact, signal frequency can differ from pump frequency up to 20 THz. You can experiment how the value of Stokes shift affects the gain by changing the frequency of the pump signal. Overall optical gain is a function of signal frequency and pump intensity (pump power divided by effective area of the fiber). To test this, you can change the effective area of the fiber or the pump signal power.

Notes:

Raman Gain Saturation

Forward-Backward Raman gain saturation.osp

Project file "*Forward-Backward Raman gain saturation.osp*" demonstrates the gain saturation due to pump depletion in forward and backward pumped Raman amplifier in a 4-channel WDM system. In Raman amplifier, since the pump supplies energy for signal amplification, it begins to deplete as the signal power increases. A decrease in the pump power reduces the optical gain. This reduction in the gain is referred to as gain saturation. In this example, we see how the gain saturation differs depending on forward or backward pump configuration. You can see this by clicking on results table for both cases and comparing them.

Notes:

Broadband Flat Gain Raman Amplifier

Broadband flat gain Raman amplifier.osp

The characteristics of the stimulated Raman scattering effect allow for an interesting new technique for gain flattening of broadband Raman amplifiers. Project file "*Broadband flat gain Raman amplifier.osp*" demonstrates that multi-pump can be used to flatten the Raman amplifier gain in a broad band. In this example, several pumps are arranged in 90 nm broad spectral range and they are used to pump in 100 km of SMF-28 in backward direction. This gain flattening technique requires only a suitable multiple-pump configuration and does not rely on any passive gain equalizing optics. The key feature of this technique is the proper choice of number of pumps, pump wavelengths, and pump powers. You can experiment by altering the power distribution and wavelengths of the pumps.

Notes:

Pumping Requirements

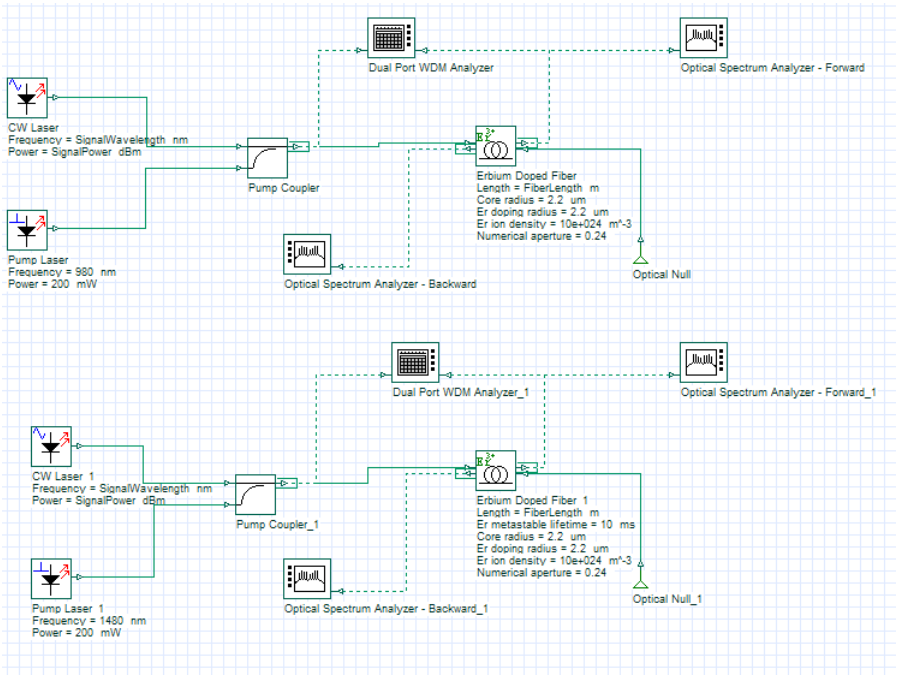
Pumping requirements - Co-propagating.osp

Pumping requirements - Counter-propagating.osp

Pumping requirements - Bidirectional.osp

The amplifier performance characterized by the signal output power, gain and noise figure depends on the pump wavelength. The project file "*Pumping requirements - Co-propagating.osp*" (Figure 7-81) shows two different configurations, "Pump @ 980 nm" and "Pump @ 1480 nm". The 980 nm and 1480 nm pump wavelengths are the most important ones to be used in EDFAs.

Figure 7-81: Layout - Pumping requirements - Co-propagating

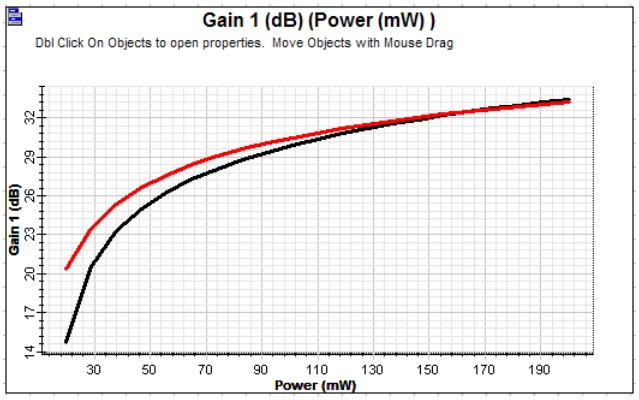


High amplifier gains in the range of 30 ~ 35 dB can be obtained in this project file by sweeping the pump power from 10 mW to 200 mW. The signal input power considered in this case is -20 dBm. Results obtained with these versions are shown in Figure 7-82.

EDFAs can be designed to operate in such a way that the pump and signal beams propagate in opposite directions, a configuration referred to as backward pumping to distinguish it from forward-pumping configuration in which both beams propagate along the same direction. Backward or counter-propagating pump scheme is discussed in the project "*Pumping requirements - Counter-*

propagating.osp". The pump power is swept from 10 to 150 mW with the signal input power kept to be -20 dBm.

Figure 7-82: Gain vs. pump power considering a co-propagating pump schemes @ 980 nm (black) and @ 1480 nm(red) pump wavelength



The layout considering backward or counter-propagating pump scheme is shown in Figure 7-83. Figure 7-84 shows the gain versus pump power when 980 nm and 1480 nm are considered as pump wavelength. The influence of the selected pump scheme on the amplifier performance can be seen by considering unsaturated or saturated regime by just changing the signal input power range.

Figure 7-83: Layout of pumping requirements - counter-propagation

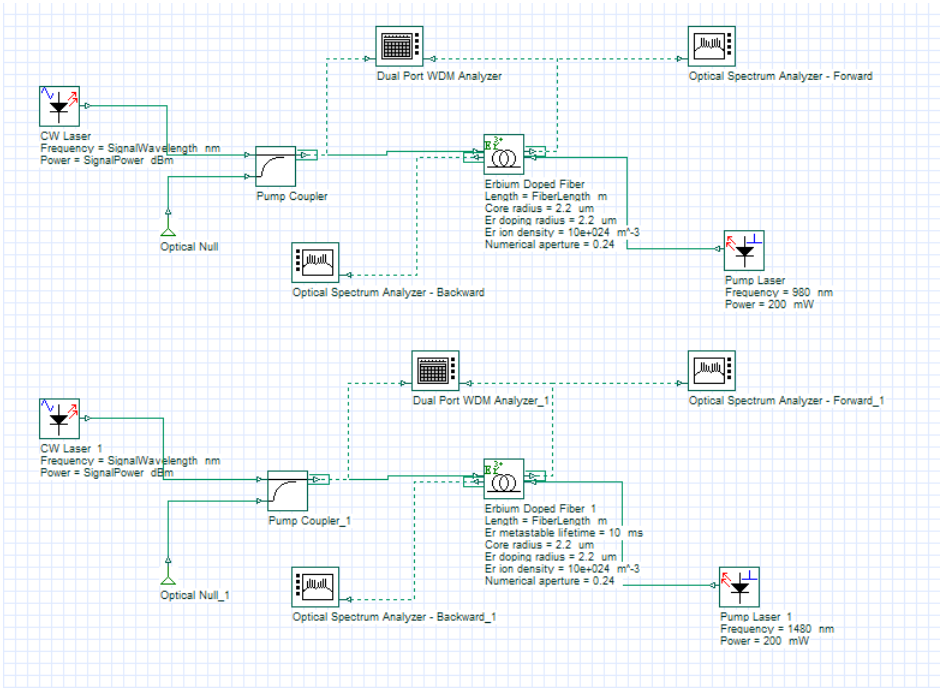
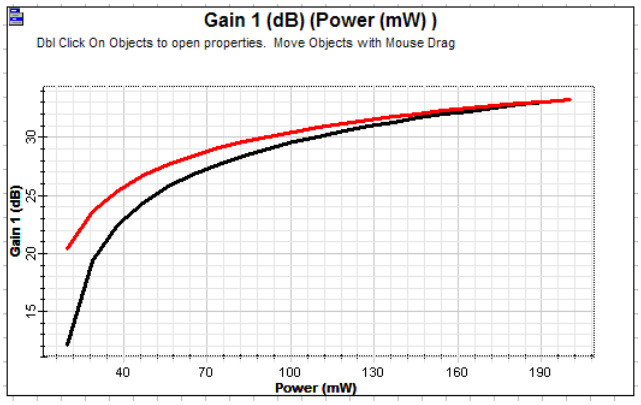


Figure 7-84: Gain vs. pump power considering a counter-propagating pump schemes @ 980 nm (black) and @ 1480 nm (red) pump wavelength



The project "Pumping requirements - Bidirectional.osp" considers the bidirectional pumping configuration, where the amplifier is pumped in both directions simultaneously by using semiconductor pump lasers located at the two fiber ends. The advantage of this pump scheme can be checked by setting small-signal or large-signal input and observing the amplifier performance.

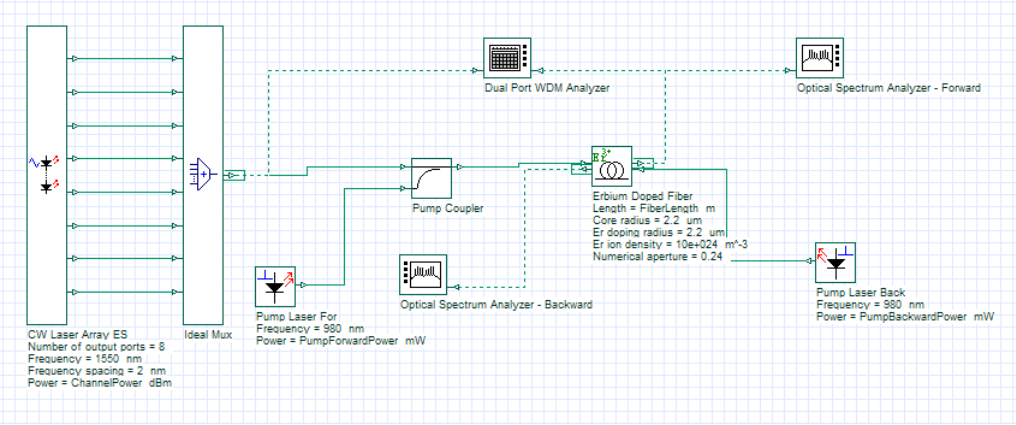
Notes:

Multichannel Amplification

Multichannel amplification.osp

EDFA performance is evaluated considering multiple signal input. The amplifier is setup in a bidirectional pump scheme, as shown in Figure 7-85.

Figure 7-85: Layout - Multichannel amplification



In the project, the amplifier is setup in a bidirectional pump scheme that enables extending the analysis to co-propagating or counter-propagating pump schemes.

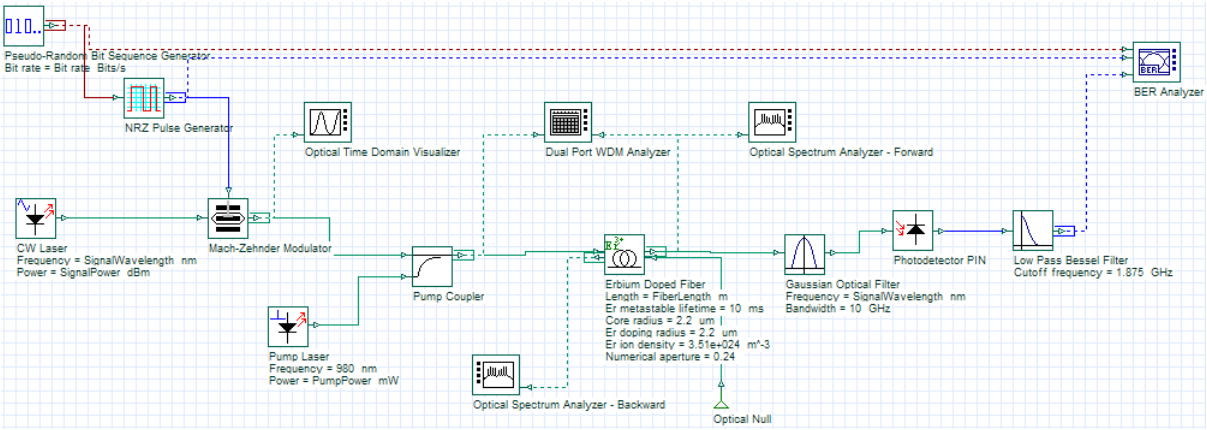
Notes:

Optical Preamplifiers

Preamplifier system.osp

The performance of a preamplifier positioned at the receiver input is evaluated in the project "*Preamplifier system.osp*" (Figure 7-86). Characteristics of noise, gain and the improvement in the sensitivity of the photodetector/receiver can be analyzed.

Figure 7-86: Layout - Preamplifier system

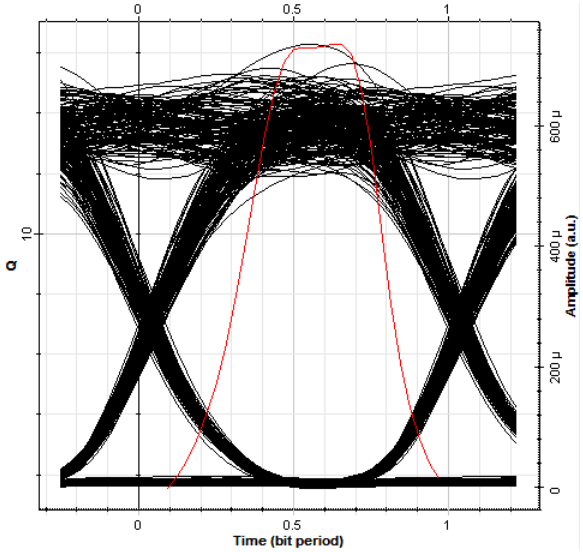


A modulated signal is coupled to the EDFA preamplifier and the corresponding characteristics are displayed on Dual Port WDM Analyzer by double clicking on this visualizer.

The direct-detected signal on the receiver is pre- and post- filtered and the BER is evaluated through the BER Analyzer. The eye diagram is shown in Figure 7-87.

The amplifier performance will affect the eye diagram observed at the BER Analyzer. Input conditions, such as signal wavelength, signal and pump power, and fiber length specifications will affect the amplifier performance when being modified.

Figure 7-87: Eye diagram



Power Boosters

Booster system.osp

Booster amplifiers are usually positioned at the transmitter output or for amplifying the multiple outputs of nodes in broadcast networks.The project "*Booster system.osp*" (Figure 7-88) presents the characteristics of a booster amplifier positioned at the transmitter output.

Two different types of modulation are considered in this project: direct and external modulation. In the first case, the electrical signal is directly modulated on the signal laser. The other option uses an electroabsorption modulator to modulate the signal source laser. Both schemes can be observed by coupling the modulated signal to the EDFA and evaluating the obtained results.

Figure 7-89 and Figure 7-90 show the eye diagram obtained after detecting the signal using direct modulation and external modulation, respectively.

Figure 7-88: Layout - Booster system

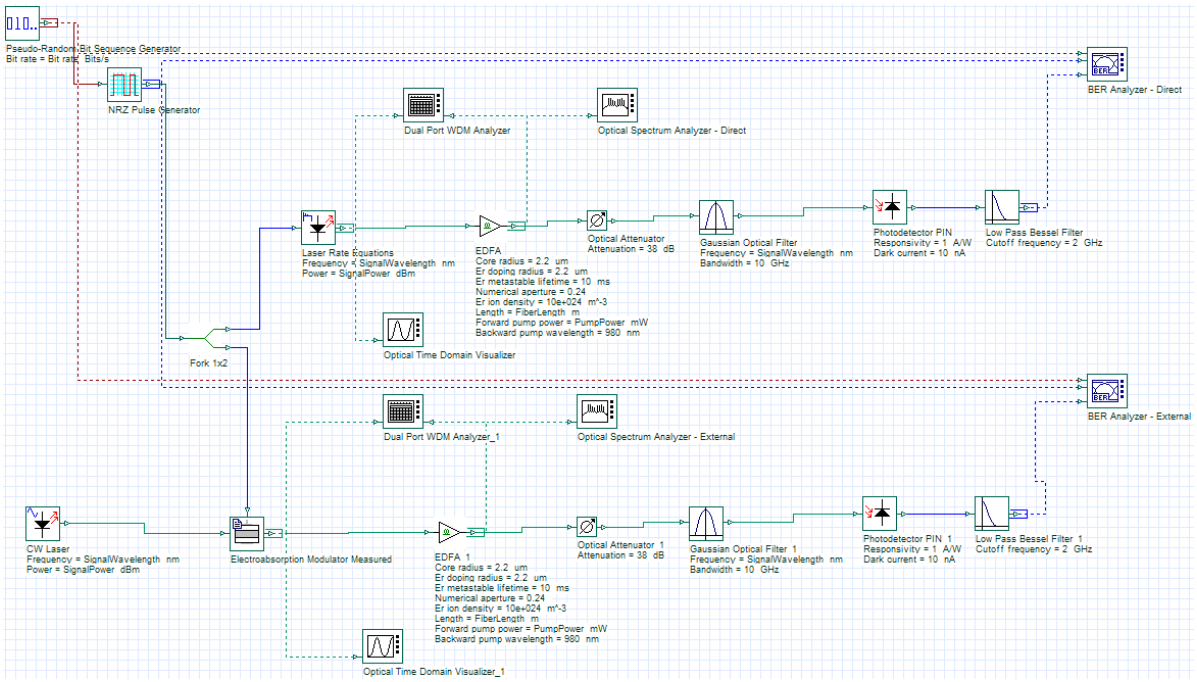


Figure 7-89: Eye diagram observed after detecting the signal using direct modulation

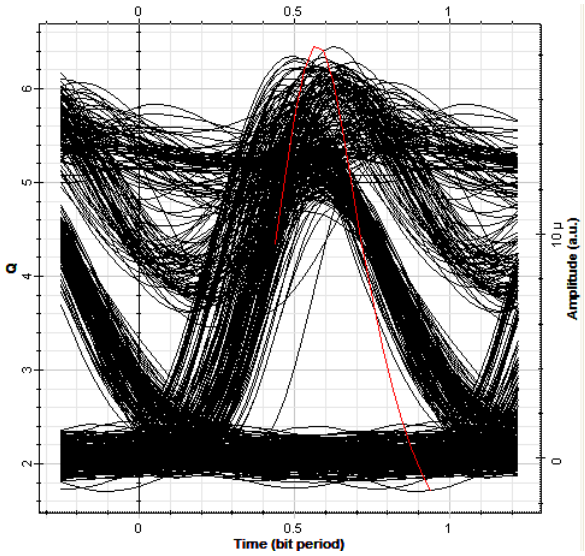
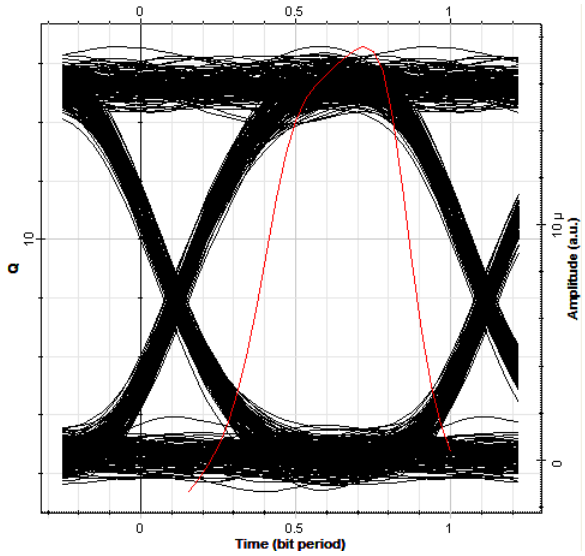


Figure 7-90: Eye diagram observed after detecting the signal using external modulation



Metro EDFA

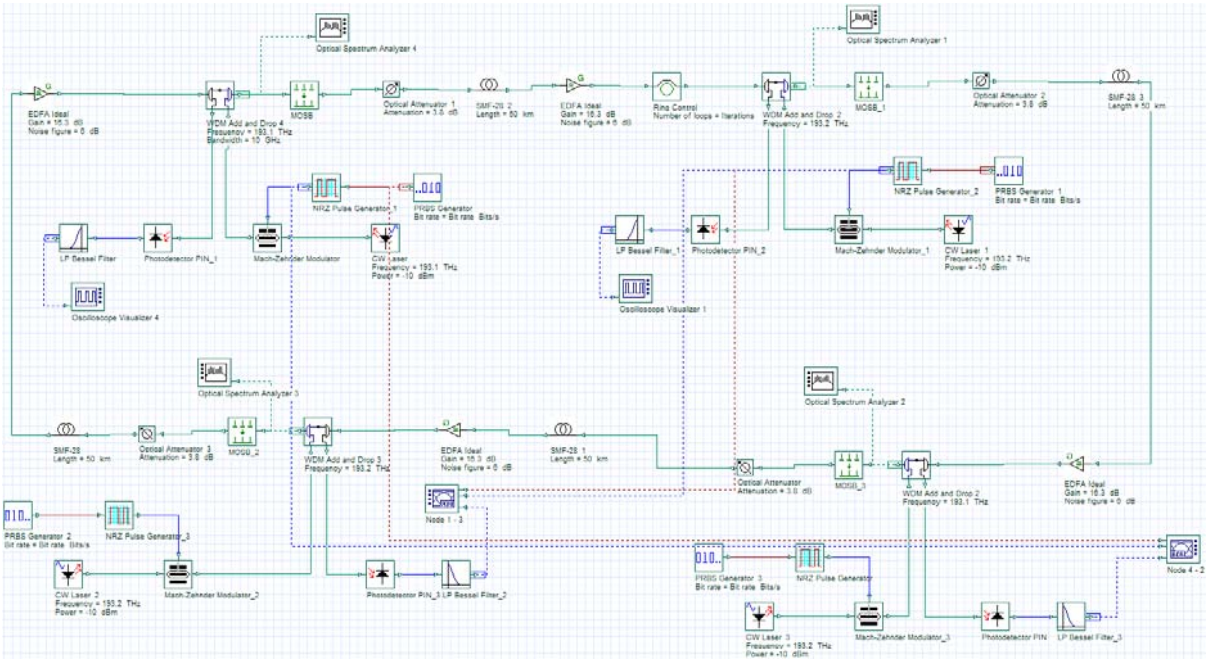
Metro EDFA.osp

This example "*Metro EDFA.osp*" illustrates EDFAs included in a four nodes network setup in a ring topology where Node 1 communicates with Node 3 at 193.2 THz, and Node 2 communicates with Node 4 at 193.1 THz. Add-drop components enable the selective signal input/output in each node. Ideal amplifiers are included in these simulations. Subsystems like this can be found in metropolitan area networks. Figure 7-91 shows the layout used to evaluate the amplifier performance in a metropolitan network.

The component Ring Control determines the number of loops considered in the two nodes connected in a ring topology. The signal output and bit error rate are visualized in the Optical Spectrum Analyzer and BER Analyzer for different loops where signal index 0 refers to the first turn in the loop and 1 is related to the second turn in the loop.

The signal going through Node 1 to Node 3 on channel 1 at 193.2 THz as well as the communication between Node 2 and Node 4 at 193.1 THz can be observed using different visualizers inserted in the project file.

Figure 7-91: Layout - Metro EDFA



The amplified signal observed at the Node 3 output is shown in Figure 7-92. The eye diagram is shown in Figure 7-93.

Figure 7-92: Spectrum observed at OSA referring to the turn 1 in the loop

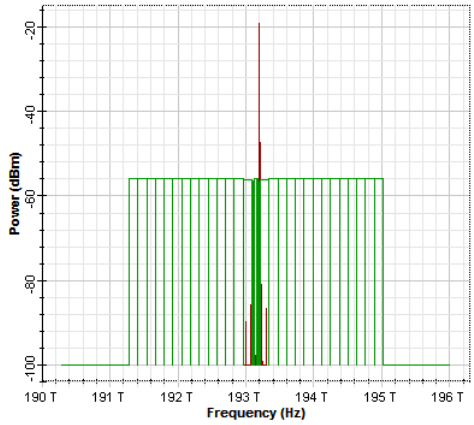
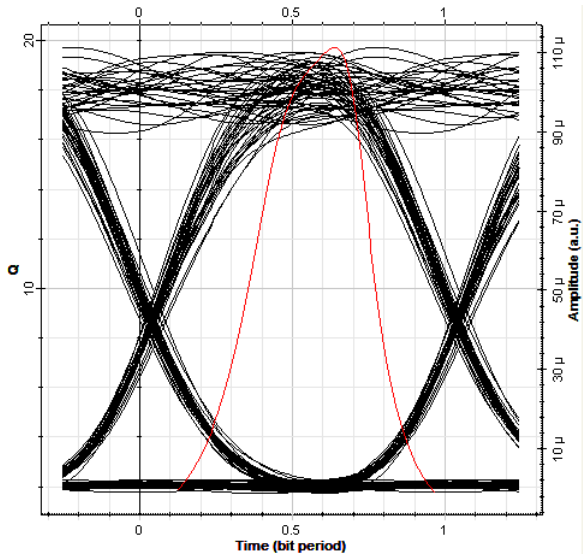


Figure 7-93: Eye diagram observed at the BER analyzer referring to the turn 1 in the loop



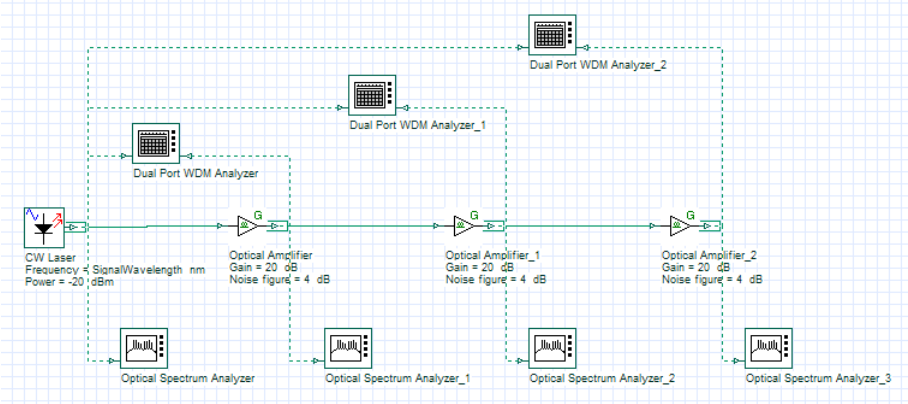
Cascaded In-Line Amplifiers

In-line cascade.osp

In the example "*In-line cascade.osp*", ideal amplifiers are cascaded to simulate the propagation of signal along the system. A signal laser source is coupled to the cascaded amplifiers and the amplifier performance can be evaluated.

The effective noise figure for this cascaded chain amplifier can be calculated after running the simulation. One can change the input signal power as well as gain and noise figure for each amplifier in the system. Figure 7-94 shows three ideal cascaded amplifiers at the output of a signal laser source. The Dual Port WDM Analyzer inserted in the layout enables checking the amplifier performance. The effective noise figure for a cascaded chain can be compared considering different amplifier gains and noise figures.

Figure 7-94: Layout - Cascaded in-line amplifiers



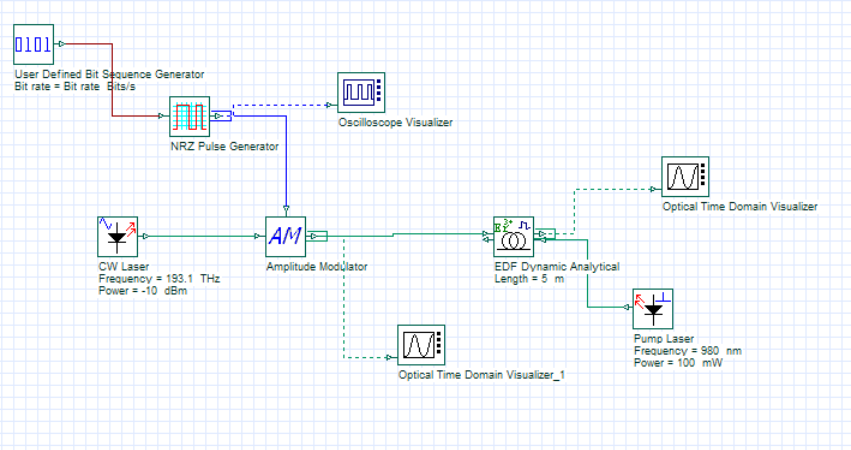
Notes:

EDFA Dynamic

EDFA dynamic.osp

In the example "*EDFA dynamic.osp*" (Figure 7-95) we simulate the function response of a C-band EDFA to a step excitation at a signal wavelength. The step function has a period of 1.0 ms, longer enough to enable the amplifier to achieve the steady-state solution. The pump power is constant over the time and is counter-propagating with relation to the signal. Power transients which occur in the amplifier can be studied as a function of the pump power and the signal power.

Figure 7-95: Layout - EDFA dynamic



The Optical Time Domain Visualizer enables the observation of power decay at the amplifier output.

The signal input coupled to the amplifier that enables dynamic analysis is shown in Figure 7-96, while the signal output is shown in Figure 7-97.

Figure 7-96: Input signal observed at the output of the amplitude modulator

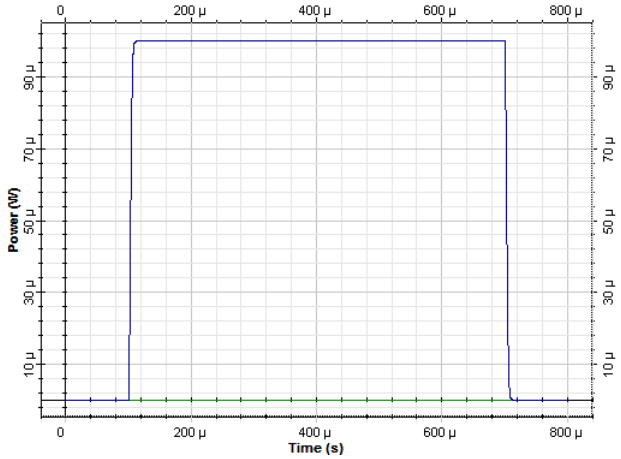
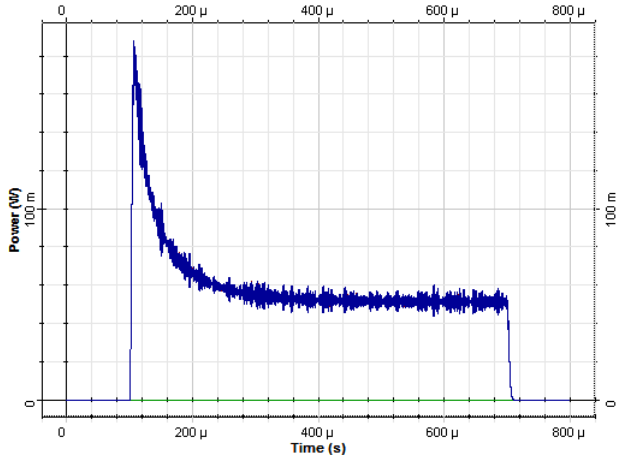


Figure 7-97: Power versus time oberved at the amplifier output



Chapter 8 - Dispersion Management

This section contains the following examples.

- Dispersion Compensation Techniques
- Precompensation Technique using SOA
- 40 Gbps Transmission System
- Dispersion Compensation with FBG
- Fiber Nonlinearities and Dispersion
- Negative Dispersion Fiber and Applications for Metro Networks
- Migrating to 10 Gbps Metro System and Dispersion Limited Transmission

Notes:

Dispersion Compensation Techniques

Dispersion compensation techniques.osp

Project file "*Dispersion compensation techniques.osp*" (Figure 8-1) compares three different dispersion compensation techniques, namely pre-, post-, and symmetrical dispersion compensations by using DCFs. These examples consider just one channel. The bit rates used for the examples are 2.5 Gb/s and 10 Gb/s, respectively.

Although there are several forms of dispersion, the main form of dispersion we are concerned with is chromatic dispersion or group velocity dispersion (GVD). Pulse broadening effect of chromatic dispersion causes the signals in the adjacent bit periods to overlap. This is called inter-symbol interference (ISI). Broadening is a function of distance as well as dispersion parameter D. Dispersion parameter is given in ps/nm-km and changes from fiber to fiber. D is also a function of wavelength and is usually about 17 ps/nm-km in the 1.55 μm wavelength range for a standard single mode fiber (SMF). It is about 3.3 ps/nm-km in the same window for a dispersion-shifted fiber (DSF). Nonzero dispersion shifted fiber (NZDSF) has a chromatic dispersion between 1 and 6 ps/nm-km for (+) NZDSF and –1 and –6 ps/nm-km for (-) NZDSF.

For externally modulated sources, transmission distance limited by chromatic dispersion is given by [1]:

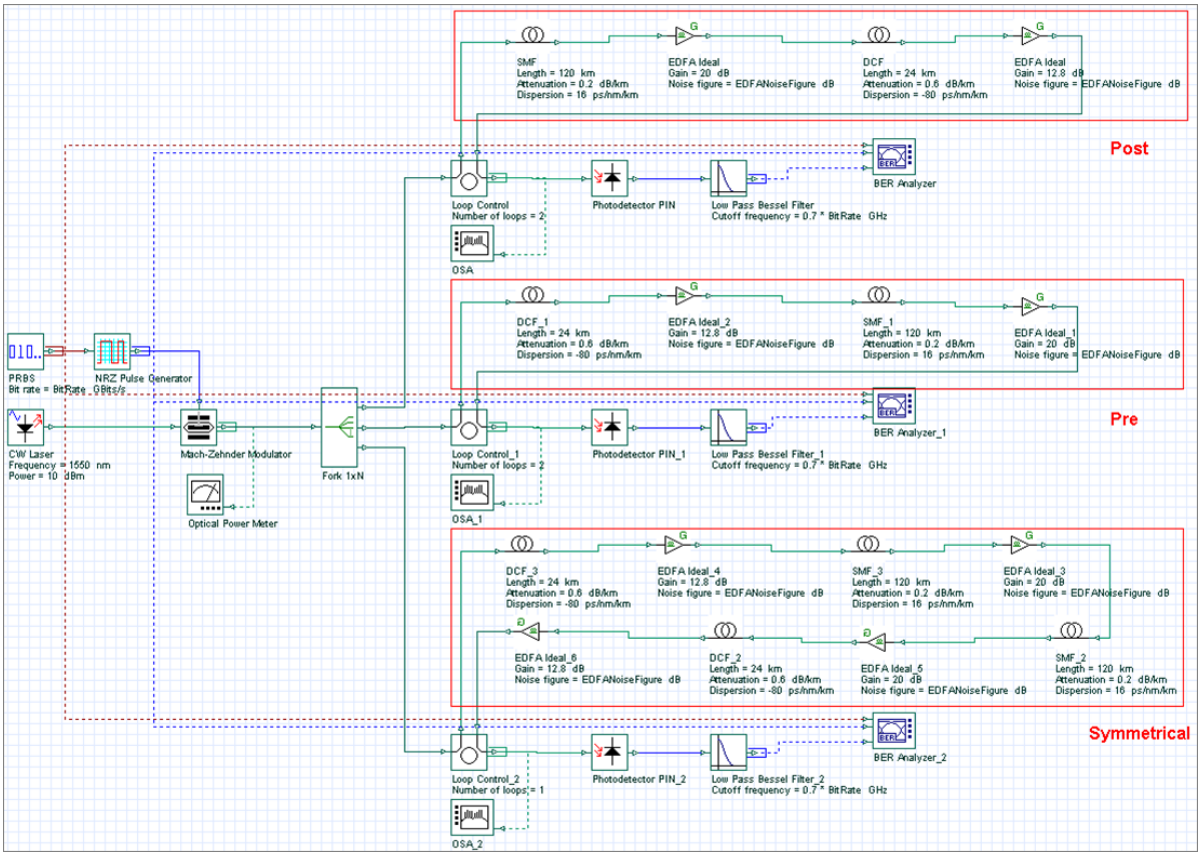
$$L < \frac{2\pi c}{16|D|\lambda^2 B^2} \qquad \textbf{(8-1)}$$

For D = 16 ps/nm-km and B = 2.5 Gb/s, L ~ 500 km whereas it drops to 30 km at 10 Gb/s bit rate.

Several techniques such as dispersion compensating fiber or fiber Bragg grating can be used to compensate the accumulated dispersion in the fiber. In this example we will show three different schemes, namely pre-, post-, and symmetrical compensation, to compensate the fiber dispersion. We will then show how the amount of accumulated dispersion from the dispersion compensator affects the performance.

Pre-, post-, and symmetrical compensation configurations are shown in Figure 8-1. In our simulations we have used optical amplifiers after each fiber to compensate for the fiber loss. Dispersion parameter of SMF is 16 ps/nm-km and it is 120 km long. Therefore, total accumulated dispersion is 16 x 120 = 1920 ps/nm. This amount of dispersion can be compensated by using a 24 km long DCF with – 80 ps/km-nm dispersion. In post-compensation case, DCF is placed after SMF whereas in pre-compensation case it is inserted before SMF. In symmetrical compensation case, fiber placement follows the sequence of DCF, SMF, SMF, DCF.

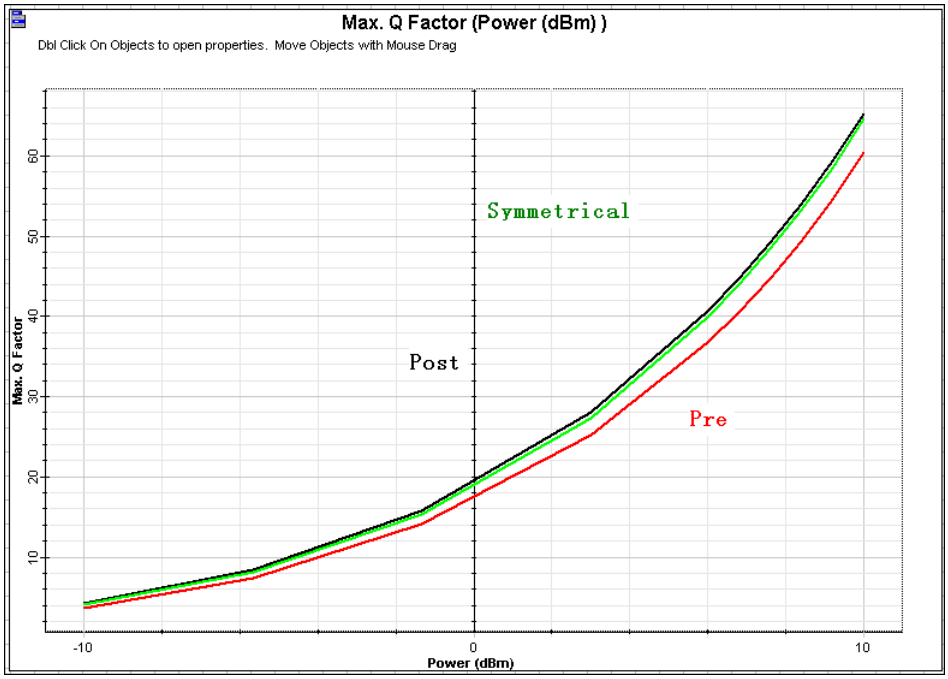
Figure 8-1: Layout - Dispersion compensation techniques



Simulation results are shown in Figure 8-2 and Figure 8-3. Figure 8-2 shows Q factor of received signal versus CW laser power for these three schemes at 2.5 and 10 Gb/s bit rates, respectively. These figures are obtained by sweeping the power from -10 dBm to 10 dBm and using the software's report page. From these figures, we can conclude that the best performance is obtained by using symmetrical dispersion compensation. The worst case is dispersion pre-compensation. Post- compensation gives a result as good as symmetrical compensation [2,3]. This can also be seen from the eye diagrams given in Figure 8-3.

Figure 8-2: Q factor vs. CW laser power at 2.5 Gbps and 10 Gbps for pre-, post-, and symmetrical dispersion compensations

B = 2.5 Gbps



B = 10 Gbps

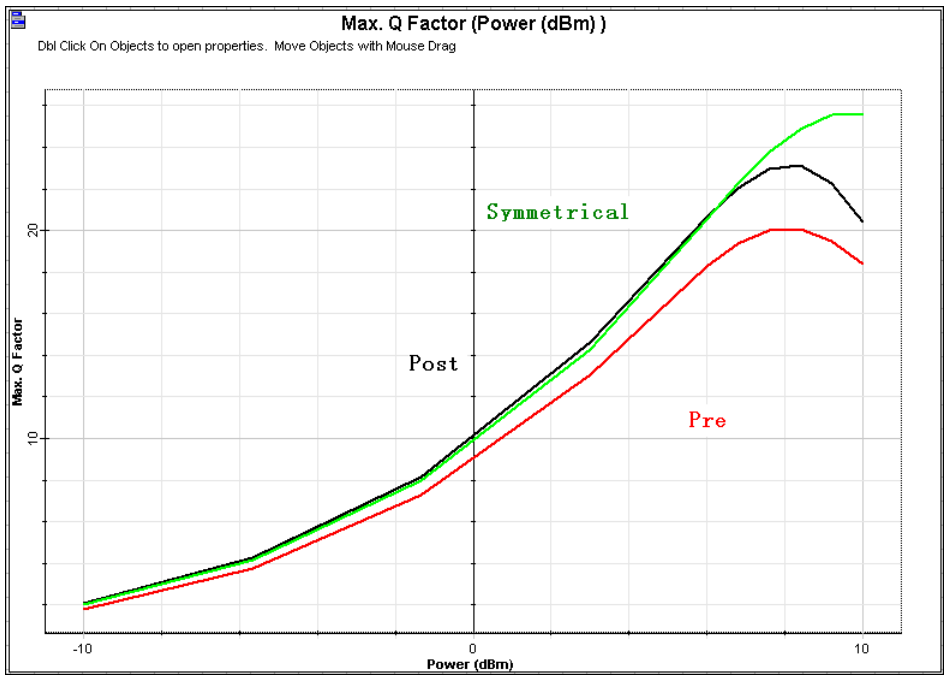
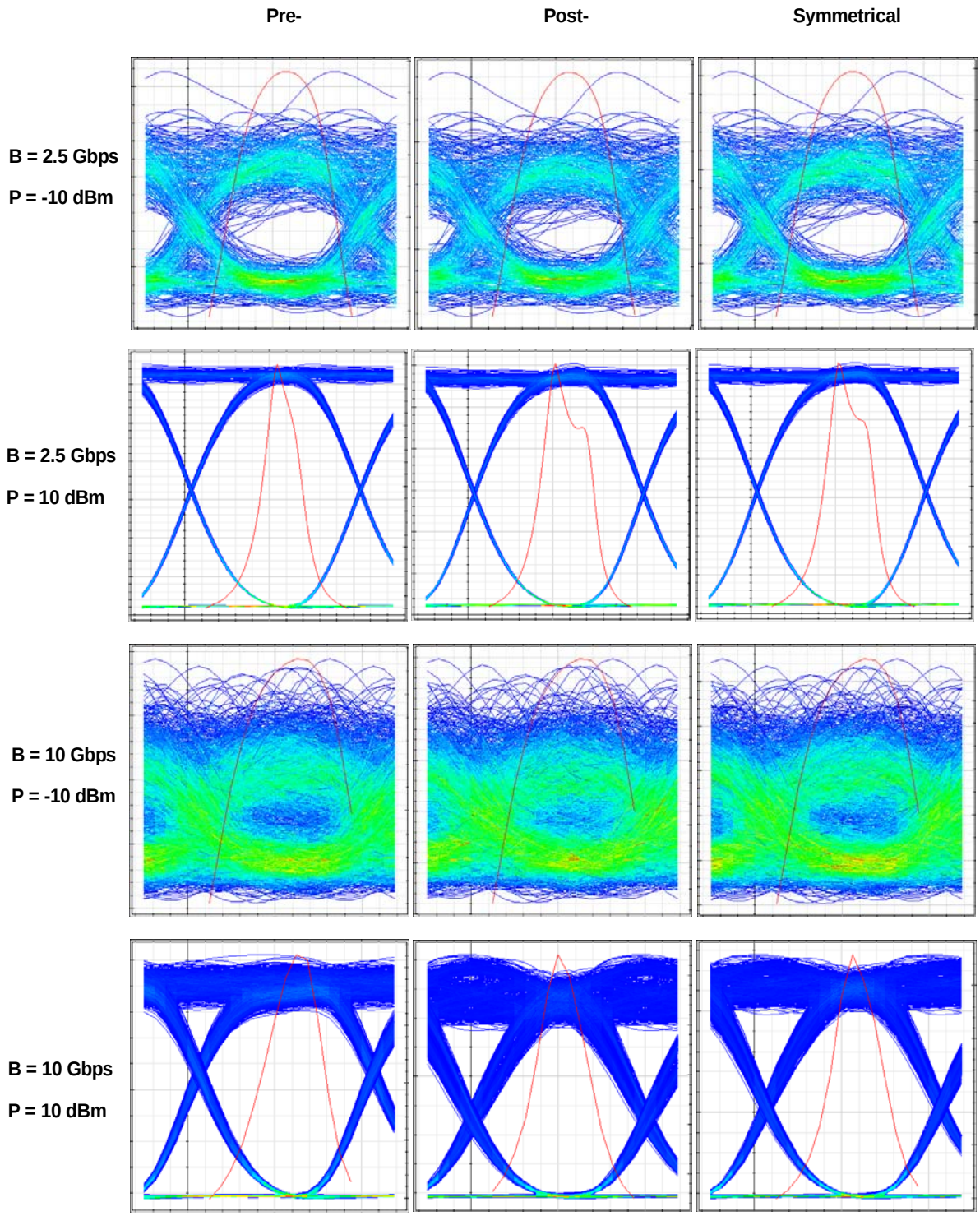


Figure 8-3: System performance for pre-, post-, and symmetrical dispersion compensations.



References:

[1] G.P. Agrawal, *Fiber-Optic Communication Systems*, 4th ed., John Wiley & Sons, INC., 2010.

[2] R. Ramaswami and K.N. Sivarajan, *Optical Networks: A practical Perspective*, Morgan Kaufmann, 1998.

[3] M.I. Hayee and A.E. Willner, “Pre- and post-compensation of dispersion and nonlinearities in 10-Gb/s WDM systems”, IEEE Poton. Tech. Lett. 9, pp. 1271, 1997.



Notes:

Precompensation Technique using SOA

Amplifier induced chirp SLA compression.osp

The gain saturation induced self-phase modulation in SOA affects in the formation of chirp of the pulse in the process of amplification. From the theory of propagation of phase modulated optical signals in dispersive medium [1], we know that depending on the signs of the chirp of signal and the chirp of the dispersive medium, different scenarios are possible. For equal signs of chirps the dispersion effect is amplified. On other hand, in the case of different signs of the chirps the effect of pulse dispersion can be reduced which effectively leads to pulse compression.

If we would like to use the red frequency shift created in the process of pulse amplification in SOA for compression, we have to propagate this pulse in a dispersive medium that creates a blue frequency shift. Such medium could be standard single mode fiber used for wavelengths larger than the zero dispersion wavelength or in other words in the region of anomalous group velocity dispersion. This idea has been proposed and realized in [2]. In this project, using SOA component we will try to interpret results obtained in [2].

Following parameters of SOA have been used in [2]: Unsaturated single pass gain G_0 = 30 dB; linewidth enhancement factor α = 5; saturation energy E_{sat} ~ 6 pJ. Ratio E_{in} / E_{sat} has been varied over the range from 0.01 to 0.2. Typical values for the carrier lifetime are given as 200 ~ 300 ps. Pulses for which the condition T_0 / T_{sat} << 1 is valid have been considered.

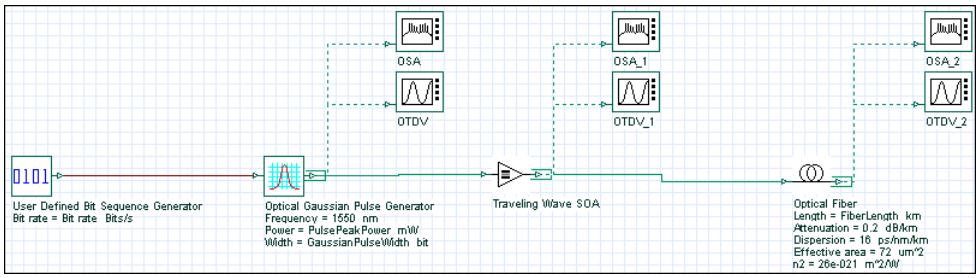
Following simulation parameters are used: bit rate B = 40 Gb/s -> T_B = 25 ps. We also consider pulses width T_{FWHM} = 12.5 ps -> T_0 ~ 7.5 ps. The default values of the SOA component, i.e., the carrier lifetime and the saturation energy are τ_C ~ 1.4 ns and E_{sat} ~ 5 pJ, respectively.

To satisfy the conditions T_0 / T_{sat} << 1 and E_{in} / E_{sat} ~ 0.01 to 0.2 we can use the Gaussian pulse with T_0 ~ 7.5 ps for which T_0/T_{sat} ~ 0.0055 and initial peak pulse powers as 4 mW, 40 mW, and 80 mW (which correspond to E_{in} / E_{sat} = 0.01, 0.1 and 0.2 respectively).

Dispersion length L_D in standard single mode fiber (D ~ 16 ps /nm-km) for pulse with T_0 ~ 7.5 ps will be L_D ~ 2.76 km.

To satisfy the condition L_C / L_D ~ 0.3 as given in [1], where L_C is the length of the fiber used for compression, the value of L_C ~ 0.828 km has been used. The layout for the project is shown in Figure 8-4.

Figure 8-4: Layout - Amplifier induced chirp SLA compression



Initial pulse shape and spectrum with T_{FWHM} = 12.5 ps and initial pulse peak power = 4 mW have been shown in Figure 8-5 and Figure 8-6, respectively.

Figure 8-5: Initial shape of pulse

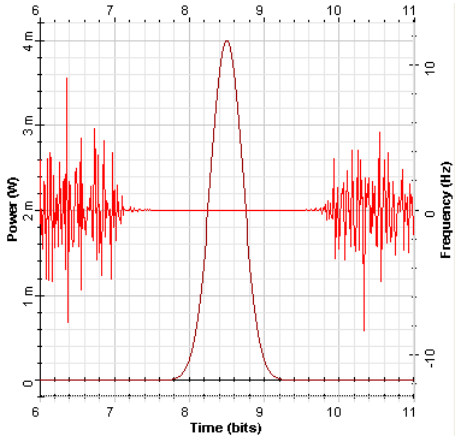


Figure 8-6: Initial spectrum of pulse

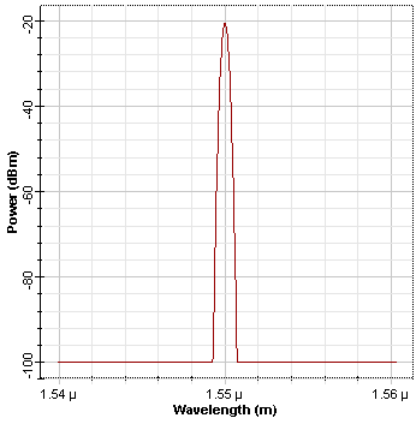


Figure 8-7 and Figure 8-8 show the shape (with corresponding positive chirp) and spectrum after amplification with SOA (G_0 = 30 dB and linewidth enhancement factor α = 5).

Figure 8-7: Shape after amplification with SOA

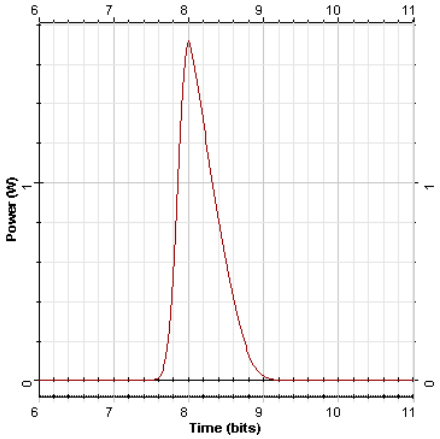


Figure 8-8: Spectrum after amplification with SOA

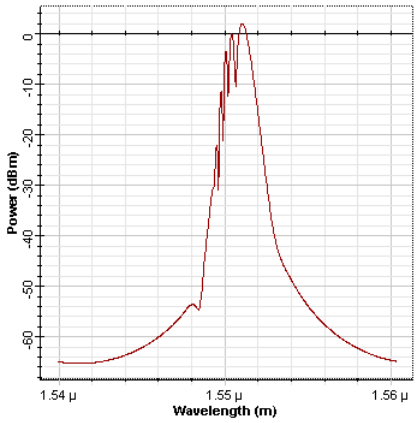


Figure 8-9 and Figure 8-10 show, the shape and spectrum of the amplified pulse after passing through 0.828 km of standard single mode fiber (SMF).

Figure 8-9: Shape of the amplified pulse after propagating through SMF

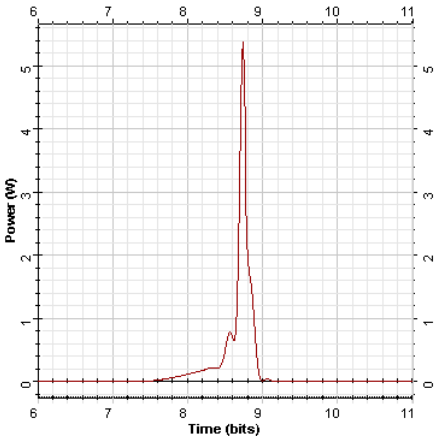
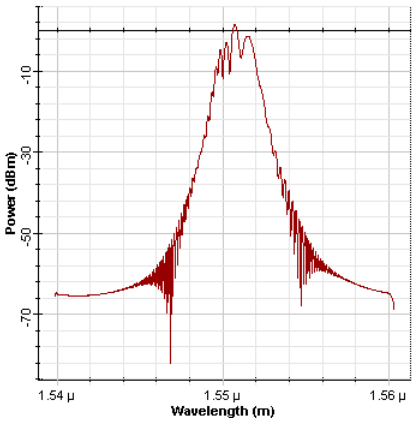


Figure 8-10: Spectrum of the amplified pulse after propagating through SMF



The comparison of the width of the pulse after fiber shows a compression factor of about 5 times with peak power enhanced by a factor of several hundreds. Two important physical facts should be mentioned in the Figure 8-9. First, there is a broad pedestal on the leading side of the pulse that leads to increased dispersion of this part of the pulse. The second point is connected with the shift of the pulse towards later time. This fact is due to the red shift of central frequency of the amplified pulse that in anomalous group velocity dispersion region leads to time delay of the pulse.

As is mentioned in [2], the compression factor depends on several input parameters, such as the pulse energy, the pulse width, the amplifier gain, and the compressor length. For non optimal parameters, another type of phenomena can appear, for example, pulse breaking as demonstrated in Figure 8-11 and Figure 8-12, where the shapes and spectrum of pulses with initial peak powers of 4, 40 and 80 mW are presented.

Figure 8-11: Shape of the pulse for non-optimal parameters

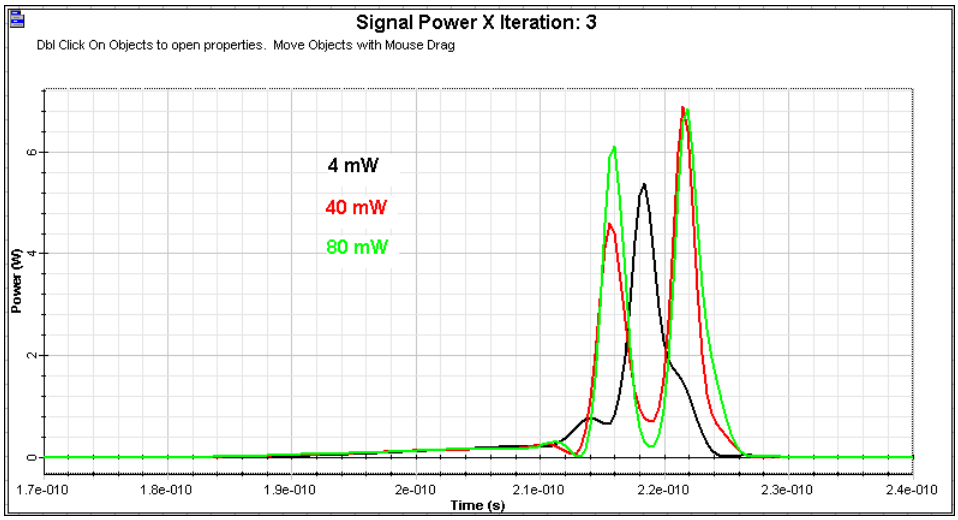
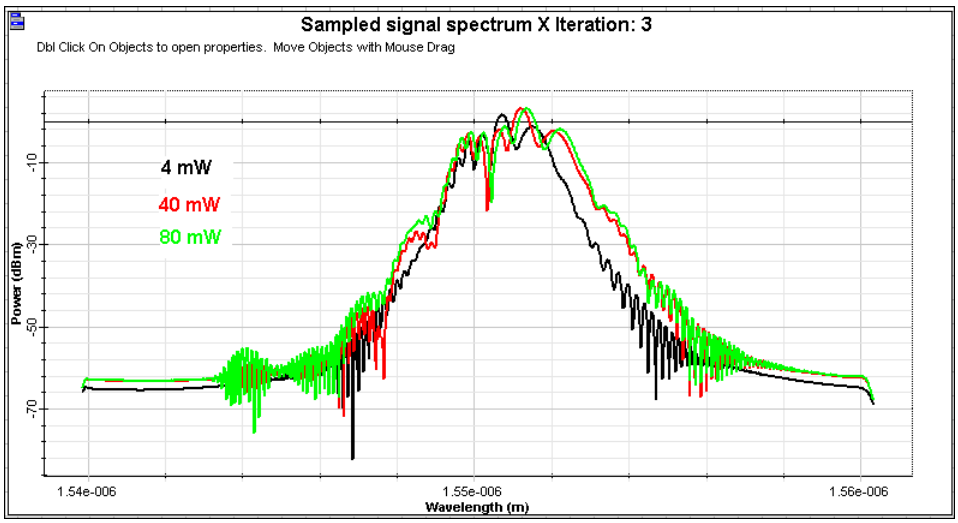


Figure 8-12: Spectrum of the pulse for non-optimal parameters



As we can see from Figure 8-11, larger input peak power can lead to pulse breaking phenomena with connected complicated spectrum structures.

We have demonstrated pulse compression of weak pulses (peak energy smaller than pJ) based on the gain saturation induced self-phase modulation effect in SOA.

References:

[1] G.P. Agrawal, *Nonlinear fiber optics*, third edition, Academic press, 2001.

[2] G.P. Agrawal and N.A. Olsson, “Amplification and compression of weak picosecond optical pulses by using semiconductor laser amplifier”, Optics Letters, vol.14, pp. 500-502, 1989.

Notes:

40 Gbps Transmission System

40 Gbps - RZ and NRZ.osp

40 Gbps - Amplifier noise and SPM for RZ.osp

40 Gbps – Post- and pre- dispersion compensation for RZ.osp

The fundamental limitation to high speed communication systems over the standard single mode fiber at 1.55 μm is the linear chromatic dispersion. Typical value of β_2 = -20 ps^2/km at 1.55 μm for SMF leads to D = 16 ps/nm-km. For bit rate B = 40 Gb/s, the slot duration will be T_B = 25 ps. For duty cycle = 0.5 -> T_{FWHM} = 12.5 ps -> T_0 = 7.5 ps, the corresponding dispersion length will be approximately L_D ~ 2.8 km.

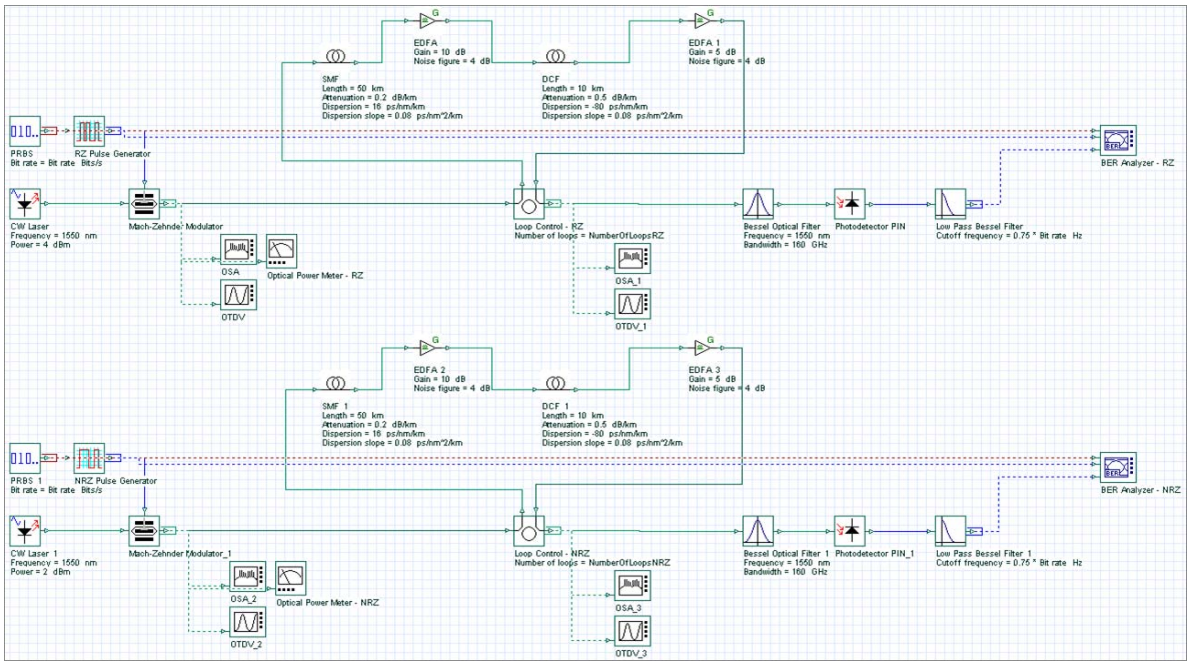
The aims of this project are as follows:

a) to compare RZ versus NRZ modulation format transmission in SMF at 40 Gb/s taking into account: group velocity dispersion, self-phase modulation due to the Kerr nonlinearity, linear losses and periodical amplification with ASE noise. The large group velocity dispersion is compensated with post- dispersion compensation scheme.

b) to analyze influence of accumulated amplifier noise and self-phase modulation for RZ modulation format transmission in SMF at 40 Gb/s.

c) to compare post- and pre- dispersion compensation schemes for RZ modulation format transmission in SMF at 40 Gb/s.

Figure 8-13: Layout - RZ and NRZ modulation formats



Global parameters used for this project are: Bit rate = 40 Gb/s, Sequence length = 256 Bits and Samples per bit = 64.

RZ generator has following properties: rectangle shape is Gaussian; duty cycle= 0.5 bit; rise time= 0.15 bit; fall time = 0.25 bit.

As an optical source, an externally modulated CW Laser with carrier wavelength = 1550 nm and linewidth = 10 MHz is used.

The standard single mode optical fiber used has dispersion coefficient D = 16 ps/nm-km, the slope $(\partial D)/(\partial \lambda)$ = 0.08 ps/nm^2-km, the nonlinear-index coefficient n_2 = 3 x 10^{-20} m^2/W, effective mode area A_{eff} = 80 μm^2, linear losses α = 0.2 dB/km and fiber length L_{SMF} = 50 km.

After each segment of SMF an amplifier compensates the linear losses. Dispersion compensation fiber has dispersion coefficient D = -80 ps/nm-km, the slope $(\partial D)/(\partial \lambda)$ = 0.08 ps/nm^2-km, the nonlinear-index coefficient n_2 = 3 x 10^{-20} m^2/W, effective mode area A_{eff} = 23 μm^2, linear losses α = 0.5 dB/km and fiber length L_{DCF} = 10 km. After each segment of DCF an amplifier compensates the linear losses.

Properties of Bessel optical filter used are: carrier wavelength = 1550 nm and bandwidth = 4 x Bit rate. The cutoff frequency of the low pass Bessel electrical filter used is 0.75 x Bit rate.

Ideal periodical amplification is performed with the help of ideal EDFA component of OptiSystem that also takes ASE noise into account. The amplifier used after SMF has a gain of 10 dB and noise figure of 4 dB and the amplifier used after DCF has a gain of 5 dB with the same noise figure value.

Part I: Comparison of RZ and NRZ formats

In the project "*40 Gbps – RZ and NRZ.osp*" (Figure 8-13) the transmission over a distance of 1000 km SMF (20 loops x 50 km) with periodical amplification after every 50 km of fiber has been considered. For the RZ modulation format, the result for the dependence of the max Q on the transmitter power (after the MZM modulator) is shown in Figure 8-14. Figure 8-15 shows the eye diagram for the optimal point when transmitter power ~ 0.3 mW (cf. Figure 8-14).

Figure 8-14: Max Q vs. transmitter power (RZ modulation)

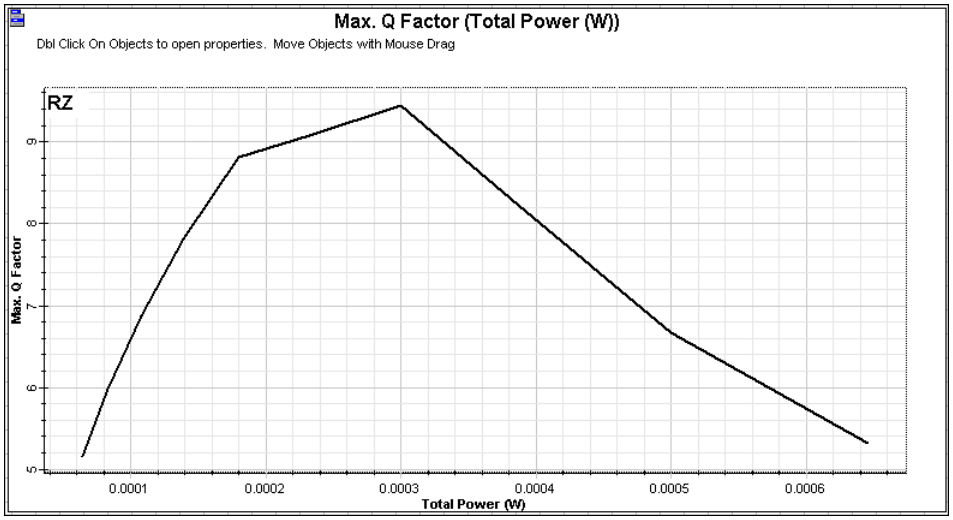
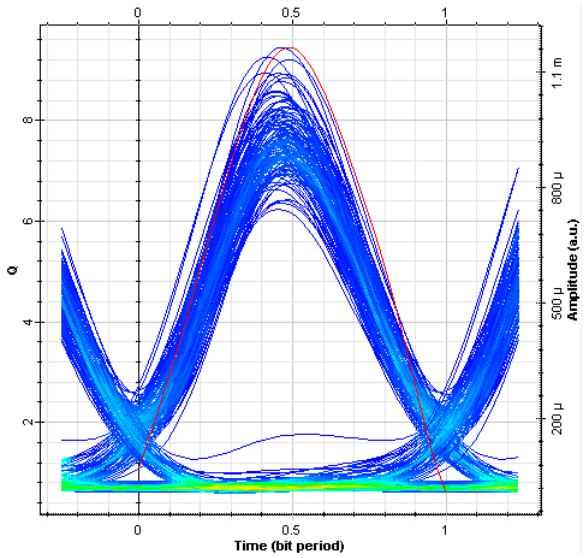


Figure 8-15: Eye diagram when transmitter power ~ 0.3 mW



For the NRZ modulation format, the same transmission link and receiver structure is used, and the result of the dependence of the max Q vs. transmitter power is shown in Figure 8-16. Figure 8-17 shows the eye diagram for the optimal point when input power ~ 0.17 mW (cf. Figure 8-16).

Figure 8-16: Max Q vs. transmitter power (NRZ modulation)

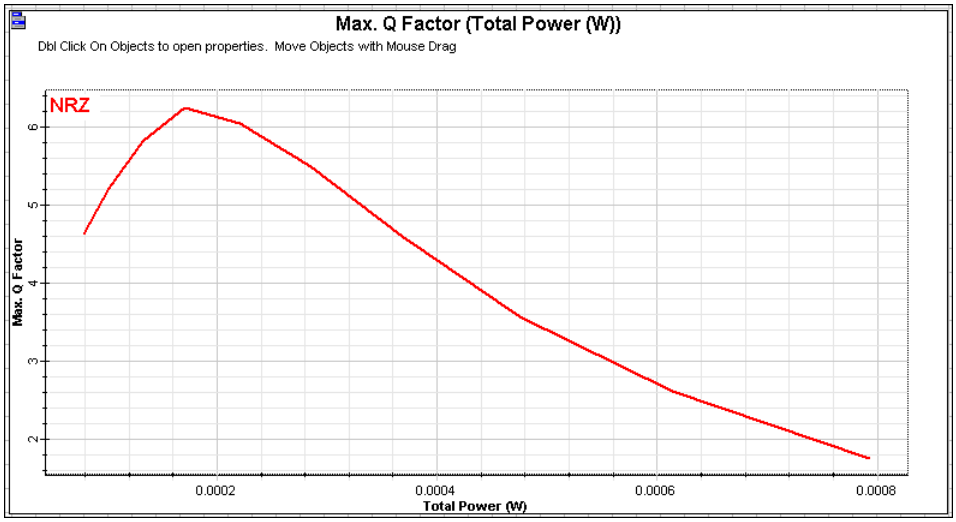
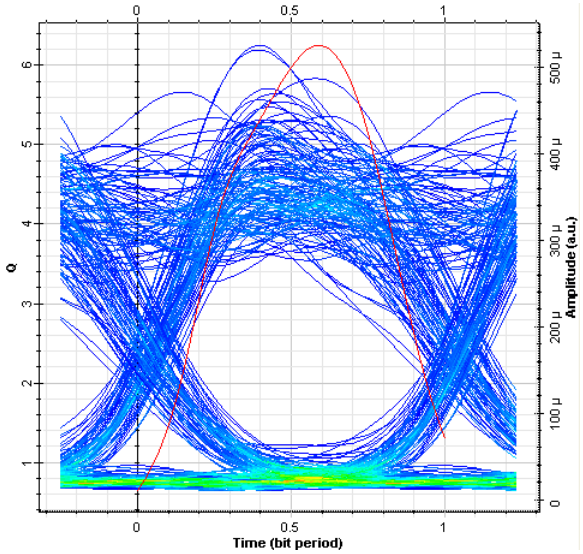


Figure 8-17: Eye diagram when transmitter power ~ 0.17 mW

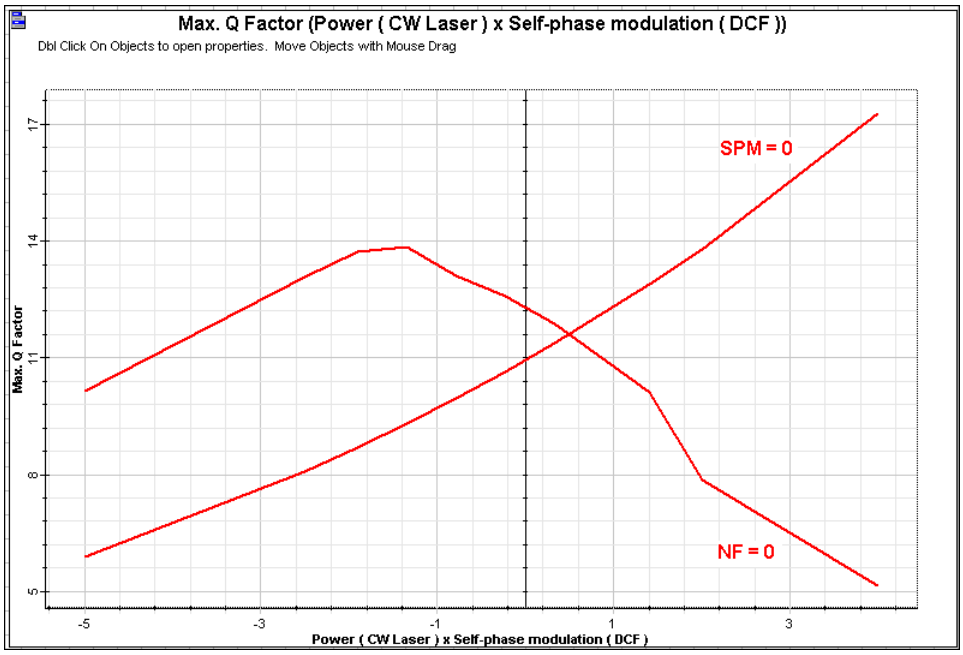


Comparing positions of the maximums of both curves we can clearly see the shift toward larger input powers for the RZ format. Obtained results show that the RZ modulation format with duty cycle = 0.5 is superior compared to conventional NRZ modulation format.

Part II: Influence of accumulated amplifier noise and self-phase modulation on RZ signal transmission

In this project we have considered two different situations. In the first case, the self-phase modulation was assumed to be zero, and in another case the noise figure was not taken into account. Obtained results are presented in Figure 8-18.

Figure 8-18: Max Q vs. input CW laser power (dBm) for two separate cases (Case I: SPM = 0; Case II: Noise figure = 0)

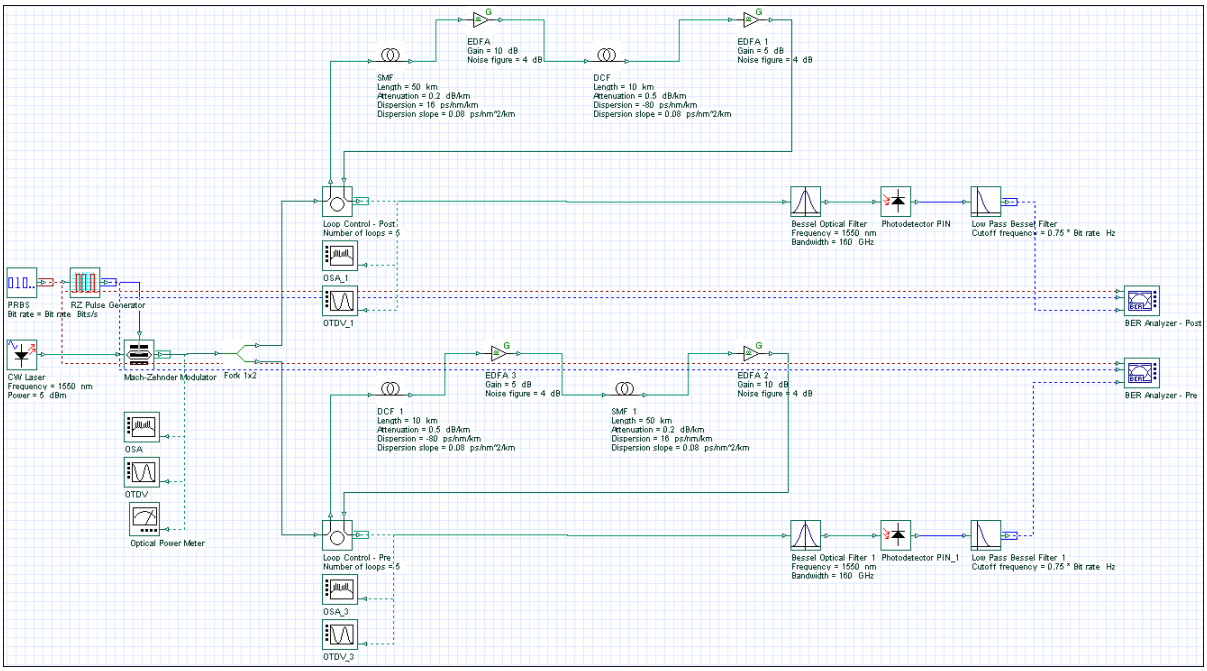


As we see, at low power levels, the performance is mainly hampered by the accumulated amplifier noise. At high input power levels, the transmission distance is significantly reduced due to the self-phase modulation. As we see, just these effects determine the well expressed maximum in the Q curve in Figure 8-14. The optimum Q happens when CW laser power is 0.55 dBm, which corresponds to a power of ~ 0.3 mW after the modulator, matches with Figure 8-14.

Part III: Post- and pre- dispersion compensation for RZ modulation format

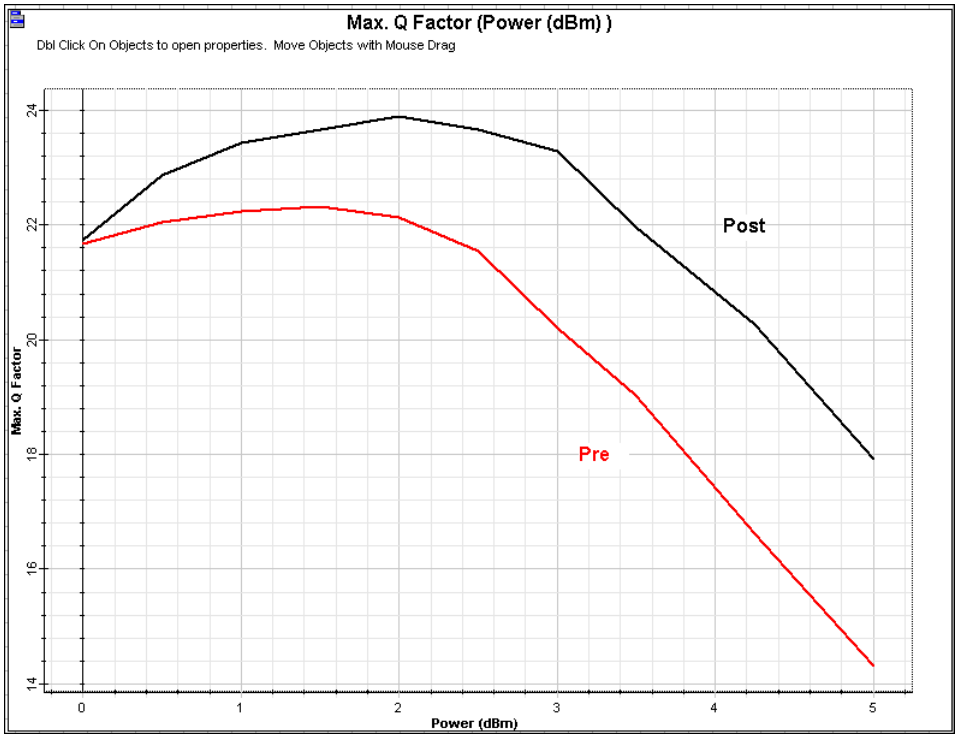
In the project "*40 Gbps – Post and pre dispersion compensation for RZ.osp*" (Figure 8-19), two schemes of dispersion compensation are studied, i.e., post- and pre- compensation.

Figure 8-19: Layout - 40 Gbps - Post and pre dispersion compensation for RZ



The corresponding results for the RZ signal transmission in SMF at 40 Gb/s are shown in Figure 8-20.

Figure 8-20: RZ modulation format transmission at 40 Gb/s over 250 km in SMF. Max Q vs. CW laser power



Results indicate that post-compensation scheme is superior compared to pre- compensation in dispersion compensated system at 40 Gbps in SMF.

We have thus shown that for upgrading the existing standard fiber network at 1.55 μm to 40 Gb/s:

a) Dispersion compensation is necessary

b) RZ is superior compared to conventional NRZ modulation format

c) At low power levels, the performance is mainly hampered by the accumulated amplification noise and at higher input power levels, the transmission distance is significantly reduced by self-phase modulation

d) Post compensation scheme is superior compared to pre-compensation scheme.

References:

[1] D. Breuer and K. Petermann, "Comparison of NRZ and RZ- modulation format for 40 Gbit/s TDM standard-fiber system", IEEE Photon. Technol. Lett., vol. 9, pp.398-400, 1997.

[2] M.I. Hayee and A.E. Willner, "NRZ Versus RZ in 10-40 Gb/s Dispersion – Managed WDM Transmission systems", IEEE Photon. Technol. Lett., vol. 11, pp.991-993, 1999.

[3] C.M. Weinert, R. Ludvig, W. Papier, H.G. Weber, D. Breuer, K. Petermann and F. Kuppers, "40 Gbit/s Comparison and 4 x 40 Gbit/s TDM/WDM Standard Fiber Transmission", Journal of Lightwave Technology, vol. 17, pp.2276-2284, 1999.

Notes:

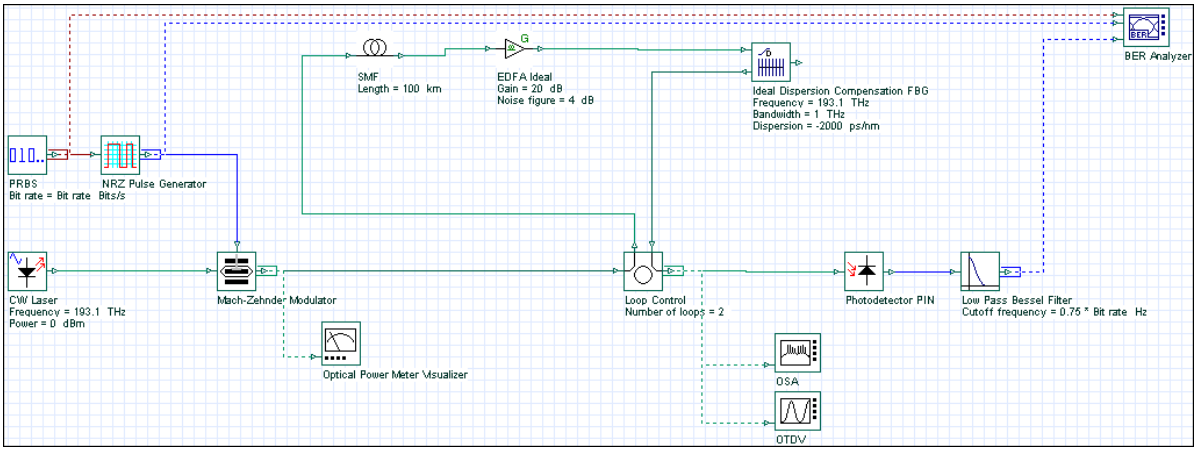
Dispersion Compensation with FBG

Dispersion compensation – Post with FBG.osp

Project "*Dispersion compensation - Post with FBG.osp*" (Figure 8-21) shows the dispersion compensation by using fiber Bragg grating. It shows how the amount of compensating dispersion affects the system performance.

In the project we prefer post-compensation scheme because of its simplicity comparing to symmetrical compensation scheme. Its performance is also as good as symmetrical compensation scheme.

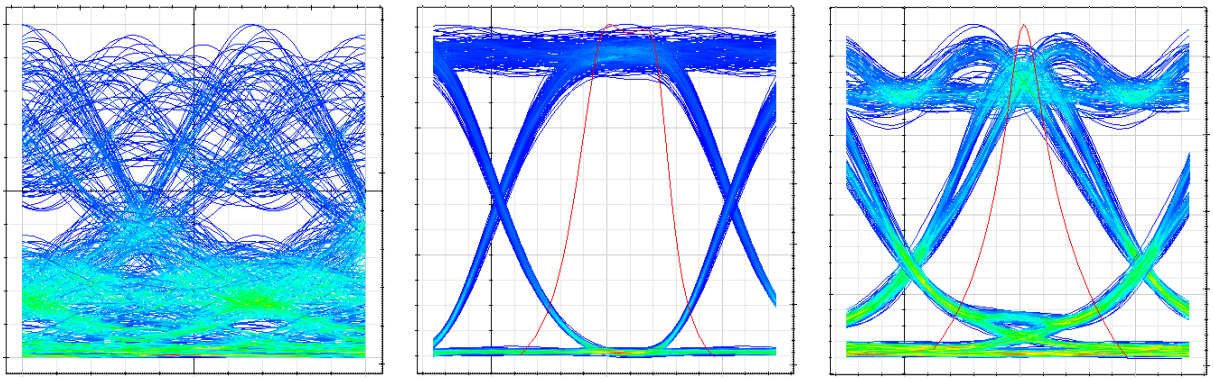
Figure 8-21: Layout - Dispersion compensation - Post with FBG



In this case, the total accumulated dispersion of the SMF is 16 x 100 = 1600 ps/nm. We swept the total dispersion of FBG from 0 to -2000 ps/nm. In this simulation, we just want to see the dispersion-limited performance of the system.

Therefore we keep the CW laser power at 0 dBm. This is needed to avoid triggering of any fiber nonlinearity. Effects of residual dispersion to nonlinear effects will be considered in other examples. Figure 8-22 shows the eye diagrams at the receiver end for several total compensation dispersion values. This simulation shows that, in the linear regime (low input signal power), compensate fiber dispersion completely gives the best result. Over compensation degrades the system performance.

Figure 8-22: Eye diagrams at the receiver end when the FBG dispersion is (a) 0 (b) 1600 and (c) 2000 ps/nm



(a) **(b)** **(c)**

Fiber Nonlinearities and Dispersion

Fiber nonlinearities and dispersion – Single channel.osp

Fiber nonlinearities and dispersion – Multi channel equal spacing.osp

Fiber nonlinearities and dispersion – Multi channel unequal spacing.osp

As long as the optical power within an optical fiber is small, the fiber can be treated as a linear medium. However, when the power level is high, we have to consider the impact of nonlinear effects. They can be classified into two categories. Some of them occur in multi channel WDM systems where interaction of signals at different wavelengths is possible. These categories and nonlinear effects in single channel and multi-channel systems are shown in Table 8-1.

Table 8-1: Nonlinear effects in the fiber

	Single channel	**Multi channel**
Refractive index related	Self phase modulation (SPM)	Cross phase modulation (XPM) Four wave mixing (FWM)
Scattering related	Stimulated scattering (SBS)	Stimulated raman scattering (SRS)

SPM and XPM affect the phase of signals and cause spectral broadening, which in turn, leads to increase in dispersion penalties. SBS and SRS provide gains to some channels at the expense of depleting power from other channels. The nonlinear interaction depends on transmission length and effective area of the fiber. Since loss in the fiber decreases the signal power, we use an effective instead of physical length. In practice, SPM can be a significant consideration in designing 10 Gbps systems, and restricts maximum power per channel below a few dBm. XPM becomes an important consideration when the channel spacing is of the order of a few tens of GHz. FWM efficiency depends on signal power and dispersion, as well as channel separation in WDM systems. If the channel is close to zero dispersion wavelength of the fiber, considerably high power can be transferred to FWM components. Using unequal channel spacing can reduce the effect of FWM.

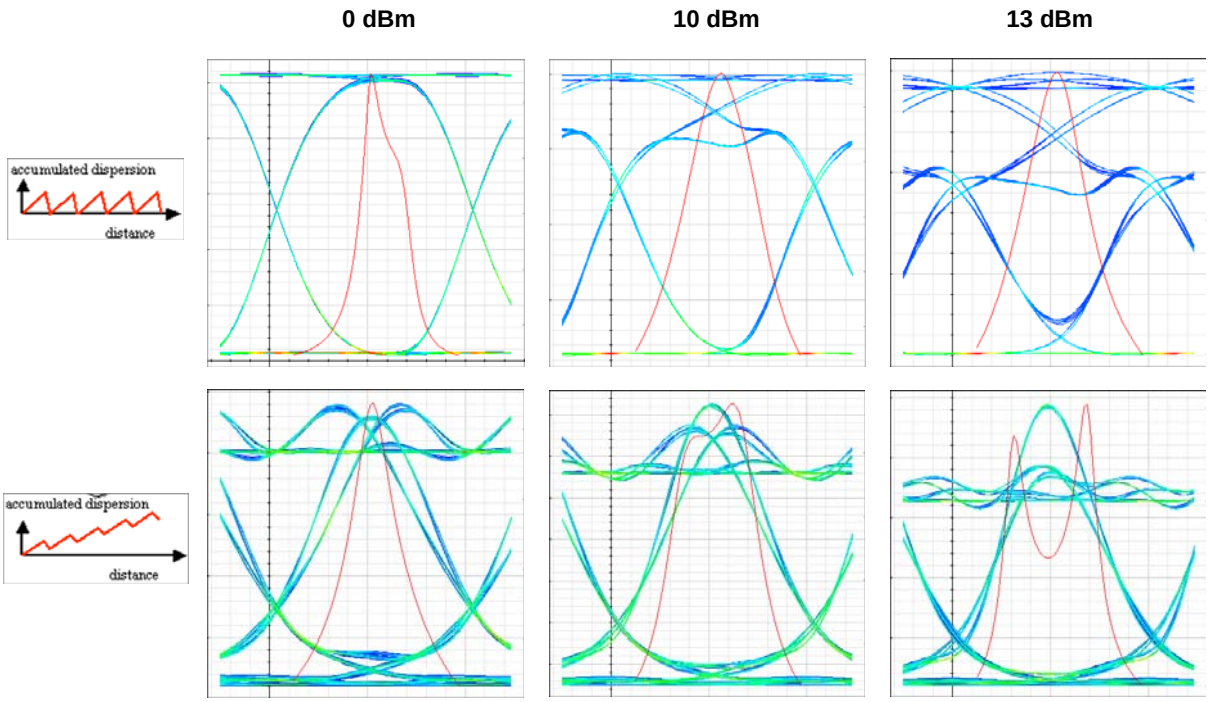
Dispersion plays a key role in reducing the effects of nonlinearities. However, dispersion itself causes inter-symbol interference. Fortunately, the good thing is that we can engineer systems with zero total dispersion but with a certain amount of local dispersion along the link.

Fiber nonlinearities and dispersion – Single channel

In this section we will consider effects of dispersion compensation to system performance in high power regime where nonlinearities are active. Let us first consider a dispersion post-compensated system with single channel. The project is given in "*Fiber nonlinearities and dispersion - Single channel.osp*" file. In

this file, we have two different versions of the transmission link. In the first version, system residual dispersion is 0, whereas it is 800 ps/nm in the second version. Transmission link contains 5 spans and bit rate is 10 Gbps. Dispersion of the 100 km SMF is 16 ps/nm-km and its effective area is 72 micron-square. Dispersion of the 20 km DCF is – 80 ps/nm-km for the first version, and –72 ps/nm-km for the second one. Effective area of DCF is 30 micron-square. SMF and DCF losses are compensated by an EDFA with 35 dB gain. Noise figure of the EDFA is set to zero, because the purpose of this example is to deal with nonlinear and dispersion effects. If we only consider the SMF and also include the effect of amplification (5 times), we can estimate the threshold power for SPM [1,2]. If we do so, we find that after about 10 dBm average power, SPM becomes a limiting effect. However, we need to investigate if that is the case then how the residual system dispersion affects it. Figure 8-23 shows the eye diagrams for two different residual dispersion values and three different signal input powers.

Figure 8-23: Eye diagrams of the received signal for several signal input powers when system residual dispersion is (a) 0 and (b) 800 ps/nm. Inset on the left shows the dispersion map for each case.



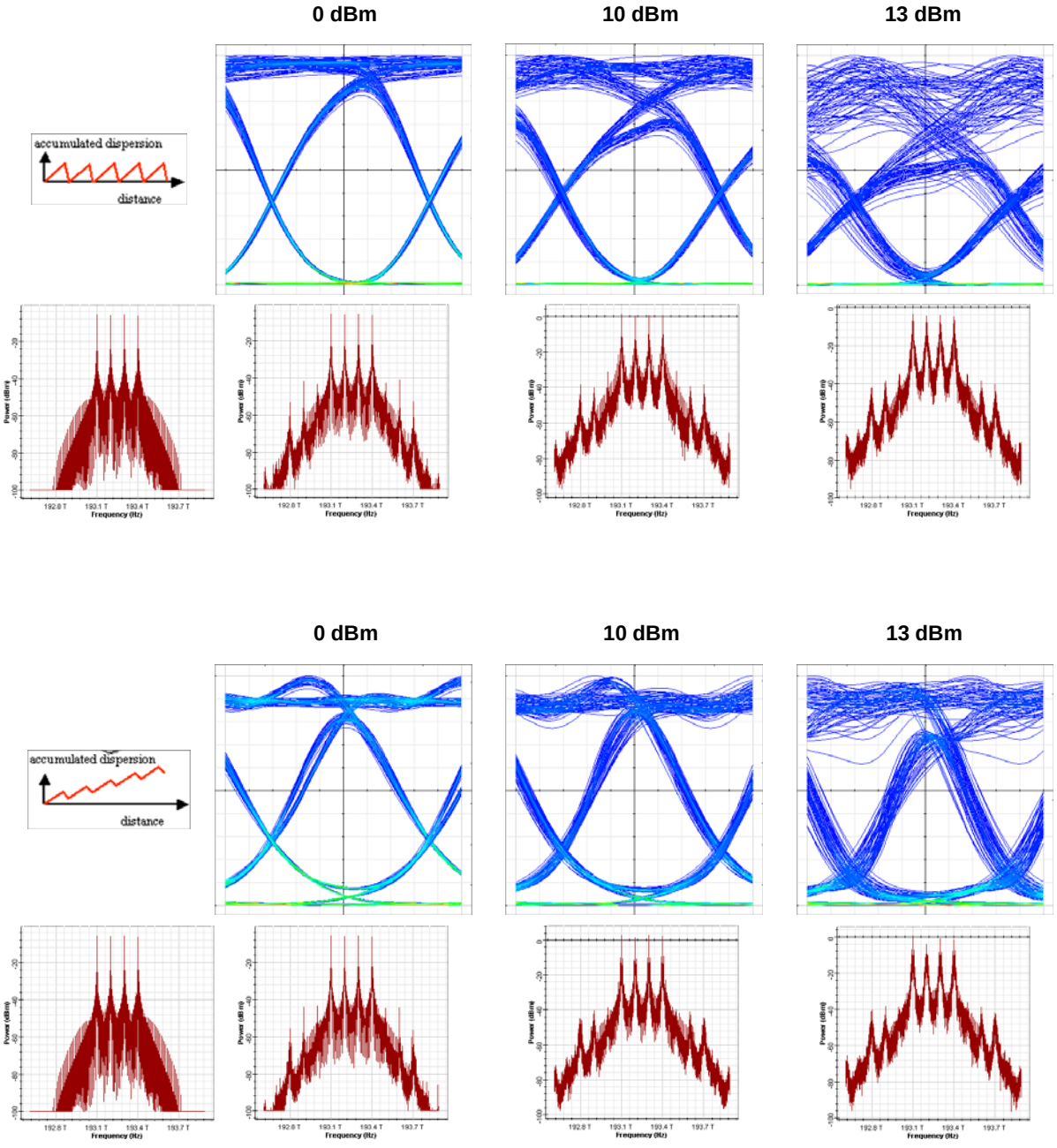
This simulation shows that the effect of SPM can be reduced by not completely compensating the dispersion, but leaving some residual dispersion in the system. Notice how the increase of power results in eye closure in zero residual dispersion case.

Fiber nonlinearities and dispersion – Multi channel equal spacing

Let us now consider a multi-channel system with 4 channels. The first channel is at 193.1 THz and they are separated with 100 GHz. SMF and DCF parameters are same as above. Even though the dispersion of fiber depends on wavelength, we set both fibers' dispersion to constant values. This will not affect the basic idea that we want to show here. We again have two versions of the design. The project is given in "*Fiber nonlinearities and dispersion - Multi channel equal spacing.osp*" file. In this file, we have two different versions of the transmission link. In the first version, system residual dispersion is 0, whereas it

is 800 ps/nm in the second one. In Figure 8-24, simulation results are given for these two cases with several channel powers.

Figure 8-24: Eye diagrams of the received signal for several signal input powers when system residual dispersion is (a) 0 and (b) 800 ps/nm. Insets on the left show the dispersion map as well as the input power spectrum for each case.



For a four-channel system, the threshold power for nonlinear effects is about 10 dBm per channel. Simulation results justify this finding. In this simulation, both SPM and XPM affect the system

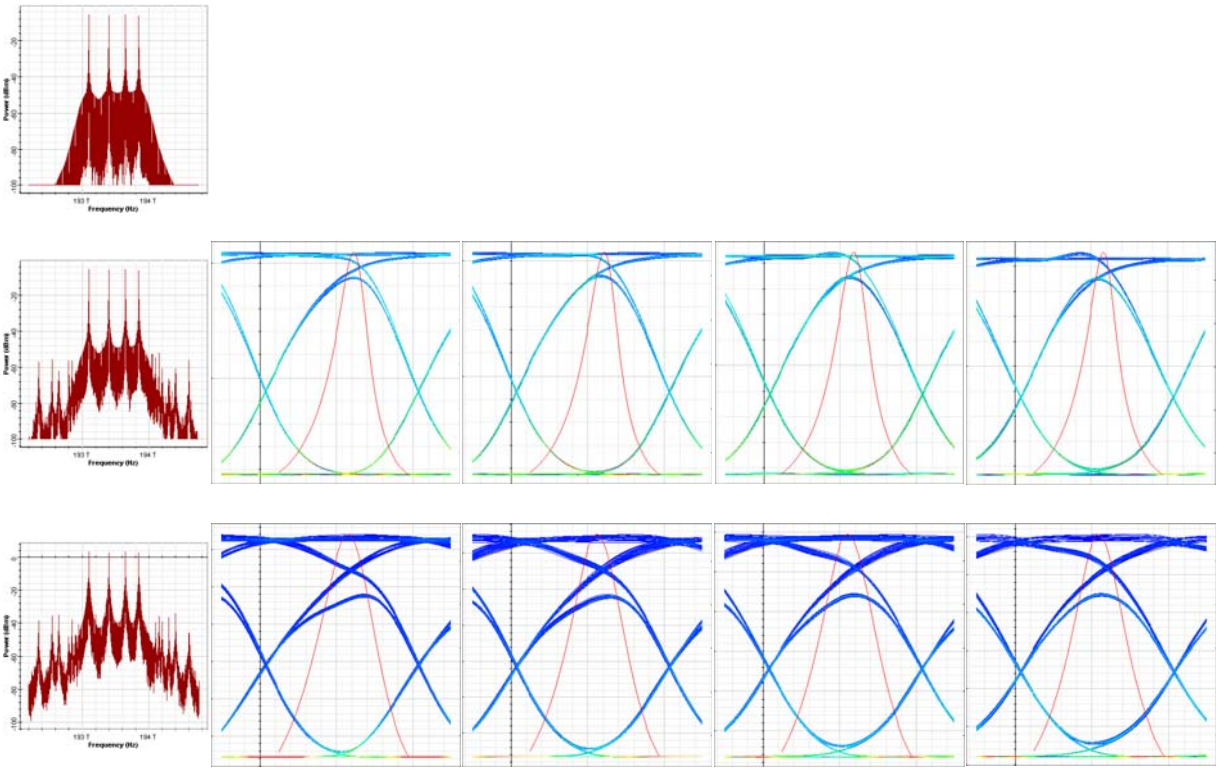
performance. This simulation shows that nonlinear effects can be reduced by local dispersion. Better performance is obtained with nonzero residual dispersion [3].

Fiber nonlinearities and dispersion - Multi channel unequal spacing

We will now show another example with 4 unequally spaced channels. Channels are at 193.1, 193.4, 193.65, and 193.85 THz. Bit rate is 10 Gb/s. In this case, we used wavelength dependent dispersion profile. Dispersion of the SMF is 16 ps/nm-km and DCF is -80 ps/nm-km @ 1550 nm. Dispersion slope of both SMF and DCF are set to 0.08 ps/nm^2-km. Project is given in "*Fiber nonlinearities and dispersion - Multi channel unequal spacing.osp*".

In the output spectrum, note the FWM generated spectrum components. Since they do not overlap with channels, FWM effect is decreased. Figure 8-25 shows the eye diagrams for each channel.

Figure 8-25: Eye diagrams of channels as obtained from the simulation. The first row shows the input signal spectrum; the second row shows the output spectrum as well as the eye diagrams for the four channels when channel input power is 0 dBm/ch; the third row is the same as the second row except that channel power is 10 dBm/ch.



References:

[1] G.P. Agrawal, *Fiber-Optic Communication Systems*, 4th ed., John Wiley & Sons, INC., 2010.

[2] R. Ramaswami and K.N. Sivarajan, *Optical Networks: A practical Perspective*, Morgan Kaufmann, 1998.

[3] G. Bellotti et. al., “Dependence of self-phase modulation impairments on residual dispersion in 10 Gb/s based terrestrial transmission using standard fiber”, IEEE Poton Tech. Lett. 11, pp. 824, 1999.

[4] H. Taga, “Long distance transmission experiments using the WDM technology”, J. Lightwave Tech. 14, pp. 1287, 1996.



Notes:

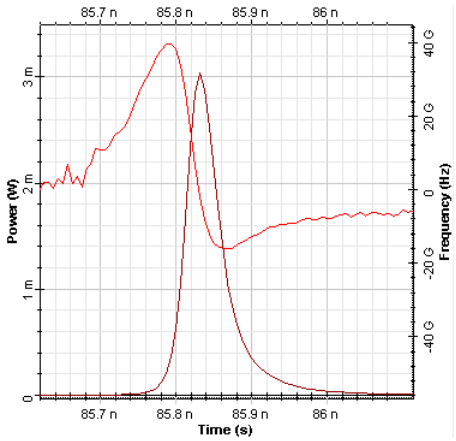
Negative Dispersion Fiber and Applications for Metro Networks

Negative dispersion fiber and applications for metro networks.osp

Project file "*Negative dispersion fiber and applications for metro networks.osp*" compares two types of fibers namely Corning's MetroCor and SMF-28 Fibers. MetroCor Fiber has a negative dispersion parameter whereas SMF-28 has a positive dispersion parameter in the EDFA band where we run our simulations. We also consider effects of source chirp on the network performance. For metro applications, directly modulated sources are preferred because of their low cost, but they result in more chirp, and more penalty due to dispersion when classic positive dispersion SMF is used. One option to overcome this effect is to use a fiber with negative dispersion. This example shows that, with the same amount of accumulated dispersion, MetroCor fiber performs better when a directly modulated source is used.

In the project, directly modulated laser sources are used with bit rate equals to 2.5 Gb/s. Three channels at 191.9 THz, 192.3 THz, and 192.5 THz are multiplexed and propagated in a fiber loop, which consists of either MetroCor or SMF-28 fiber followed by an amplifier. Noise from the EDFA is neglected in the simulation. The chirp of the pulse at the source is shown in Figure 8-26.

Figure 8-26: Pulse shape and chirp at the output of the directly modulated laser



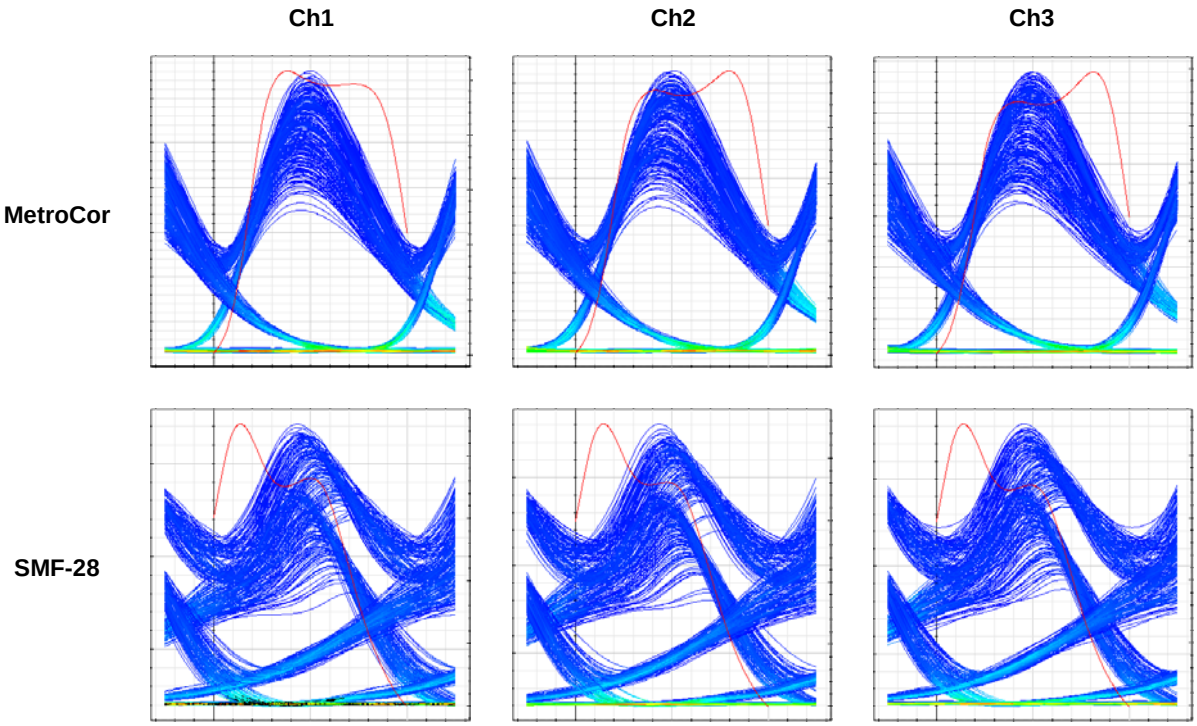
It is known that the linewidth of the source affects the broadening factor [3]. It is given as

$$\frac{\sigma^2}{\sigma_0^2} = \left[\left(1+\frac{C\beta_2 z}{2\sigma_0^2}\right)^2 + (1+(2\sigma_\omega\sigma_0)^2)\left(\frac{\beta_2 z}{2\sigma_0^2}\right)^2\right] \quad \textbf{(8-2)}$$

Where σ_ω is the RMS width of the Gaussian source spectrum. Directly modulated sources have broader spectrums and this contributes more in the broadening of the pulse. It can even dominates the broadening originated from the group velocity dispersion (GVD) itself when $(2\sigma_\omega\sigma_0)^2 \gg 1$.

Figure 8-27 shows eye diagrams of each channel after propagate in 300km MetroCor where total accumulated dispersion is about 1680 ps/nm and 100 km SMF-28 where the total accumulated dispersion is about 1675 ps/nm.

Figure 8-27: Eye diagrams of each channel after propagation in MetroCor and SMF-28, respectively.



Even though the accumulated dispersion is the same for both tested links, we have clearer eye in the case of MetroCor fiber link. This is achieved from the interplay between the negative chirp of the directly modulated laser and the opposite chirp introduced by the negative dispersion parameter for the case of MetroCor fiber. Note that in the transmission band, the dispersion parameter of MetroCor is negative whereas that of SMF is positive.

These results show that with the same amount of accumulated dispersion, MetroCor fiber performs better when a directly modulated source is used. Moreover, we can conclude that the use of negative dispersion fiber increases transmission distance.

References:

[1] C. Kennedy et. al., “The performance of negative dispersion fiber at 10 Gbps and significance of externally and directly modulated lasers”, NFOEC’01, 2001.

[2] D. Culverhouse et. al., “Corning MetroCore Fiber and its Application in Metropolitan Networks”, Corning’s White Paper WP5078.

[3] G.P. Agrawal, *Nonlinear Fiber Optics*, Second Edition, Academic Press, 1995.

Notes:

Migrating to 10 Gbps Metro System and Dispersion Limited Transmission

Migrating to 10 Gbps - No dispersion compensation.osp

Migrating to 10 Gbps - Dispersion compensation at each node.osp

Migrating to 10 Gbps - Lumped dispersion compensation.osp

In project files "*Migrating to 10 Gbps – No dispersion compensation.osp*", "*Migrating to 10 Gbps - Dispersion compensation at each node.osp*", and "*Migrating to 10 Gbps - Lumped dispersion compensation.osp*", we investigate the issues at high data bit rate, particularly 10 Gb/s (OC-192) systems in metro area ring networks. For high bit rates, in addition to loss compensation, we need to consider the chromatic dispersion compensation. Two possibilities, namely "lumped" and "at each node" dispersion compensation schemes are shown and compared for metro applications.

For this case, the receiver sensitivity is –16 dBm which reduces the allowable loss to $L_{allowable}$ = 3 – (-16) = 13 dB. Assuming again a power of 3 dBm per channel, the amount of amplification needed in the ring is $G_{required}$ = - (3 - 4 x 0.25 x 50 - 4 x 3.8 - (-16) - 3) = 49.2 dB. We can again use unity gain segment approach for power compensation. This calculation shows that migration is easily done in terms of power budgeting since the total loss is not changed, even though the allowable loss is changed.

Let us now look at the criteria for dispersion and try to see if it is a real issue for metro networks.

In the case of directly modulated DFB lasers, the GVD limited transmission distance is calculated by [1,2]

$$L < \frac{1}{4B|D|\sigma_\lambda} \qquad \textbf{(8-3)}$$

Where σ_λ is root-mean-square spectruml width, with a typical value around 0.15 nm, for D = 16 ps/nm-km and 2.5 Gbps, L ~ 42 km.

For an externally modulated source, the GVD limited transmission distance is

$$L < \frac{2\pi c}{16|D|\lambda^2 B^2} \quad \textbf{(8-4)}$$

Again for D = 16 ps/nm-km and 2.5 Gbps, L ~ 500 km. therefore group velocity dispersion (GVD) is not a limiting effect in the above example for a 2.5 Gb/s communication network.

No dispersion compensation

At high bit rates, GVD may become a limiting parameter for the transmission distance. When the bit rate is increased to 10 Gb/s, GVD limited transmission distance drops to ~ 30 km for an EML and ~ 10 km for DML. Figure 8-29 shows the eye diagram when the bit rate is 10 Gb/s and transmitter (DML) power is 3 dBm/channel. In this example, we have used unity gain segment approach, which means the loss in each fiber span and node is compensated immediately before the following node. This project is given in "*Migrating to 10 Gbs - No dispersion compensation.osp*" file.

Figure 8-28: Layout - Migrating to 10 Gbps - No dispersion compensation

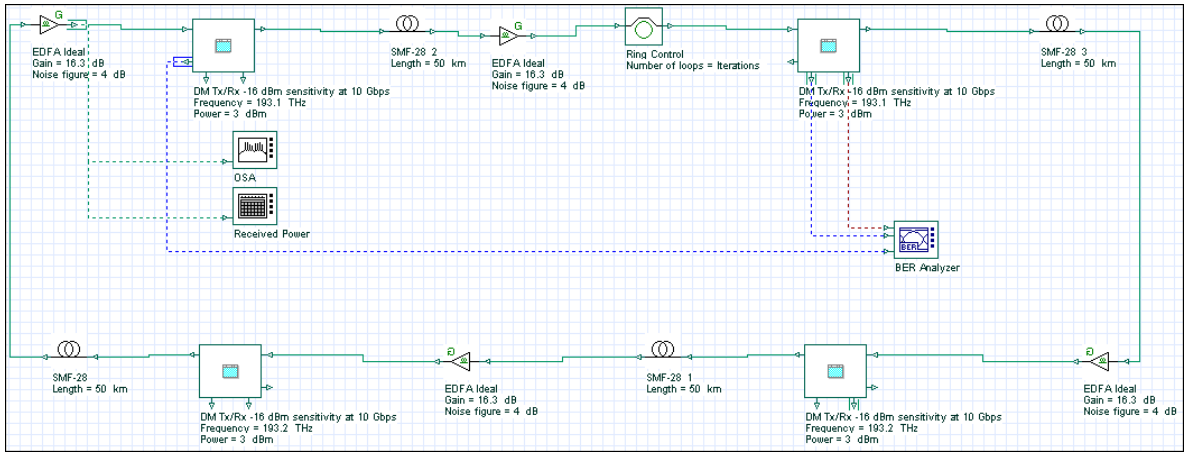
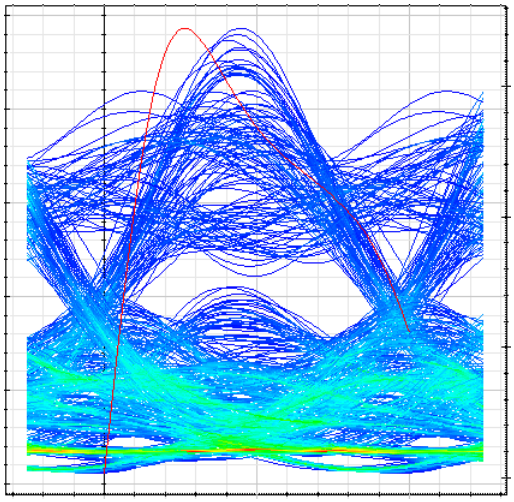


Figure 8-29: Eye diagram of channel 1 at node 4 when the transmitter power is 3 dBm and bit rate is 10 Gb/s



Therefore, at this rate one has to consider dispersion management. Total dispersion per 50 km span is around 16 x 50 = 800 ps/nm. This will require 10 km of dispersion compensating fiber (DCF) with D = -80 ps/nm-km for each fiber span. We can again follow several avenues to compensate the accumulated dispersion.

"Per span" dispersion compensation

For example, DCF can be used after each span or total accumulated dispersion can be compensated at a certain point. Again for the scalability of the network and considering the dynamic structure of the metro traffic, it seems to be the best choice to distribute the dispersion compensation to every node. This will also make sure that dispersion experienced by dynamically routed signals will be compensated properly. For this case, you also need to compensate the power loss of DCFs. For that purpose 2.5 dB more gain is added to each amplifier. The simulation project is given in "*Migrating to 10 Gbps - Dispersion compensation at each node.osp*" file. Figure 8-30 shows the network layout when unity gain approach and per node dispersion compensation is used.

Figure 8-30: Ring network layout when unity gain approach and per span dispersion compensation is used

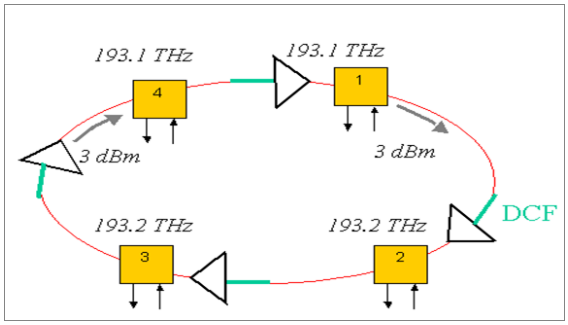


Figure 8-31: Layout - Dispersion compensation at each node

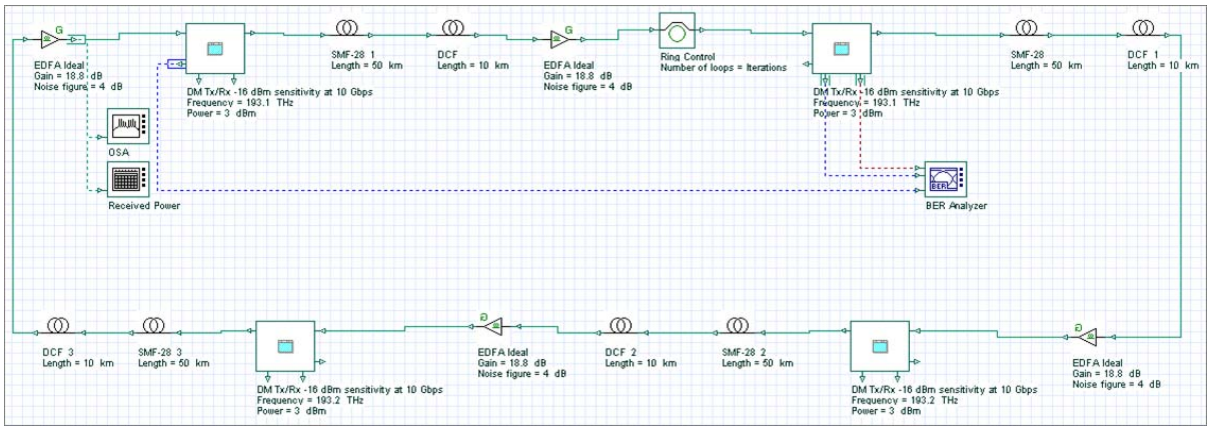
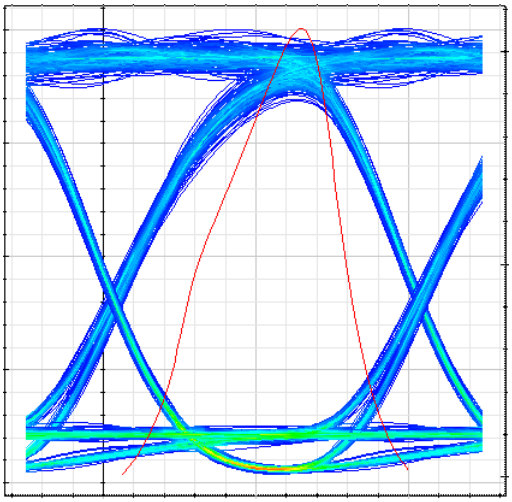


Figure 8-32 shows the eye diagram at the receiving end when per span dispersion compensation is used.

Figure 8-32: Eye diagram at node 4 when per span dispersion compensation is used



"Lumped" dispersion compensation

Now consider the "lumped" dispersion compensation case. In this case, one DCF and extra amplifier is inserted just before node 2 to compensate the total dispersion and extra loss of DCF. This project is given in "*Migrating to 10 Gbps - Lumped dispersion compensation.osp*" file. Figure 8-34 shows the eye diagram at node 4 for this configuration. As can be seen from the eye diagram, this configuration definitely improves the network performance for the considered channel comparing with the uncompensated case, but worse than the case with distributed compensation. Moreover, "lumped" dispersion compensation is not suitable for metro networks in which the wavelength routing path cannot be estimated.

Figure 8-33: Layout - Lumped dispersion compensation

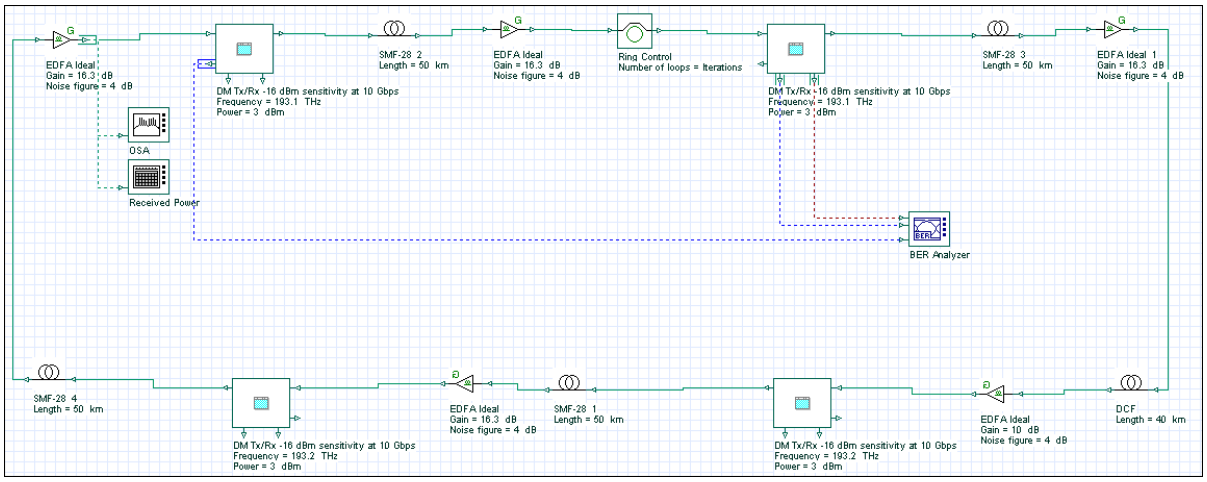
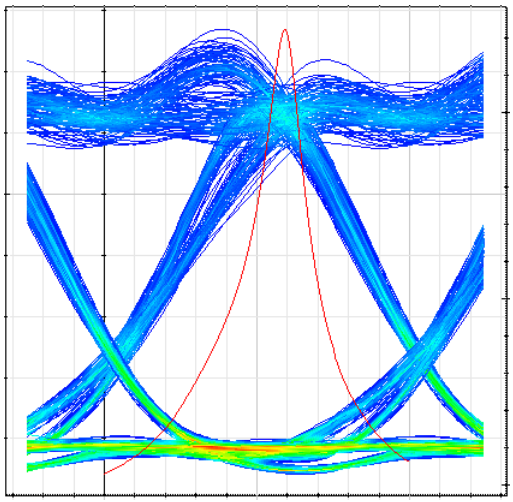


Figure 8-34: Eye diagram at node 4 when "lumped" dispersion compensation is used



References:

[1] G.P. Agrawal, *Fiber-Optic Communication Systems*, 4th ed., John Wiley & Sons, INC., 2010.

[2] R. Ramaswami and K. N. Sivarajan, *Optical Networks: A practical Perspective*, Morgan Kaufmann, 1998.

Notes:

Chapter 9 - Soliton Systems

This section contains the following examples.

- Fundamental and Higher-Order Solitons
- Interaction of A Pair of Fundamental Solitons
- Average Soliton Regime
- Interaction of Multicolor Solitons

Notes:

Fundamental and Higher-Order Solitons

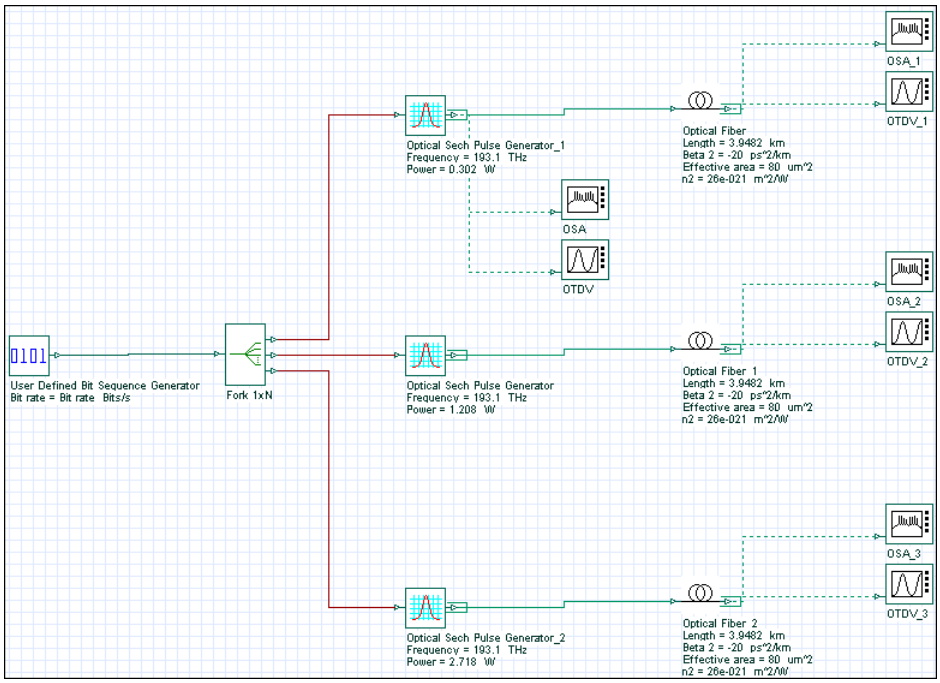
Fundamental and higher-order solitons.osp

The aim of this example is to present numerical results for fundamental and higher-order solitons in SMF at 1.55 μm.

The basic parameter N is defined by $N^2 = \gamma P_0 L_D$, where $\gamma = 2\pi n_2/(\lambda A_{eff})$ is nonlinear coefficient, $L_D = T_0^2/|\beta_2|$ is the dispersion length, P_0 is the peak power, n_2 is the nonlinear refractive index, A_{eff} is the effective core area, $T_0 = T_{FWHM} / 1.763$, and $\beta_2 = (\partial^2\beta)/(\partial\omega^2)$ at ω_0 where β is the propagation constant. The basic parameter N represents a dimensinonless combination of the pulse and fiber parameter.

The optical pulse which corresponds to N = 1 is called fundamental soliton. Pulses with N = 2, and 3 are called second and third-order solitons. The layout for generation of the solitons is shown in Figure 9-1.

Figure 9-1: Layout - Soliton generation



As an optical source, an optical sech pulse generator has been chosen. A 40 Gb/s transmission at 1.55 μm in SMF (β_2 = -20 ps^2/km or D = 16 ps/nm-km) is considered. We consider T_B = 25 ps, T_{FWHM} = 12.5 ps (duty cycle = 0.5) -> L_D = 2.51 km and A_{eff} = 80 μm^2, n_2 = 2.6e-20 m^2/W -> γ = 1.3 $W^{-1}km^{-1}$ -> the peak power of the fundamental soliton P_0 ~ 0.302 W. The power required for obtaining the second- and third-order solitons are 1.208 W and 2.718 W, respectively.

Distance at which the three types of solitons were propagated is equal to so-called soliton period ($Z_0 = \pi/2*L_D$). In our case Z_0 = 3.9482 km. The evaluation of fundamental, second order and third order solitons is shown in Figure 9-2, Figure 9-3, and Figure 9-4.

Figure 9-2: Evolution of the fundamental soliton over one soliton period

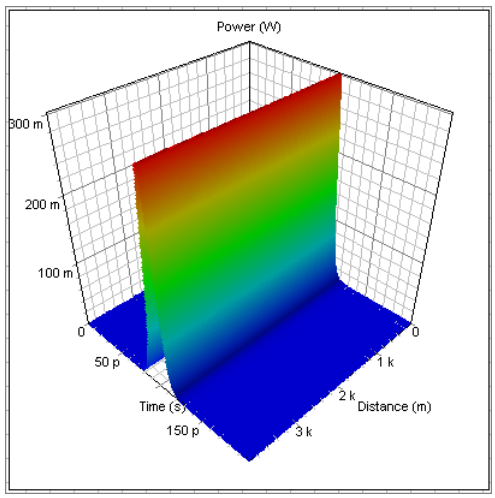


Figure 9-3: Evolution of the second-order soliton over one soliton period

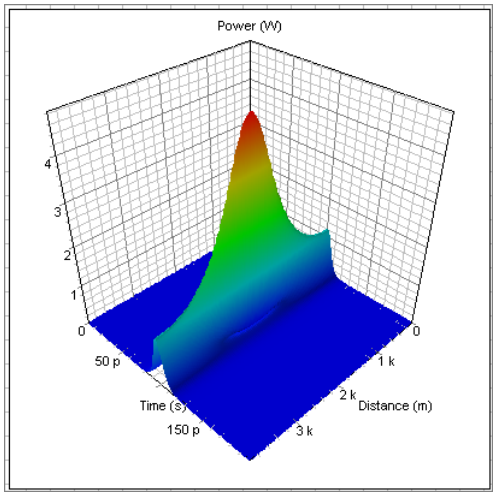
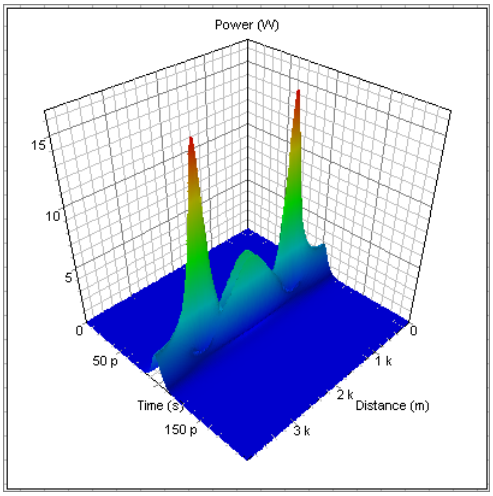


Figure 9-4: Evolution of the third order soliton over one soliton period



References:

[1] G.P. Agrawal, *Nonlinear Fiber optics*, third edition, Academic Press, 2001.

[2] G.P. Agrawal, *Fiber-Optic Communication Systems*, 4th ed., John Wiley & Sons, INC., 2010.

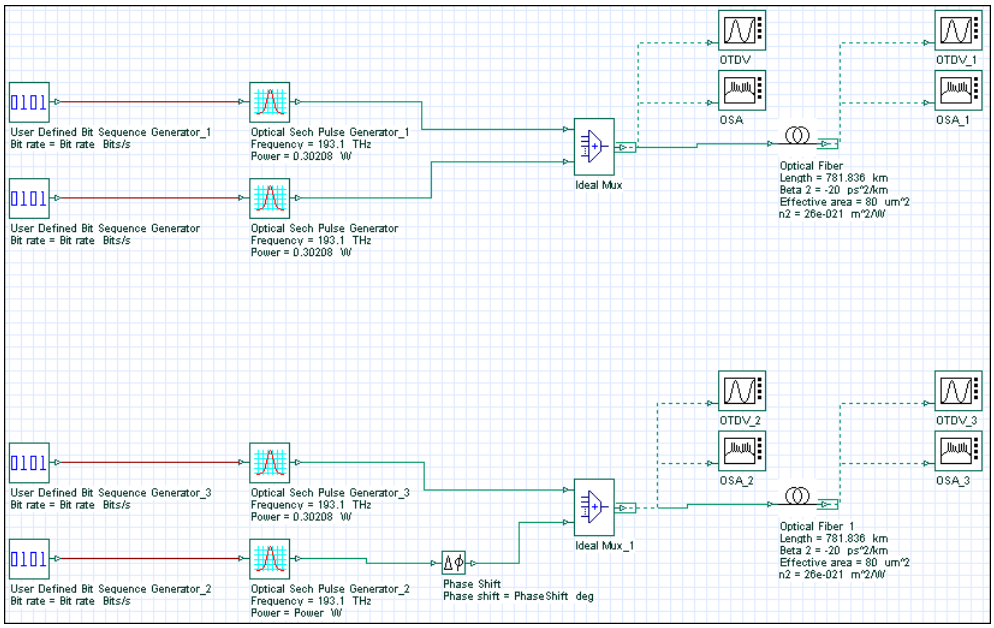
Notes:

Interaction of A Pair of Fundamental Solitons

Interaction of a pair of fundamental solitons.osp

Project file "*Interaction of a pair of fundamental solitons.osp*" demonstrates the interaction of two adjacent solitons. If the solitons are not well separated in time, depending on their phases they will either periodically collide or repeal from each other. In this example, two in phase soliton pulses are launched into a nonlinear dispersive fiber. They periodically collide inside the fiber. The collision period depends on the input time shift between the pulses. As a comparision, the propagation of two π-out-of-phase soliton pulses in a fiber is also shown.

Figure 9-5: Layout - Interaction of a pair of fundamental solitons



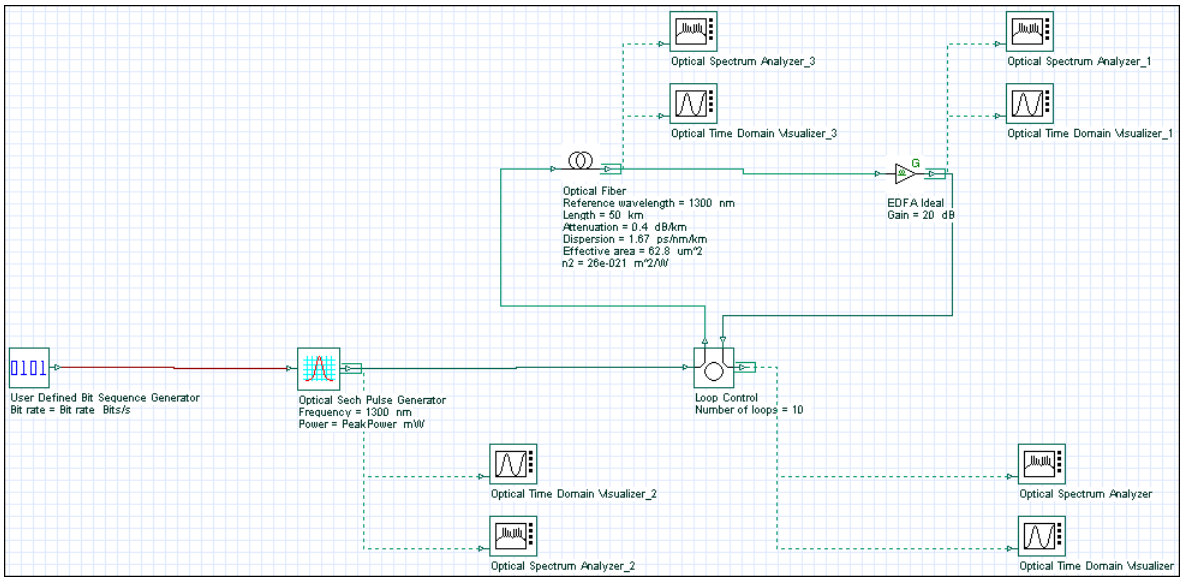
Notes:

Average Soliton Regime

Average soliton regime.osp

The aim of this example is to demonstrate the average soliton regime at 10 Gb/s transmission over a 500 km optical link consisted of SMF. The corresponding layout has been shown below in Figure 9-6.

Figure 9-6: Layout - Average soliton regime



We fixed B = 10 Gb/s -> T_B = 100 ps. The sequence length is 16 bit. The carrier wavelength of the pulse is ~ 1300 nm. T_{FWHM} = 20 ps -> $T_0 = 0.567 \times T_{FWHM} \sim 11.34$ ps. The input pulse peak power is 27.1 mW.

We have considered SMF with a length of 50 km and loss of 0.4 dB/km. D = 1.67 ps/nm-km -> L_D = 85 km. (The effects of group delay and third order dispersion are not taken into account). After every 50 km of fiber, the signal will be amplified using an EDFA, therefore, L_A = 50 km. Note tha the condition $L_A < L_D$ is satisfied.

The value of Kerr nonlinearity coefficient $\gamma = n_2\omega_0/(cA_{eff})$ can be calculated with $n_2 = 2.6 \times 10^{-20}$ m^2/W and $A_{eff} = 62.8$ μm^2. The value comes out to be 2 $W^{-1}km^{-1}$.

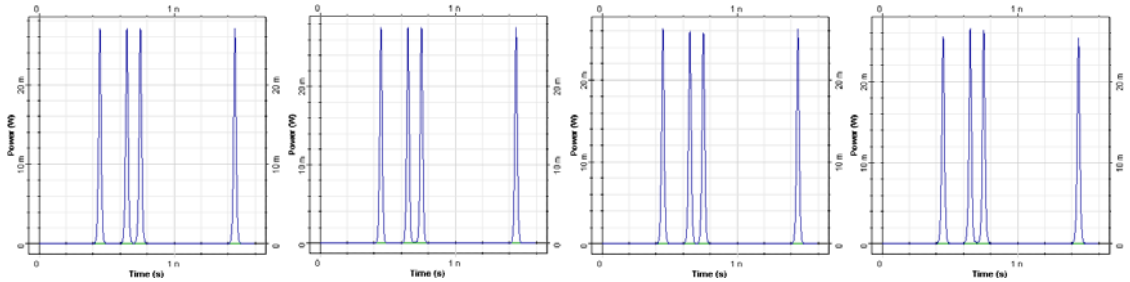
The linear loss for 50 km SMF is 20 dB. The loss is periodically compensated with an ideal EDFA with 20 dB gain.

Soliton peak power for this fiber is 5.8 mW. The pulse peak power of the average soliton is 27.1 mW. To demonstrate the importance of the input pulse peak power of the average soliton, we will consider soliton propagation in 500 km of SMF with two different input pulse peak power values: 5.8 mW (usual soliton peak power) and 27.1mW (modified soliton peak power) which takes into account the periodical

amplification, respectively. Each case includes sweeps on the number of loops: 0, 4, 7 and 10 which represent the propagation distances of 0, 200, 350 and 500 km in SMF.

Figure 9-7 shows the initial pattern of pulses and the pattern of pulses after 200, 350 and 500 km of SMF, respectively. The periodic amplification has been done with EDFA at every 50 km of SMF with 27.1 mW as the peak power.

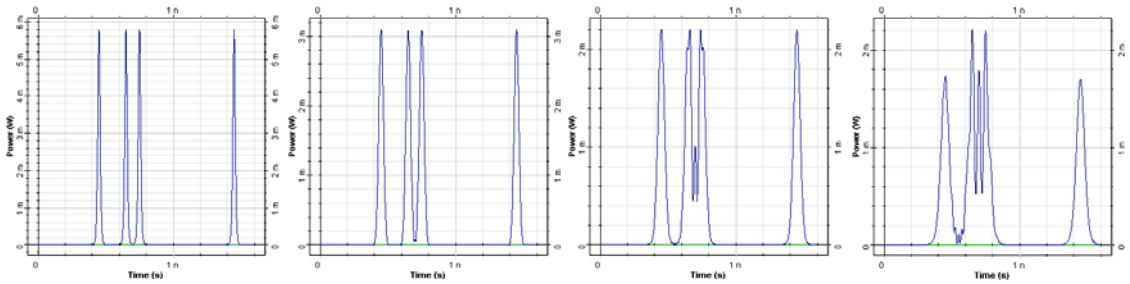
Figure 9-7: (a) Initial pulse pattern (b) Pulse pattern after 200 km of SMF (c) Pulse pattern after 350 km of SMF (d) Pulse pattern after 500 km of SMF



As can be seen, the pattern of pulses is well-preserved. The average soliton concept is valid for these pulse, fiber, and amplifier parameters.

Figure 9-8 shows the initial pattern of pulses and the pattern of pulses after 200, 350 and 500 km of SMF, respectively. The periodic amplification has been done with EDFA at every 50 km of SMF with 5.8 mW as the peak power.

Figure 9-8: (a) Initial pulse pattern (b) Pulse pattern after 200 km of SMF (c) Pulse pattern after 350 km of SMF (d) Pulse pattern after 500 km of SMF



Because of the improper pulse peak power used, the pulses do not preserve their original forms. As a result, pulses broaden and complicated structures appear.

References:

[1] G.P. Agrawal, *Applications of nonlinear fiber optics*, Academic Press, 2001.

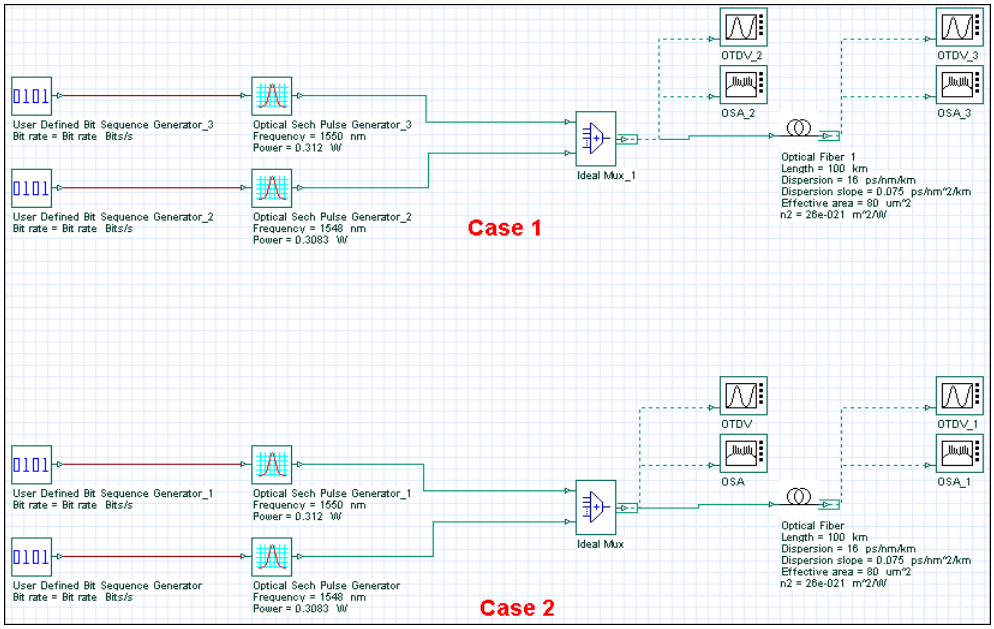
[2] G.P. Agrawal, *Fiber-Optic Communication Systems*, 4th ed., John Wiley & Sons, INC., 2010.

Interaction of Multicolor Solitons

Interaction of multicolor solitons.osp

Project file "*Interaction of multicolor solitons.osp*" demonstrates a 2 channel soliton communication system. The first case shows the interaction of two isolated pulses carried on two different carrier frequencies. In this case, power of each channel must be adjusted according to the value of dispersion at that specific wavelength to satisfy the soliton condition for each soliton pulse from different channels. In the second case, each channel contains two soliton pulses; they interact among themselves and with the pulses in other channels.

Figure 9-9: Layout - Interaction of multicolor solitons



Notes:

Chapter 10 - Advanced Lightwave Systems

This section contains the following examples.

- Intensity Modulation Formats (NRZ, RZ, AMI, DB)
- DPSK Modulation and Demodulation
- QPSK Modulation and Demodulation
- 100 Gbps PM-QPSK
- OD8PSK Modulation and Demodulation
- 4-QAM OFDM Modulation and Demodulation

Notes:

Intensity Modulation Formats (NRZ, RZ, AMI, DB)

NRZ (NonChirped, Chirped, Alternate-Chirp, VSB).osp

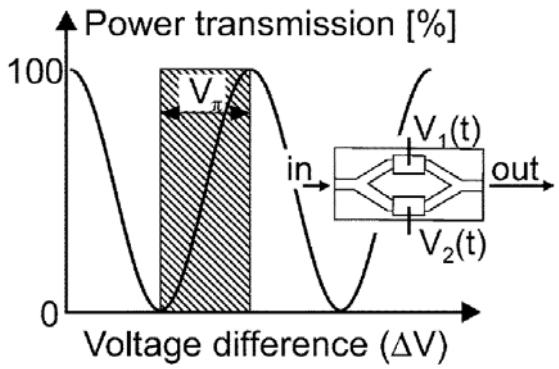
RZ (50%RZ, 33%RZ, 67%CSRZ, Chirped, Alternate-Chirp, VSB).osp

DB.osp

AMI.osp

For a dual-drive Mach-Zehnder modulator (MZM), the power transfer function is shown in Figure 10-1.

Figure 10-1: Power transfer function of a dual-dirve MZM (from Ref. [1])



The optical field transfer function $T_E(V_1,V_2)$ of the MZM is [1]:

$$T_E(V_1, V_2) = e^{j\left(\pi\frac{V_1+V_2}{2V_\pi}+\frac{\psi}{2}\right)}\cos\left[\pi\frac{V_1-V_2}{2V_\pi}-\frac{\psi}{2}\right] \quad \textbf{(10-1)}$$

where V_1 and V_2 are the voltages applied on the two MZM arms, and ψ is an additional, temporally constant phase shift in one of the arms, referred to as the modulator bias.

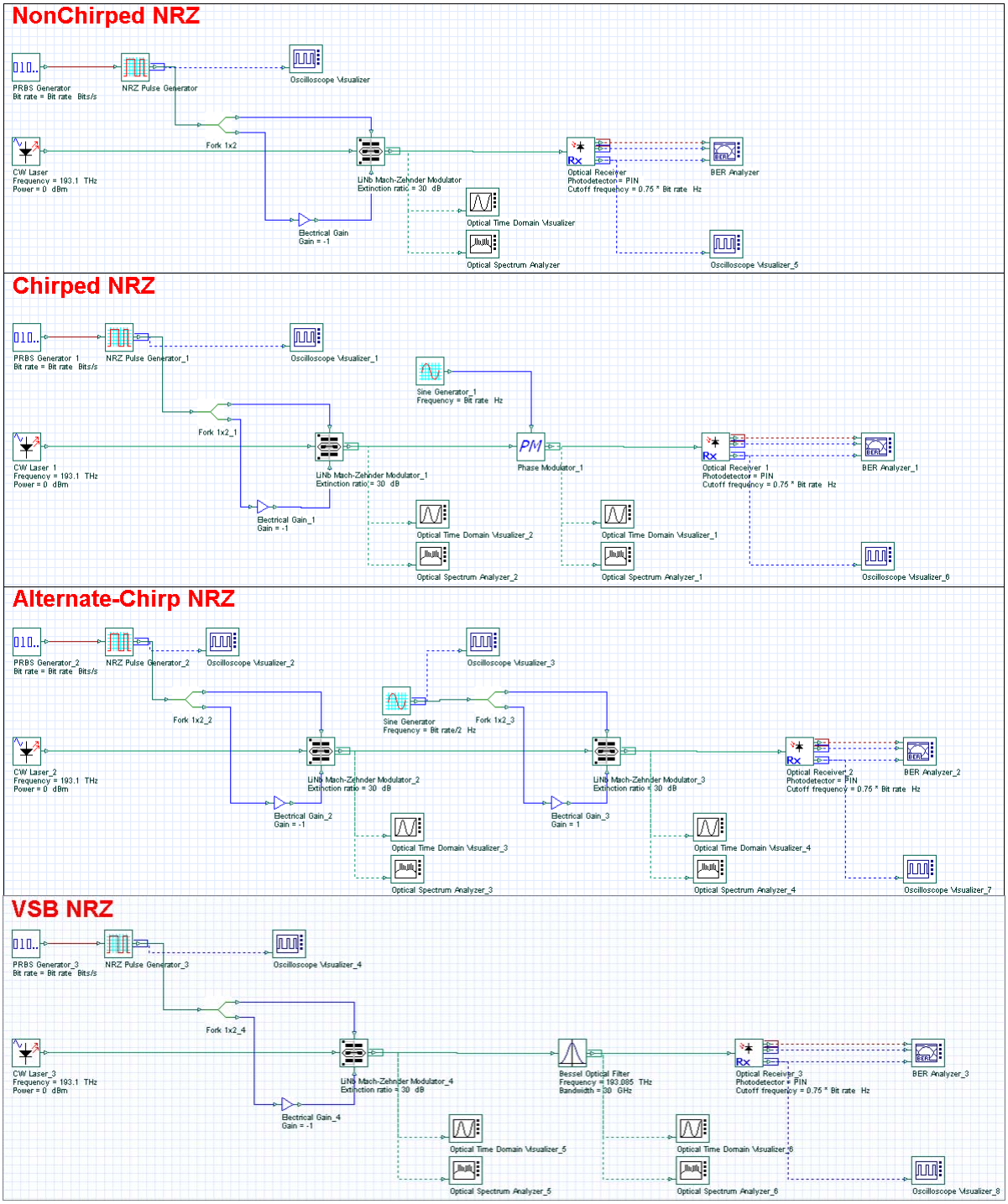
As can be seen, when $V_1 = V_2$, we can achieve a constant power transmission with some phase modulation added to the signal; when $V_1 = -V_2$, the MZM won't add any phase modulation to the input signal, but the intensity of input signal is modulated.

For all the projects we discussed in the example Intensity Modulation (NRZ, RZ, AMI, DB), the Bit Rate is set to a constant value of 10 Gbps, so readers can compare the spectrum of different intensity modulation formats directly.

(a) NRZ (NonChirped, Chirped, Alternate-Chirp, VSB) modulation format

Figure 10-2 shows the layouts for generating NonChirped, Chirped, Alternate-Chirp, and VSB NRZ signals, separately.

Figure 10-2: Layout - NonChirped, Chirped, Alternate-Chirp, and VSB NRZ signals



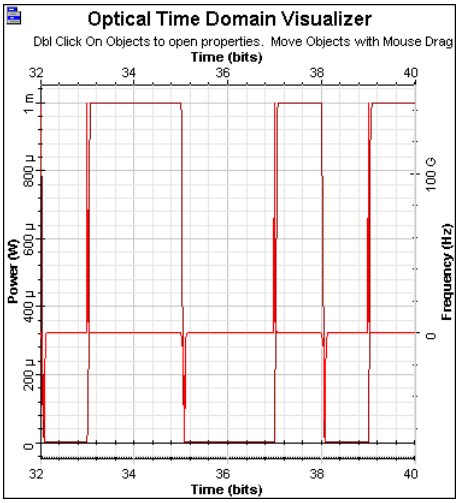
The nonchirped NRZ signal is generated by biasing the dual-drive MZM modulator at the quadrature point, which is 50% transmission, and driving from minimum to maximum transmission with a voltage swing of V_{pi} [1]. For the chirped NRZ signal, it is generated by sending the nonchirped NRZ signal to an

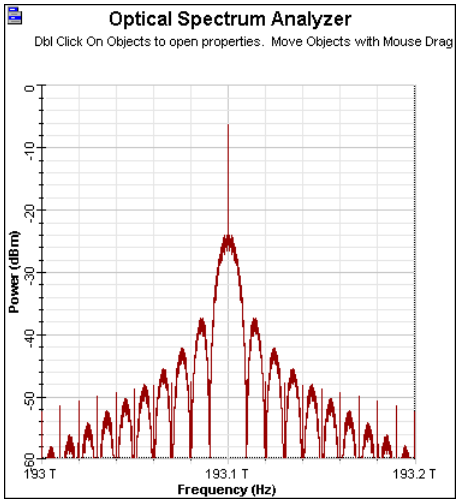
additional phase modulator, which is driven by a sine wave generator working at the same bit rate as the NRZ signal. When it comes to the alternate-chirp NRZ signal, a dual-drive MZM modulator (acting as a phase modulator by setting equal voltage on the two arms) driven by a sine wave generator at half the bit rate is used after the generation of nonchirped NRZ signal. VSB NRZ signal is generated by applying an optical filter (centered with an offset from the optical carrier frequency) to the nonchirped NRZ signal to suppress major parts of one sideband as well as perform some filter action on the other [1].

The output signal profile (both intensity and chirp) as well as the spectrum for NonChirped, Chirped, Alternate-Chirp, and VSB NRZ signals can be seen in Figure 10-3.

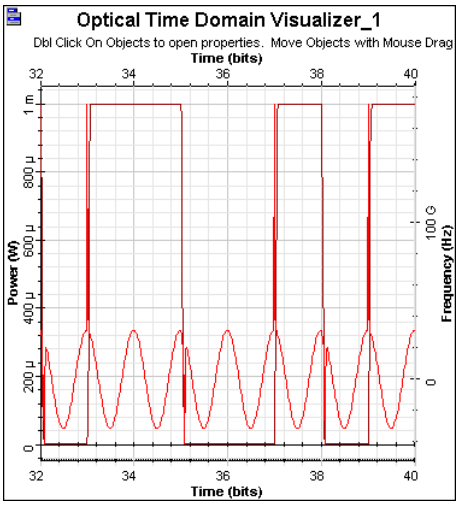
Figure 10-3: Output signal profile (intensity and chirp) and spectrum of NRZ signals

NonChirped





Chirped



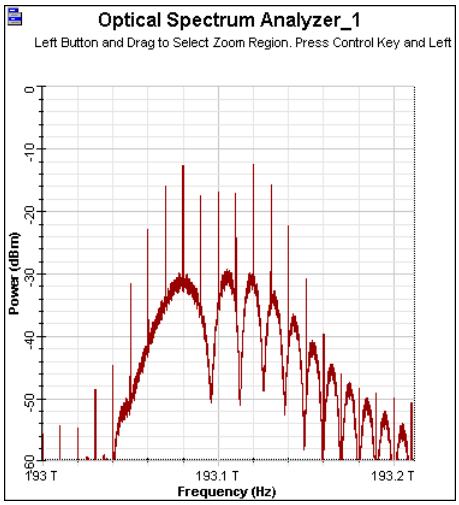
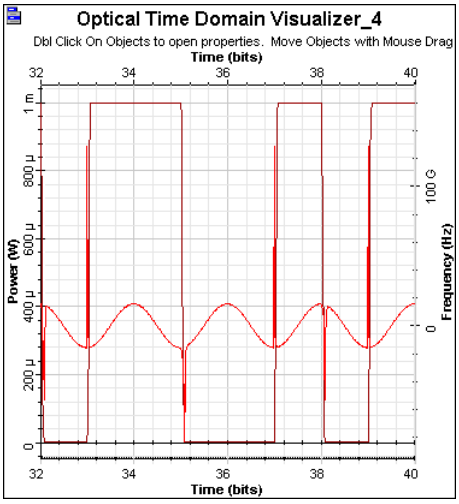
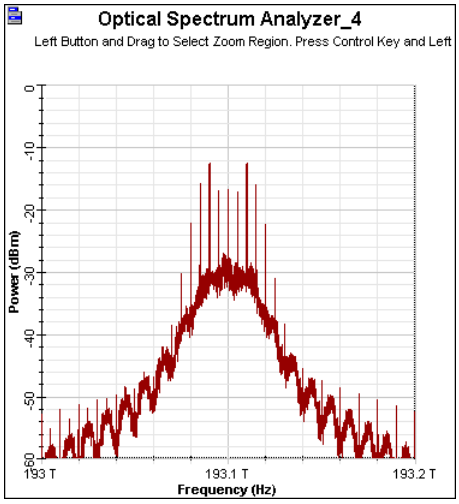


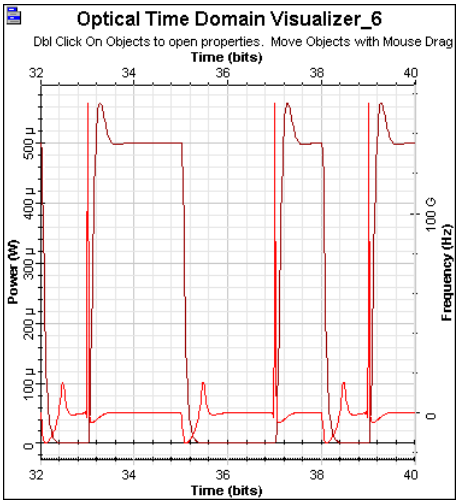
Figure 10-3: Output pulse profile (intensity and chirp) and spectrum of NRZ signals

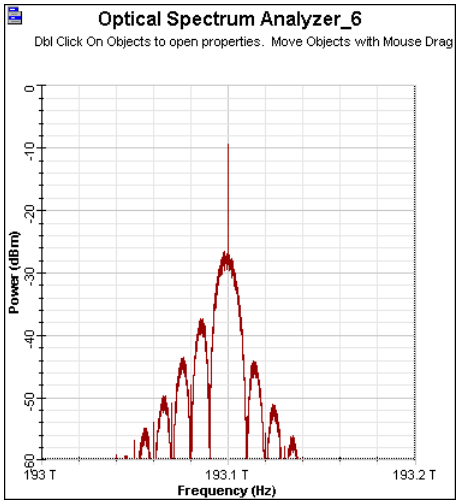
Alternate-Chirp





VSB





(b) RZ (50%RZ, 33%RZ, 67%CSRZ, Chirped, Alternate-Chirp, VSB) modulation format

The layouts for generating 50%RZ, 33%RZ, 67%CSRZ, Chirped, Alternate-Chirp, and VSB RZ signals are shown in Figure 10-4, separately.

Figure 10-4: Layout - 50%RZ, 33%RZ, 67%CSRZ, and Chirped RZ signals

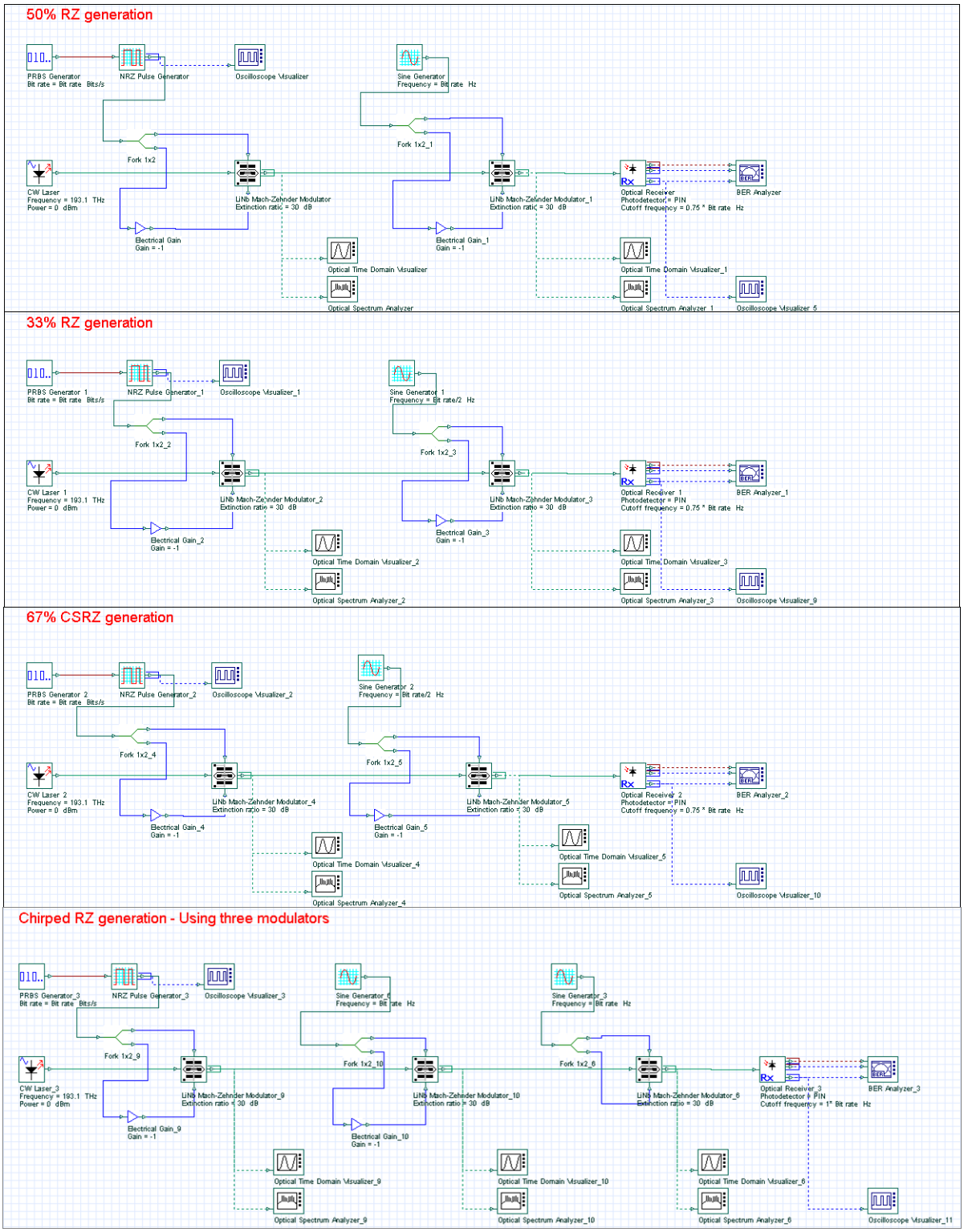
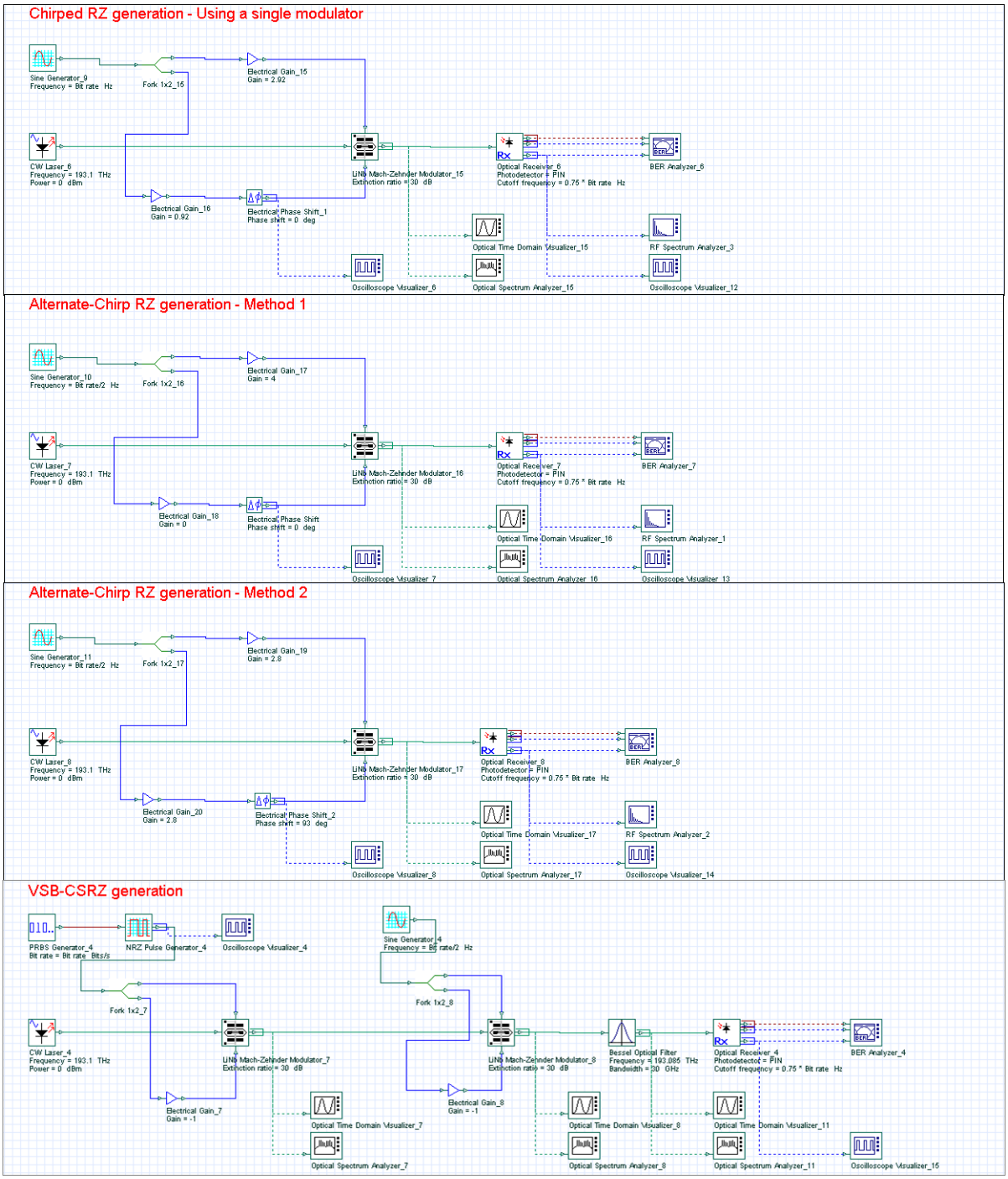


Figure 10-4: Layout - Chirped, Alternate-Chirp, and VSB RZ signals



RZ signal is usually obtained by carving a NRZ signal using an additional modulator. If this additional modulator is sinusoidally driven at the data rate between minimum and maximum transmission, 50%RZ (RZ pulse with a FWHM of 50% of the bit duration) signal can be generated; if this additional modulator is sinusoidally driven at half the data rate between its transmission minima, then 33%RZ signal is

generated; if this additional modulator is sinusoidally driven at half the data rate between its transmission maxima, then 67%CSRZ (phase inversion between adjacent bits is caused because the field transfer function of the MZM changes its sign when crossing the transmission minimum) signal can be obtained [1].

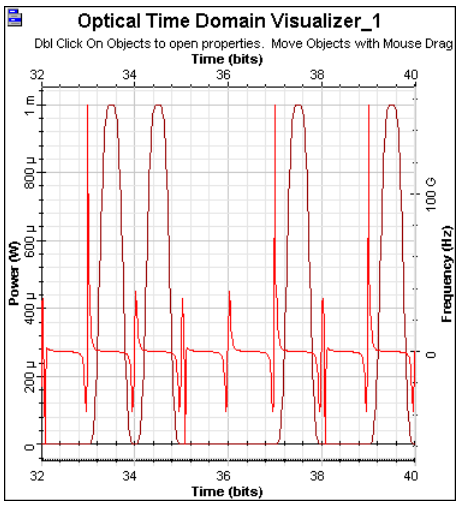
For the chirped RZ signal, one way is to use a third MZM to introduce the additional phase modulation; alternatively, chirped RZ signal can be generated using only one MZM, as shown in Figure 10-4. Two methods of generating alternate-chirp RZ signal are also shown in Figure 10-4. More details about the principles of the *Chirped RZ generation - Using a single modulator*, *Alternate-chirp RZ generation - Method1*, and *Alternate-Chirp RZ generation - Method 2* can be found in [2].

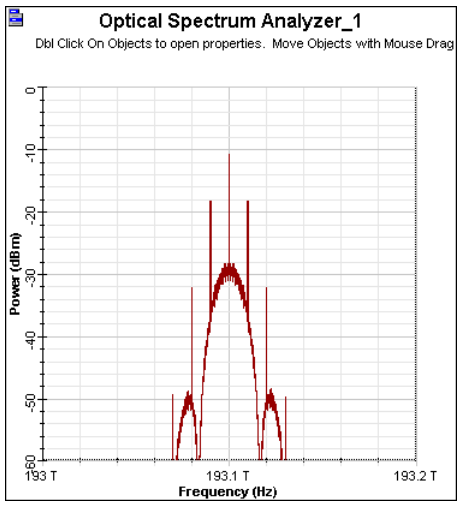
Similar to the generation of VSB NRZ signal, the VSB-CSRZ signal can be obtained by applying a filter on the CSRZ signal.

The output signal profile (intensity and chirp) and spectrum for the 50%RZ, 33%RZ, 67%CSRZ, Chirped, Alternate-Chirp, and VSB RZ signals are shown in Figure 10-5:

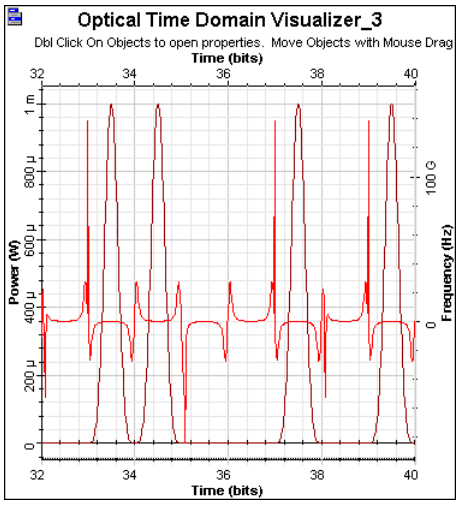
Figure 10-5: Output signal profile (intensity and chirp) and spectrum of RZ signals

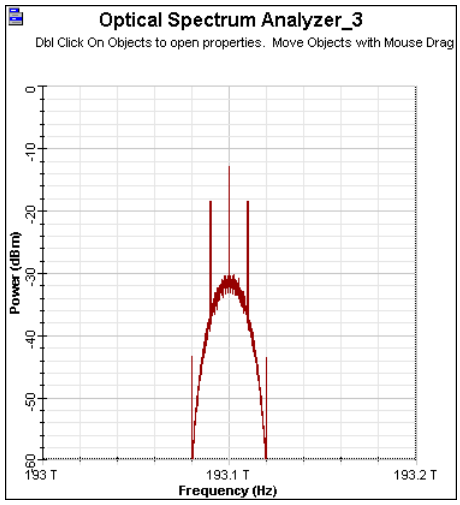
50% RZ



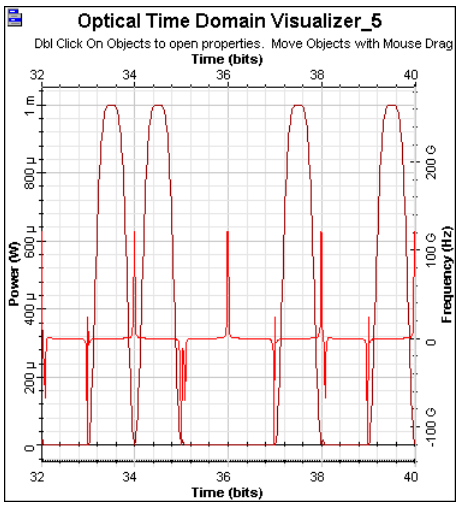


33% RZ





67% CSRZ



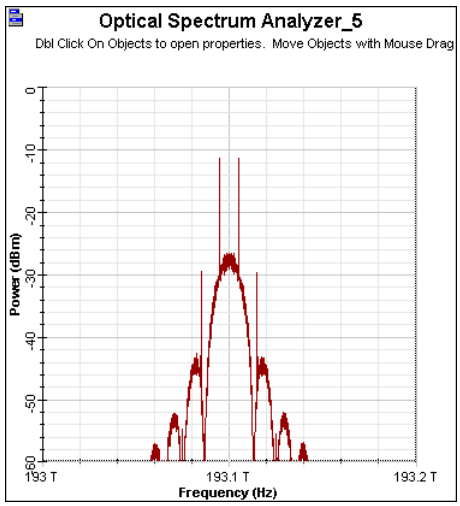
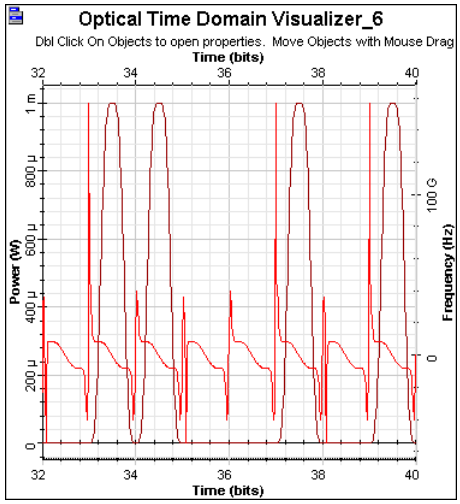
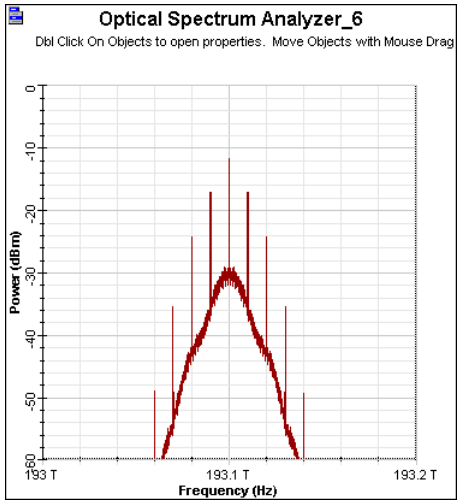


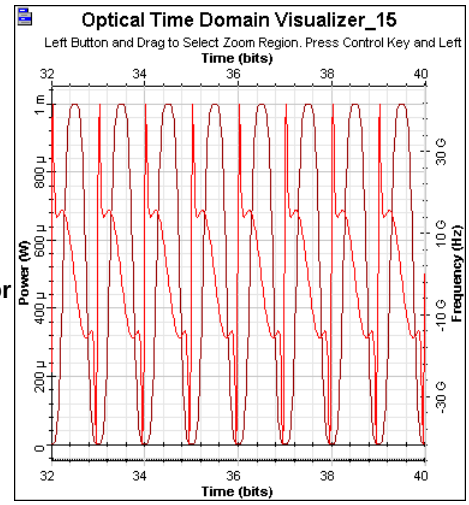
Figure 10-5: Output signal profile (intensity and chirp) and spectrum of RZ signals

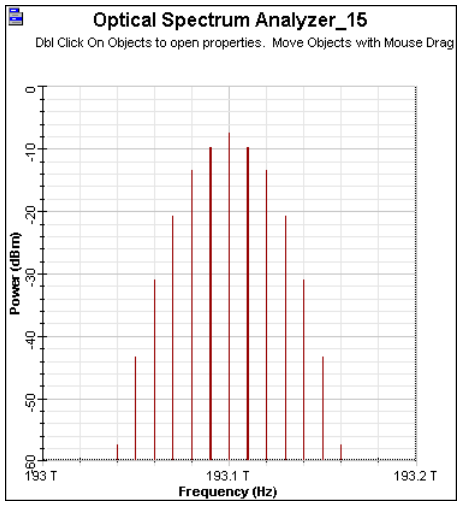
Chirped RZ with three modulators



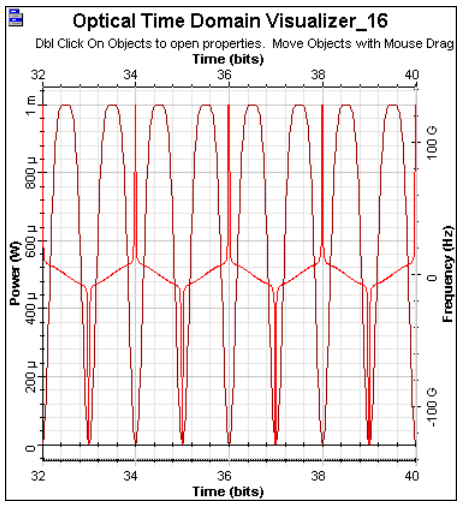


Chirped RZ with a single modulator





Alternate-Chirp RZ - Method 1



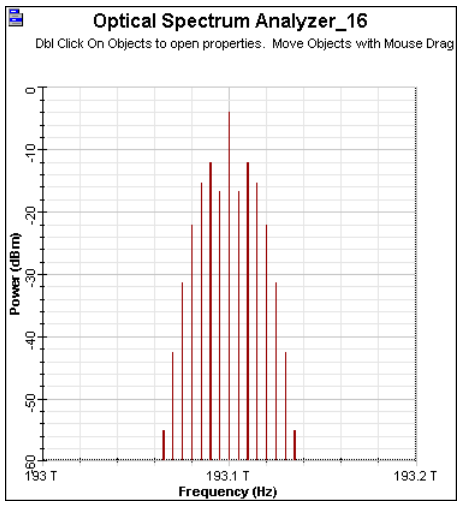
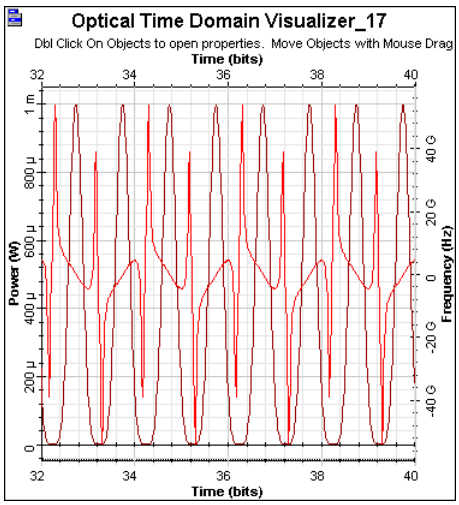
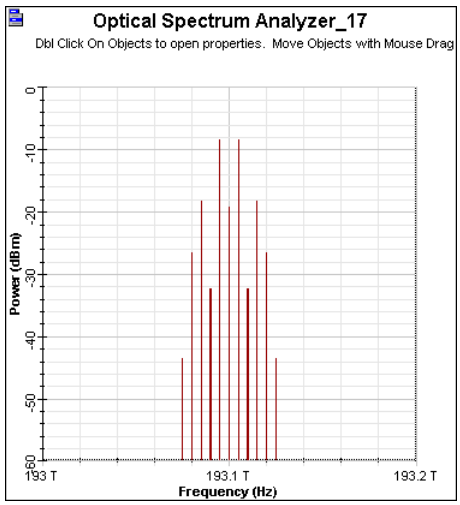


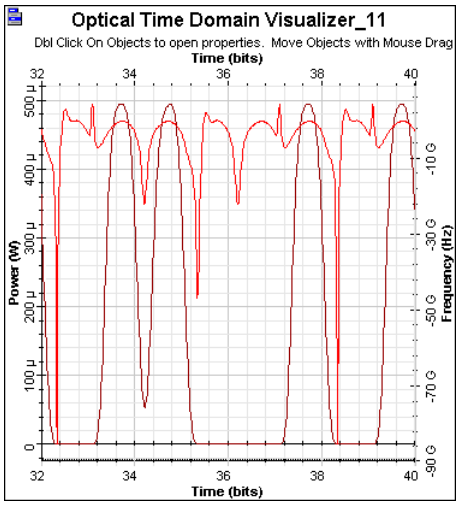
Figure 10-5: Output pulse profile (intensity and chirp) and spectrum of RZ signals

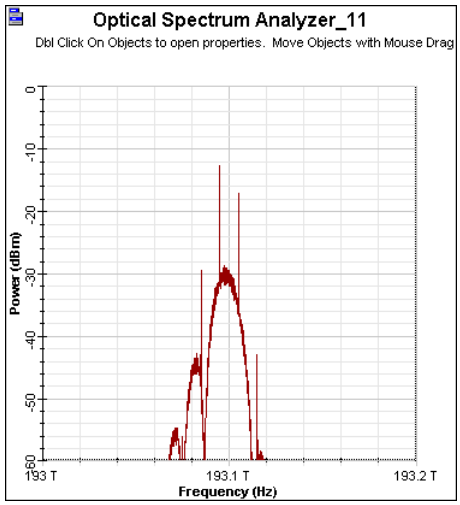
Alternate-Chirp RZ - Method 2





VSB-CSRZ

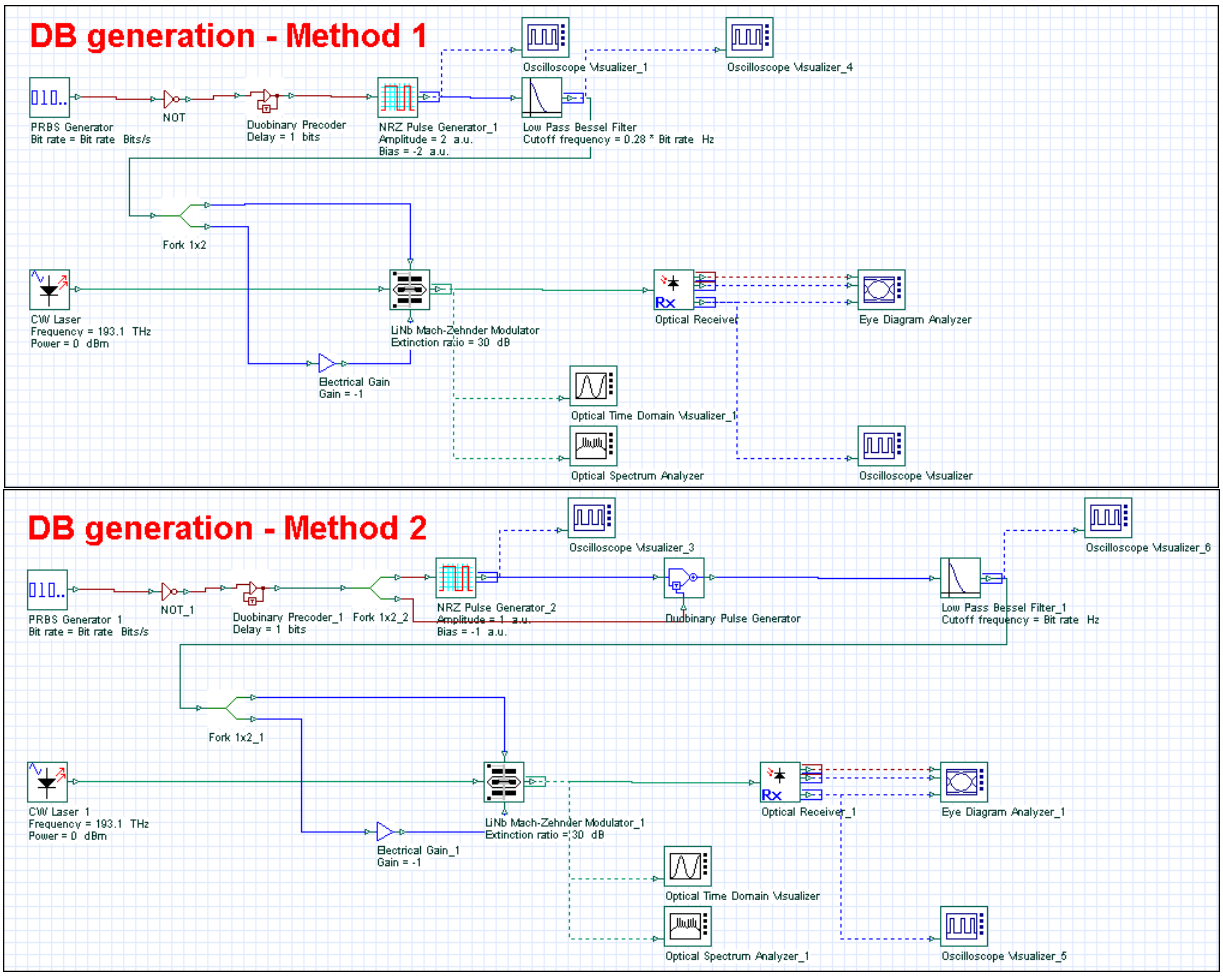




(c) Duobinary modulation format

Two methods of generating a duobinary signal are shown in Figure 10-6, with details of principles explained in [1].

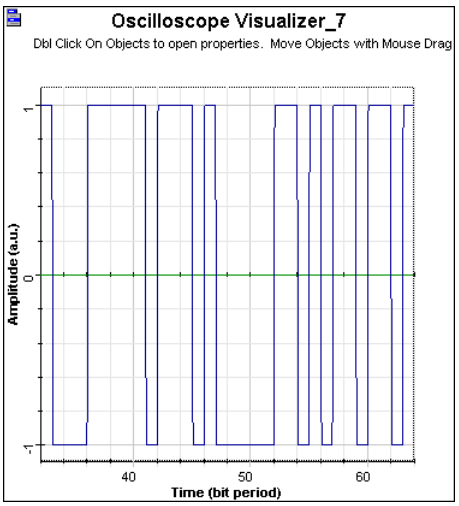
Figure 10-6: Layout - Duobinary signals



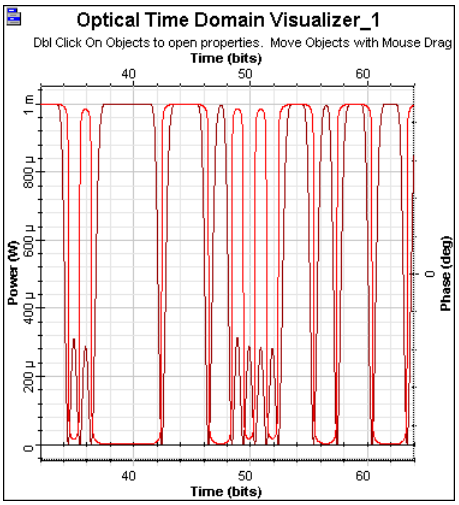
The corresponding output signal profile (intensity and phase) as well as spectrum are shown in Figure 10-7.

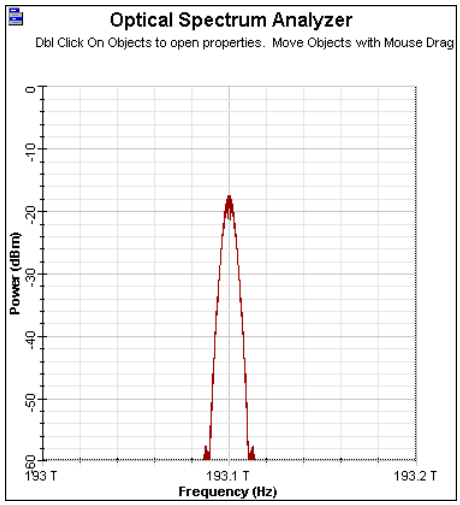
Figure 10-7: Output signal profile (intensity and phase) and spectrum of Duobinary signals

Input bit sequence

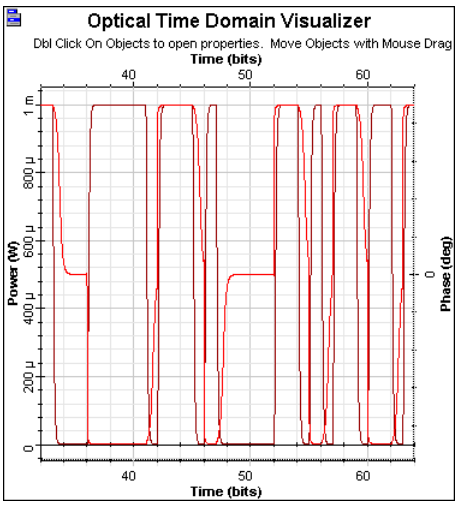


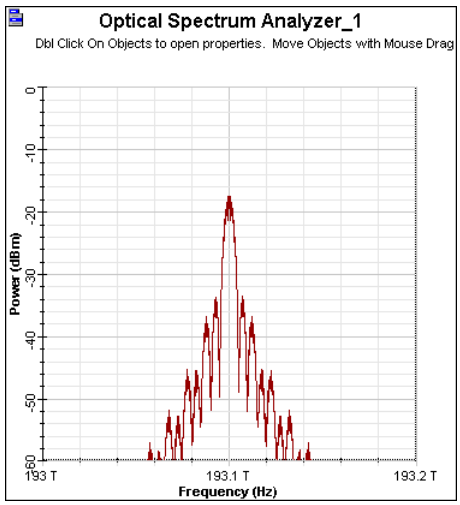
Output Method 1





Output Method 2

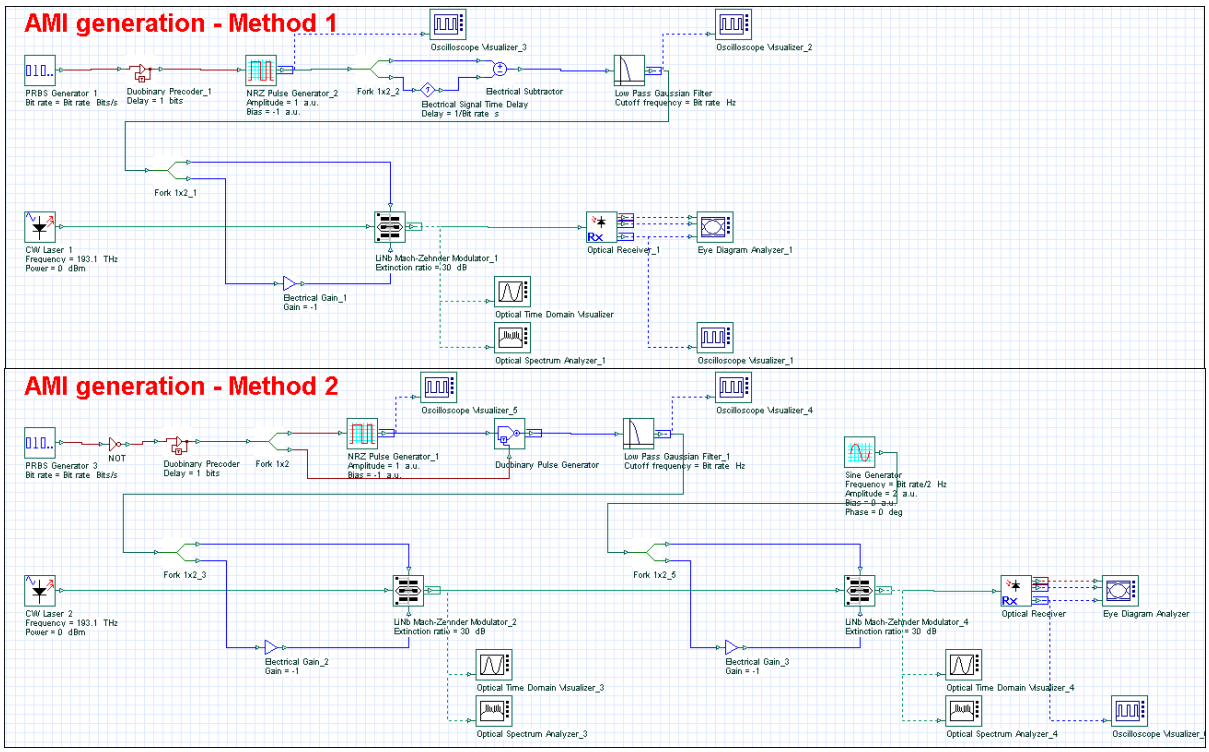




(d) Alternate-mark inversion (AMI) modulation format

Two methods of generating an AMI signal are shown in Figure 10-8, with details of principles explained in [1].

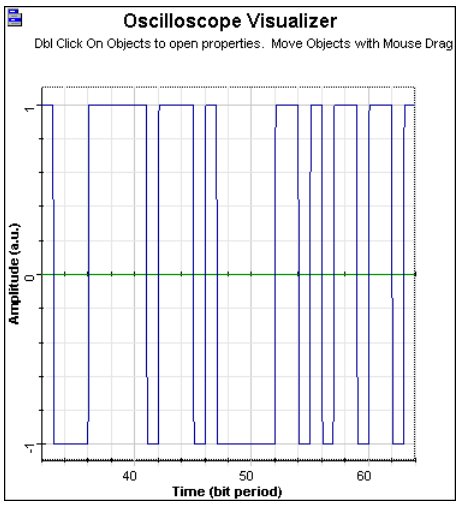
Figure 10-8: Layout - AMI signals



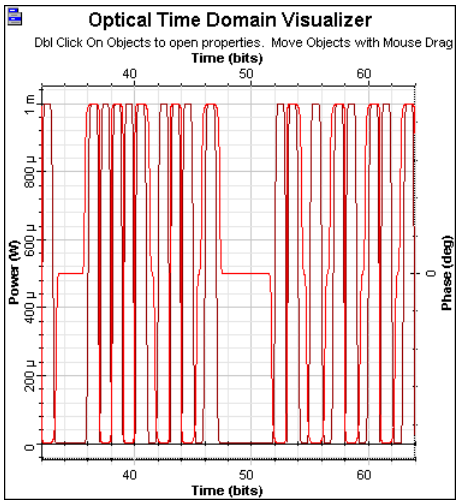
The corresponding output signal profile (intensity and phase) as well as spectrum are shown in Figure 10-9.

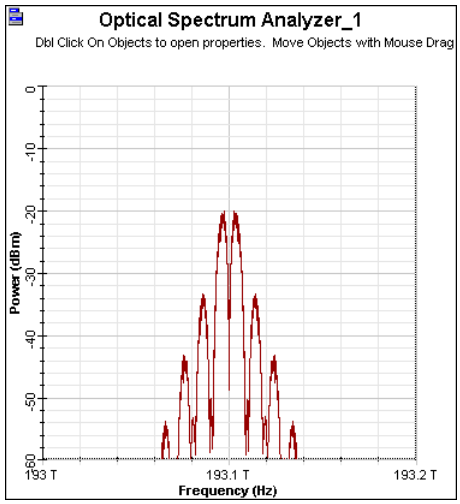
Figure 10-9: Output signal profile (intensity and phase) and spectrum of AMI signals

Input bit sequence

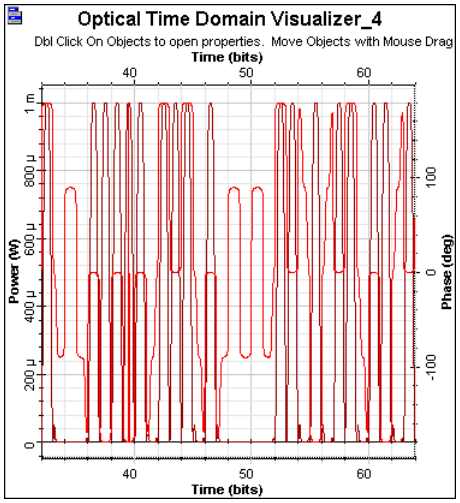


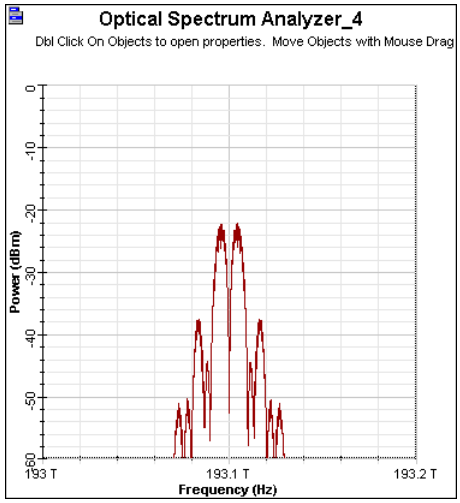
Output Method 1





Output Method 2





References:

[1] P. J. Winzer, R.-J. Essiambre, “Advanced optical modulation formats“, Proceedings of the IEEE, Vol. 94, No. 5, May 2006

[2] P. J. Winzer, C. Dorrer, R.-J. Essiambre, and I. Kang, “Chirped retrun-to-zero modulation by imbalanced pulse carver driving signals“, IEEE Photonics Technology Letter, Vol. 16, No. 5, May 2004

DPSK Modulation and Demodulation

NRZ-DPSK.osp

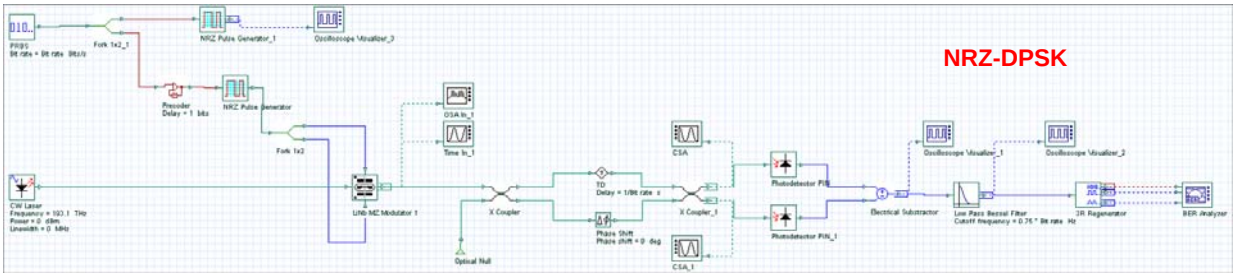
33% RZ-DPSK.osp

50% RZ-DPSK.osp

67% RZ-DPSK.osp

In contrast with the intensity modulation formats, information of the differential binary PSK (DPSK) is encoded on the binary phase change between adjacent bits: a 1 bit is encoded onto a pi phase change, whereas a 0 bit is represented by the absence of a phase change [1]. The layouts for generating NRZ-DPSK, 33% RZ-DPSK, 50% RZ-DPSK, and 67% RZ-DPSK signals are shown in Figure 10-10. Again, all the simulation projects presented in this example have a bit rate equals to 10 Gbps.

Figure 10-10: Layout - NRZ-DPSK and 33% RZ-DPSK signals



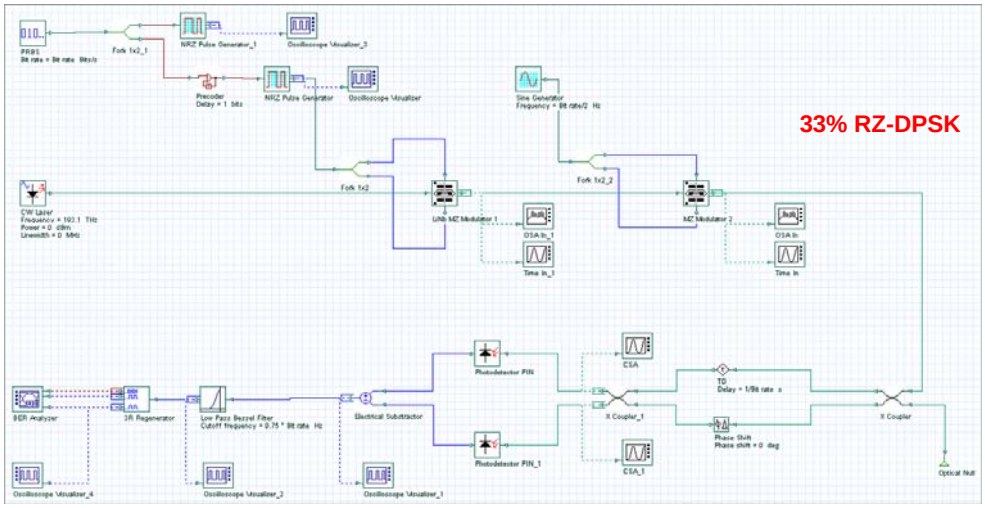
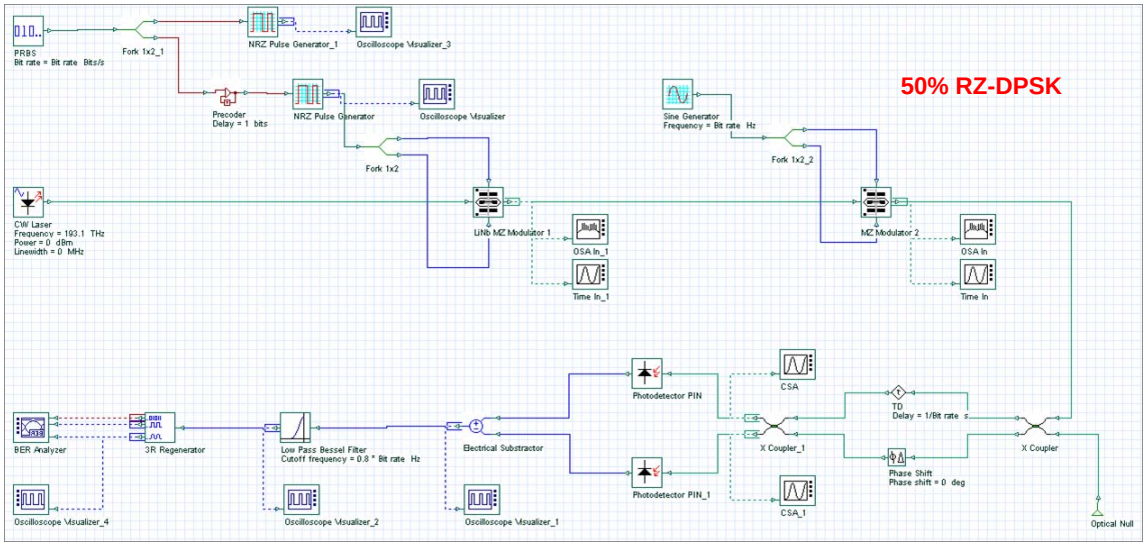
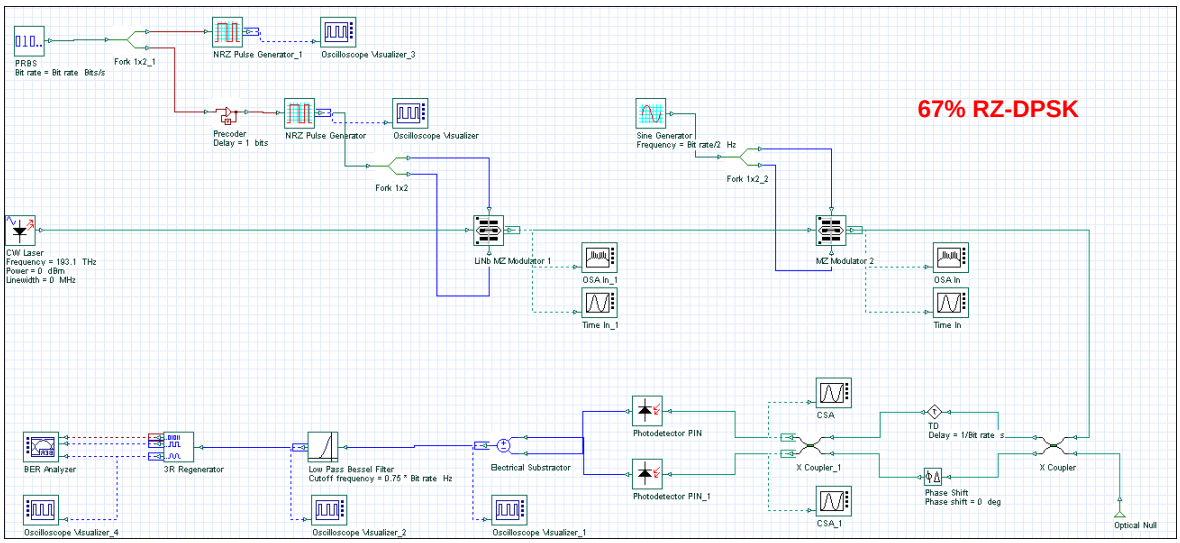


Figure 10-10: Layout - 50% and 67% RZ-DPSK signals



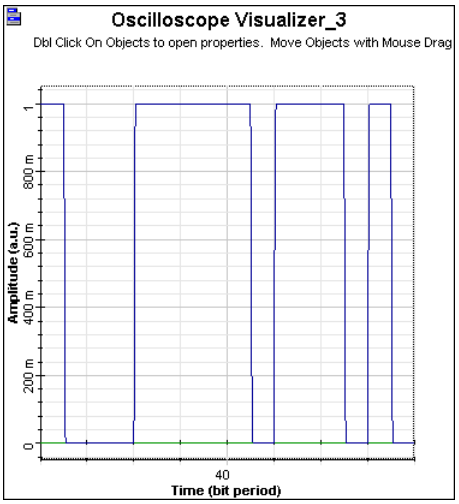


For the NRZ-DPSK signal generation, the dual-driven MZM is biased at the maximum transmission point and driven with voltage $V_1 = V_2$, so only the phase of the input light is being modulated. To get a RZ-DPSK signal, a second modulator is used to carve the NRZ-DPSK signal, in a way similar to the generation of RZ signal from NRZ signal. For the demodulation, the delay demodulation scheme is being employed.

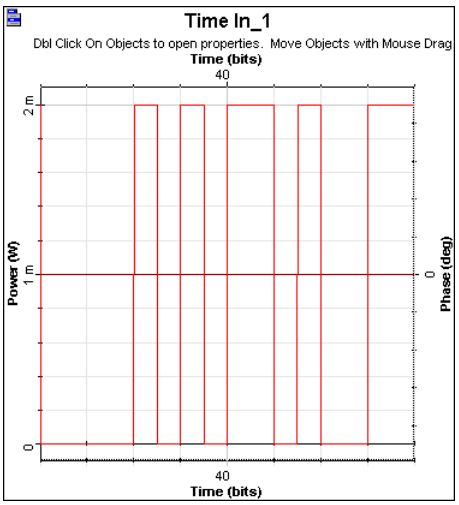
The corresponding output signal profile (intensity and phase) as well as the spectrum are shown in Figure 10-11:

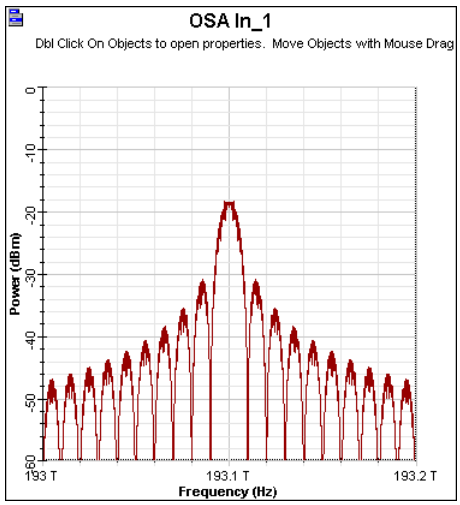
Figure 10-11: Output signal profile (intensity and phase) and spectrum of DPSK signals

Input bit sequence

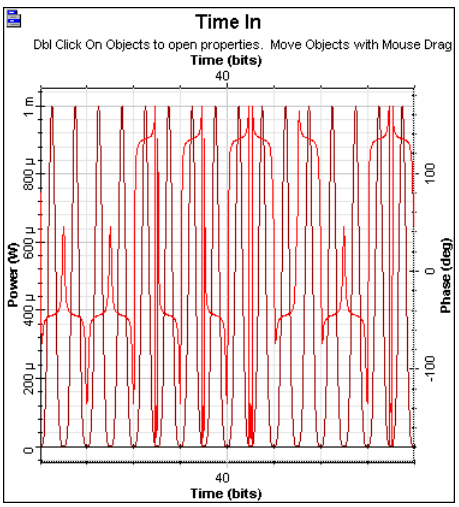


NRZ-DPSK





33% RZ-DPSK



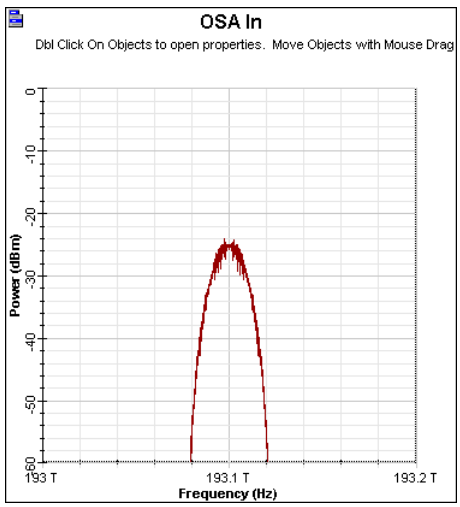
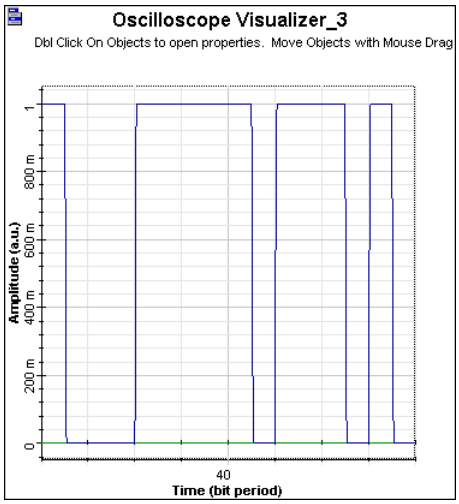
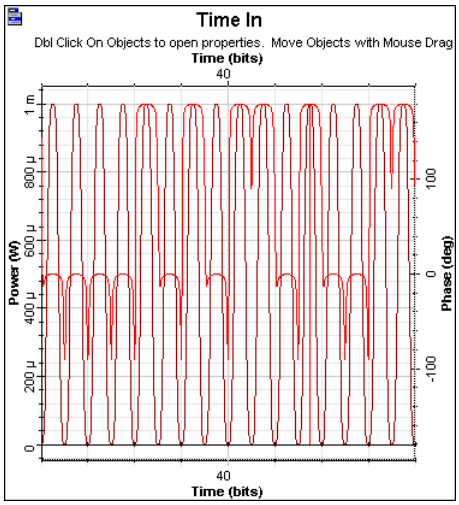


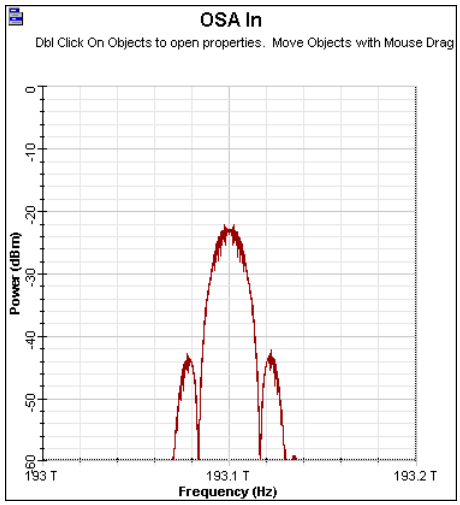
Figure 10-11: Output signal profile (intensity and phase) and spectrum of DPSK signals

Input bit sequence

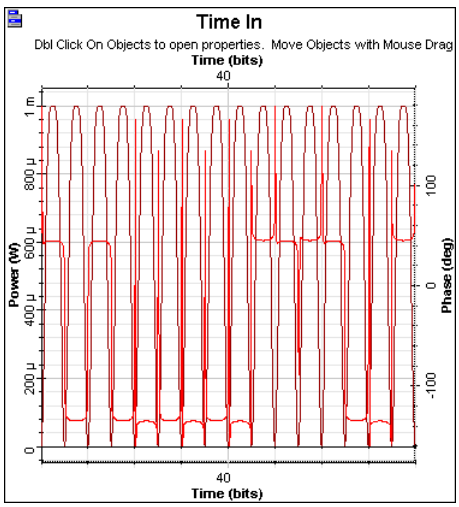


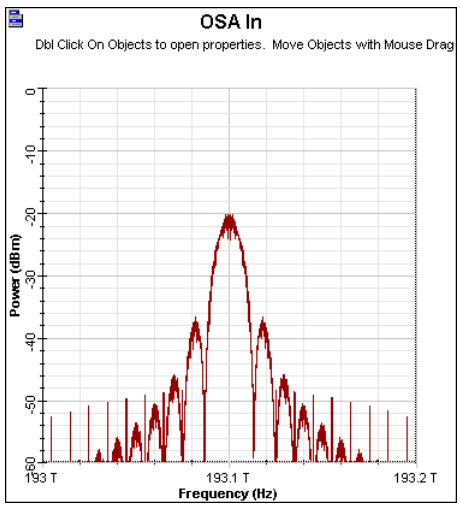
50% RZ-DPSK





67% RZ-DPSK





Reference:

[1] P. J. Winzer, R.-J. Essiambre, “Advanced optical modulation formats“, Proceedings of the IEEE, Vol. 94, No. 5, May 2006.

Notes:

QPSK Modulation and Demodulation

NRZ-QPSK.osp

33% RZ-DQPSK-Method 1.osp

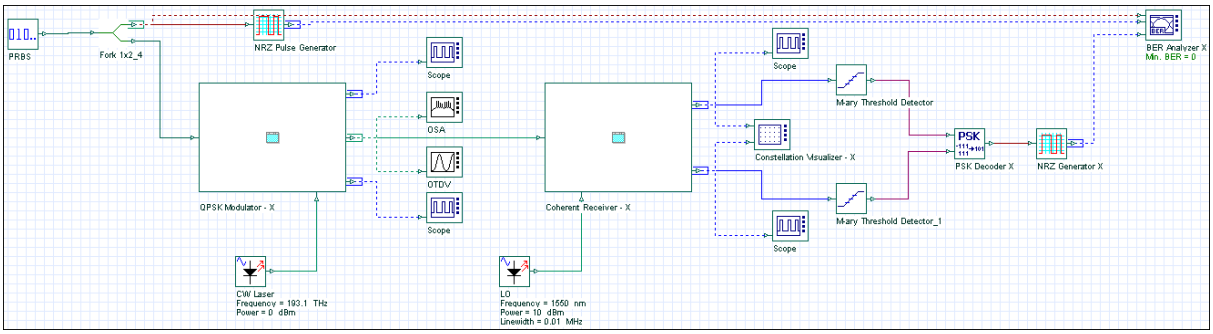
33% RZ-DQPSK-Method 2.osp

Compared with DPSK signal, the carrier phase of QPSK signal is allowed to take four different values, thus leading to a transmission rate of 2 bits per symbol and an increased spectral efficiency. For the projects presented in this example, the bit rate is set to 10 Gbps, and we can clearly see that the bandwith of QPSK signals is half as that of BPSK signals.

(a) NRZ-QPSK modulation format

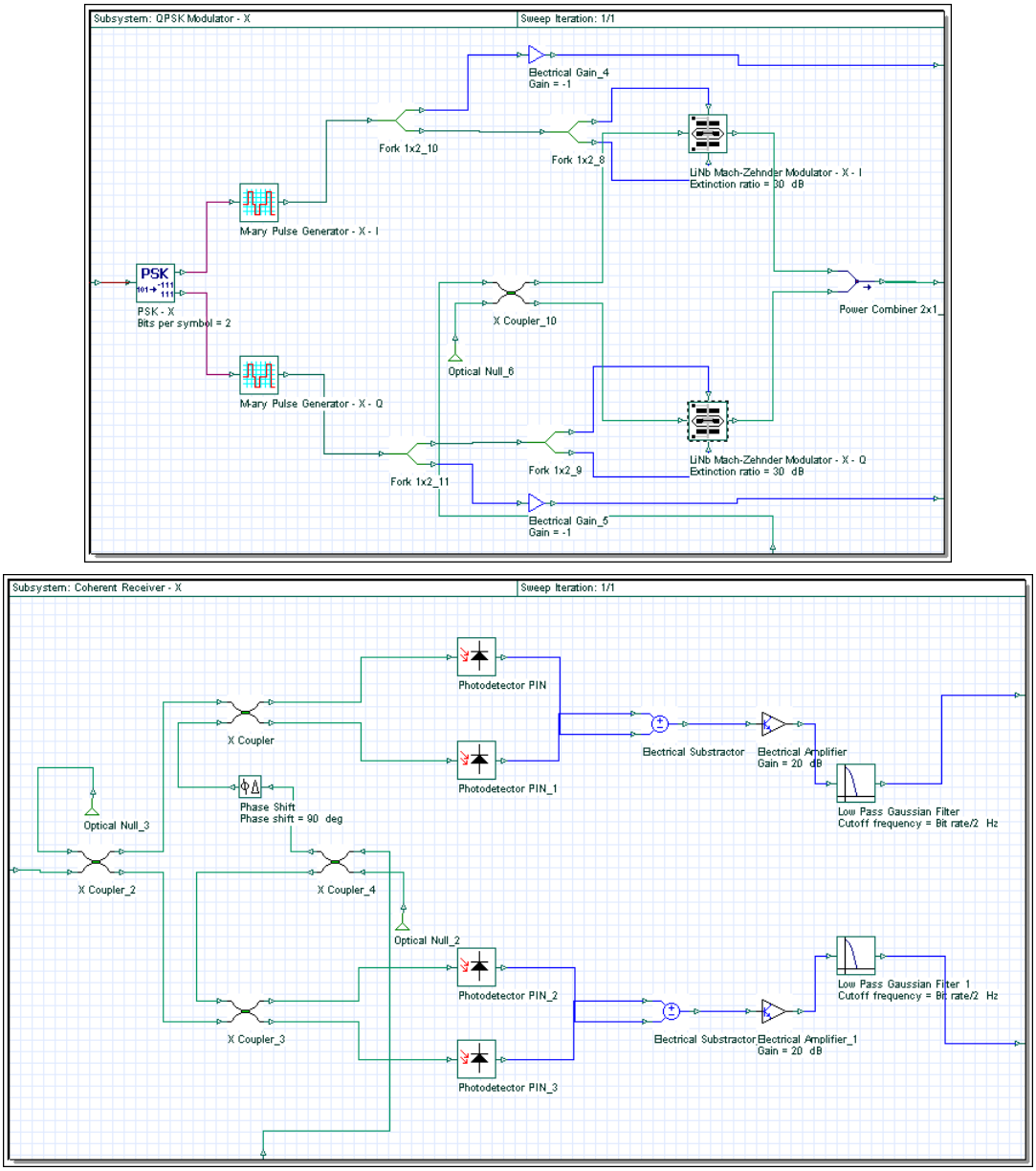
The layout for the generation of NRZ QPSK signal is shown in Figure 10-12.

Figure 10-12: Layout - NRZ-QPSK signal



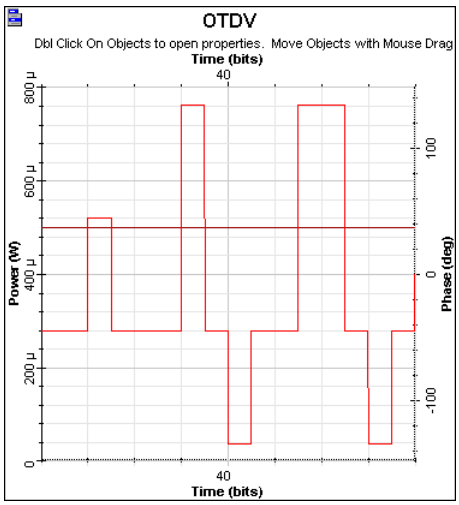
The inner structures for the subsystems *QPSK Modulator* and *Coherent Receiver* are shown in Figure 10-13.

Figure 10-13: Subsystems - QPSK Modulator and Coherent Receiver

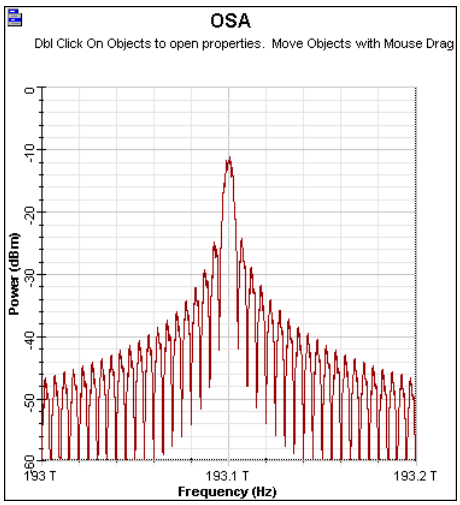


The corresponding NRZ-QPSK signal profile (intensity and phase), spectrum, as well as the constellation diagram (after the coherent receiver) are shown in Figure 10-14.

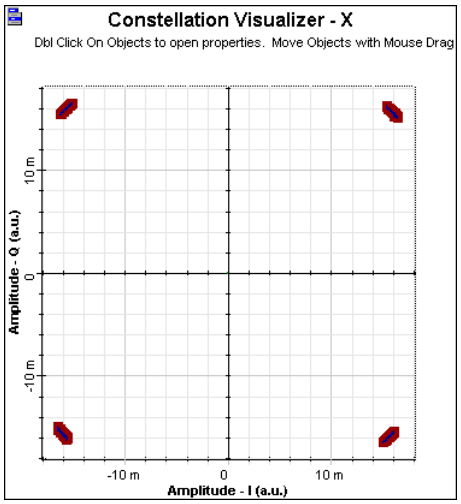
Figure 10-14: (a) NRZ-QPSK signal profile (intensity and phase) (b) NRZ-QPSK signal spectrum and (c) the constellation eye diagram after the coherent receiver.



(a)



(b)



(c)

(b) RZ-DQPSK modulation format

Two methods for generating 33% RZ-DQPSK signals are shown in Figure 10-15 and Figure 10-16 separately. For the one shown in Figure 10-15 [1], the signal generated after the first MZM is a NRZ-DPSK signal, a second MZM (acting as the phase modulator) is then used to generate the NRZ-DQPSK signal. The third MZM, sinusoidally driven at Bit Rate / 4, is used for pulse carving. For the one shown in Figure 10-16 [2], the first MZM is used for RZ pulse carving, and the next two MZMs in parallel are used for RZ-DQPSK signal generation.

For the demodulation, the delay demodulation scheme is being employed.

Figure 10-15: Layout - 33% RZ-DQPSK signal generation - Method 1

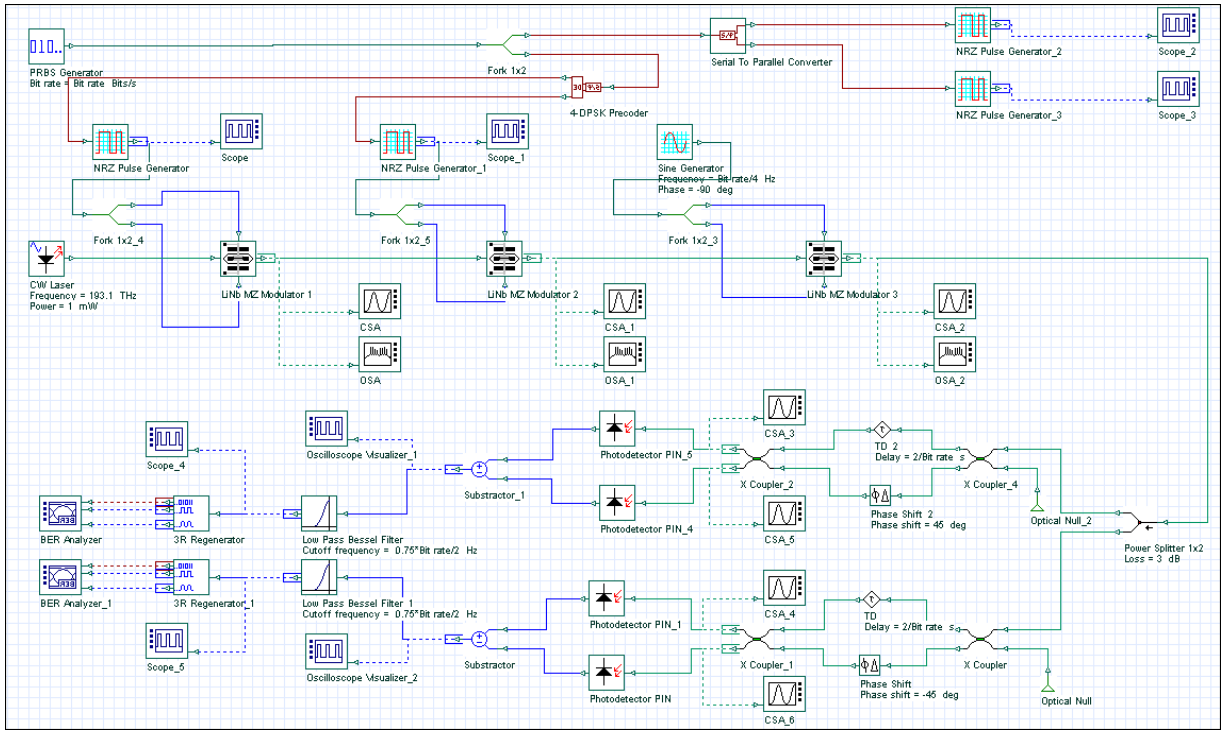
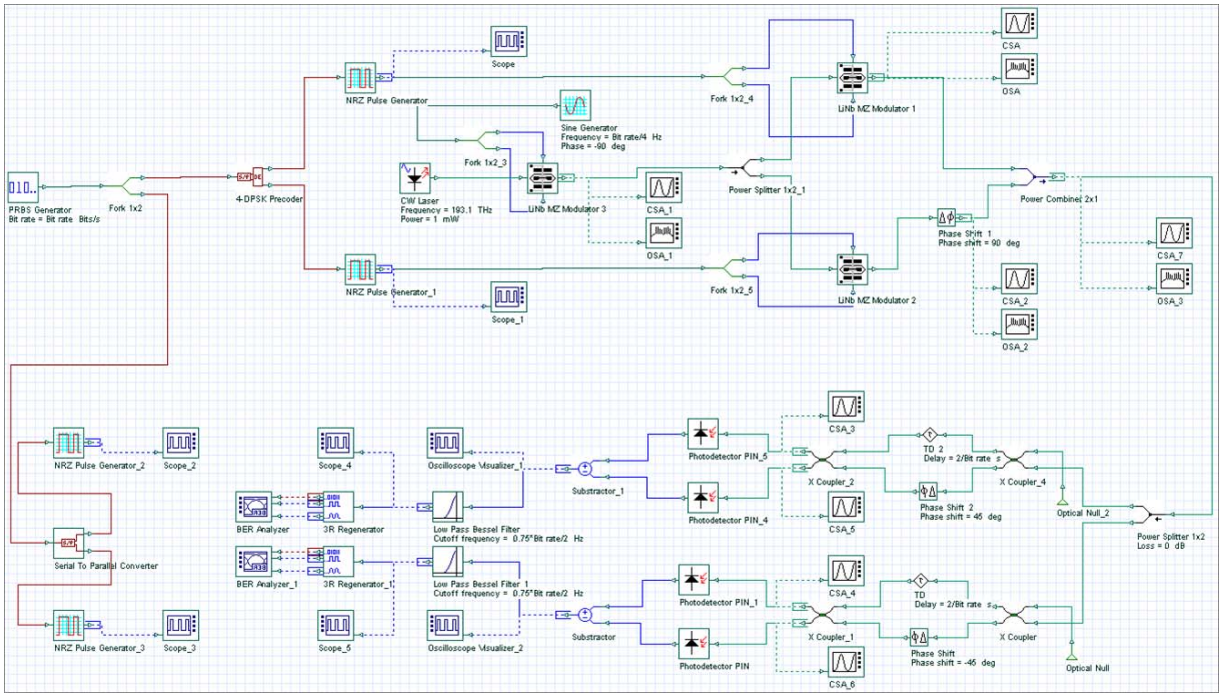


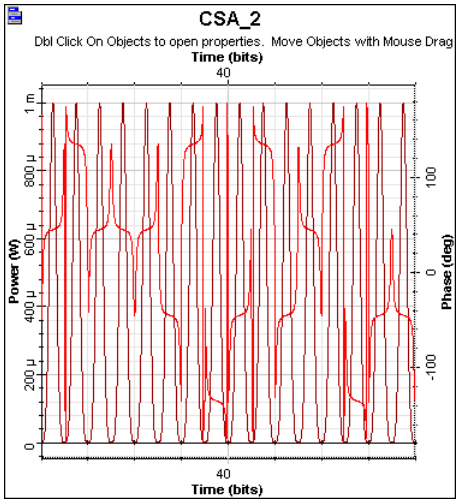
Figure 10-16: Layout - 33% RZ-DQPSK signal generation - Method 2

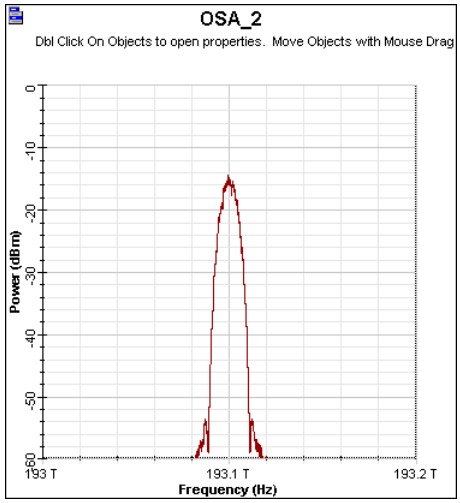


The corresponding RZ-DQPSK signal profile (intensity and phase) as well as the spectrum are shown in Figure 10-17.

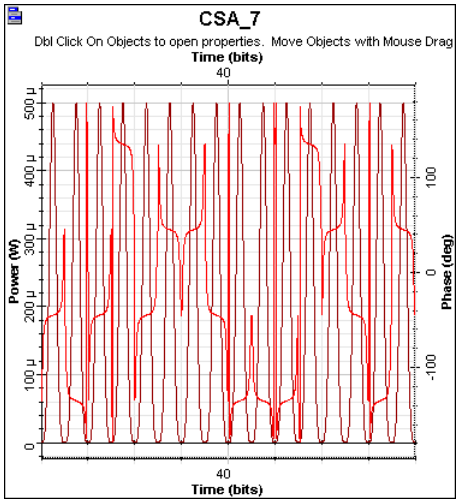
Figure 10-17: Output signal profile (intensity and phase) as well as spectrum of 33% RZ-DQPSK signals

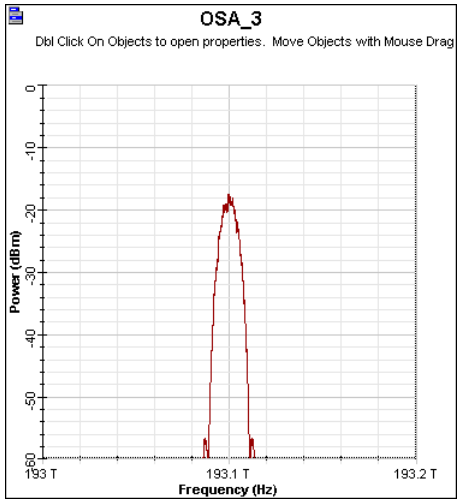
Method 1





Method 2





References:

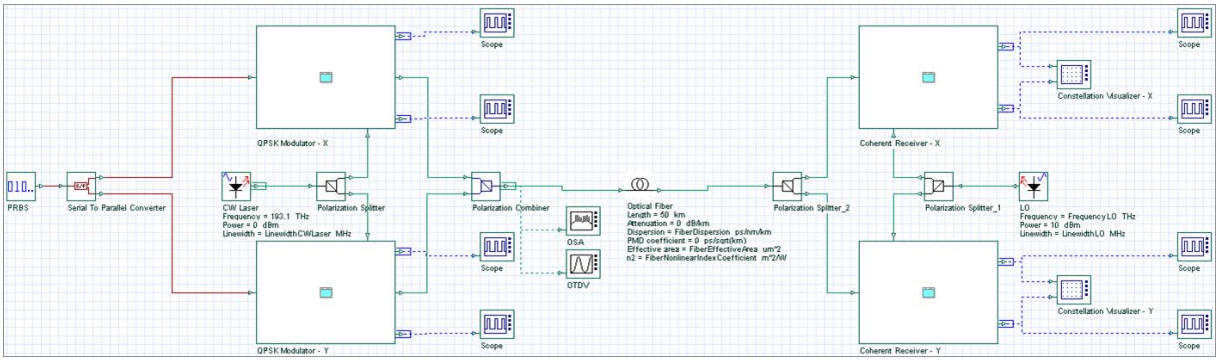
[1] C. Wree, J. Leibrich, and W. Rosenkranz, “RZ-DQPSK format with high spectral efficiency and high robustness towards fiber nonlinearities,” in *Proc. ECOC’02*, 2002, paper 9.6.6.

[2] P. J. Winzer, R.-J. Essiambre, “Advanced optical modulation formats“, Proceedings of the IEEE, Vol. 94, No. 5, May 2006.

100 Gbps PM-QPSK

A design example of a 100 Gbps polarization-multiplexed quadrature phase-shift-keying (PM-QPSK) system is shown in Figure 10-18.

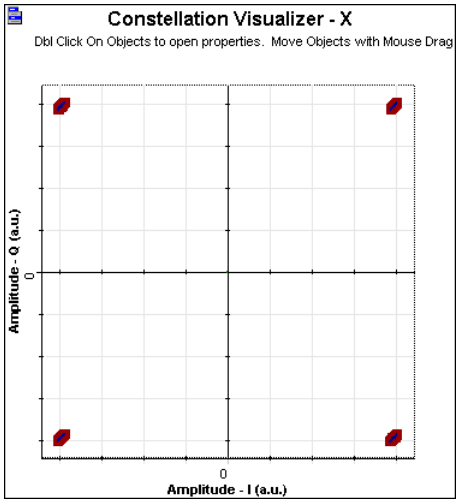
Figure 10-18: Layout - 100 Gbps PM-QPSK system

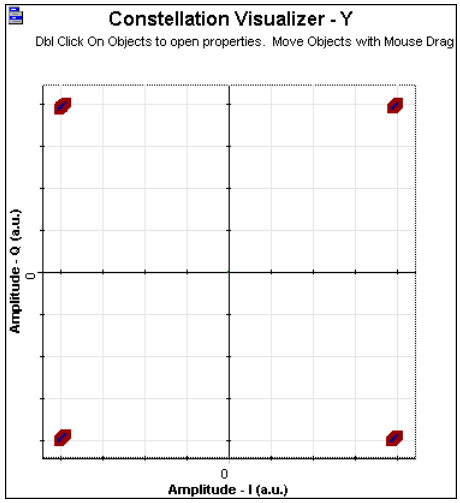


The ideal constellation diagram and the degraded constellation diagram (when both CW laser and LO linewidth are set to 1 MHz, fiber dispersion = 5ps/nm-km) are shown in Figure 10-19. The user can play with different parametes in this project to see how they affect the received constellation diagram.

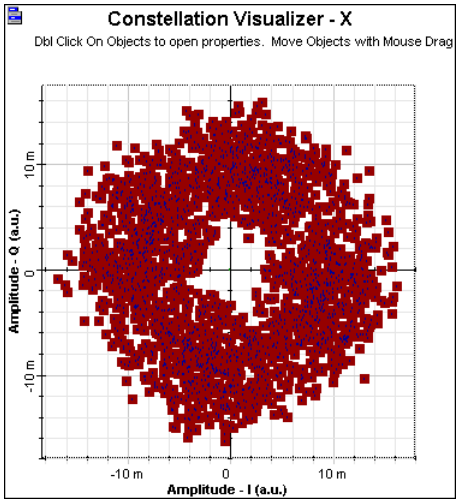
Figure 10-19: Ideal and degraded constellation diagrams

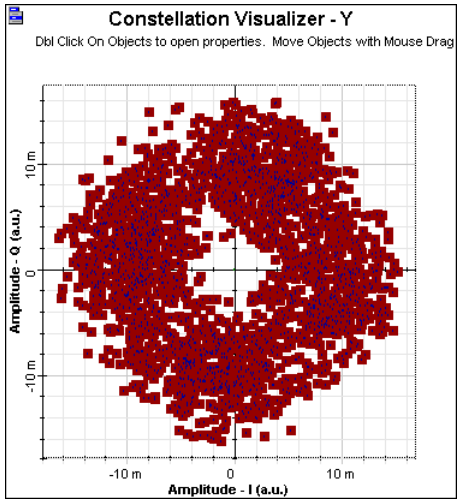
Ideal





Degraded





OD8PSK Modulation and Demodulation

OD8PSK.osp

The layout of the OD8PSK modulation format is shown in Figure 10-20, with the inner structures of the subsystems *Optical Encoder* and *Optical Demodulators and Receivers* shown in Figure 10-21 and Figure 10-22, separately.

Figure 10-20: Layout - OD8PSK signal

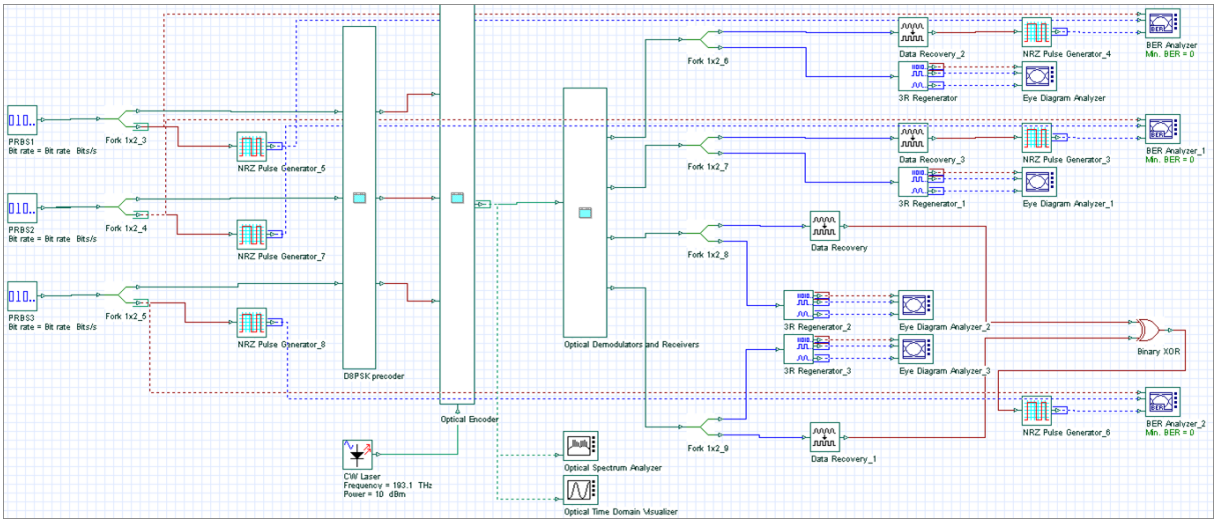


Figure 10-21: Subsystem - Optical Encoder

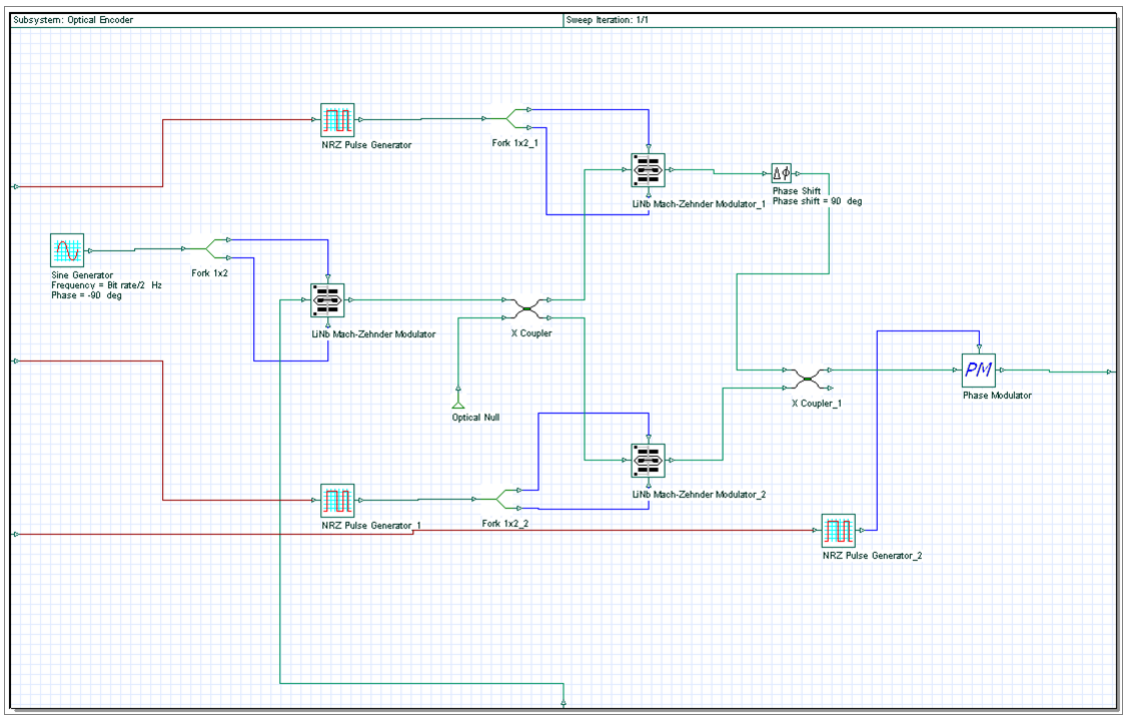
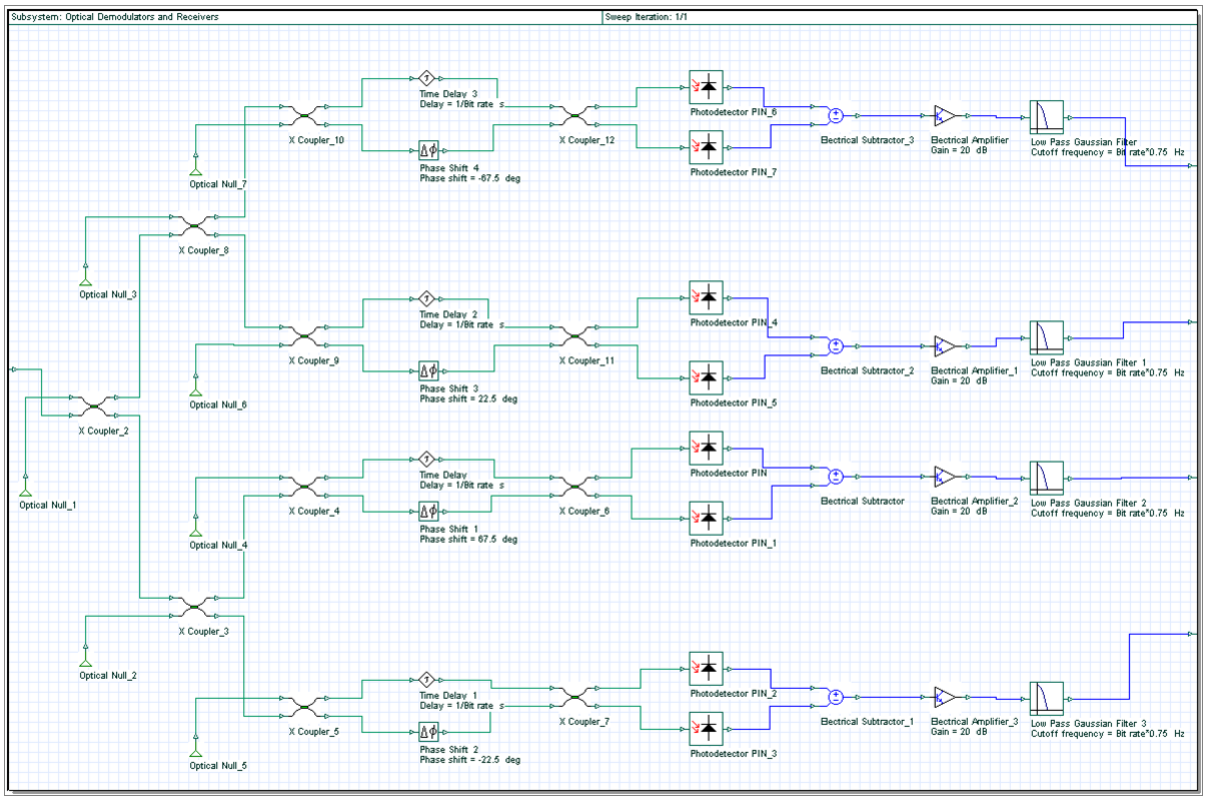
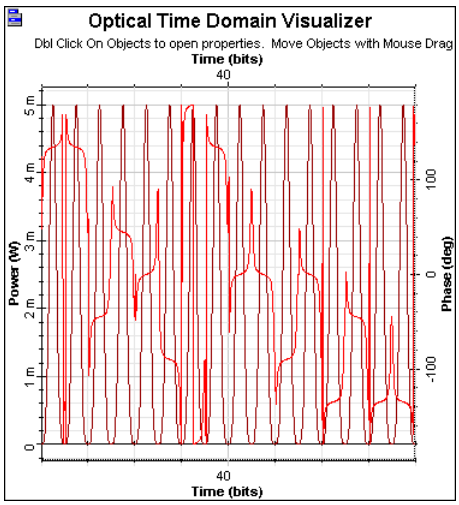


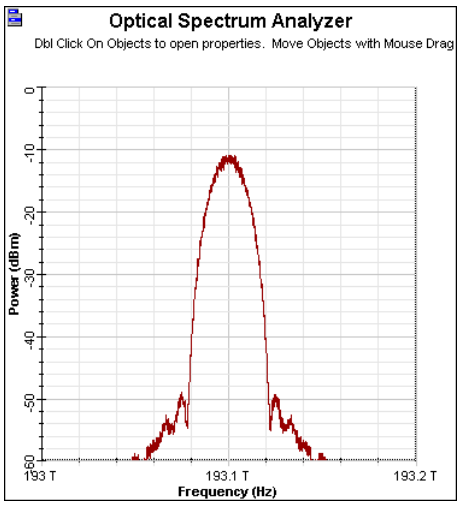
Figure 10-22: Subsystem - Optical Demodulators and Receivers



The electrical encoder, optical encoder, and the optical demodulators and receivers are implemented according to [1]. The generated OD8PSK signal profile (intensity and phase) as well as spectrum are shown in Figure 10-23.

Figure 10-23: Output signal profile (intensity and phase) as well as spectrum of OD8PSK signals





Reference:

[1] C. Kim and G. Li, “Direct-detection optical differential 8-level phase-shift keying (OD8PSK) for spectrally efficient transmission,“ Optics Express, Vol. 12, No. 15, July 2004

4-QAM OFDM Modulation and Demodulation

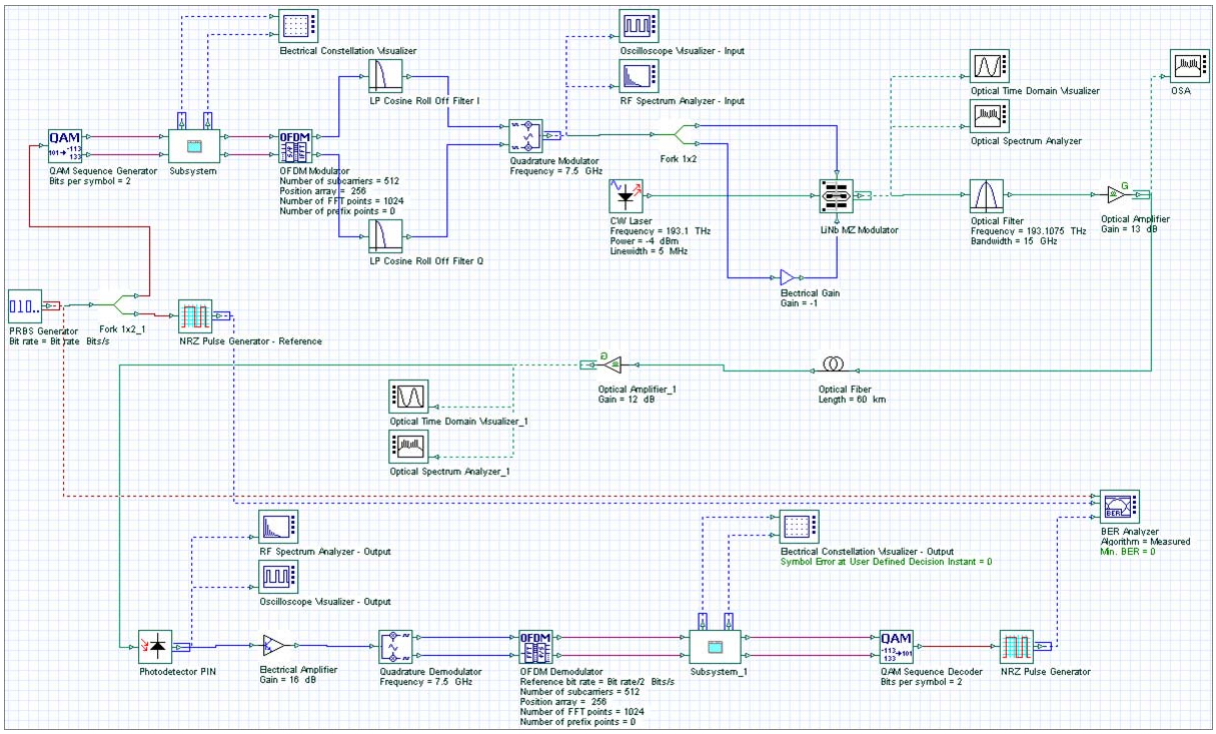
Direct-detection optical OFDM.osp

Coherent-detection optical OFDM.osp

(a) Direct-detection optical OFDM design

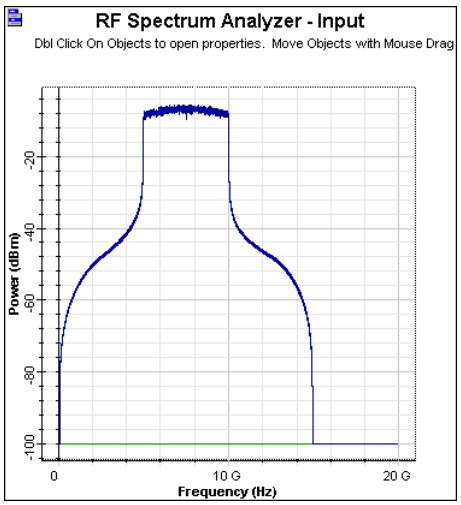
The layout of a direct-detection optical OFDM system is shown in Figure 10-24.

Figure 10-24: Layout - Direct-detection optical OFDM system



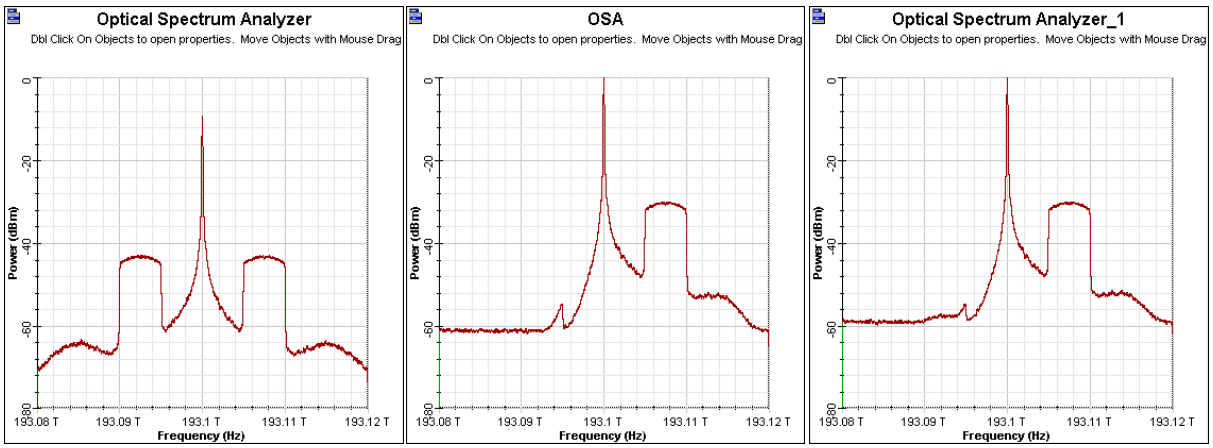
The generated RF OFDM signal spectrum after the quadrature modulator is shown in Figure 10-25.

Figure 10-25: RF OFDM signal spectrum after the quadrature modulator



The optical OFDM signal spectrum after the MZM modulator, filtering, and fiber propagation are shown in Figure 10-26.

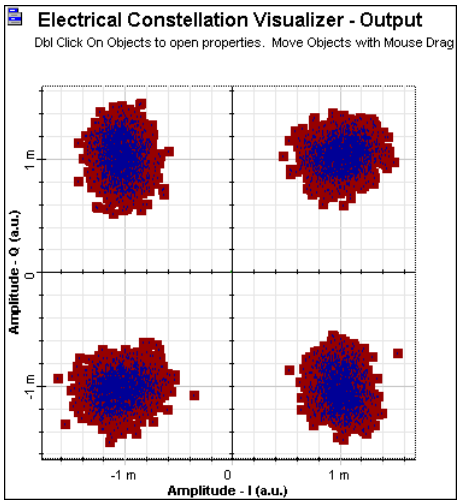
Figure 10-26: Optical OFDM signal spectrum after (a) MZM modulator (b) filtering and (c) fiber propagation



(a) **(b)** **(c)**

The received constellation diagram after quadrature demodulation and OFDM demodulation is shown in Figure 10-27.

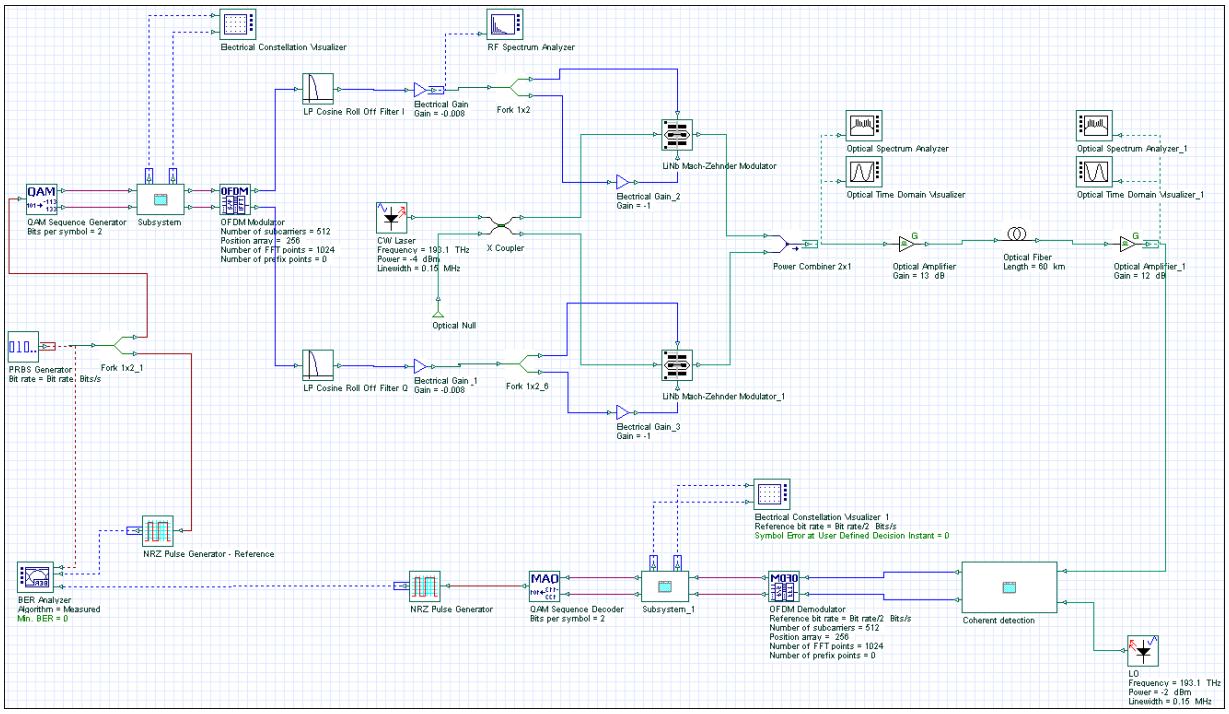
Figure 10-27: Received constellation diagram after demodulation



(b) Coherent-detection optical OFDM design

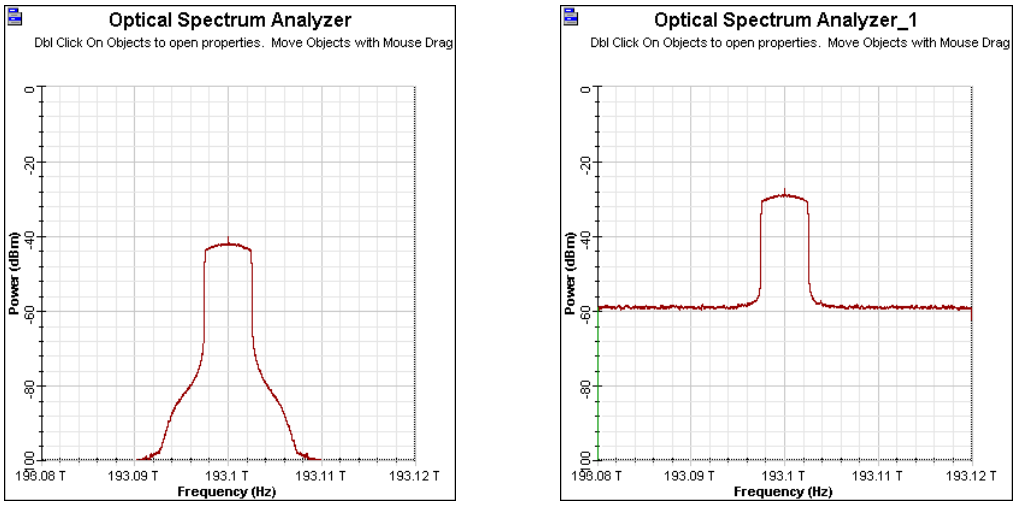
The layout of a coherent-detection optical OFDM system is shown in Figure 10-28.

Figure 10-28: Layout - Coherent-detection optical OFDM system



The generated optical OFDM signal spectrum before and after fiber propagation are shown in Figure 10-29.

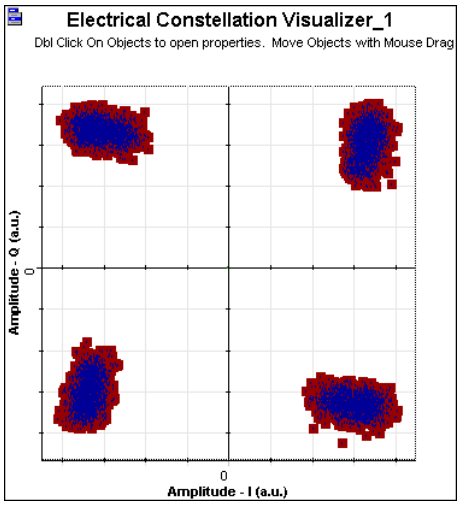
Figure 10-29: Optical OFDM signal spectrum before and after the propagation in fiber



Before **After**

The received constellation diagram after demodulation is shown in Figure 10-30.

Figure 10-30: Received constellation diagram after demodulation



Chapter 11 - Optical Signal Processing

This section contains the following examples.

- Nonlinear Optical Loop Mirror
- Parametric Amplifiers
- Wavelength Conversion Based on FWM in SOA
- Wavelength Conversion Based on XGM in SOA
- Wavelength Conversion Based on XPM in HNLF
- Data-Format Conversion Based on XPM in HNLF
- SPM Based 2R Regenerator for RZ Signal
- XPM Based 3R Regenerator for RZ Signal

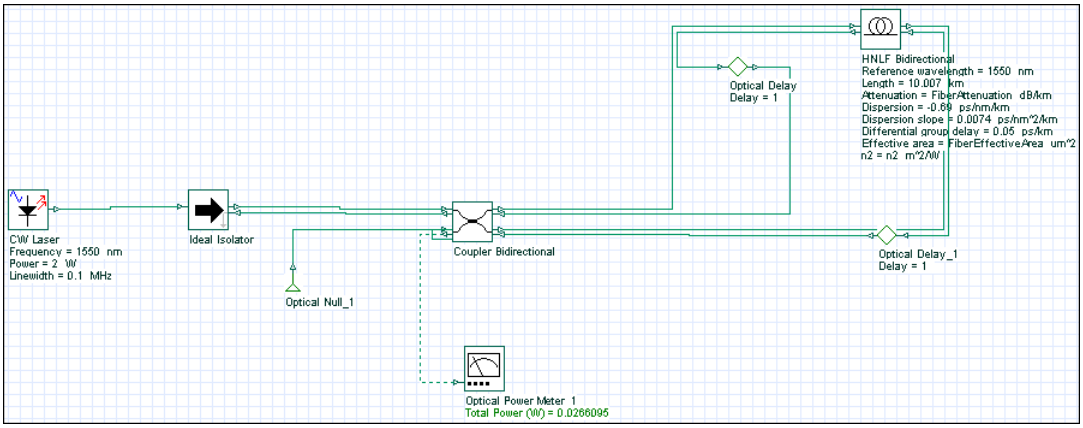
Notes:

Nonlinear Optical Loop Mirror

Nonlinear optical loop mirror.osp

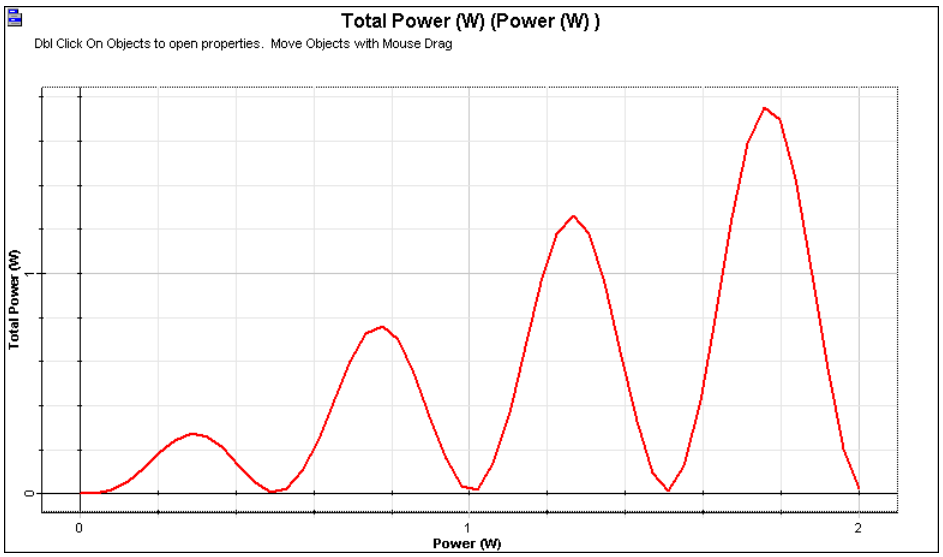
A nonlinear optical-loop mirror (NOLM) is a Sagnac interferometer in which different nonlinear phase shifts are acquired by the counter-propagating waves inside the fiber loop [1]. The layout of the NOLM example is shown in Figure 11-1:

Figure 11-1: Layout - Nonlinear optical loop mirror



The incoming light is splitted into two counterpropagating parts by the coupler. At the output, whether the light is transferred or reflected is determined by the relative phase difference of the two counterpropagating waves. The transmitted power as a function of the incident power is shown in the report page, as in Figure 11-2:

Figure 11-2: Transmitted power vs the incident power



Reference:

[1] G.P. Agrawal, Fiber-Optic Communication Systems, 4th ed., John Wiley & Sons, INC., New York, 2010.

Parametric Amplifiers

Parametric amplifiers.osp

Project file "*Parametric amplifiers.osp*" shows an example of a single-pump parametric amplifier. The pump wavelength is fixed at 1542.4 nm, while the wavelength of probe light is swept from 1450 nm to 1650 nm, so the parametric gain for different pump-signal detunings can be characterized. The gain experienced by the probe light is calculated using the Dual Port WDM Analyzer component. The layout and obtained parametric gain spectrum are shown in Figure 11-3 and Figure 11-4, respectively.

Figure 11-3: Layout - Parametric amplifiers

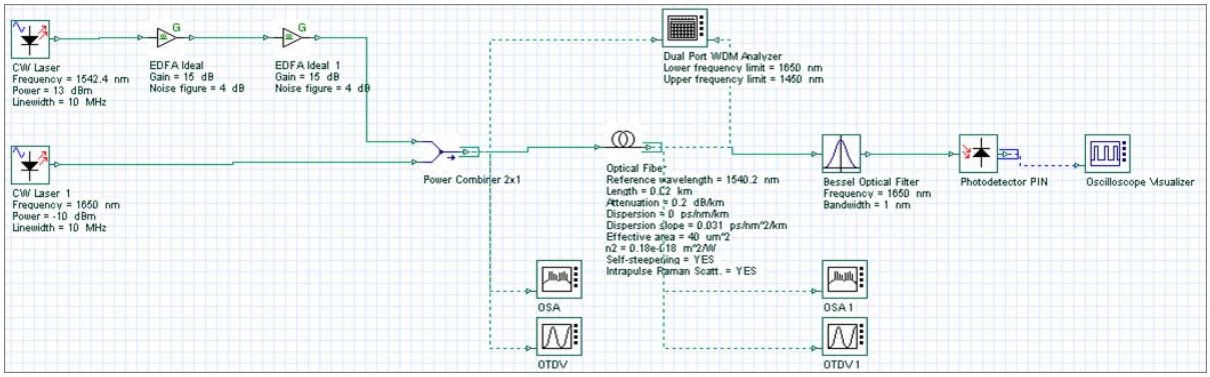
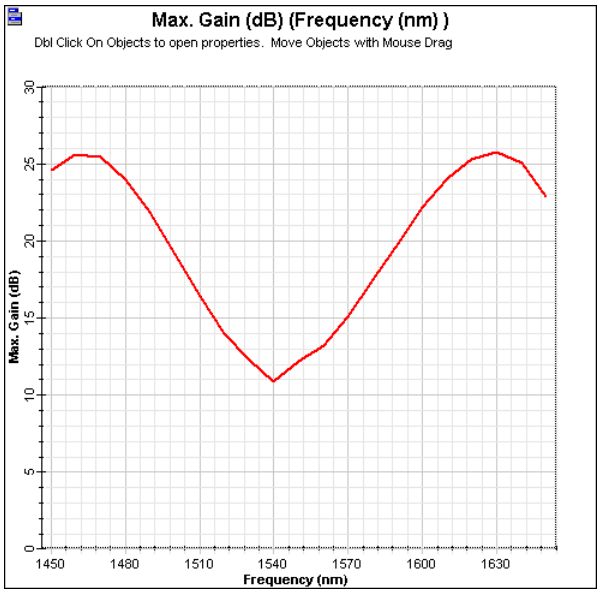


Figure 11-4: Parametric gain spectrum



Reference:

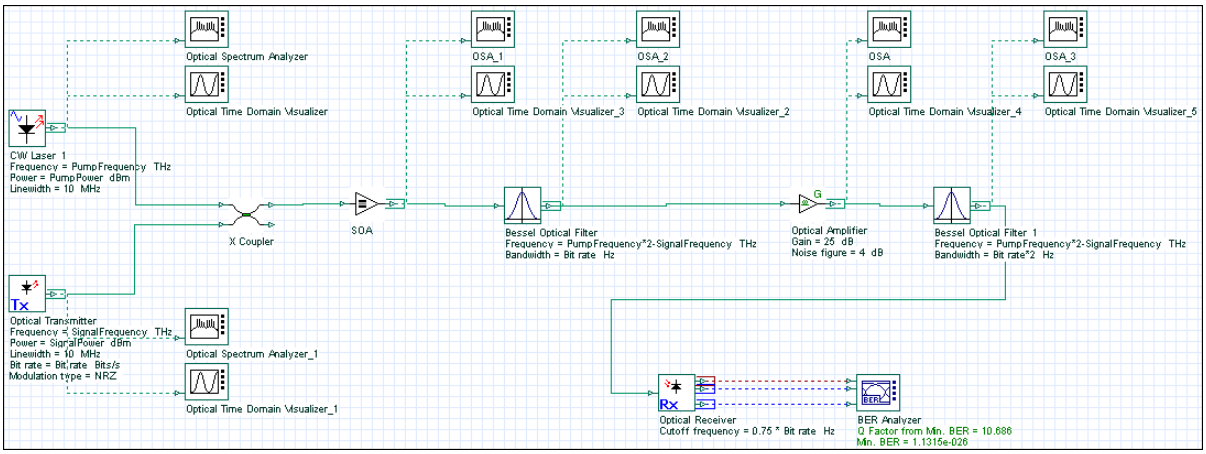
[1] M.-C. Ho, K. Uesaka, M. E. Marhic, Y. Akasaka and L. G. Kazovsky, “200-nm-Bandwidth fiber optical amplifier combining parametric and raman gain,” IEEE Journal of Lightwave Technology, Vol. 19, No 7, pp. 977-981, July 2001.

Wavelength Conversion Based on FWM in SOA

Wavelength conversion based on FWM in SOA.osp

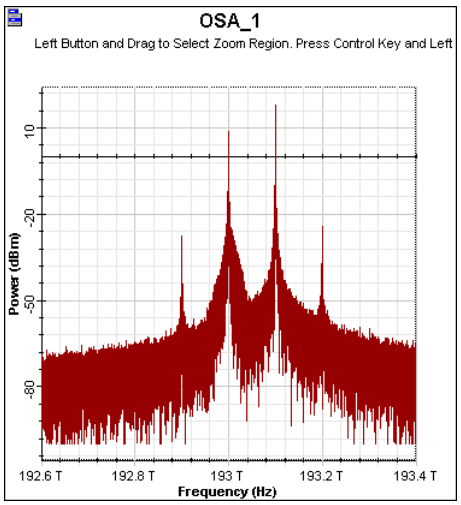
A wavelength converter based on FWM in SOA operating at 2.5 Gb/s is shown as an example in the project file "*Wavelength conversion based on FWM in SOA.osp*". The layout for the wavelength conversion scheme is shown in Figure 11-5:

Figure 11-5: Layout - Wavelength conversion based on FWM in SOA



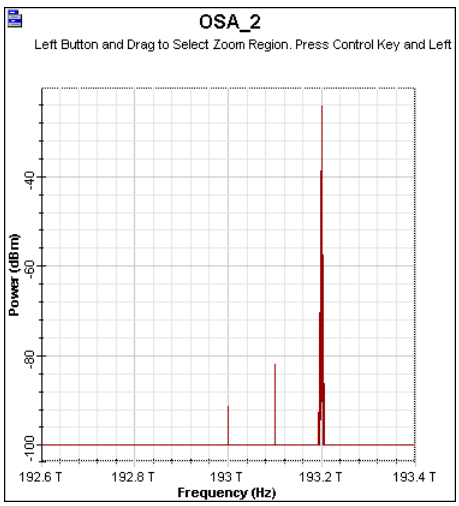
The pump laser has a frequency of 193.1 THz and a power of 10 dBm; while the NRZ signal has a frequency of 193 THz and power of 5 dBm. The pump and signal light are combined using a 3 dB coupler and then copropagate in a SOA, where the FWM effect occurs. After the SOA, an optical filter centered at (2 x PumpFrequency - SignalFrequency) is used to select the FWM generated new frequency component. The optical spectrum after the SOA is shown in Figure 11-6, where we can clearly see the FWM generated new frequency components.

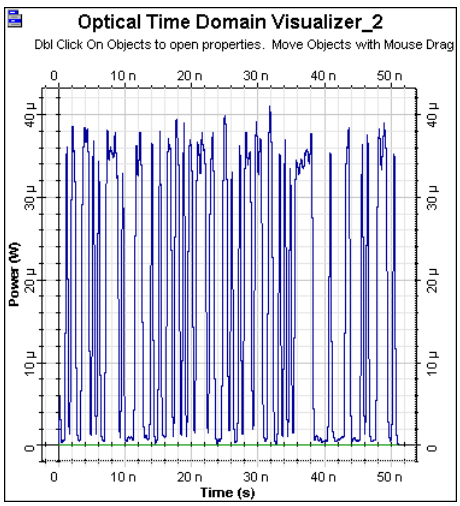
Figure 11-6: Spectrum after the SOA



The optical spectrum as well as time domain signal profile after the first optical filter are shown in Figure 11-7.

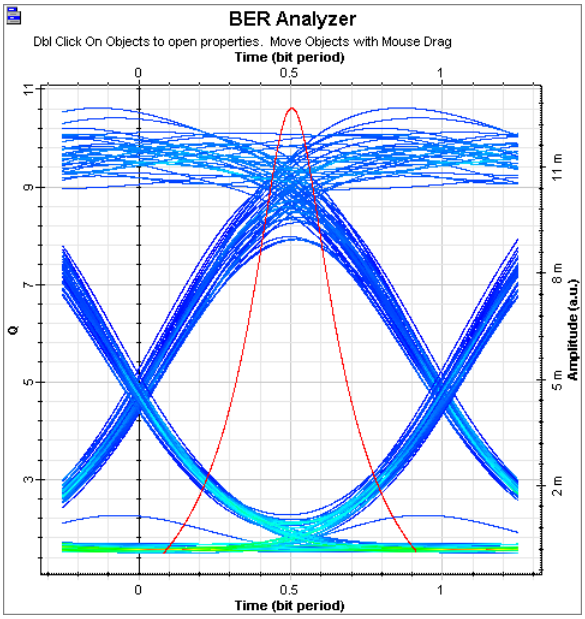
Figure 11-7: Spectrum and time domain signal profile after the first optical filter





After amplifying and filtering out-of-band noise, the eye diagram obtained after the wavelength conversion process is shown in Figure 11-8.

Figure 11-8: Eye diagram of the wavelength converted output



References:

[1] J. M. H. Elmirghani and H. T. Mouftah, "All-optical wavelength conversion: Technologies and applications in DWDM networks," IEEE Communications Magazine, March 2000.

[2] G.P. Agrawal, *Fiber-Optic Communication Systems*, 4th ed., John Wiley & Sons, INC., New York, 2010.

Notes:

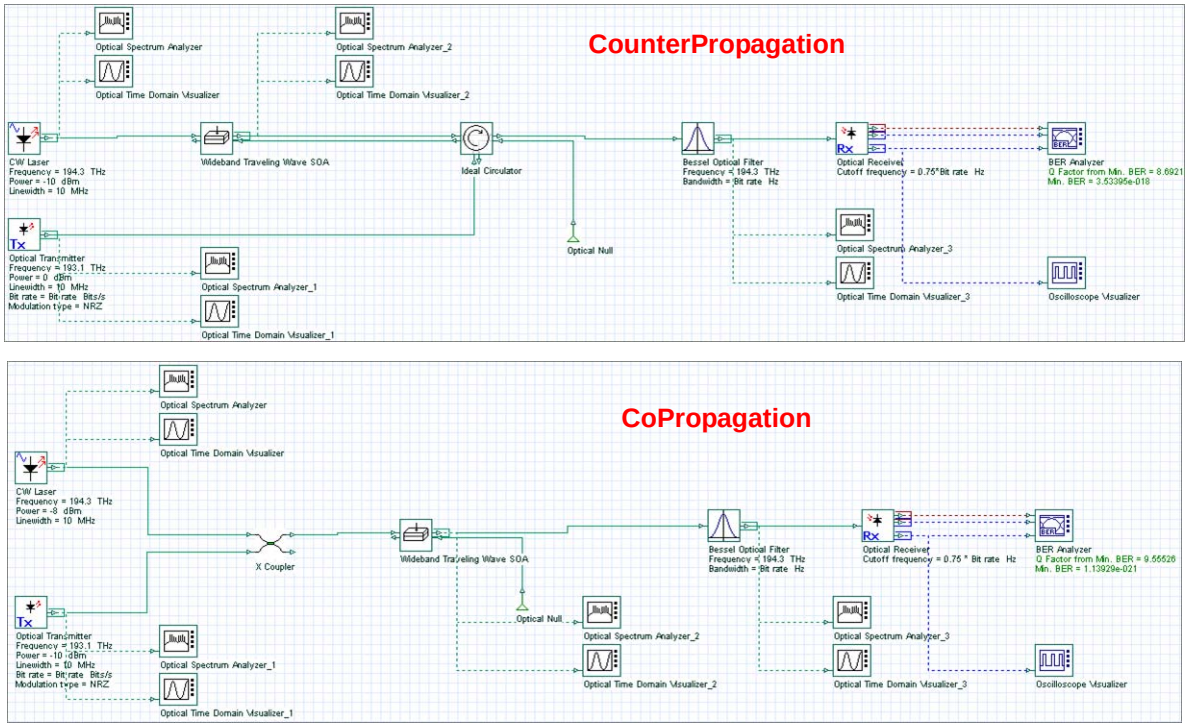
Wavelength Conversion Based on XGM in SOA

Wavelength conversion based on XGM in SOA - CounterPropagation.osp

Wavelength conversion based on XGM in SOA - CoPropagation.osp

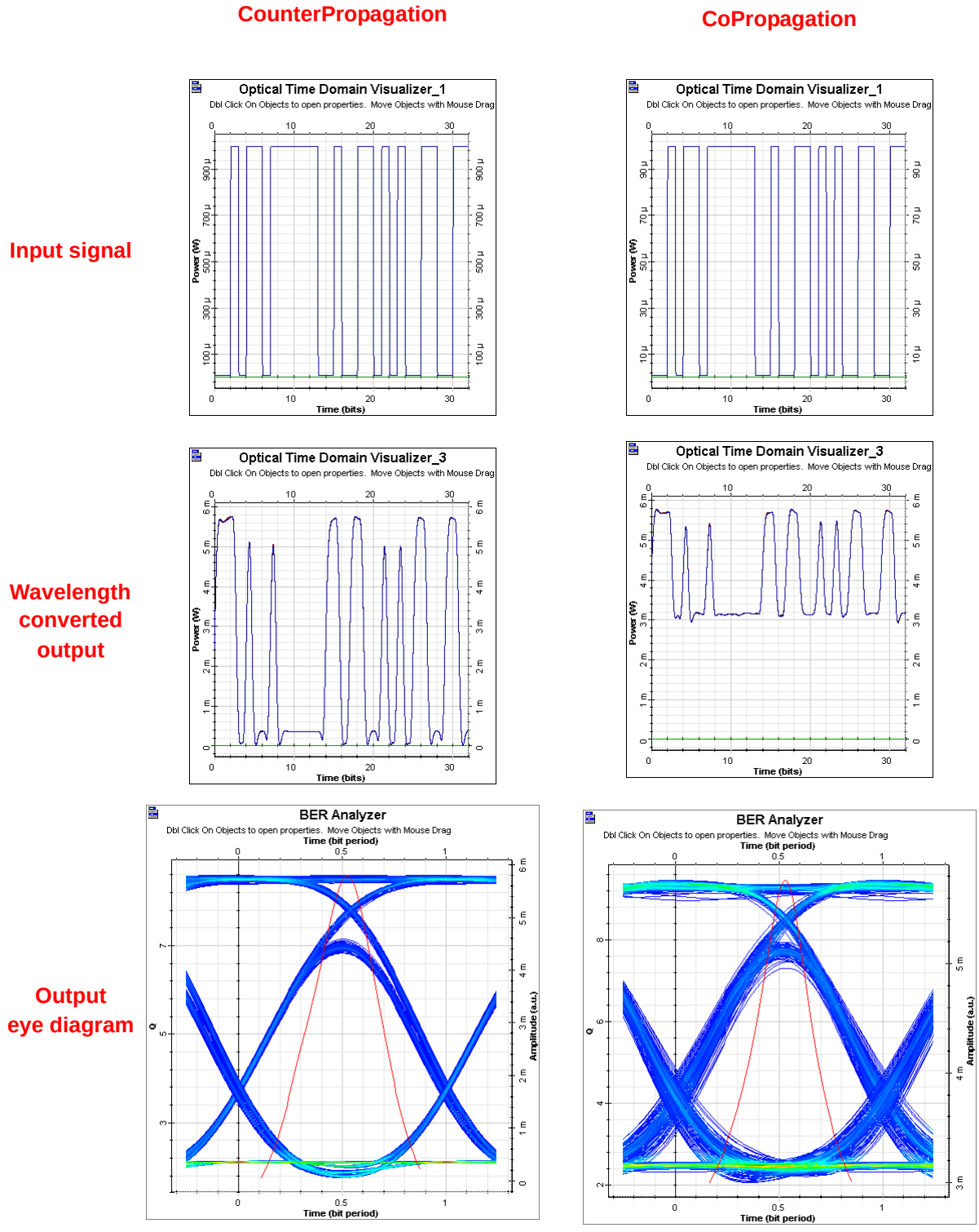
Two schemes of wavelength conversion based on XGM in SOA, namely, CounterPropagation and CoPropagation, are shown in this example. The bit rate for both scheme is set to 2.5 Gb/s.

Figure 11-9: Layout - Wavelength conversion based on XGM in SOA



The original signal profile, wavelength-converted signal profile, as well as the eye diagram of the wavelength converted output,are shown in Figure 11-10.

Figure 11-10: Comparison of the signal profiles before and after wavelength conversion



Reference:

[1] J. M. H. Elmirghani and H. T. Mouftah, “All-optical wavelength conversion: Technologies and applications in DWDM networks,” IEEE Communications Magazine, March 2000.

[2] G.P. Agrawal, *Fiber-Optic Communication Systems*, 4th ed., John Wiley & Sons, INC., New York, 2010.

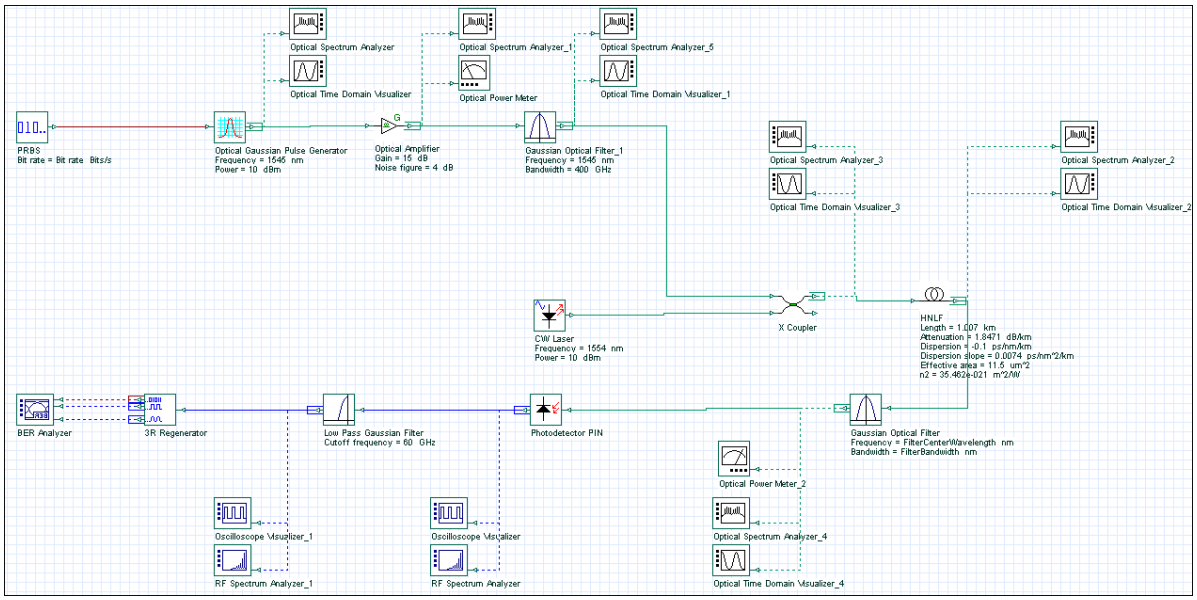
Notes:

Wavelength Conversion Based on XPM in HNLF

Wavelength conversion based on XPM in HNLF.osp

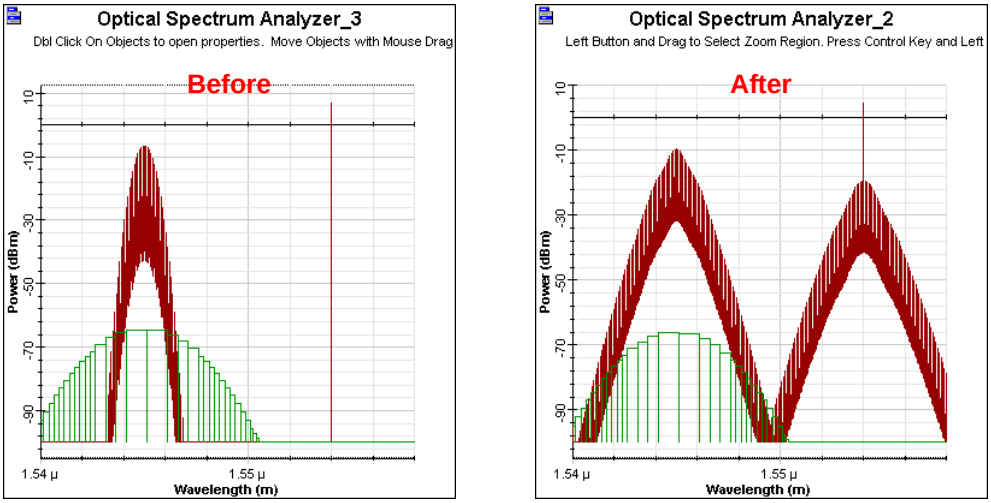
In the project file "*Wavelength conversion based on XPM in HNLF.osp*", the nonlinear phenomenon of XPM is employed to achieve the wavelength conversion. The layout is shown in Figure 11-11:

Figure 11-11: Layout - Wavelength conversion based on XPM in HNLF



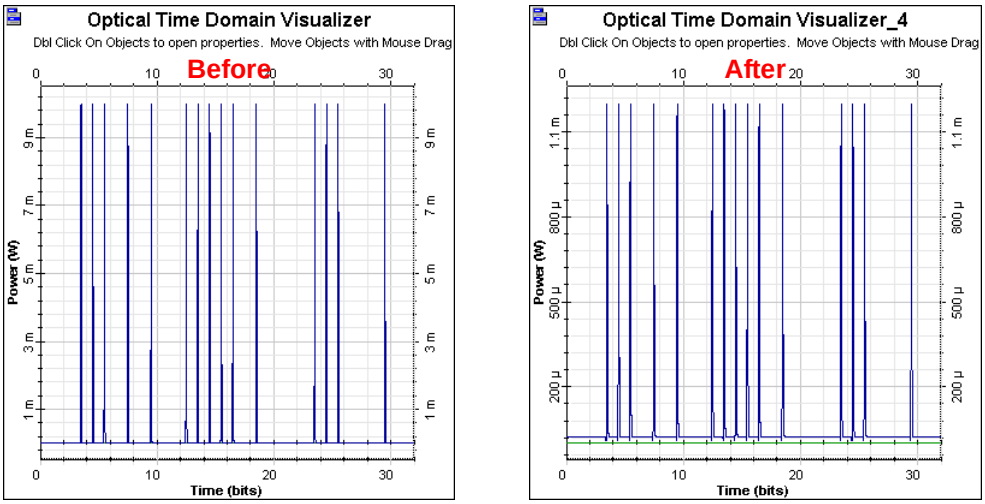
The wavelength conversion scheme is demonstrated at 10 Gb/s. The signal (@ 1545 nm), which is a sequence of gaussian pulses, is amplifed and then copropagate with a CW probe (@ 1554 nm) in a HNLF. The CW probe will experience XPM induced spectral broadening, and the optical spectrum before and after the HNLF are shown in Figure 11-12.

Figure 11-12: Spectrum before and after the HNLF



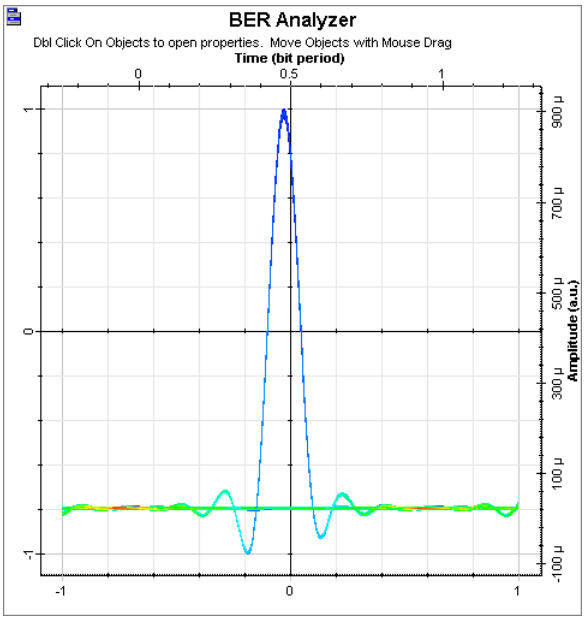
After the HNLF, a BPF, which is 0.8 nm offset from the center wavelength of the CW laser, is used to filter out the original frequency components at 1554 nm and keep the spectral components that have been shifted by XPM. The original signal profile and the wavelength-converted output after the BPF are shown in Figure 11-13.

Figure 11-13: Comparison of the signal profile before and after wavelength conversion



The eye diagram of the wavelength-converted output is shown in Figure 11-14.

Figure 11-14: Eye diagram of the wavelength converted output



If the BPF is aligned exactly to the CW laser wavelength, then a polarity-inversed output can be obtained. The reader can play with the filter center wavelength as well as the bandwidth to see how the output will be affected.

Reference:

[1] G.P. Agrawal, *Fiber-Optic Communication Systems*, 4th ed., John Wiley & Sons, INC., New York, 2010.

Notes:

Data-Format Conversion Based on XPM in HNLF

NRZ to RZ format conversion based on XPM in HNLF.osp

RZ to NRZ format conversion based on XPM in HNLF.osp

The project file "*NRZ to RZ format conversion based on XPM in HNLF.osp*" shows an example of 10 Gb/s all-optical NRZ to RZ format conversion using single HNLF assisted by optical bandpass filter. A 10 Gb/s NRZ signal at 1554 nm (acting as the probe) is combined with a synchronized RZ clock (acting as the pump) at 1545 nm and then launched into the HNLF. The pulsewidth of the RZ clock is ~ 5 ps. Due to the high power of the RZ clock, the NRZ signal will experience XPM induced spectral broadening. An subsequent optical BPF is then used to extract the sideband spectrum with an offset to the original NRZ wavelength. Since the spectral shift occurs only during the RZ pulse duration, a RZ pulse train which has the same data information as the NRZ signal can thus be obtained after the offset filtering. More details about the principle of this simulation can be seen in [1].

The project file "*RZ to NRZ format conversion based on XPM in HNLF.osp*" shows the example of spectral filtering from a cross-phase modulated signal for RZ to NRZ format conversion. The principle is similar to the XPM based wavelength conversion and is detailed in [2].

Reference:

[1] J. Dong, X. Zhang, J. Xu, D. Huang, S. Fu, and P. Shum, "40Gb/s all-optical NRZ to RZ format conversion using single SOA assisted by optical bandpass filter," Opt. Express 15, 2907-2914 (2007).

[2] S. H. Lee, K. Chow, and C. Shu, "Spectral filtering from a cross-phase modulated signal for RZ to NRZ format and wavelength conversion," Opt. Express 13, 1710-1715 (2005).

Notes:

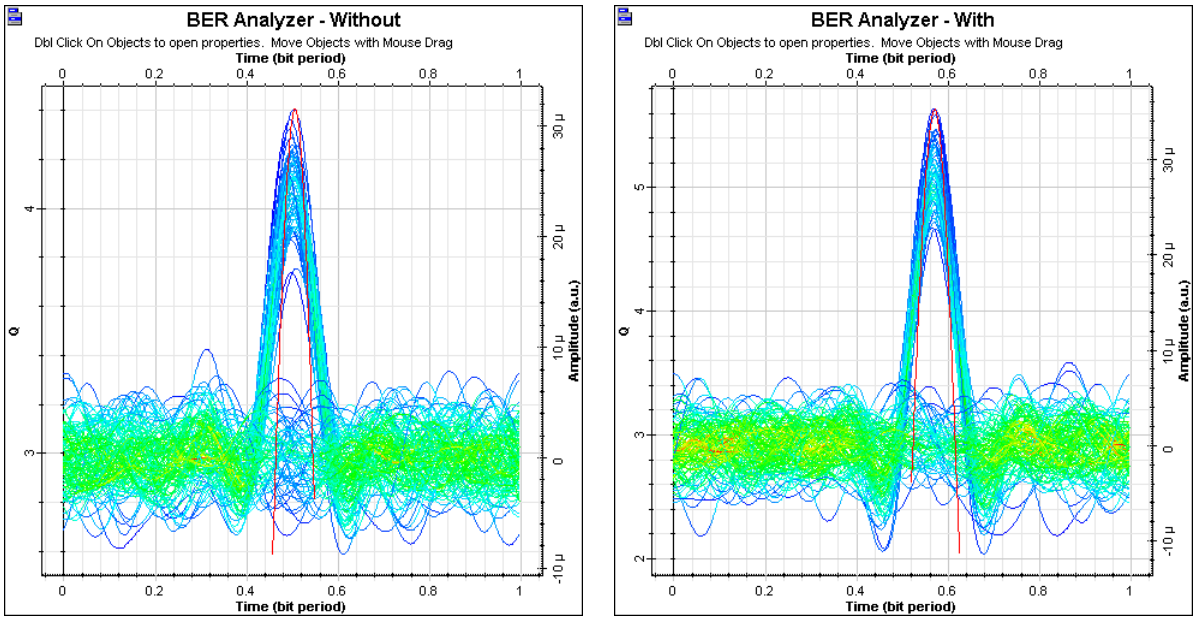
SPM Based 2R Regenerator for RZ Signal

SPM based 2R regenerator for RZ signal.osp

Project file "*SPM based 2R regenerator for RZ signal.osp*" shows the improvement of eye diagram after passing the signal throught the SPM based 2R regenerator. The principle of SPM based 2R regenerator is already explained in [1-2] and the regeneration property comes from the different power transfer function for "0"s and "1"s.

At the same receiver power level of -29.3 dBm, the recovered eye diagrams without/with 2R regeneration are shown in Figure 11-15. We can clearly see the improvement with 2R regeneration.

Figure 11-15: Eye diagrams without and with 2R regeneration



Reference:

[1] G.P. Agrawal, *Fiber-Optic Communication Systems*, 4th ed., John Wiley & Sons, INC., New York, 2010.

[2] M. Rochette, L. Fu, V. Ta'eed, D. J. Moss, and B. J. Eggleton, "2R optical regeneration: An all-optical solution for BER improvement," IEEE Journal of Selected Topics in Quantum Electronics, Vol. 12, No. 4, July/August 2006.

Notes:

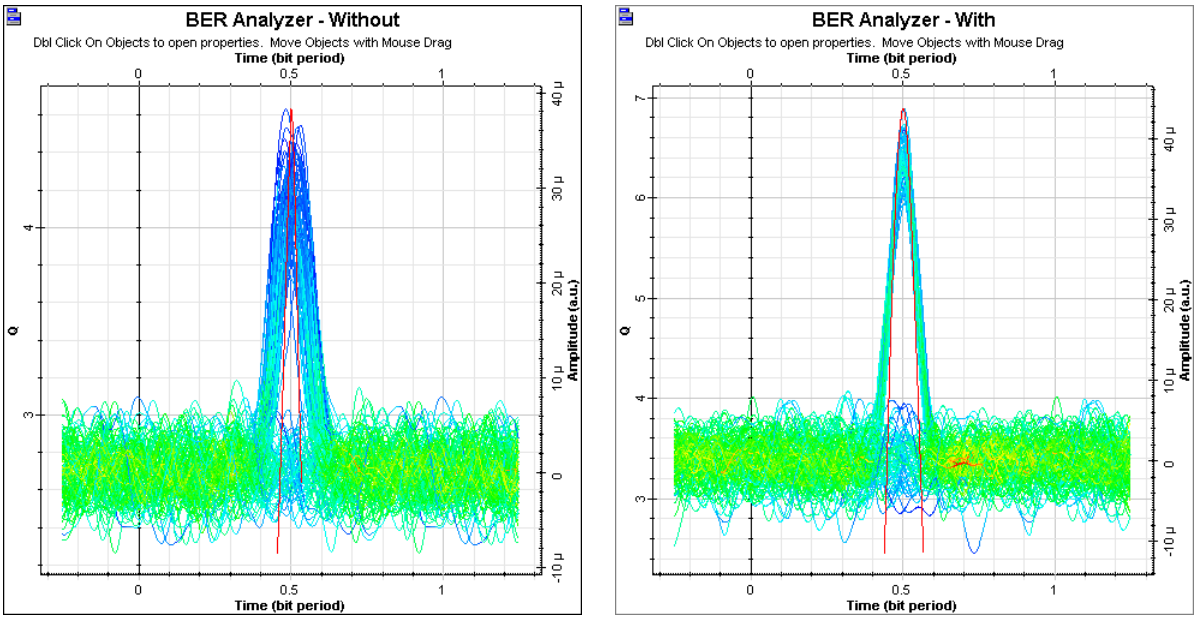
XPM Based 3R Regenerator for RZ Signal

XPM based 3R regenerator for RZ signal.osp

Compared with 2R regenerator, a 3R regenerator also performs the retiming function and reduces the timing jitter of a bit stream. Project file "*XPM based 3R regenerator for RZ signal.osp*" shows an example of 3R regenerator based on XPM in HNLF [1-2].

Time jitter and white light source are added to the input signal to degrade the input signal quality. At the same receiver power level of -26.9 dBm, the recovered eye diagrams without/with 3R regeneration are shown in Figure 11-16. We can clearly see the improvement with 3R regeneration.

Figure 11-16: Eye diagrams without and with 3R regeneration



References:

[1] G.P. Agrawal, *Fiber-Optic Communication Systems*, 4th ed., John Wiley & Sons, INC., New York, 2010.

[2] M. Rochette, J. L. Blows, and B. J. Eggleton, "3R optical regeneration: An all-optical solution with BER improvement," Optics Express, Vol. 14, No. 14, July 2006.

Notes:



Optiwave
7 Capella Court
Ottawa, Ontario, K2E 7X1, Canada

Tel.: 1.613.224.4700
Fax: 1.613.224.4706

E-mail: support@optiwave.com
URL: www.optiwave.com